The University of Adelaide

Doctoral Thesis

Mechanisms of inclined stress corrosion cracks

Author:
James Griggs

Supervisors:
Dr. Erwin Gamboa
A/Prof. Andrei Kotousov

A thesis submitted in fulfilment of the requirements for the degree of Doctor of Philosophy

in the

School of Mechanical Engineering

December 2016

Declaration of Authorship

I certify that this work contains no material which has been accepted for the award of any other degree or diploma in my name, in any university of other tertiary institution and, to the best of my knowledge and belief, contains no material previously published or written by another person, except where due reference has been made in the text. In addition, I certify that no part of this work will, in the future, be used in a submission in my name, for any other degree or diploma in any university or other tertiary institution without the prior approval of the University of Adelaide and where applicable, any partner institution responsible for the joint-award of this degree.

I give consent to this copy of my thesis, when deposited in the University Library, being made available for loan and photocopying, subject to the provisions of the Copyright Act 1968.

I also give permission for the digital version of my thesis to be made available on the web, via the University's digital research repository, the Library Search and also through web search engines, unless permission has been granted by the University to restrict access for a period of time.

Signed: _____

Date: _____

"Aim for the bushes."

D. T. R. Johnson

Abstract

Inclined high pH stress corrosion cracking (SCC) is a type of intergranular environmental cracking in gas pipelines which differs from typical SCC by propagating at an angle from axial-radial plane. Prior investigations of Australian and Canadian inclined SCC colonies have not provided a clear indicator of the mechanism behind the abnormal crack growth direction. This thesis addresses the issue of why SCC has inclined in the cases in Australia and Canada, as well as the implications of this inclination on industry management techniques. This research was also a project under the energy pipelines cooperative research centre as a collaboration between industry and university, with various publications and industry reports produced as a result of the work.

The phenomenon of inclined SCC is investigated primarily through the use of simulations along with some supporting experiments. A survey of the literature is first conducted to identify possible mechanisms that could cause inclined SCC. The simulations developed then have the aim of first testing those mechanisms for feasibility with a developed crack path model validated with existing field data, and then clarifying the effect of that mechanism on SCC crack growth rates and interaction.

Key results include that the likely mechanism governing SCC inclination is crack-tip strain enhanced electrochemistry, where the highly strained areas around the crack tip cause an increase in current density and hence dissolution rate. Another result is that growth rates of inclined SCC should always be slower than straight SCC to a depth of approximately 1mm for the surveyed cases, but that the growth rates could be higher after the first 1 mm depth of growth depending on the degree to which current density is affected by strain. Lastly, existing SCC interaction guidelines were shown to still be valid for inclined SCC in the conditions reported in prior studies on SCC colonies from Australia and Canada. The simulations on inclined SCC interaction were also extended to consider conditions outside of those reported in prior studies to demonstrate the regions where existing interaction guidelines would be at risk of being unconservative.

The findings of this thesis not only add to the literature of SCC research with various publications, but also could be made use of with the real world applications of pipeline SCC management and pipeline manufacture to control inclination, as has been documented in various reports to industry.

Future work which could benefit the knowledge gained from this work is also suggested. In particular, some experiments are suggested which could provide further information as to the sensitivity of crack inclination to the material, electrochemistry, and loading conditions.

Acknowledgements

It seems so unjust that a PhD is awarded to just one person when so many people have an influence on the result through either professional or personal support throughout. Those people will have to settle for the brief mention here.

Firstly, I'd like to convey my sincerest gratitude to my primary adviser Dr. Erwin Gamboa for his support of my PhD study. The lessons both in corrosion and life will stay with me forever. I hope you have a great life in Canada.

Besides Erwin I'd also like to thank A/Prof. Andrei Kotousov for his assistance whenever I've come with a difficult question, and for stepping in as primary supervisor at the end. Your speedy work in providing informative feedback is greatly appreciated.

My sincere thanks also goes to thank those from the EPCRC who have provided not only the funding and their time but also integral pieces of knowledge to help me wrap my head around the world of pipelines. Prof. Valerie Linton, Geoff Callar, Craig Clarke, Craig Bonnar, Colin Beasley, Dr. Daniel Fabijanic, Dr. Ivi Cicak and Dr. Michael Law, your input and advice has been invaluable.

I also need to show my appreciation to those others at university who have helped me technically throughout. Dr. Olivier Lavigne has always been able to help when I have questions about some experiments or need a paper to be checked. He has been like another supervisor to me, for which I am grateful. Dr. John Codrington has also provided an irresponsible amount of help with bug-checking my terrible ANSYS codes and training with the precious Instron machines. Thankfully his quotes were not the only knowledge he instilled upon me. Lastly the soon to be Dr. Rahim Kurji gave me the opportunity to collaborate and learn ANSYS at the same time in my first year of study by introducing me to the terrors of simulating welding. I'll never forgive you.

It would be remiss for me to not also acknowledge all my friends and family who've not only sat through my explanations of stress corrosion cracking without looking too bored. They've also continued to provide love and support despite my decision to pursue higher education. Your emotional support has helped me stay focussed to get to this point that I never dreamed I would be at even months ago. You all know who you are. I love all of you.

Lastly, I need to thank you. You who are reading this. The work I've done is for nothing if noone ever reads it, and the fact that you have even gotten this far fills me with joy. I wish you good luck in your journey through this thesis.

This work was funded by the Energy Pipelines CRC, supported through the Australian Government's Cooperative Research Centres Program. The cash and in-kind support from the APGA RSC is gratefully acknowledged.

Contents

List of Figures

List of Tables

Abbreviations

AR	**A**spect **R**atio
CEPA	**C**anadian **E**nergy **P**ipeline **A**ssociation
CT	**C**ompact **T**ension
EBSD	**E**lectron **B**ack**s**catter **D**iffraction
E-FEM	**E**nriched **F**inite **E**lement **M**ethod
FEA	**F**inite **E**lement **A**nalysis
FEM	**F**inite **E**lement **M**ethod
ILI	**I**n-**L**ine **I**nspection
L/D	**L**ength to **D**epth Ratio
PDF	**P**robability **D**ensity **F**unction
PDS-FEM	**P**article **D**iscretization **S**cheme **F**inite **E**lement **M**ethod
SCC	**S**tress **C**orrosion **C**racking
SCE	**S**aturated **C**alomel **E**lectrode
SHE	**S**tandard **H**ydrogen **E**lectrode
SMYS	**S**pecified **M**inimum **Y**ield **S**trengh
X-FEM	E**x**tended **F**inite **E**lement **M**ethod

Physical Constants

Faraday's Constant	F	=	96490 C mol^{-1}
Rice's Coefficient	β	=	5.08

Symbols

a	crack depth or half crack surface length depending on context	m
$\dot{a}$	crack growth rate	m s^{-1}
$\dot{a}_e$	crack growth rate without fatigue effects	m s^{-1}
$\dot{a}_f$	crack growth rate with fatigue effects	m s^{-1}
$\bar{C}$	vector containing crack path coordinates in simulation	-
c_1	depth of straight section	m
c_2	radial depth of inclined section	m
d_1	axial centreline offset of two adjacent parallel surface cracks	m
d_2	half hoop offset if two adjacent parallel surface cracks	m
E	elastic modulus	Pa
F_i	mode i shape factor	-
F_I	mode I shape factor	-
F_{II}	mode II shape factor	-
F_n	current density ratio for inclined angles	-
i_a	crack tip peak current density	A m^{-2}
J	J integral	J m^{-2}
J_0	J integral for straight crack of equal depth to inclined crack	J m^{-2}
J_{crit}	critical J integral for inclination	J m^{-2}
K_i	mode i stress intensity factor	Pa $\sqrt{m}$
K_I	mode I stress intensity factor	$Pa\sqrt{m}$
K_{II}	mode II stress intensity factor	$Pa\sqrt{m}$
K_{ISCC}	critical stress intensity factor for SCC in X65	$Pa\sqrt{m}$
K_M	mean stress intensity factor in a cycle	$Pa\sqrt{m}$

L_i	surface length of a crack i	m
M	molar mass of iron	kg/mol
M_w	molecular weight of a given metal	kg
n	repassivation kinetic exponent	-
N	strain hardening exponent	-
Q_F	charge passed between two film ruptures	C
r	distance from crack tip	m
r_0	specific length for crack tip strain rate calculation	m
t_0	incubation time for repassivation	s
x	specific coordinate along the modelled microstructure field width	mm
X	modelled microstructure field width	mm
y	specific coordinate along the modelled microstructure field depth	mm
Y	modelled microstructure field depth	mm
z	valence	-

α	surface interaction angle	degrees
$\dot{\epsilon}_{ct}$	strain rate	s^{-1}
ϵ_F	rupture ductility of passive film	-
θ	inclination angle	degrees
ν	Poisson's ratio	-
ρ	density	kg/m^3
σ	stress	Pa
σ_Y	yield strength	Pa

Publications from this work

1. Griggs, J., Gamboa, E. and Lavigne, O. (2016), A review of modelling high pH stress corrosion cracking of high pressure gas pipelines. Materials and Corrosion, 67: 251-263. DOI:10.1002/maco.201508454

2. Griggs, J., Gamboa, E. and Lavigne, O. (2016), 2D modelling of inclined intergranular stress corrosion crack paths. Fatigue and Fracture of Engineering Materials, DOI:10.1111/ffe.12514.

3. Lavigne O, Gamboa E, Griggs J, Luzin V, Law M, Roccisano A (2016). High-pH inclined stress corrosion cracking in Australian and Canadian gas pipeline X65 steels. Materials Science and Technology, 32: 684-690, DOI: 10.1080/02670836.2015.1132030

4. Griggs, J., Lavigne, O. and Gamboa, E. (2016), Influence of strain on current densities and its effects on stress corrosion cracking growth rates in X65 pipeline steel. Corrosion, Accepted for publication 11/10/2016.

5. Griggs, J., Lavigne, O. and Gamboa, E. (2016), Modelling 3D interaction limits of inclined stress corrosion cracking. EUROCORR 2016, 11–15 September 2016, Montpellier, France.

Copies of all publications presented in Appendix B

For my family.

Chapter 1

Introduction

Stress corrosion cracking (SCC) is a type of environmentally assisted cracking that can occur with the combined presence of sufficient stresses, an aggressive environment and a susceptible material. One such case in which SCC can occur is on the outer surface of buried pipelines, which has been observed since the 1960s [1]. The majority of SCC research prior to the year 2000 found that the cross section of stress corrosion cracks presents either as perpendicular to the outer surface or highly branched depending on the pH of the environment [2–10]. As such, industry guidelines for managing SCC on pipeline steels are developed with the assumption that the crack is either straight or branched [11].

Recently, this theory has become incomplete in describing SCC in pipeline steels, with X65 pipelines in Canada and Australia presenting with SCC that instead grows at an angle of between 30 and 50 degrees from the perpendicular [12–14]. This is known as inclined SCC, and an example crack shape is shown in Figure 1.1.

Inclined SCC raises various problems. The cause of the inclination is unknown, as is the potential impact of inclined SCC on the industry used guidelines. If these unknowns could be better understood, then industry would have more confidence in assessing pipes which display inclined SCC. Additionally new pipe designs may be able to avoid or encourage inclined SCC crack paths depending on whether or not it is preferential to straight SCC with regards to crack interaction and crack growth rates.

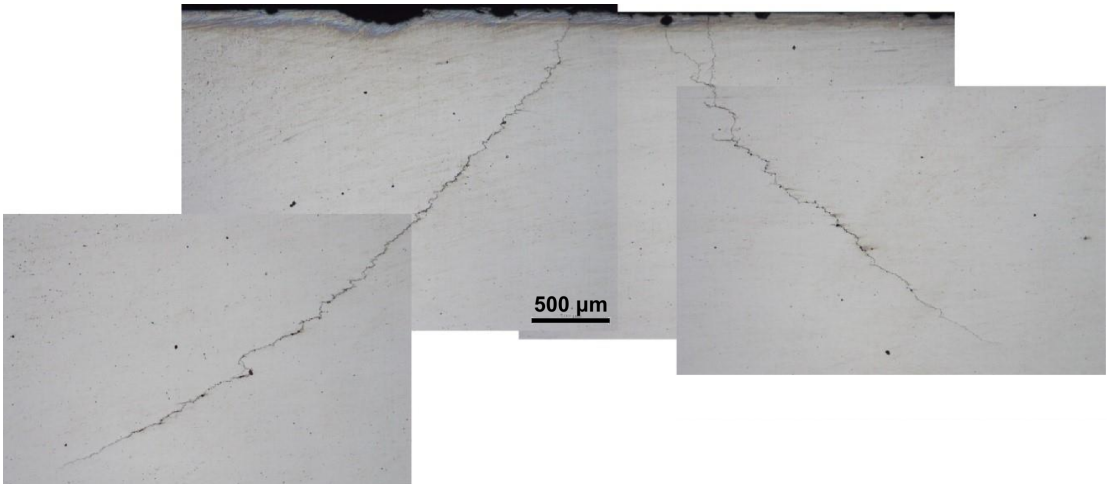

FIGURE 1.1: 2D cross section of two inclined SCC cracks in Australian X65 pipe transverse to pipe main axis [15].

The problem of the lack of understanding of inclined SCC is addressed in this thesis through the development of mechanistic hypotheses to describe the inclination, creation of a mathematical model to evaluate these hypotheses, then the development of further models which evaluate the impact of inclination on industry SCC management guidelines. The first step toward building an understanding of this new phenomenon is to analyse the existing SCC theory and SCC industry management techniques.

SCC of pipeline steels can refer to either high pH SCC or near neutral SCC. Traditional theory suggests high pH SCC produces straight intergranular crack paths, while near neutral SCC typically presents with branched crack paths and transgranular growth [5]. High pH or intergranular SCC is of interest in this research, as these are also the conditions that are seen for inclined SCC.

The life cycle of high pH SCC can begin when a defect in the coating of the pipe surface allows for contact between corrosive media and the outer steel surface. This can cause crevice corrosion and pitting on the steel surface. These pits act as stress concentrators which can allow cracks to initiate [8].

The initiated cracks propagate through a dual mechanism. Anodic dissolution dissolves the material along the grain boundaries ahead of the crack, while passive film formation on the crack walls and front act to prevent this dissolution [8]. The applied stresses then can fracture the passive film which allows dissolution to resume. This cycle allows the crack to grow at stresses below those that would reach the fracture toughness of the steel since the film has a lower fracture toughness than the steel (critical stress intensity factor for SCC is of the order of 20 MPa$\sqrt{mm}$ with fracture toughness in the order of 50 MPa$\sqrt{mm}$) [2, 16].

The film fracture typically governs the growth direction. The film will fracture in the direction perpendicular to the highest stress (Figure 1.2), which in pipeline scenarios (away from welds, bends and other stress field altering features) is the hoop stress [8, 17]. This causes high pH SCC to appear axially oriented on the surface, with an axial-radial subsurface growth plane. Usually SCC presents in a colony (Figure 1.3), with many pits allowing multiple cracks to initiate near to

one another. These cracks will grow both along the surface and into the steel until its stress field intersects with that of another crack [18]. This interaction can cause either shielding or acceleration depending on the relative positions of the cracks [19]. Should the cracks accelerate each other, they will most likely coalesce and combine to form one larger crack. This process continues and multiple cracks coalescing start to form longer and deeper cracks. If left unmanaged, these long and deep cracks can then grow deep enough for the pipe to fail through fast fracture.

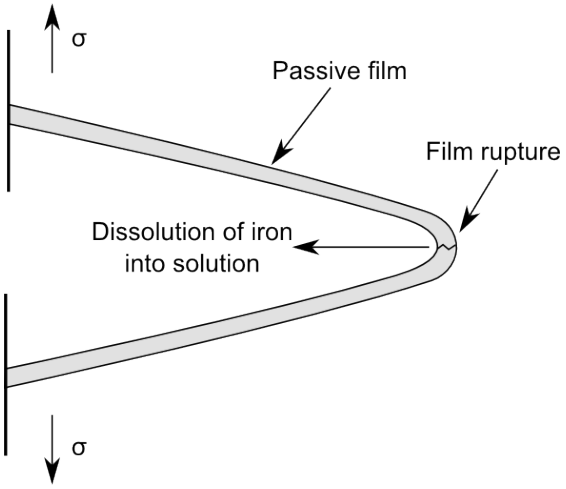

FIGURE 1.2: 2D schematic of film rupture perpendicular to the highest stresses and subsequent dissolution of the bare metal into the solution.

FIGURE 1.3: Surface view of an SCC colony with axial direction from left to right [14].

Industry management techniques have been developed to predict where SCC will occur and prevent these cracks from causing failures. Ground surveys combined with predictive models can identify the high risk areas for SCC before it has initiated. Once SCC colonies have initiated, they can be detected with in-line inspection (ILI). ILI returns data of crack locations down the pipe length. The locations with the deepest cracks can then be assigned for field inspection, which involves exposing the pipe surface and applying high contrast paint and magnetic particles to visualise the SCC colony. The colony can then be assessed to determine which is the longest potential crack using interaction limit guidelines [11]. This could then be used as an input into historical data trends or crack growth rate predictive models [20, 21] to determine the duration of time allowed before either a new inspection should be conducted, or whether a repair is necessary.

These management techniques are based on theory that assumes a straight crack path [11, 19], which means that the tortuous crack paths seen in inclined SCC (Figure 1.1) could potentially fall outside of the predictions of the existing tools. Inclined SCC appears the same as straight SCC on the surface of the pipe, however it differs through the thickness [12–14, 22]. Inclined SCC begins with a through thickness straight section of approximately 0.55 mm depth before gradually inclining to an angle of 30-50 degrees from the axial-radial plane [14, 22]. This is not predicted by the existing theory, as the film fracture perpendicular to the hoop stress should encourage the cracks to grow in the axial-radial plane. Metallographic studies of inclined SCC show the same intergranular growth of high pH SCC, along with passive film on the crack faces [12, 14]. Both Canadian and

Australian X65 pipeline steels have shown inclined SCC, but the full global extent is unknown due to the rarity and cost of reviewing the subsurface crack path.

The studies to date on inclined SCC have postulated various reasons for the inclination, however there has been no clear case for the cause of the inclination. Additionally the extent of the impact on interaction limits and growth rates is unknown. This presents the gap for this research, with the aim being to identify the mechanism behind inclined SCC and determine the impact on industry used interaction limits and growth rate predictions. Simulations are developed with test various possible causes for the inclination, with strain enhanced electrochemistry being the most promising, and to test the effects on growth rates and interaction. Some experiments are also conducted to confirm the mechanism, and to provide inputs to the model where existing theory is insufficient.

This thesis will first cover a review of the literature in Chapter 2. This review will provide some background on the theory of SCC, present the gaps related to inclined SCC, identify possible mechanisms that could cause the inclination and examine previous models in various fields for methodologies that are applicable to an inclined SCC model. Following the review, the aims, objectives and scope are presented in Chapter 3. Chapter 3 also states the research aim of developing an understanding of the mechanism behind inclined SCC, and using that understanding to assess industry growth rate and interaction guidelines. Chapters 4-6 discuss the methodology behind the three models built to answer the three main objectives, as well as presenting and discussing the key results from those models. The methodology is combined in these chapters rather than in its own separate

chapter as the methods used to develop the three models are specialised with little overlap. Finally, a summary of the work is given in Chapter 7. Chapter 7 also summaries the importance of the results for practical application by identifying the implications for industry, along with suggestions for future research directions.

Chapter 2

Literature review

2.1 Introduction

High pH stress corrosion cracking (SCC) of high pressure gas pipelines usually presents in the axial-radial plane, and various management techniques are available to industry. However, recently SCC cracks have been seen to instead incline away from the perpendicular and grow at an angle of between 30 and 50 degrees from the axial-radial plane. The reason for this inclination is unknown, as is the impact on industry assessment techniques of growth rates and crack interaction limits. There is a need for new understanding that can identify the mechanism behind the growth of inclined SCC, whether that growth could be faster than straight SCC and whether the inclination can lead to interaction that would not be predicted with existing methods. In this chapter, a review of the existing SCC theory, inclined SCC studies and the proposed theories behind the inclination is conducted. Following this, a range of models are investigated to identify the various modelling

methods that would be appropriate to fill the gaps in knowledge that surround inclined SCC. The review focus on high pH SCC of high pressure gas pipelines, with some knowledge gained from allied fields of research when pipeline specific research is lacking.

2.2 Classical SCC background

High pH SCC of gas pipelines occurs on the outer surface of the pipelines with the the combined presence of sufficient stresses and a susceptible material-environment pair [2]. Each of these elements is required for SCC propagation to occur, with the environment-metal pair resulting in dissolution along the crack front and the stresses resulting in the fracture of the passive oxide layer that inhibits dissolution. When viewed from the outer surface, pipeline SCC usually presents as many axially oriented cracks in a colony, perpendicular to the hoop stress; however proximity to welds or notches can change the stress field and lead to cracks with different orientations [23]. The traditional view of a crack growth cycle is presented below and has been covered extensively by numerous other authors [2, 5, 6, 8, 9, 17, 23, 24].

Initiation of high pH SCC in pipelines usually occurs under a defect in the coating, where the some of the cathodic protection is accessible in the potential range of stress corrosion cracking. Pitting can then occur on the surface and the cracks can initiate at these stress concentrators [5].

Once the crack is initiated, growth continues intergranularly via a combination of anodic dissolution and film cleavage [2, 5]. Anodic dissolution acts to dissolve the bonds between adjacent grains into the solution. The speed of propagation has a ceiling of the Faradaic limit determined experimentally of approximately 10^{-6} mm/s [8]. Growth in the field rarely reaches this limit though, as the propagation is rate limited by passive film fracture [8, 17]. The electrochemical conditions at the tip of the crack are usually conducive to both dissolution and passive film formation. This passive film prevents further dissolution and advancement of the crack front. The film is brittle and much weaker than the base metal and can break through either creep or fatigue, depending on the loading pattern [17]. The crack can then advance a small amount through dissolution, as well as some penetration into the base metal from the fracture of the film. Overall, this results in fairly slow growth rates in the order of $2 \cdot 10^{-8}$ mm/s for individual cracks [8].

Cracks can start to grow with a faster crack tip velocity once the colony develops and coalescence begins. The coalescence of neighbouring cracks can cause both temporary dormancy of some cracks due to stress shielding, and coalescence with crack acceleration depending on the relative position of the cracks [25]. Cracks that are configured favourably relative to each other begin to link up, causing a much longer crack with greater stress concentration. The increased stresses and strains at the crack tip cause the time between brittle fractures to reduce resulting in an increase in crack tip velocity [18]. Failure occurs rapidly once the cracks reach a depth and length such that the fracture toughness of the material is exceeded by the mechanical stresses alone, with inspections of the final fracture surface often

showing no corrosive damage in the overload region [4].

The aforementioned growth cycle revolves around the rate limiting film fracture [8, 20, 26]. The cracks grow perpendicular to the outer surface of the pipe as this fracture will occur perpendicular to the principle stress, which is usually dominated by the applied hoop stress. A change in direction of the cracks is evidence of either a shift in the mechanism, or a change in the stress field due to interaction, welds or other stress concentrators. Within the last decade, examples of significant deviations from straight crack growth have been seen in both Canada and Australia [12, 13, 15, 22, 27], with the full global impact unknown due to the inconvenience of sample extraction when repairing SCC colonies in the field resulting in few reports of SCC growth direction.

In pipelines where high pH SCC is present, various prevention and subsequently management techniques must be taken to ensure safe operation of the asset. Techniques for prevention include applying coatings to the outer surface of the pipe and application of cathodic protection to prevent SCC initiation. However, there may at some points be a defect in the coating or damage to the coating that allows contact between the corrosive media and the steel, while also shielding the cathodic protection [2]. If a pipe and its coating have shown to be susceptible to SCC initiation, then prediction of where the pipe is most likely to experience SCC as well as management is critical.

Prediction of the location of SCC is possible with the results of soil surveys and knowledge of the temperature profiles of the pipe. Higher temperatures and different soil chemistries can increase the rate at which SCC grows, and the likelihood of

it occurring [2, 8, 20]. Proximity to compressor stations is one of the principle factors which influence temperature, and areas nearer to the stations are considered at a higher risk for SCC [2].

Prediction alone is insufficient to find a SCC colony however, as there are many kilometers of buried pipeline that cannot easily be manually inspected for small cracks. In-line inspection (ILI) is the method commonly used to detect areas where SCC may be present. SCC detecting ILI involves sending a unit through the centre of the pipeline, and using non-destructive techniques such as ultrasonics to determine areas with SCC [28]. Different locations on the pipeline can then be prioritised based on the length and depth of cracks found for urgency of visual inspection. The data from ILI can also be used to empirically approximate growth rates of SCC in the pipeline based on extrapolation of the measured crack depths. Although some models have been produced which can predict growth rates where empirical data is unavailable [20, 21]

Visual inspection in accordance with the Canadian Energy Pipeline Association (CEPA) SCC guidelines [11] involves exposing the buried pipeline at the point of interest, performing a number of cleaning techniques and spraying the pipe with magnetic paint which allows easier visualisation of the cracks [11]. The cracks are then inspected for potential interaction, with two cracks considered interacting if their hoop and axial spacing is within 14% and 25% respectively of their average lengths. Depending on the severity of the findings, the section will be scheduled for repair or reinspection at a date determined with the assistance of empirical growth rate predictions [20].

While management techniques are well established, their scientific basis is founded on the assumption that SCC will grow entirely within the axial-radial plane [6, 8, 10]. This has been shown to not always be the case in recent years, with X65 pipelines in Australia and Canada showing SCC that instead grows at an angle to the perpendicular [12, 13, 22, 27, 29]. This means that the empirical data from previous pipes with straight SCC, crack growth rate predictive models that assume straight SCC, and interaction rules that assume straight SCC could all be invalid for the inclined case.

2.3 Inclined SCC background

Inclined SCC occurs when an SCC crack diverts from a crack path perpendicular to the surface and instead follows a new trajectory that is offset by a varying angle, often in the range of 30–60 degrees. It has been documented in both Australian [22] and Canadian [12, 13] pipelines since 2004. Figure 2.1 shows the three cross sectional shapes of SCC found from a Canadian study [13]. These studies documented cracks in high pressure gas pipelines that were inclined (Figure 2.1c), as well as some that were straight (Figure 2.1a). This occurrence has only been documented to date in X65 steels (0.085% C, 0.33% Si, 1.58% Mn, 0.0045% S, 0.054% Nb, 0.022% P [29]). Other occurrences of cracks growing in unusual directions have been observed in stainless steels in high temperature water [30–32], though these cases usually present simultaneously with branching, providing some

mechanical explanation. The inclined SCC phenomenon could have some implications for both growth rates of individual cracks, as well as interaction zone limits for multiple cracks.

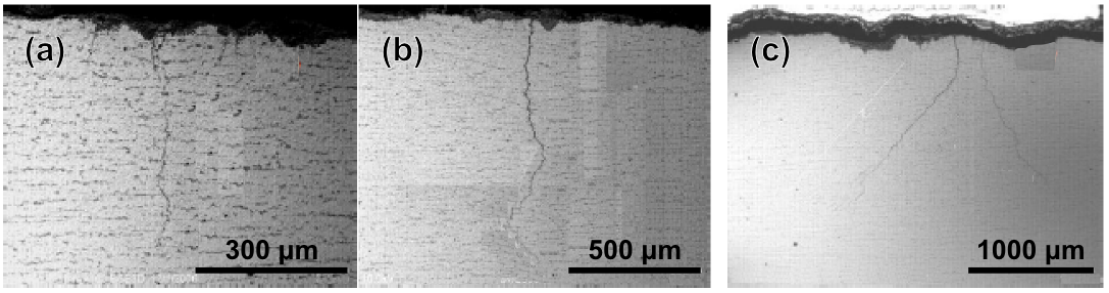

FIGURE 2.1: Three categories of SCC documented by Xie et al. [13]: (a) straight, (b) zig-zag and (c) inclined.

The first study into inclined SCC by Sutherby and Weixing [12] showed inclined SCC that grew perpendicular to the outer surface for 1.5 mm or less, before inclining at an angle of 30 to 60 degrees. They found that the entire crack was intergranular, both before and after inclination, and the shape of the crack front was not semi-elliptical as is usually observed for SCC. They also determined that the crack inclination angle was generally proportional to the crack length and postulated that the crack does not incline at any one point, rather undergoing a slow turning process. Most of the cracks they showed supported this hypothesis (Figure 2.2a: a slowly curving crack), although there were some exceptions (Figure 2.2b: sharp kinks in a zig-zag pattern). Sutherby and Weixing [12] also proposed a 3D schematic sketch of an inclined crack, Figure 2.3a, which rather than showing a semi-elliptical crack with a bend in the middle, shows the crack post-inclination behaving more like a centre crack, with the cross sectional chord peaking in the middle. Tomographical work performed later by Lavigne et al. [27] and Gamboa et al. [15] showed that the shapes are in fact far more complex due

to the interaction intrinsic to SCC, and cannot simply be approximated as semi-elliptical. Figure 2.3b shows that the cracks can appear semi-elliptical, as in the light blue crack, but also have steeper edges and a more rectangular shape, such as the dark blue crack. This presents the possibility that the inclined SCC could also be deeper and longer below the surface than would be expected from surface inspection alone. Sutherby and Weixing [12] theorised that the crack inclination was caused by microstructural variance through the wall thickness that was itself caused during manufacture. This hypothesis was reinforced by their presentation of SEM images of the microstructure both at the surface and half way through the thickness, which showed banding as the depth increased. A hardened surface was also observed in the first 1.5 mm of pipe thickness, consistent with surface hardening techniques, which is the similar to the length of the perpendicular section of growth in these specimen.

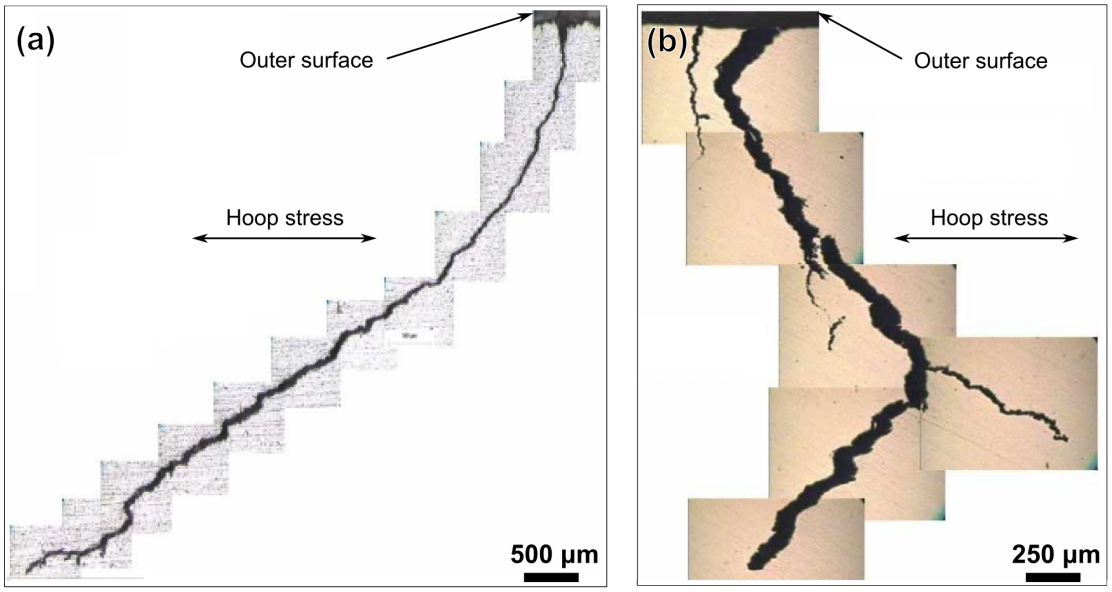

FIGURE 2.2: Some of the cracks surveyed by Sutherby and Weixing [12], (a) smooth curve, (b) sharper kinks.

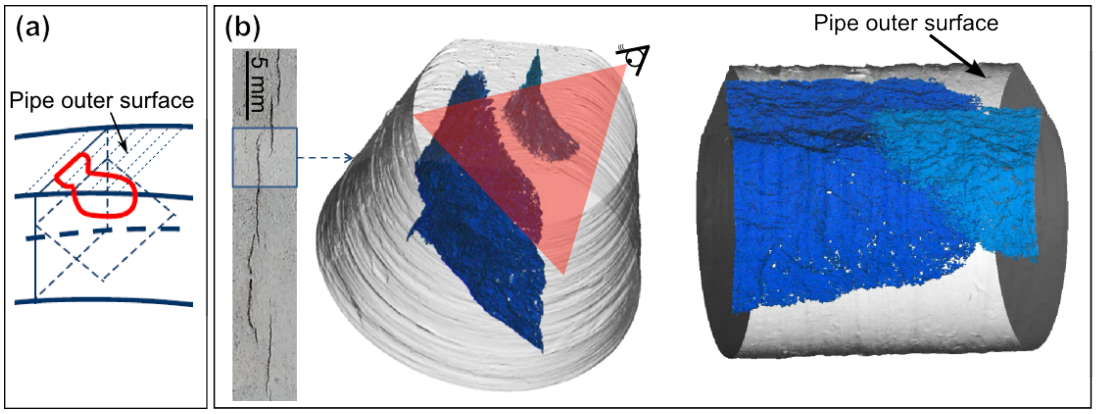

FIGURE 2.3: (a) Sketch of the 3D profile of an inclined crack [12]. (b) 3D tomography of an inclined crack in an Australian SCC colony, adapted from Gamboa et al. [15].

A follow up study was performed by Xie et al. [13]. Xie found that the cracks generally inclined in the range of 0.2–0.6 mm from the surface, with an inclination angle of 30–50 degrees, with more than 50% of all cracks with a straight depth of 0.2 mm or more being inclined. The cracks Xie examined generally showed sharp kinking, as previously shown in Figure 2.1b, but they also presented some cracks which curved rather than kinked, similar to the findings of Sutherby and Weixing [12]. Banding of the microstructure was also found, however no significant change in the banding was observed where the crack inclined. Contrary to Sutherby's findings, no significant change in hardness was present in the inclination zone and this result was also supported by Zadow [14] in the Australian case. Xie's [13] mechanistic analysis prompted the hypothesis, contrary to Sutherby and Weixing's proposals, that a combination of residual stresses and some abnormal corrosion were the causes of the inclination.

Zadow et al. [22] conducted a survey of a section of pipe from an Australian pipeline. They found that the straight section of significant cracks was between

0.2–0.9 mm, while the angle was between 30–60 degrees, with deeper cracks generally having a larger angle. 81% of significant cracks showed some inclination. 32% of all cracks analysed had some crack interaction occurring and 44% of those cracks had inclined and coalesced within the pipe thickness, but not necessarily on the surface [14]. Cracks showed both kinking and gradual curving towards the final inclination angle, as is seen in Figure 2.4. The authors ascertained that the longitudinal subsurface travel may be significant, however other work involving tomography is required to confirm this. While none of the interactions breached the guidelines for crack interaction provided by CEPA, Zadow et al. [22] suggest more work is required to quantify how conservative are the guidelines.

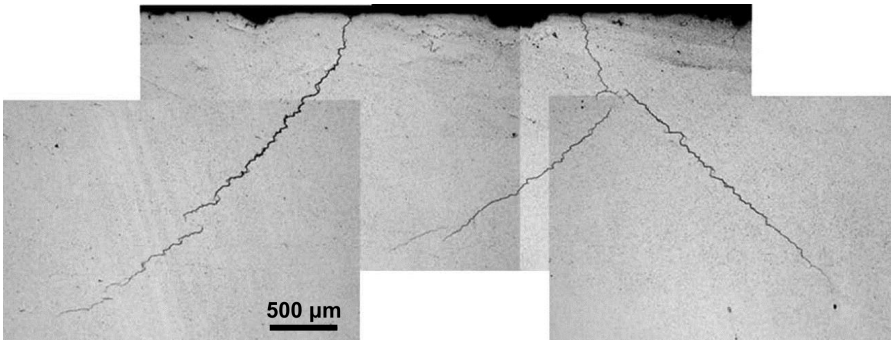

FIGURE 2.4: 2D cross section of inclined SCC in Australian X65 pipe, with curving seen on the left and kink-like branching on the right [22].

The studies to date on inclined SCC seem to imply that some of the influencing factors of inclined SCC could be fracture mechanics based (crack interaction or other stress field altering circumstances), microstructural variance (texture or residual strain), or other unspecified electrochemical mechanisms. One such mechanism could be a preference towards dissolution or heterogeneous film formation at areas of high strain, as seen by Tang and Cheng [33], Yaguchi and Yonezawa [30] and Lavigne et al. [27] which could explain the angular deviation. These ideas

should be explored further to gain an idea as to which is the most likely cause for the inclination.

2.4 Current hypotheses for SCC inclination

The cause behind inclined SCC is unknown, as are the suitability of the management techniques used by industry. This section will examine the postulated reasons for the inclination proposed in the previous section, being fracture mechanics, microstructural variance, or an electrochemical mechanistic change. Once the suitable reason for the inclination is identified, the remaining sections will address the methods of evaluating the suitability of the management techniques.

2.4.1 Mechanical hypotheses

Straight SCC is rate limited by passive film rupture, and this rupture is also understood to govern the crack path [8, 34]. Fracture mechanics can be used to predict in which direction the film will fracture, and this theory will be examined for the requirements for inclination to occur. Additionally, studies into kinked cracks in the literature can be investigated for the equations that govern crack kinking. The possible reasons can then be explored for their applicability to the case of inclined SCC.

The stress intensity factor is a parameter used to quantify the stress singularity around a crack tip. The general equation for a stress intensity factor is shown in

Equation 2.1, where K_i is the stress intensity factor, F_i is a constant dependant on crack geometry and loading conditions, with the subscript i referring to the mode of fracture. σ is the nominal stress for the cross section, and a is the crack length [35].

$$K_i = F_i \sigma \sqrt{\pi a} \tag{2.1}$$

The stress intensity factor can then be related to the local stress field, and is proportional to $r^{-0.5}$ where r is the distance of a stress element from the crack tip. This describes the singularity at the crack tip, clearly as r tends to 0, local stress tends to infinity [36]. This relationship provides a continuity in the stress field, and would imply that if crack curving were to occur, it would occur slowly rather than a sharp kink. This may not always be the case however as SCC cracks grow in steps, often going in and out of dormancy [6], and the stress field can vary significantly from one time to another.

There are three types stress intensity factor which describe the different modes of fracture. The opening mode, the sliding mode, and the tearing mode, often abbreviated to modes I, II and III, provide the three degrees of freedom necessary to describe both opening, and shear in two planes. Various theories have been developed which can describe the crack growth path under the presence of varied loading conditions, however under purely mode I loading, the results are identical. The theory of local symmetry, first proposed by Goldstein and Salganik [37], is based around these three stress intensity factors. It dictates that a crack will tend

to the path that results in only mode I fracture, with the resultant lack of mode II and III indicative of the symmetry. If this condition of local symmetry were to be met for inclined cracks, the maximum stress intensity factor must be at an angle, and some mode II stress must be present, either from mixed mode loading or interaction with other features.

Various studies have used fracture mechanics theories to develop models which can describe curved and kinked crack growth, such as Cotterell and Rice [38]. Cotterell and Rice developed methods of calculating stress intensity factors of kinked cracks with a kink length approaching to zero, and also a crack path prediction method based on these stress intensity factors, in combination with the theory of local symmetry. Since then others have expanded on the criteria [39, 40], and many have calculated stress intensity factors for combinations of kinked, zigzag, and slant cracks [41–43]. An important result stemming from a finite element model of Bechtle et al. [43] is a kinked crack with a projected kink length of at least 15% of the total projected crack length results in the same stress intensity factor as for a slant crack of equal projected length. This provides an easier source of verification, as stress intensity factors for slant cracks are relatively simple to calculate.

While the studies mentioned above provide stress intensity factors for kinked or slant cracks, the resultant stress intensity factor in response to pure mode I loading (hoop stress) is still perpendicular growth. In pipelines, mixed mode stresses will not be applied in normal operation due to the pipe being a pressure vessel. Interaction with other features such as cracks, welds or defects could cause the mixed mode loading required. None of these seem to fit however, as the survey

performed by Zadow et al. [22] shows crack inclination away from other cracks and welds for extended periods where defects would not have such an effect.

The conditions surrounding inclined SCC seem to imply that the fracture mechanics of the film fracture cannot account for frequent and consistent inclination of the cracks over long distances. This suggests that film fracture may not be entirely governing the crack path, as the fracture should still occur in the direction of highest stress if the film is equally strong at all angles. One possible explanation is that the film is not homogeneous around the crack tip or weaker at some angles about the crack tip, which could explain the fracture through the energy method, where the energy required for fracture is lower at some angles due to heterogeneity [44–46]. It can be concluded that some electrochemical effect could be weakening the film along the inclination angles if film rupture is to still govern the crack path. Alternatively, the film could still fracture in the direction of the highest stress intensity factor, but other electrochemical effects could cause a greater degree of dissolution along the inclination angles.

2.4.2 Microstructural effects for inclination

Various microstructural reasons have been proposed as a cause of the inclination. Among these are directional residual strains, textural effects and defects such as vacancies. There exists reasonable data on the microstructure of the inclined affected pipe [27, 29]. This allows analysis of these reasons to be quantitative and simple.

Residual stress/strain effects have been proposed as a potential cause of the inclination, possibly induced during rolling of the steel. Due to the cracks having a propensity to incline in either the clockwise or counter-clockwise direction, the effects of residual stress and strain would need to be present in a symmetrical fashion, which would also somewhat enhance the growth of straight cracks. Zadow et al. [22] found some strain patterns around the crack paths of existing inclined cracks, however these were likely caused by the growth of the crack itself. Zadow et al. [22] also found some shear residual strains that appear to be preferentially located around boundaries located perpendicular to the radial direction, which could encourage growth in that direction. No significant change was seen at the 0.55 mm depth where the cracks begin to incline, leading this to possibly be a contributing factor, but not the governing mechanism.

Texture has also been postulated as an influencing factor behind inclined SCC. A link between SCC susceptibility and crystallographic texture is already identified in literature [47–49]. High angle boundaries have been shown to be more susceptible to SCC, while low angle boundaries and other special boundaries have been shown to be resistant to SCC [47–49]. Investigation by Lavigne et al. [29] has found that the inclined SCC affected pipe has a lower density of texture that is resistant to SCC initiation than non-affected steel from the same pipeline, however no comparison to straight SCC affected pipe has been made. Additionally there is no data that shows a preference of high angle boundaries along the inclination angles, and further work still needs to be conducted to determine the influence of texture on crack path.

Lastly the cracks could incline if there existed long chains of vacancies or dislocations, or segregation. The crack could follow the higher stresses near these defects and incline. This is highly improbable however as the majority of cracks were inclined. This leaves residual strain and texture having a possible influence on the crack path, but still not likely to be the sole causes for the inclination.

2.4.3 Crack tip strain enhanced electrochemistry

As mentioned in Section 2.4.1, some electrochemical effect seems to be required along the inclination angles to explain the inclination. The angles that the cracks tend to follow align with the highest strain direction under the plane strain criterion [50]. Further evidence even exists of higher degrees of strain in the direction of kinking under mode I loading [51], which would explain the continued inclination in the same direction unless disturbed by interaction. This suggests that the crack tip strain may be influencing the electrochemistry and either weakening the film or enhancing the dissolution. This idea will be explored in the literature.

There is experimental evidence that supports the concept of the impact of electrochemical dependency on areas of high strain [52–59]. Not only does the strain result in an increase in current density, which is a driver of the dissolution rate in Faraday's law (Equation 5.1), but also a shift in the relative propensity for dissolution and filming at the crack tip potential, which could mean a change in the charge passed between film ruptures, which is a driver of Equation 2.3 and hence the crack growth rate. A plasticity dependant electrochemical response would result in different degrees of filming and dissolution at different angles (and grain

boundaries) around the crack tip and thus angular dependant SCC susceptibility, possibly explaining the inclined cracks discussed in Section 2.3. This has not been considered to a great extend in SCC before, as historically the film cleavage has been the rate limiting factor of the crack growth rate.

The electrochemical response of a metal in an environment can be described by its polarisation curve. The polarisation curve for a material in a given solution is often used for the design of preventative measures for corrosion in pipelines, but numerous studies have shown that the polarisation response shifts when the material is strained [52–56, 59]. The plastic strain causes an increase in the dislocation density in the material, which in turn provides higher diffusivity into the grain boundaries. This can cause a change in the effective current density (which is proportional to the dissolution rate) as well as the relative propensities for filming and dissolution.

The studies reviewed in this section have evaluated the effect of applying uniform plastic strain to a material and looking at the effect on the polarisation curves, with the exception of Yaguchi and Yonezawa [30]. This condition differs from that at the crack tip which is a non-uniform strain field, but the results should be transferable, especially with the evidence of Yaguchi and Yonezawa [30]. Some of the earliest work on this phenomenon was performed by Despic et al. [60], who demonstrated that the current density of iron in hydrochloric acid increased with strain fairly linearly until failure (Figure 2.5). Later, Wells et al. [53] performed some slow strain rate tests on 304 stainless steel in dilute thiosulphate

at different potentials in the cathodic range and documented the change in current density. Figure 2.6a shows some results from that study, including that the corrosion current varies strongly with the applied potential and goes through a maximum with the applied strain (aside from the most cathodic applied potential of -300mV SCE). It can be seen also that the current density increases with the potential in the cathodic direction (aside again from the -300mV SCE potential). Similar behaviour was observed for 316L stainless steel in $0.1Na_2SO_4 + 5\%H_2SO_4$ solution (Figure 2.6b) [61], that showed an increase of the current densities with the increase of the potential in the anodic direction and a maximum in the current with the applied strain.

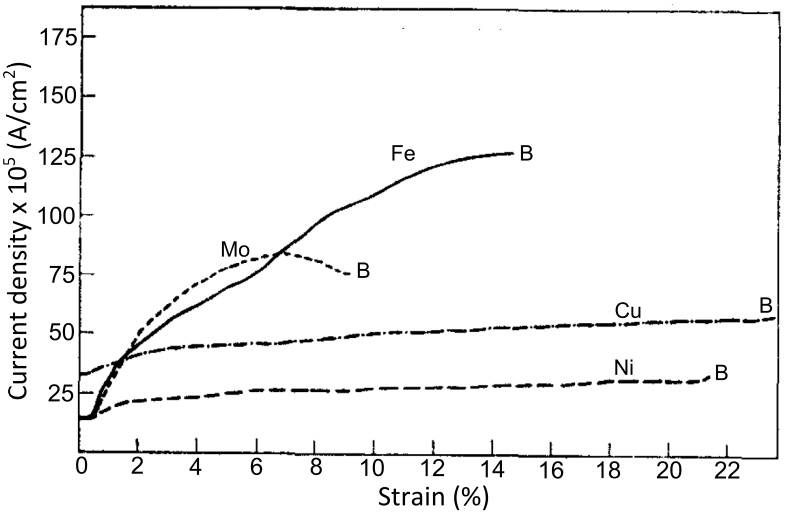

FIGURE 2.5: Current density variation with strain of iron, molybdenum, nickel, and copper in various solutions. B represents breaking point. [60].

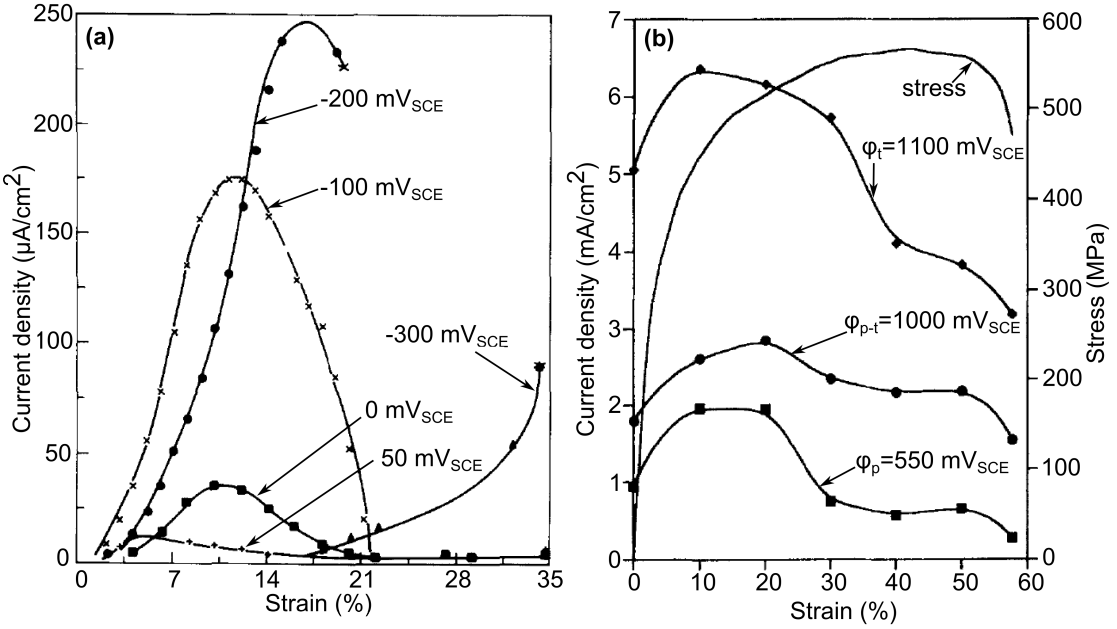

FIGURE 2.6: Current density variation with plastic strain of (a) type 304 austenitic stainless steel in $0.5MS_2O_3^{2-}$ for different levels of cathodic potential [53], and (b) type 316L stainless steel in $0.1Na_2SO_4$+5%H_2SO_4 for different levels of anodic potential (vs SCE) [61].

Sahal et al. [52] went further and looked at the potentiodynamic curves of pre-strained nickel in sulphuric acid (Figure 2.7). Figure 2.7a shows the different zones of the curve, where Section A is active dissolution, Section B is the transition zone comprising both filming and dissolution, Section C is the passive region and D is the film breakdown. Figure 2.7b shows that changing the strain shifts the active dissolution and transition zones negatively relative to the potential, as well as changing the peak current density. The results indicate that a small amount of strain increases the current density and further strain decreases it, although the current densities are still higher than the non-strained values. Some properties of the hardening of nickel could be the cause of this movement, as suggested by Sahal et al. [52], with nickel known for its strain hardening and elongation at failure. As such, the presence of dependency is applicable to pipeline steels, however the

shape could be different due to the different stress-strain properties of the metals. Further work conducted by this group has shown that a good correlation exists between dislocation distribution and current density [62].

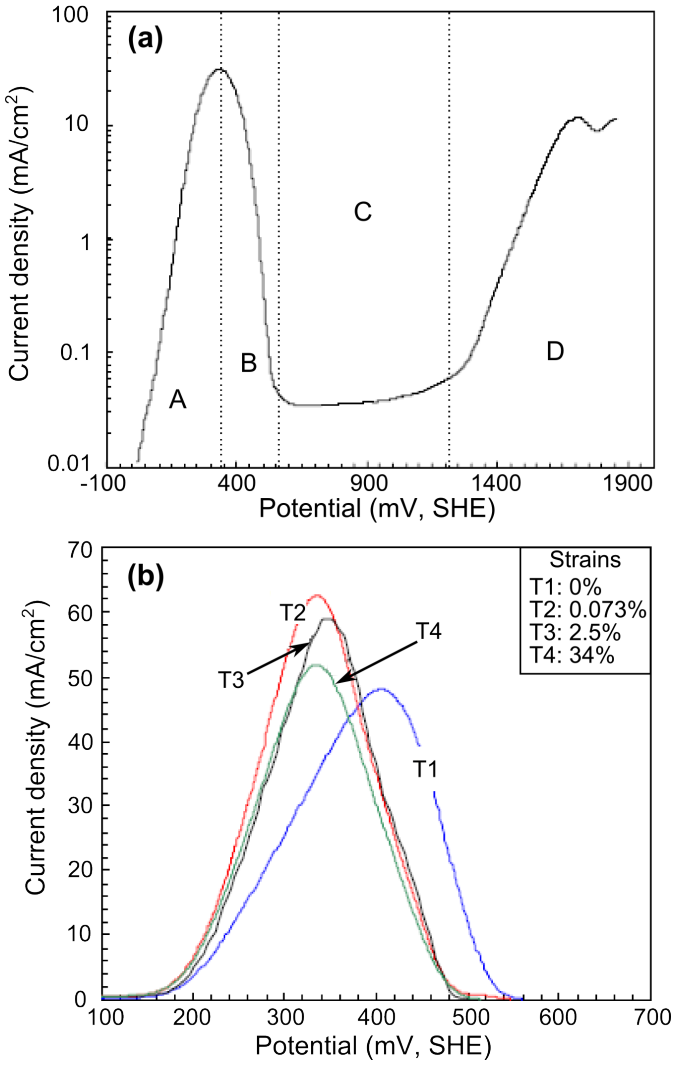

FIGURE 2.7: Effect of strain on potentiodynamic curves of nickel in H_2SO_4: (a) shows the various zones (A,B,C,D) of the curve, whilst (b) shows the current density against potential for different strains [52].

The effect of strain on the current density for X80 pipeline steel (0.055% C, 0.2002% Si, 1.3917% Mn, 0.0019% S, 0.0318% Cr, 0.2636% Ni, 0.0017% P, 0.0173% Al, 0.3184% Mo) in NaCl aqueous solution has been investigated by Wang et al.

[54] through potentiodynamic measurements (Figure 2.8a). The corrosion potential appears to become more negative when the steel is strained, with a maximal shift in potential for a strain value of 6 millistrain. The current densities tend also to increase with strain, with a maximum effect observed also at the strain of 6 millistrain. Increasing strain further shifts the polarisation curve towards the zero strain condition. At this specific strain of 6 millistrain, the corrosion current density shows a sharp increase, while above and below this value the corrosion current densities are relatively stable and low (Figure 2.8b). X80 is a higher grade of pipeline steel than the X65 on which this report focuses and has a slightly different composition. Thus, similar to the nickel results [52], the shape of the relationship between current density and strain may differ between X80 and X65, but studies done on this higher grade can still be of great interest for X65 pipes.

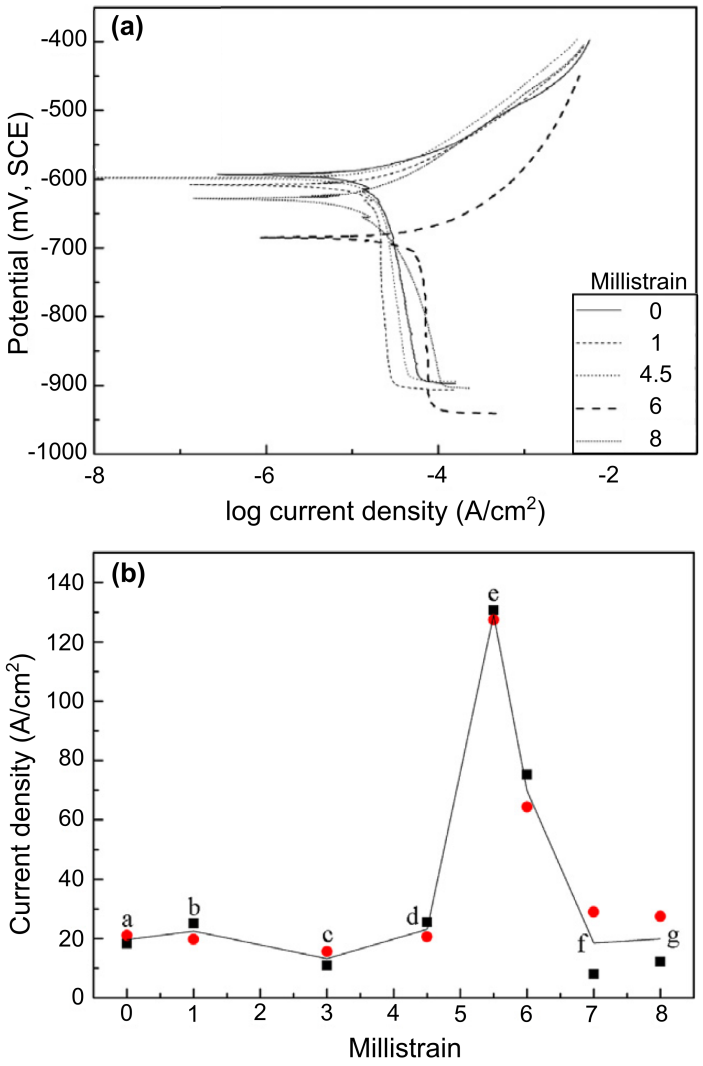

FIGURE 2.8: (a) Polarisation curve response of X80 in 0.62 M NaCl aqueous solution at different levels of strain. (b) Relationship between strain and current density at the corrosion potential. A sharp increase in the current density of X80 steel is illustrated at a strain of 6 millistrain [54].

In a study of interest, Ren et al. [55] examined the electrostatic responses of marine structural steels to elastic strain in NaCl solution. The steels used in that study were low carbon bainitic (0.08% C, 0.35% Si, 1.12% Mn, 0.0083% S, 0.38% Cu, 0.52% Cr, 0.31% Ni, 0.0037% Nb, 0.008% P) and ferritic (0.0055% C, 0.16% Si, 0.79% Mn) steels. It was found that the relationship between strain and current density was non-linear with a more stepwise response seen (Figure 2.9).

It was proposed that this current density increases in the elastic region due to microplastic deformation events at local regions of instabilities inside the steel, despite the macroelastic stresses being below the yield strength. This plastic strain then increases the current density in the same manner as is seen in other studies. Pure elastic strain is shown to have little impact on the current density, indicating that plastic strain rather than total strain is the key factor to consider for electromechanical characterisation [50, 60].

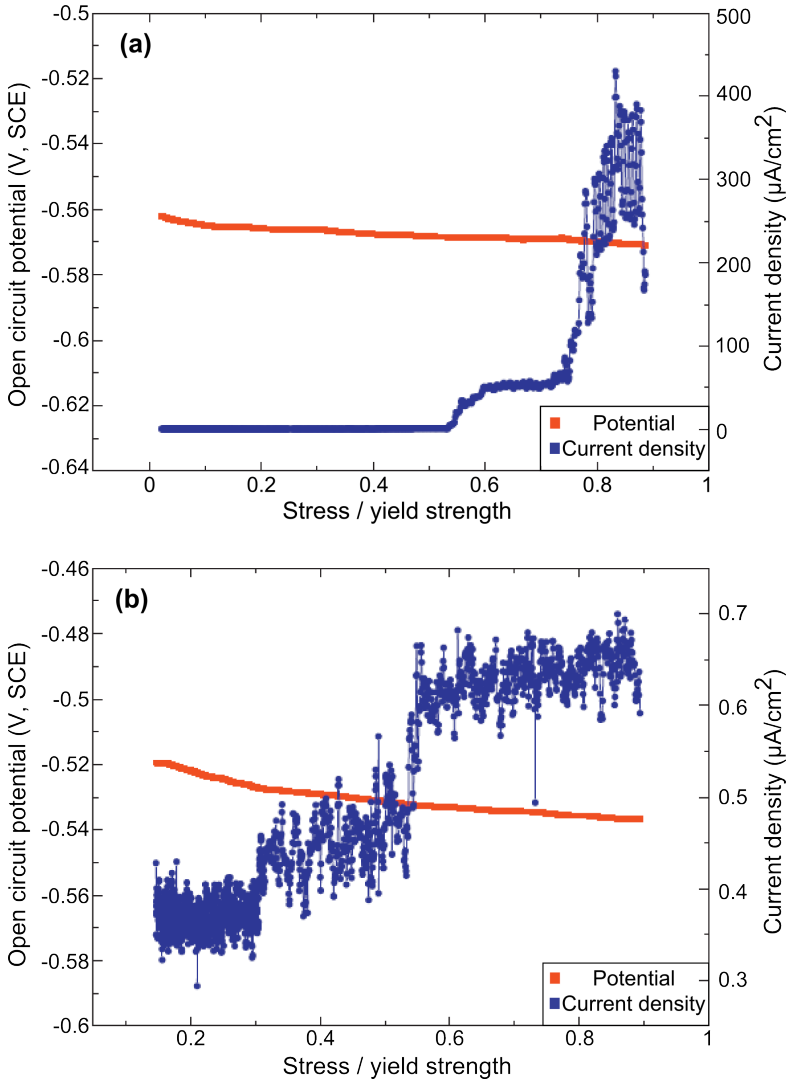

FIGURE 2.9: Change in current density and potential with increasing elastic strain for (a) low carbon bainitic steels and (b) low carbon ferritic steels, both in 3.5 wt% NaCl [55].

Feng et al. [56] considered structural carbon steel (0.37% C, 0.16% Si, 0.32% Mn, 0.053% S, 0.026% P) in cement extract solution and the effects of strain on the polarisation response. Figure 2.10 shows the relationship between strain and the polarisation response, and the results seem to be following the trend of proportionality between strain and current density seen in the aforementioned studies, however this is without the previously seen reduction in current density as the strain is increased further. Strain seems to shift the curve more positively along the current density axis, with little movement along the potential axis. One possible reason for this difference relative to Sahal et al. [52] and Wang et al. [54] is that the strains all fall below the well-defined ultimate tensile strength of the carbon steel in Feng's case (similar to X65), while the nickel [52] and X80 steel [54] studies involve materials with flatter post yielding stress-strain responses. A similarly predictable response was also shown by Wang et al. [59] on X65 steel in the elastically stressed region (Figure 2.11), however the presence of pits and defects allowed regions of plastic strain. This could mean that for grade X65 and below steels, with strains below the ultimate tensile strength, strain may have a somewhat predictable effect on the polarisation response.

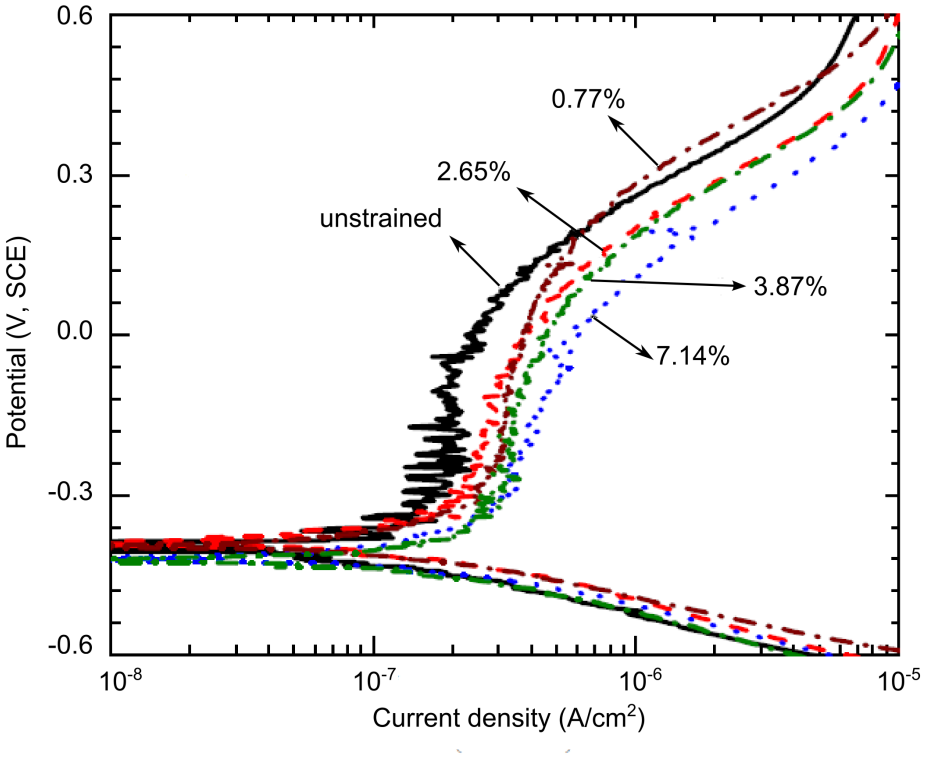

FIGURE 2.10: Effect of strain on polarisation response of carbon steel in cement extract [56].

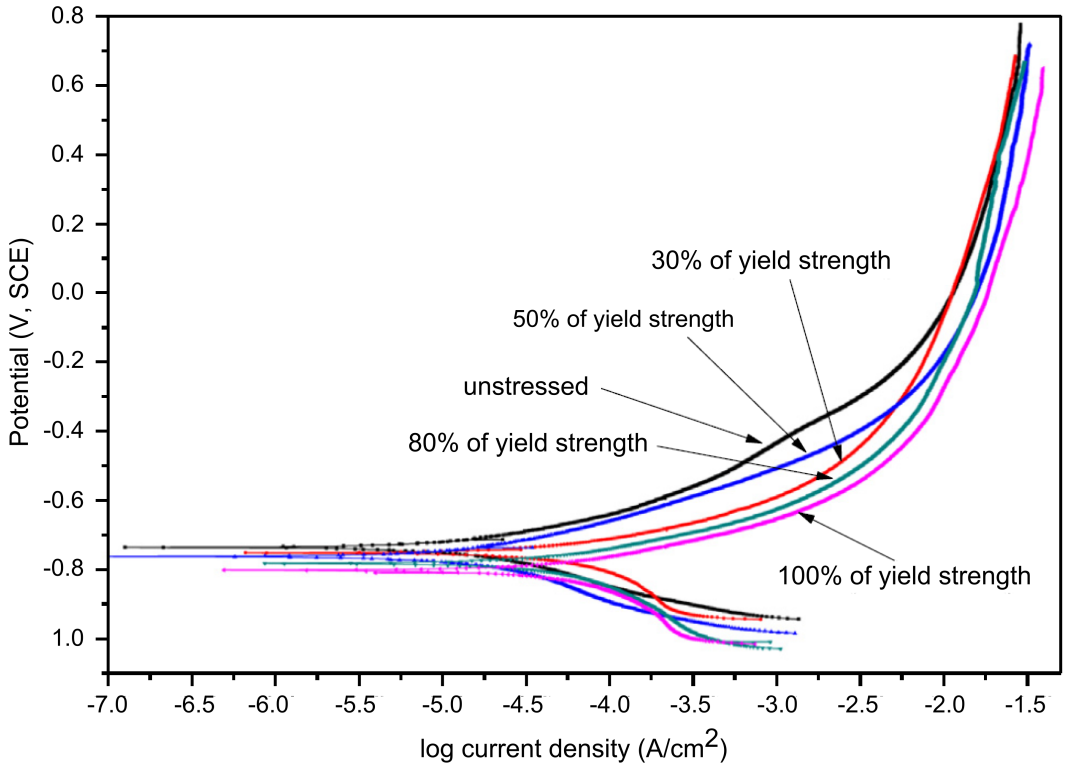

FIGURE 2.11: Effect of elastic stress on the polarisation response of pitted X65 steel in a soil representing alkaline solution [59].

Yaguchi and Yonezawa [30] have shown intergranular SCC crack growth parallel to the applied stress. Their study subjected an existing fatigue crack to a corrosive environment and constant load conditions and showed SCC growth perpendicular to the crack, along its edge (Figure 2.12). The cracks were deemed to be SCC rather than intergranular corrosion due to the formation of an oxide on the crack surface that was sufficient to halt extension after a small portion of growth. Higher zones of plasticity are present close to the crack walls due to its growth history as well as from the rolling process of manufacture. Yaguchi and Yonezawa [30] hypothesise that plasticity induced growth along susceptible grain boundaries. This result presents a possible case of polarisation curve shifting where the highly strained areas provide a weaker film and stronger dissolution and the less highly

strained areas result in a stronger film, preventing dissolution. Crack tip plasticity enhanced dissolution has also been shown by Tang and Cheng [33] where the face of a pre-cracked X-70 pipeline steel was exposed to corrosive media and significant attack was present in the crack tip plastic zone (Figure 2.13). This increase in current density on the microscale was also reported by Li et al. [50], who showed that the current density of anodic dissolution increased significantly during plastic deformation of a single crystal (but not elastic deformation). They related this increase in current density to the higher dislocation density in the plastic region around an SCC crack tip. This reinforces the idea that the increase in current density seen with the bulk strained samples should be relatable to plasticity on the microscale ahead of a crack tip.

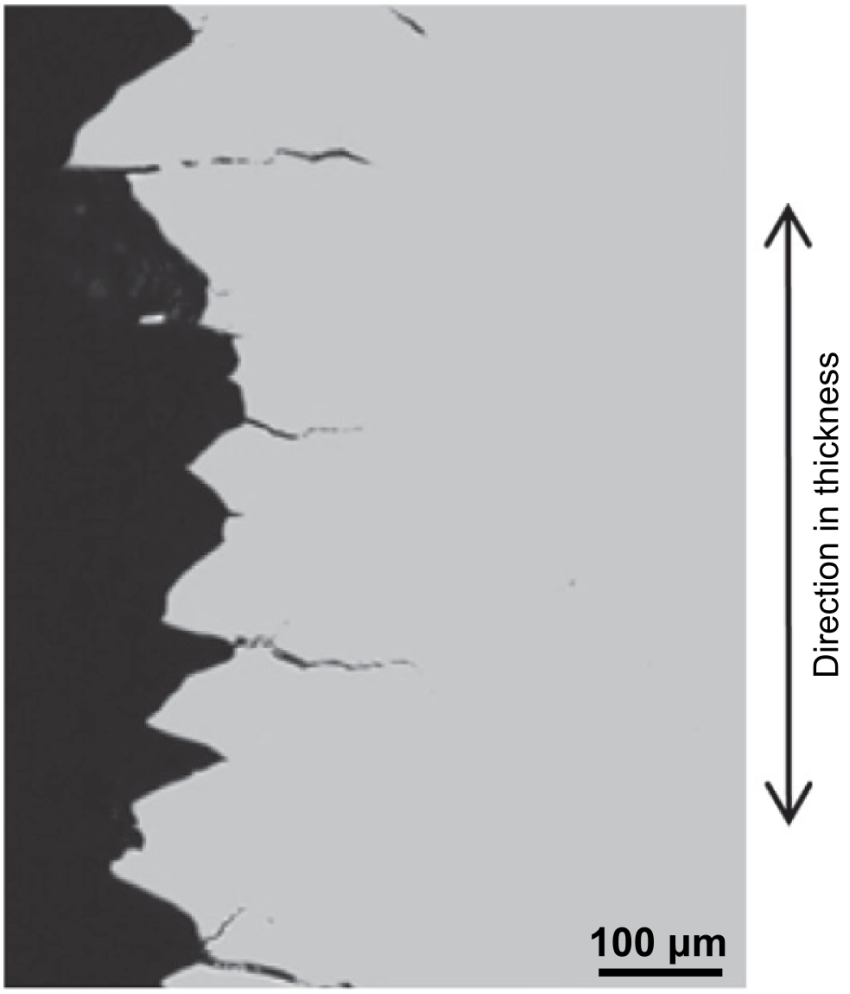

FIGURE 2.12: SCC cracks (horizontal) growing off parent fatigue crack (vertical on left of image) [30].

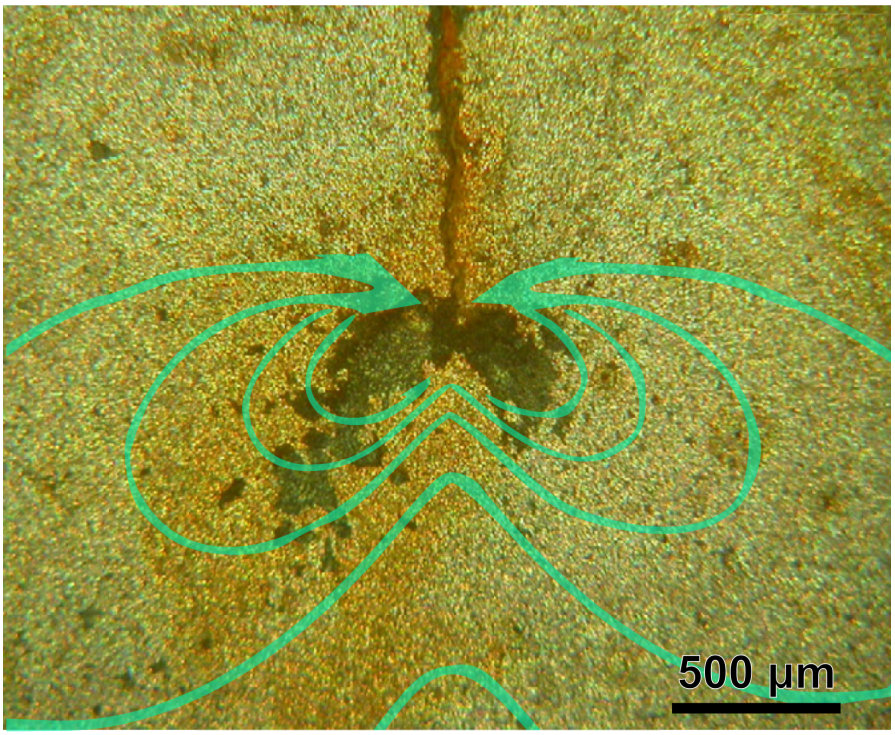

FIGURE 2.13: Preferential corrosion in the highly strained areas of pre-cracked X70 pipeline steel [33], with the theoretical linear elastic fracture mechanics strain contours overlayed.

Overall this means that SCC crack growth may not follow a constant, strain independent potentiodynamic curve. The higher and varied strains around the crack tip could result in different conditions for dissolution along differently strained grain boundaries. A model which represents intergranular SCC growth should be able to include not only the traditional stress response, microstructure, and filming and dissolution kinetics, but also demonstrate how those kinetics change radially around the crack tip. Additionally, as the cathodic protection differs down the length of the pipe, so too will the SCC equilibrium point. This could mean that the same pipeline could experience straight and inclined SCC along its length as the material properties, stresses and cathodic protection changes and thus these factors should also be considered when modelling SCC.

2.5 Modelling

The reasons for inclination proposed in the previous section are expensive and time consuming to test experimentally, so computer simulations can be utilised to assess the viability of the suggested causes of inclination. Furthermore, models can identify the sensitivity of the parameters involved, and provide guidance on whether the industry techniques identified in Section 2.2 are valid for inclined cracks.

2.5.1 Crack path modelling

The mechanism behind the crack path of inclined SCC is controversial with no proposed mechanism proven, and a model is desirable to test the varied hypotheses proposed in prior studies on inclined SCC [12–14, 22]. These various proposed hypotheses include microstructural effects such as texture, crack tip plasticity enhanced dissolution and altered stress fields. Thus a model that can assess the impact of these potential influencing factors should have the ability to:

- Represent a microstructure similar in appearance to those seen in prior studies [27] and have the ability to apply properties to those grain boundaries such as texture.
- Calculate the stress field around an intergranular crack to determine the stress intensity factor and crack tip stress/strain fields.

- Incorporate crack propagation with a customisable growth algorithm over many grains (at least 1mm of depth) to see the full shape of the crack path over long distances, as well as what the crack paths may look like at crack depths beyond what has been seen in field studies.
- Produce results that can be validated through comparison to field grown crack paths.
- Do all of the above without being too computationally expensive.

A new model that is applicable to inclined SCC can be informed by straight SCC theory and simulation techniques. Previous SCC models and theory can be analysed for relevant theory and techniques that can apply to the items above, such as techniques for representing microstructure. The most applicable methods for inclined SCC can then be selected for incorporation into an inclined SCC crack path model.

Crack path modelling has been noticeably absent in the field of stress corrosion cracking of pipelines, however some knowledge can be borrowed from fatigue models as well as SCC in nuclear power plants.

Tafreshi [63] performed a study on a 2D aerospace de-lamination problem using a boundary element method. He examined the effects of anisotropy on the crack propagation direction and rate, and found they had a significant effect. The model did not explicitly incorporate microstructural effects or electrochemistry. Propagation was determined with an energy based criterion.

Chin [64] considered the fatigue of a titanium bracket used in the aerospace industry. The 3D model analysed corner cracks, using a combination of ANSYS and FRANC3D. A crack was manually placed in the bracket, and propagation was calculated using linear elastic fracture mechanics. Grain structure and corrosion were not relevant to this model.

Sun et al. [65] considered intergranular crack growth in a creep-fatigue system of a nickel based superalloy. A damage model is used where damage from fatigue, creep, and oxygen diffusion are considered simultaneously to determine whether the crack front will advance. The 2D model used a cohesive zone model that assumes the intergranular crack path as predefined, and linear.

Kamaya and Kitamura [66], Kamaya and Itakura [67] considered pure intergranular growth of SCC in stainless steel in high temperature water, for a nuclear power plant application. A combination of C++ and an in-house finite element analysis (FEA) solver were used to calculate the local stresses in 3D, and subsequently propagate the crack. They modelled a 3 mm by 1 mm by 0.5 mm polycrystalline block of stainless steel, of which the grain structure was randomly generated using a grain growth algorithm [66], or 3D Voronoi tessellation [67], with a Monte Carlo analysis to account for different grain structures, and grain boundaries given varying resistance to the load. They considered both the initiation and growth mechanisms, both of which were governed by damage mechanics in the most recent paper, whereby a grain boundary would break once the cumulative damage exceeded a threshold value. Corrosion was accounted for by accumulating damage on the grain boundaries.

In a similar vein to Kamaya and Itakura [67], Stoll and Wilkinson [68] focused on calculating growth rates of intergranular stress corrosion crack colonies in a 2D stainless steel/water environment. The propagation of the cracks is governed by a power-law type crack growth rate equation dependant on the stress intensity factor in a boundary element method model. Voronoi tessellation was used to generate the grain structure. The power law implemented to describe the crack growth kinetics was also used by Kamaya and Kitamura [66].

Jivkov has also looked into simulating intergranular stress corrosion cracking in both 2D [69, 70] and 3D [71, 72] for austenitic stainless steels in the power generation industry. In each model he uses a combination of a Java master code with ABAQUS for the finite element calculations. His focus is on the role of special grain boundaries and grain size on the early stages of growth, generally considering no more than 30 grains in depth. The model is based on simplified continuum damage mechanics, whereby the entire model is comprised of beam elements. The rate of crack growth was not considered important for their project, hence the corrosion mechanism was unaccounted for. The grains were modelled as uniformly distributed hexagons and truncated octahedrons in the 2D and 3D models respectively, and crack propagation could only occur along grain boundaries.

Musienko and Cailletaud [73] considered the transition from intergranular SCC to transgranular SCC in Zircaloy tubes subjected to iodine in nuclear power plants. Continuum damage mechanics is used in this model, with Voronoi tessellation to represent the grain structure. A combination of C++ and a finite element solver were used to determine the stresses and propagate the cracks. Both 2D and 3D

models were considered, and in each case the transgranular propagation occurred at such a point in the microstructure where it was geometrically preferable for the crack to propagate into the grains, rather than along the grain boundaries. Thin elements were placed between the grains to represent grain boundaries. Corrosion was considered by including the diffusion of iodine into the grain boundaries and, to a smaller degree, into the grains. This diffusion is damage dependent and governed by Fick's laws. It is coupled using the code ZéBuLoN, which adds damage to the grain boundary based on the amount of diffusion.

Unlike the aforementioned authors, Rimoli [74] modelled SCC of a gun barrel rather than a component in a nuclear power plant. Gun barrels experience SCC during the high heat and physical loading associated with the shot, which accelerates the corrosion by the residual gun powder. He used a 3D finite element analysis to simulate a grain structure, apply stresses, and simulate corrosion with a continuum damage mechanics approach. The microstructure was modelled as a repeating pattern, and the grain shape simplified to allow for a reasonable amount of grains to be analysed. The corrosion was simulated using Fisher's model, which is based on Fick's laws of diffusion, with three types of corrosion kinetics considered; however hydrogen diffusion was the corrosion mechanism analysed. Crack propagation was restricted to the grain boundaries, when combined with the microstructure model, causes crack paths where branching and interaction are discouraged.

2.5.1.1 Representing the microstructure

As high pH SCC in gas pipelines propagates intergranularly, the properties of the microstructure will have an influence on the growth of the cracks. Various methods of creating a representative microstructure have been utilised in previous models with each having their advantages and drawbacks [47–49, 66–77]. Some of those studies have gone on to consider the effect of various microstructural properties, such as geometrical factors (shape/size) [48, 49] and grain boundary properties (misorientation, special grain boundaries) [47, 49, 66, 67, 69–72, 75].

The least complex method of generating a geometric microstructure is uniform tessellation of a shape, usually a hexagon or truncated octahedron, and this results in a uniform grain structure (Figure 2.14a). This can be modified to add some shape skew to represent microstructural characteristics developed during fabrication and tends to be used for models where the specific path of a crack is not as important as the generic growth rate [69–72, 74].

Following this a grain growth method is sometimes employed to represent the microstructure [66]. This involves generating numerous grain nuclei, either randomly or via an algorithm, and then assigning each nuclei an incubation time and growth rate. The grain grows after an incubation period and forms a grain boundary when it collides with another grain. This requires significantly greater complexity than the uniform tessellation, but it does create geometrically realistic grain structures.

An alternate method to the grain growth method of generating a grain structure is Voronoi tessellation, which has been adopted in various models of polycrystalline

solids as the primary method of microstructural representation [48, 67, 68, 73, 77]. Originally created in mathematics as a way of randomly dividing up a finite space into convex subspaces, Voronoi tessellation places a multitude of seed points within a 2D or 3D region [78]. Each point in the space then assigns itself to the closest seed point, creating Voronoi cells. While more complex than uniform tessellation, it is less complex than the grain growth method, while producing realistic grain structures (Figure 2.14b). Furthermore, the multitude of research into Voronoi tessellation from the mathematics field has produced various algorithms for generating these diagrams more efficiently, such as with Delaunay triangulation [79]. Voronoi tessellation can even represent complex microstructural characteristics, such as banding or clusters [48] (Figure 2.15). Both the grain growth algorithm and Voronoi tessellation's random nature require a Monte Carlo analysis to be performed, so that the most likely and worst case scenarios can be determined, which results in significantly more computational time than a repeating microstructure for a representative result.

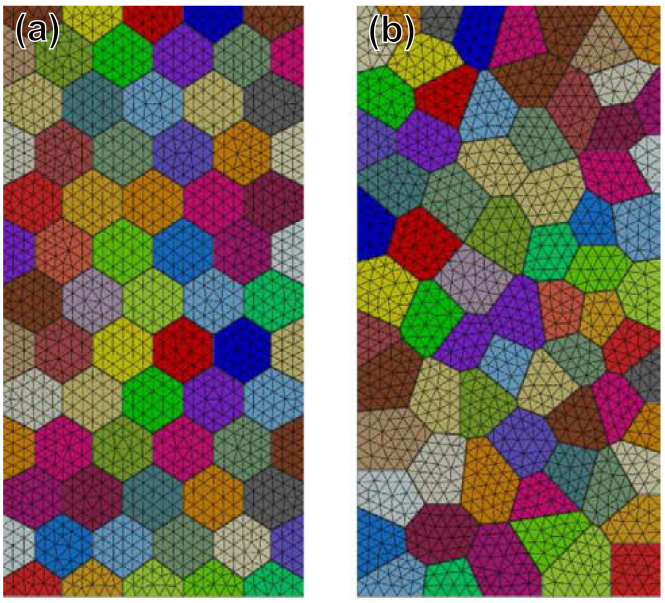

FIGURE 2.14: (a) Grains modelled using uniform tessellation; (b) Grains modelled using Voronoi tessellation [73].

Finally, the grain structure of a specific sample can be found experimentally. One such method involves using a scanning electron microscope (specifically using an electron backscattered diffraction camera) [29, 47], and then importing the experimentally determined microstructure directly into a model [76]. This method is good for validation of a model when compared with a failed component, but is generally impractical on a larger scale due to the time necessary to account for the random nature of the grains.

Voronoi tessellation seems to be the most commonly used method in the SCC models in Section 2.5.1, and also boasts benefits of good computational efficiency with good customisation available to mimic a grain structure. As such it is the best candidate for modelling inclined SCC. Whichever representative method is used, the geometrical properties of the microstructure (e.g. aspect ratio, grain diameter,

banding or clusters) should be determined experimentally and then replicated as closely as possible by one of the above methods.

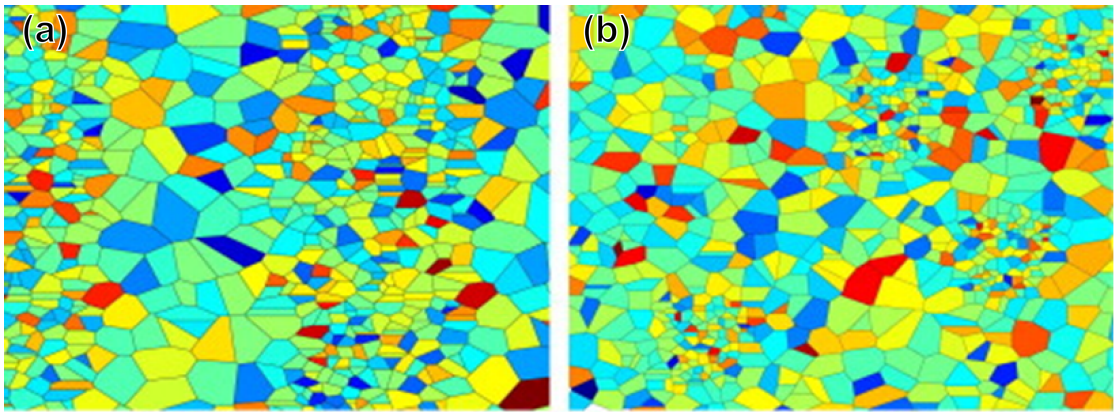

FIGURE 2.15: A Voronoi tessellation generated microstructure with (a) banding and (b) clusters [48].

The effect of special grain boundaries on stress corrosion cracking has also been a popular field of investigation. Certain textures (misorientation between grains) are more resistant to stress corrosion cracking [29, 47] and various authors have examined their effect on crack growth rates [47, 49, 66, 67, 69–72, 75]. Generally the authors considered the effect of increasing the fraction of special grain boundaries on the SCC growth rate, however not on the SCC growth direction. The exception is Itakura et al. [75] who postulated that special grain boundaries can be a site for crack branching nucleation in three dimensions (Figure 2.16). Overall, these models show that special grain boundaries play a key role in SCC and their impact on the crack velocities should be considered in a model. All the methods of generating the microstructure listed are capable of applying a variable to the grain boundaries to represent resistance, such as was done by Kamaya and Itakura [67] and Jivkov et al. [70].

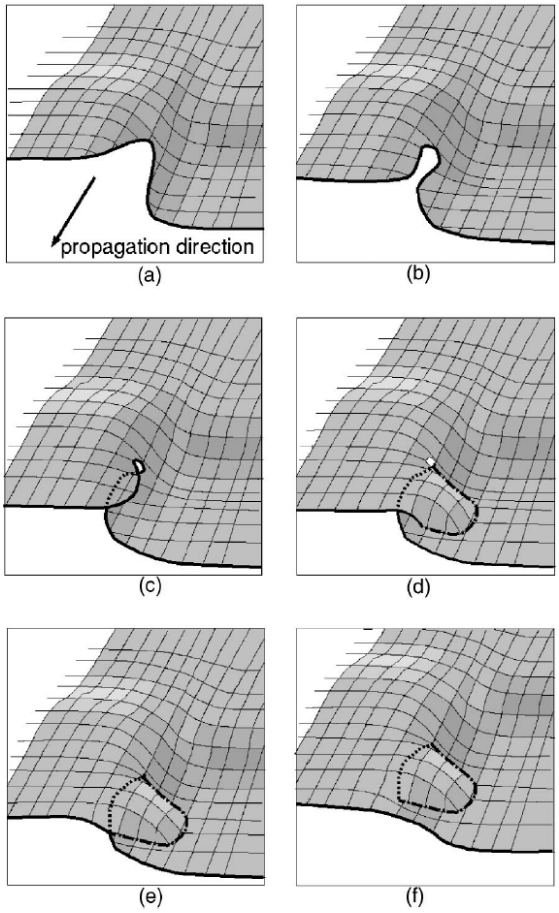

FIGURE 2.16: A step by step process of a resistant grain boundary causing crack branching in three dimensions [75].

2.5.1.2 Calculating the stress fields and propagation techniques

Regardless by which mechanism SCC grows, calculations of the stresses, strains, or stress intensity factors are required for the governing crack growth rate equations [8, 20, 52, 71, 80, 81]. Film rupture is often determined by either the stress intensity factor or strain rate, as was seen in Equation 2.3, while dissolution based mechanisms are governed by current density, which could have a dependency on plastic strain [30]. Typically, models have addressed the micro- or macro-scale growth of cracks, but the methods are generally applicable for meso-scale growth with some concessions in either accuracy or processing time.

Various methods are available to calculate the stress fields around a crack tip. For simple geometries, approximations can be made from tables or simple equations [20, 38, 41–43, 45, 80, 82]. These can provide relatively accurate stress intensity factor results with low computational effort, however for more complicated crack geometries, interaction and detailed stress field analysis, more complex methods are required. To do this, finite element solvers, such as ANSYS, ABAQUS, Franc2D, Franc3D, Z-Cracks, or self-developed finite element solvers have been used in several models [64–67, 69–74, 83] and offer robustness at a higher computational cost, particularly for three dimensions. Alternatively, boundary element methods are sometimes used [63, 68] and although they can be more efficient in some cases, no clear case is present for the use of either the boundary element method or finite element method exclusively over the other and the solution remains a matter of preference. Assorted alternative methods exist for calculating fracture parameters around a crack tip, such as enriched FEM (E-FEM) [84–87], extended FEM (X-FEM) [88–91] and the particle discretization scheme FEM (PDS-FEM) [92, 93], which often involve enriched nodes and the advantage of mesh independence, however they have scarcely been used in existing SCC models. PDS-FEM stands out from the others, as it provides a probabilistic crack path (Figure 2.17), which is of great interest to intergranular SCC. Figure 2.17 shows two cracks in a flat plate from a surface view, with different loading rates depicted in the quadrants. The coloured contours are a probability density function representing the likelihood of the crack path growing through each point, with red being more likely than blue. The spread inherent in their model is a result of varying material properties with a normal distribution to represent the variance

in material properties inherent in manufacturing. The idea of a probabilistic crack response to material properties can equally be performed with existing methods though using a Monte Carlo approach, albeit at a lower computational efficiency.

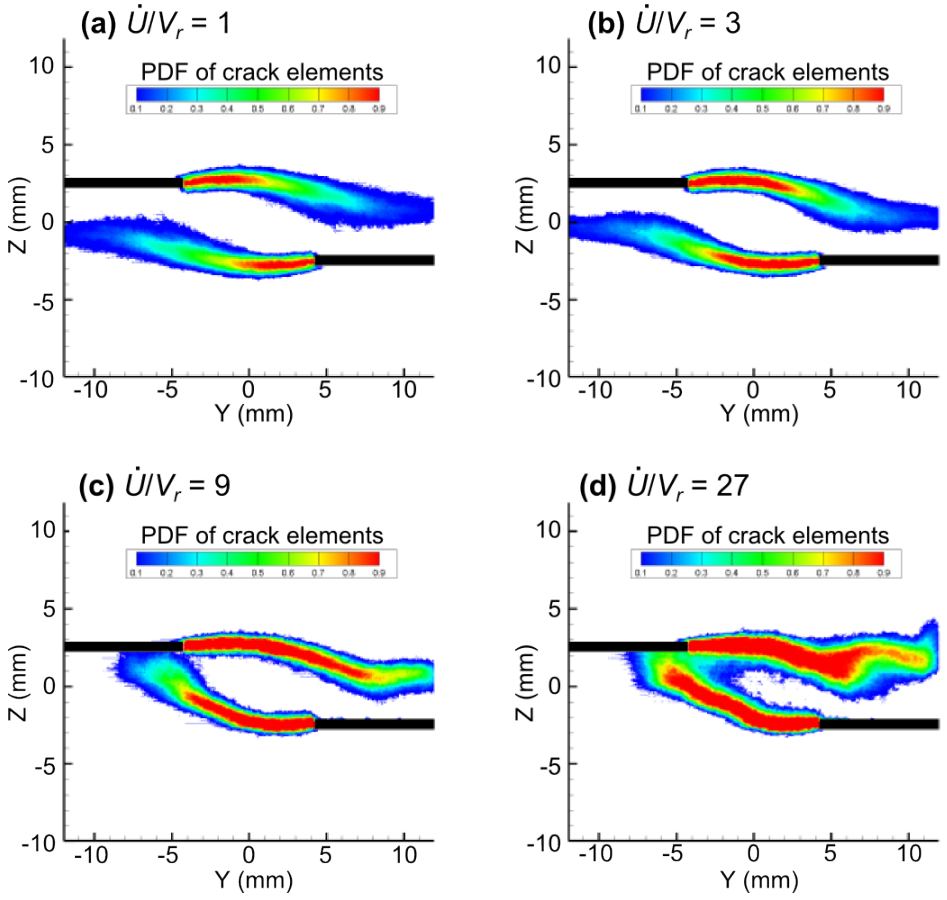

FIGURE 2.17: Plate surface view of a probability density function (PDF) of the crack path in PDS-FEM based on random material properties. Y and Z represent the coordinates of the surface, $\dot{U}$ is the loading rate (mm/s) and V_r is a constant equal to 0.1% of the P-wave velocity to non-dimensionalise the ratio [93].

Propagation has been governed by various theories in intergranular models, including fracture mechanics [64, 68], damage mechanics (often integrated with some corrosion) [65, 67, 73, 74] and the energy method [63]. The majority of the studies used an in-house code combined with an FEA solver to govern crack growth, while a small selection used auto-propagation software. Auto-propagation software will

usually be optimised and be more computationally efficient than a self-developed code, however it is also much less robust and unlikely to be able to account for the conditions of inclined stress corrosion cracking. It has yet to be seen which of the methods would be most suitable for the inclined cracking case, but the combination of an in-house code and a FEA solver provides the flexibility to input varied algorithms that might account for the inclination.

2.5.2 Crack growth rate modelling

Crack growth rate modelling of inclined stress corrosion cracking is important as existing predictions for inspection intervals may not be correct for the inclined case, since the equations and theory developed for SCC crack growth assume straight crack paths. A crack growth rate model should be founded in an equation that can account for the environmental and mechanical factors that govern SCC crack growth rates without including assumptions that relate to the crack path. This would allow the sections of the equation that need to be modified for the inclined mechanism to be easily identified and changed. A history of crack growth rate equations used in industry should be examined for their suitability to inclined SCC.

Leis and Parkins [10] stressed the importance of modelling the dissolution process at the grain boundaries, as well as the passive film rupture and repassivation of the oxide layer. They suggest that while a model can be based on existing crack growth data for a colony, a purely predictive model would be useful. They focus their study on the initiation and formation of crack colonies, with a 2D surface

model. The effects of crack interaction and coalescence were considered beyond the scope of the research. The crack growth rates they employed were based on the form of Faraday's law, shown in Equation 2.2, often favoured by Leis and Parkins. In this equation, $\dot{a}$ is the crack growth rate, M_w is the molar mass of iron, z is the valency of ions in solution, F is Faraday's constant, ρ is the density, and i_a is the peak current density.

$$\dot{a} = \frac{M_w}{zF\rho} i_a \tag{2.2}$$

Song [17] looked at the crack growth rate by considering the crack tip chemistry. He suggested an average crack growth rate which takes into account crack tip current density reduction with increasing crack depth. He claims the model is useful for areas where in line inspection is impractical, and can provide good estimates of later stages of crack growth given ILI data on the early stages of crack growth. The model was further developed into a comprehensive industry tool in 2011, with good correlation with field data, and then extended to include fatigue effects [20, 21]. This model of course assumes a typical crack growth path, rather than the potentially outlying paths that inclined SCC could generate.

Lu et al. [80] considered the crack growth rate of pipeline steels in a high pH carbonate-bicarbonate solution, by expanding Faraday's law, along with including strain rate effects. The equation they begin their derivation from is shown in Equation 2.3 [7]. Here Q_F represents the charge passed in time between two passive film ruptures, $\dot{\epsilon}_{ct}$ is the crack tip strain rate caused due to both the static

and cyclic loading present in pipelines, and ϵ_F is the strain required to rupture the film. This equation is generally considered to be representative of high pH stress corrosion cracking as it accounts for both crack tip dissolution and passive film rupture. One of the final equations derived is shown in Equation 2.4. The variables in this equation are described in Equations 2.5 and 2.6, as well as in Table 2.1.

$$\dot{a} = \frac{M_w}{zF\rho} Q_F \frac{\dot{\epsilon}_{ct}}{\epsilon_F} \tag{2.3}$$

$$\dot{a} = (A_0 B^n i_a)^{\frac{1}{1-n}} \left[ln \left(\frac{K_M^2 - K_{ISCC}^2}{3\pi r_0 \sigma_Y^2} \right) \right]^{\frac{n}{1-n}\frac{N+1}{N-1}} \tag{2.4}$$

$$A_0 = \frac{1}{1-n} \frac{M}{zF\rho} \left(\frac{t_0}{\epsilon_F} \right)^n \tag{2.5}$$

$$B = \frac{2N}{N-1} \frac{\beta \sigma_Y}{E r_0} \tag{2.6}$$

TABLE 2.1: Definition of parameters used for growth rate calculation in Equation 2.4.

Symbol	Description	Unit
$\dot{a}$	Crack growth rate	m/s
i_a	Crack tip peak current density	A/m^2
n	Repassivation kinetic exponent	non-dimensional
N	Strain hardening exponent (Ramberd-Osgood Law)	non-dimensional
K_M	Mean stress intensity factor in a cycle	$Pa\sqrt{m}$
K_{ISCC}	Critical stress intensity factor for SCC in X65	$Pa\sqrt{m}$
r_0	Specific length for crack tip strain rate calculation	m
σ_Y	Yield strength of X65	Pa
M	Molar mass of iron	kg/mol
z	Valence of iron	non-dimensional
F	Faraday constant	C/mol
ρ	Density of iron	kg/m^3
$t_0(s)$	Incubation of repassivation	s
ϵ_F	Rupture ductility of passive film	m/m
E	Elastic modulus of X65	Pa
β	Rice's coefficient	non-dimensional

Various simplifications were made in the models using these equations [20, 21, 80]. Importantly they assume the chemistry and potential at the crack mouth is equal to that at the crack tip, which is strictly speaking incorrect, however the current density is varied from crack mouth to tip. Additionally straight crack growth,

rather than potentially inclined growth, is inherently assumed in this research. With a straight crack path comes the underlying assumption that the crack growth is rate limited by film rupture. They claim their results match well with crack velocities lower than 10^{-6} mm/s, where they claim mass transfer is negligible. This is reasonable as Parkins and Fessler [2] has said that dissolution mechanisms tend to grow at or above 10^{-6} mm/s.

Overall either Equation 2.3 or 2.4 are appropriate for use in a model considering the growth rates of inclined SCC. It is important to determine the mechanism behind inclined first and see whether the assumptions fit. Equation 2.4 is the more suitable equation for this work as it is includes an expanded form of the passive film strain rate which is dependent on the stress intensity factor. The stress intensity factor is far easier to calculate either by hand or through FEA than the crack tip strain rate directly.

2.5.3 Crack interaction modelling

The tendency of SCC to grow in colonies makes interaction between adjacent cracks a common occurrence, so much so that coalescence is integral to stage 3 and 4 growth (Figure 2.18) [4]. Crack coalescence allows two cracks to join into one longer crack faster than would be possible for either crack on their own. Determining which cracks are interacting is an important tool required for industry inspections of pipelines, as the longest chain of cracks is used as a measure to assess the remaining life of the pipe section. Currently used guidelines in Canada and Australia specify that if two axially oriented cracks are spaced within 25% and 14%

of their average lengths in the axial and hoop directions respectively, then those two cracks should be considered as possibly interacting [11]. These guidelines are based on the assumption of a straight crack, and as such may not be applicable to the case of inclined SCC. There exists the possibility that two inclined cracks could incline towards each other and interact beneath the surface. This differs from the assumptions of the existing guidelines that assume surface interaction will occur first. A model will be developed which can analyse the impact of inclination on the interaction criteria. The model should both be able to identify the geometric worst case scenarios for two crack interaction, but also be able to assess the effect of shielding to determine whether cracks interact. Many models already exist both in fracture mechanics and SCC research which analyse interaction of surface cracks [19, 94–98], and some of these prior models will be examined in this section to ascertain applicable modelling methods.

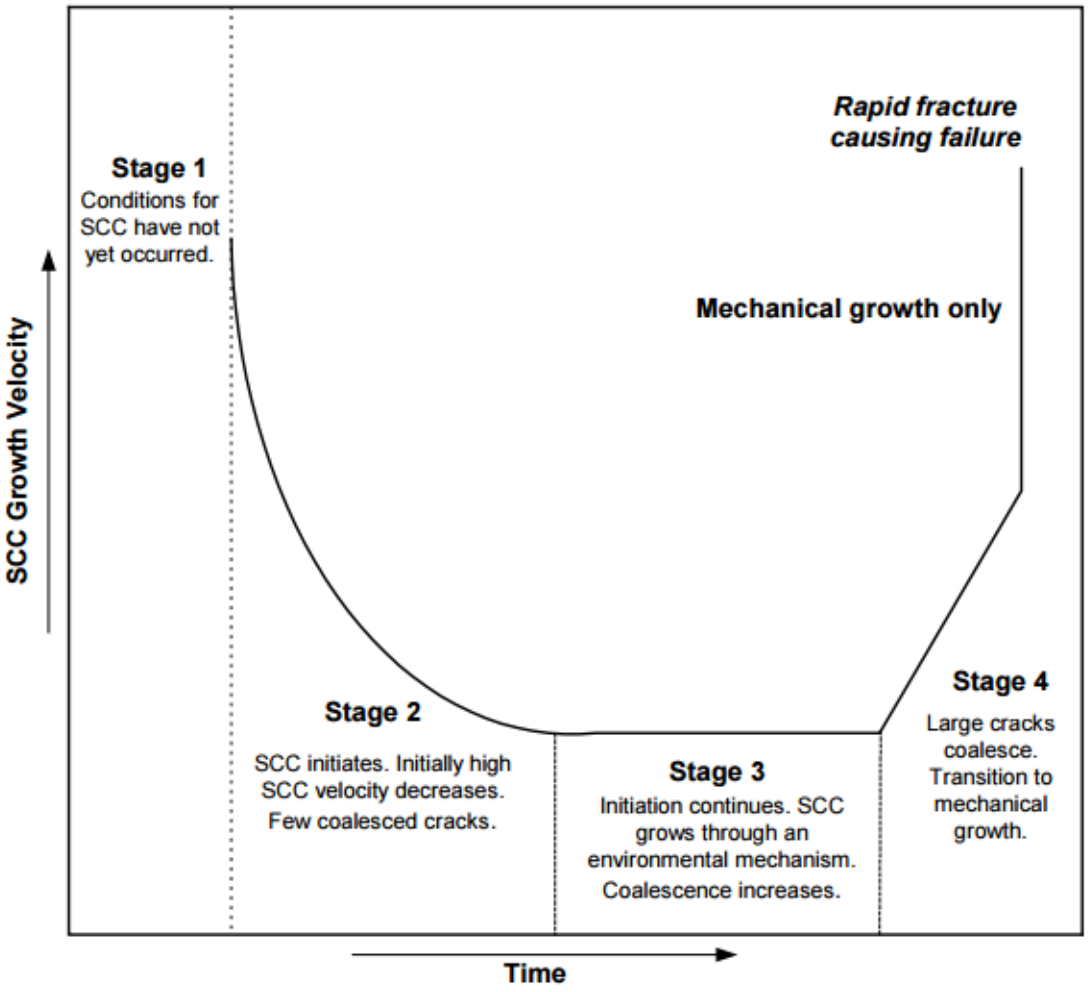

FIGURE 2.18: The Bathtub Model describing the various stages of SCC growth [4].

Stonesifer et al. [94] conducted a study to attempt to determine the stress intensity factors for interacting SCC cracks in a pipe using a finite element alternating method. They considered two equal length parallel cracks, offset in both the hoop and axial direction, in a linear elastic steel. The surface of the pipe was approximated as a plate rather than a cylinder, and the error due to this assumption was shown to be negligible as the wall thickness and crack length is much less than the radius. The cracks were given a fixed aspect ratio based on experimental observations. The results showed a good result for the 2D case, however the 3D

case could not accurately predict both the surface and crack front well. This is a well-known problem inherent in fracture mechanics theory. In any case, the stress intensity factors were highest near the surface, as SCC cracks tend to be long and shallow.

Wang et al. [19] attempted to find the interaction limits for SCC in pipe steels, using 2D FEA. Similar to Stonesifer et al. [94], they considered offset equal length cracks in a linear elastic steel with a flat plate assumption. Electrochemistry was neglected as crack growth due to interaction is dominated by mechanics. Their findings showed that with some hoop offset, as the inner crack tips near each other in the axial direction, the stress intensity factor increases. Once the crack tips pass each other, the stress intensity factor decreases. The mode II stress intensity factor also switches sign as the crack tips pass, implying the preference switches from growing toward each other to growing away. The interaction limit was found to be 14% in the hoop direction, which is the value now used in the industry guidelines [11]. The results were validated with experimentally grown cracks.

Sankar and Lesser [95] again conducted an analysis of stress intensity factors of two interacting cracks, with the intention to apply them to crack fields. 2D linear elastic FEA of offset parallel equal length surface cracks was conducted, similar to the prior studies mentioned [19, 94], however the material was a polymer. Since interaction is dominated by the stress fields and all models considered have assumed a linear elastic body, the results and method used for this material should still be applicable to steels. Equal length cracks were used as they present the worst

case. They showed the quantitative relationship which occurs as the inner crack tips pass, and demonstrates that the outer crack tips become dominant once the cracks are overlapping (Figure 2.19). They then extended their two crack model to crack fields by the use of superposition. Experimentally grown cracks were used to validate the two crack case.

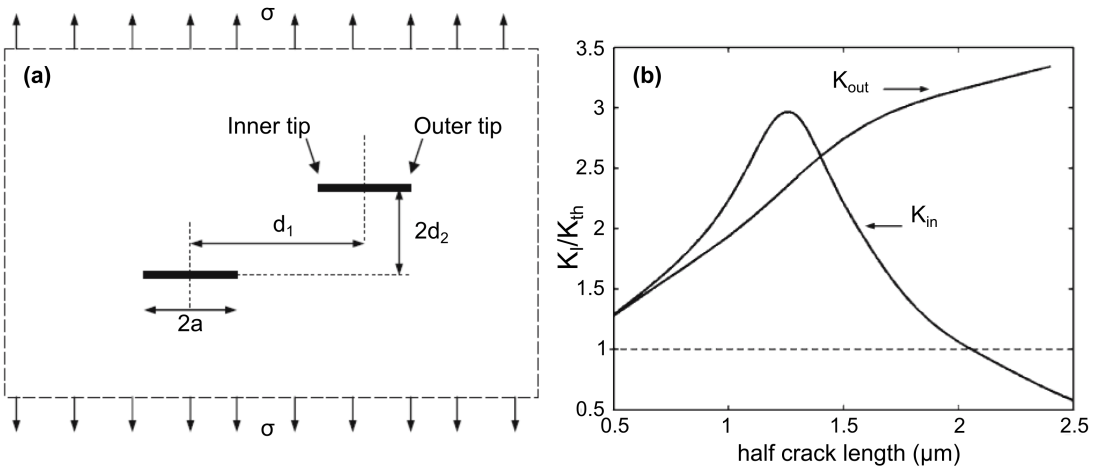

FIGURE 2.19: Crack interaction results from Sankar and Lesser [95]. (a) Equal length crack geometry used in the study. (b) Stress intensity factor normalised by the fracture toughness at the inner and outer tips for d_2=0.25μm and d_1=2.5μm showing the outer tip becoming dominant just after the crack tips pass at a half crack length of 1.4μm.

Similar to the prior studies, Kamaya [96] also considered offset parallel surface SCC cracks. This studied differed however in that it used 3D FEA rather than 2D FEA. The results showed the same outcomes as the prior studies in that the cracks tended to grow towards each other if they were not overlapping, and tended to grow apart if they were overlapping. The 3D FEA geometry was created using a standard method of a tie block joining two solid bodies with embedded cracks. This method is commonly used to ensure reasonable mesh around each crack tip, and the spacing can be altered simply by changing the size of the tie block. The use of a tie block would not be possible for inclined cracks however, as the inclination

would go through the tie block beneath the surface. This makes the methods used in this 3D FEA interaction study inapplicable to inclined SCC.

The studies analysed show that 2D FEA is widely used and gives good validated results for overlapping cracks. The differences of the inclined case to the straight crack case involve primarily the potential interaction below the surface, as the stress intensity factors at the surface should remain unchanged. However since SCC cracks tend to grow more along the surface than through the thickness, the surface stress intensity factors can still give an indication as to whether the remainder of the crack will grow beneath the surface. For instance if one crack tip is shielded on the surface, the other will grow and the crack will extend both in length and depth in that direction. Geometric conditions for the worst case of interaction can be determined based on the prior metallographical studies on inclined SCC [14, 22]. These interaction cases can then be assessed for whether they could grow to those conditions using the modelling tools and assumptions discussed [19, 94, 95]. Should the surface geometry corresponding to the subsurface interaction not be attainable, then the interaction would be considered shielded and not possible.

2.6 Summary

Inclined SCC presents three key gaps to research and industry. The mechanism behind inclined SCC is controversial, and the impact on both growth rates and crack interaction limits is unknown. Prior studies on inclined SCC as well as a

wider literature search have identified crack tip strain enhanced electrochemistry as a likely driving mechanism for inclined SCC. Modelling techniques used in multiple fields have been analysed to identify suitable methodologies to test the mechanism. Theory and simulation techniques have also been reviewed for their relevance in calculating the impact of inclined SCC on growth rates and crack interaction. These models should assist in filling the gaps and clarifying the mechanism, as well as providing industry guidance on the effect on growth rate and crack interaction limits.

Chapter 3

Scope

3.1 Overall aim

The aim of this thesis is to develop an understanding of the mechanism behind inclined SCC, and use it to assess industry growth rate and interaction guidelines.

The work also aims to fulfil the requests to the Australian pipeline industry of a model that incorporates the mechanisms of inclined SCC and can assess the safety of pipelines with inclined SCC.

3.2 Specific goals

The goals set to meet the aim are as follows.

- Determine a plausible mechanism for the inclination, and develop a model based on this mechanism that can reproduce typical inclined crack paths.

- Determine how the accuracy of crack growth rate predictions is affected by this mechanistic shift.

- Determine whether inclined SCC could interact outside of the Canadian Energy Pipeline Association (CEPA) interaction guidelines [11].

3.2.1 Exclusions

The thesis will develop simulations to achieve the aim and goals, however the following points are outside of the scope of this work.

- 3D growth of cracks.

- Incorporation and effect of local microstructural features such as vacancies.

- Growth of full colonies.

- Development of an industry ready tool for assessment.

3.3 Objectives

To meet the goals, three objectives have been created. The completion of these objectives will signify the completion of the goals, and hence the overarching aim.

1. Create a full intergranular growth model that combines microstructural properties, fracture mechanics and electrochemistry to identify the mechanism behind the inclined crack paths.

2. Combine the found mechanism with proven and compatible SCC growth equations to predict the effect of the mechanism and inclination on crack growth rate.

3. Validate the CEPA guidelines by combining the constraints of crack growth set by the mechanism with the observed crack shape parameters from previous work [14] to create a 3D interaction model.

It is hoped that the knowledge gained from this work will inform safe pipeline management practices. These objectives are covered in Chapters 4, 5 and 6 respectively, and also in the publications attached in the appendix.

Chapter 4

Factors affecting inclination

4.1 Introduction

This chapter attempts to achieve the first objective laid out in Section 3.3. Specifically, it will identify the mechanism behind crack inclination through the creation of a 2D intergranular growth model combining microstructure, fracture mechanics and electrochemistry. This helps to achieve the first part of the thesis aim, which is developing an understanding of the driving mechanism of inclined SCC. The results of this chapter will go on to inform the work done in the proceeding chapters.

The chapter will first provide a background and insight into the theory behind the model. Following this the modelling method will be explained, and the results from the model presented. Crack tip strain enhanced electrochemistry is identified as the likely mechanism, and simulated crack paths show good agreement with field

grown cracks. Further modelling results are shown, including the effects of varying the grain aspect ratio, and the significance of texture. Finally, the implications of the model results on the other thesis goals are discussed, along with the sources of error.

4.2 Background

Various findings have been made by the investigations from prior researchers on inclined cracks that lead to suggestions on what is and is not likely to be the cause of the inclination. Firstly, any similarities and differences between the Canadian and Australian inclined SCC can give some insight as to what is and is not inclination dependant, as the cause for inclination must be present in both instances. For instance, if the hardness varied significantly between the two inclined SCC cases, then it can be concluded that hardness is not likely to be part of the driving mechanism causing SCC inclination. Possible reasons for crack kinking from fracture mechanics theory must also be assessed for this case, as should the suggestions of the previous studies that a shift in mechanism could be present.

4.2.1 Australian and Canadian inclined SCC

Previous studies on both Australian and Canadian cracks have analysed the crack geometry, the mechanical properties of the X65 steel, the residual stresses and the microstructure [12, 13, 15, 22, 27, 29, 99]. The studies found that inclination usually was observed to have begun within the first 0.2 to 0.9 mm depth from the

outer surface, with an inclination angle between 30° and 60° [22], however with slightly lower inclination angles for the Canadian samples [13]. The studies also showed the majority of cracks deeper than 0.2 mm from the outer surface were inclined (81% in the Australian case [22]). The Canadian researchers reported seeing sharp kink-like inclination [12, 13], while the Australian researchers instead reported a slower curving inclination. Analysis of the cracks though shows similar crack paths in some cases (Figure 4.1), and it is unclear whether the difference is due to nomenclature, or actual differences in the crack path. Since the crack paths appear to be relatively similar, both will be assumed to follow the same mechanism.

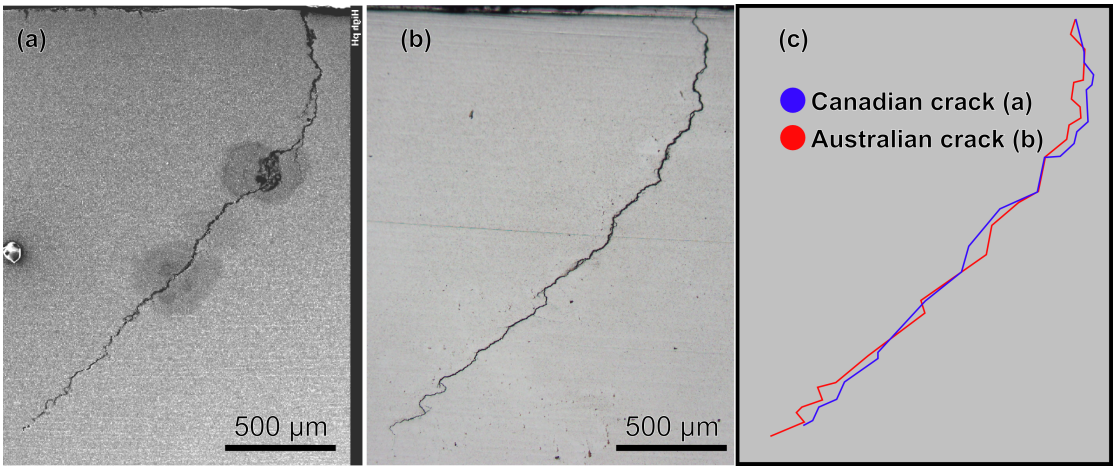

FIGURE 4.1: (a) Canadian inclined SCC crack [12], (b) Australian inclined SCC crack [14], (c) Tracings of the cracks overlayed on each other for comparison.

Analysis of the material properties and microstructure yielded little insight into the driving factors that influence SCC inclination. Studies of the mechanical properties (yield strength, tensile strength, elastic modulus, hardness) showed little differences between the Australian and Canadian samples for the X65 steels. Authors from all studies are in agreement that mechanical properties are not

indicative of propensity for inclination. Similarly, residual stresses were found to be relatively low and not in a direction such that the cracks would incline. Optical microstructural analysis showed no obvious features that could cause the inclination such as smearing [13, 22]. Other microstructural findings included an average grain aspect ratio of approximately 0.5 across the Australian and Canadian specimens [99].

One proposed reason for the inclination by the prior studies was mechanistic shift [13], since there was no evidence that the stress field could have been disturbed sufficiently from pure hoop stress. Other literature suggests the mechanistic shift may be related to strain dependant electrochemistry [52–56, 59]. This could be the case as a crack tip experiences high values of strain along the shear planes which could in turn cause the current density to rise at those angles.

4.2.2 Fracture mechanics

Typical fracture mechanics based reasons for crack kinking such as mixed mode stresses would be a simple explanation for the cracks turning, with the mixed mode stresses possibly being caused by crack-crack interaction, crack-weld interaction, and general residual stresses from pipe forming. All of these can be discounted however, as the cracks have occurred away from welds, sometimes inclined with no other nearby cracks, and inclined in both directions (69% clockwise, 31% counter-clockwise of 95 inclined cracks surveyed [22]) which discounts significant residual stress field effects. Additionally, electron backscatter diffraction (EBSD) analysis has shown no obvious residual strain patterns or microstructural features that

could explain the inclination on their own, although there is possibly some contribution from residual strain in the rolling direction [27]. Other causes must be looked at for the cracking, and the electrochemical element of SCC propagation is the logical place to look for the shift in mechanism.

4.2.3 Shifting mechanism

The existing theory for predicting SCC growth involves the balance between dissolution and passive film cleavage. Film cleavage is usually the rate limiting factor, and is represented as such in Equation 4.1 (repeated from Chapter 2 for ease of reading), which is a modified form of Faraday's law [7].

$$\dot{a} = \frac{M_w}{zF\rho} Q_F \frac{\dot{\epsilon}_{ct}}{\epsilon_F} \tag{4.1}$$

Here $\dot{a}$ is the crack growth rate, M_w is the molar mass of iron, z is the valency of the ions in solution, F is Faraday's constant, ρ is the density, Q_F represents the charge exchanged in the time between two passive film ruptures, $\dot{\epsilon}_{ct}$ is the crack tip strain rate and ϵ_F is the strain required to rupture the film. Lu et al. [80] developed a model based on this equation and they report good agreement with crack velocities lower than 10^{-6} mm/s. Their model assumed that the mass transfer is negligible and that the crack will grow via a film cleavage dominated growth mechanism.

Of note is that the dissolution is governed by charge exchanged, Q_F, which is also proportional to the current density at the crack tip [7]. Various authors [52–56, 59]

have shown that plastic deformation can change the current density at a given potential. There has also been evidence of a shift in the corrosion potential under elastically strained X65 steel [59], with pits causing microplastic events, which could suggest that the balance between dissolution and film formation could shift if the metal is locally strained. Since zones of high plasticity occur at angles to a crack tip under mode I stresses, it follows that current density may be higher at these angles, increasing the propensity for dissolution. Further support for this idea is given by the growth of SCC parallel to the applied stresses off a pre-grown fatigue crack where the strain is high [30], as well as preferential dissolution in the crack tip plastic zone of pre-cracked X70 pipeline steel [33] (Figure 2.13).

For this crack tip strain enhanced mechanism to be worth investigating, it should be able to explain the macroscopic slow curving nature of the cracks seen in the majority of isolated cracks (the small deviations and perturbations can often be attributed to microstructural features or 3D effects). This can be most easily performed by following the assumption that above a critical strain value, the current density will be sufficient to cause inclined SCC extension in the direction of highest strain. Below that critical strain the traditional film cleavage dominated mechanism will cause a straight crack extension. The J integral (as defined in Equation 4.2) is used as a relative measure of strain due to ease of calculation and comparison, and J_{crit} is defined as the J integral calculated at the critical strain criterion. In Equation 4.2, K_I is the mode 1 stress intensity factor (defined in Equation 4.3), K_{II} is the mode 2 stress intensity factor (defined in Equation 4.4), ν is Poisson's ratio and E is the elastic modulus. In Equations 4.3 and 4.4, σ is

the applied stress, F_i a geometric shape factor and c_1 and c_2 are as defined in Figure 4.2.

$$J = (K_I^2 + K_{II}^2) \cdot (\frac{1 - \nu^2}{E}) \tag{4.2}$$

$$K_I = \sigma F_I \sqrt{\pi(c_1 + c_2)} \tag{4.3}$$

$$K_{II} = \sigma F_{II} \sqrt{\pi(c_1 + c_2)} \tag{4.4}$$

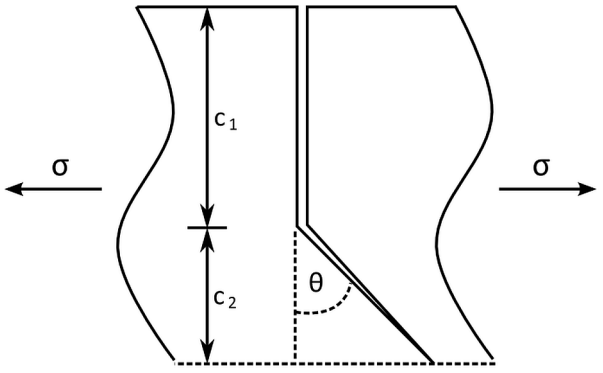

FIGURE 4.2: Definition of crack geometric parameters.

The crack would start by growing generally perpendicular to the applied stress with minor deviations due to microstructural features until the strain along the angles was sufficiently high such that the path of least resistance was along that angle, and the crack begins to incline. Using geometrical parameters defined in Figure 4.2, Table 4.1 shows that a kinked crack under hoop stress will have a lower J integral than the straight crack of equal depth (row 1). Thus it can be seen that

if J_{crit} is reached for a straight crack (ie. $J = J_{crit}$), the J integral will then fall below J_{crit} after a small extension at an angle in the direction of highest strain, and return to perpendicular film cleavage dominated growth. This alternating straight/inclined growth would continue until such a depth that the critical strain can be exceeded at a steady inclined angle, as illustrated in Figure 4.3.

TABLE 4.1: Stress intensity factors for various kink angles and length ratios Fett et al. [42], along with the J integral relative to a straight crack of equal depth, with parameters as defined in Figure 4.2, and J_0 is the J integral for a straight crack of equal length.

$\frac{c_2}{c_1+c_2}$	$\theta(^o)$	$\frac{K_I}{\sigma\sqrt{\pi(c_1+c_2)}}$	$\frac{K_{II}}{\sigma\sqrt{\pi(c_1+c_2)}}$	$\frac{J}{J_0}$
~ 0	0	1.1215	0	1
~ 0	15	1.093	0.1437	0.9662
~ 0	30	1.011	0.2695	0.8704
~ 0	45	0.877	0.3626	0.7160
0.03	15	1.05	0.159	0.8967
0.03	30	0.96	0.294	0.8015
0.03	45	0.82	0.3918	0.6566
0.05	15	1.061	0.1625	0.9160
0.05	30	0.967	0.304	0.8169
0.05	45	0.824	0.4044	0.6699
0.1	15	1.087	0.1696	0.9623
0.1	30	0.989	0.3172	0.8577
0.1	45	0.838	0.4255	0.7023
0.15 to 1	15	1.088	0.177	0.9661
0.15 to 1	30	0.989	0.329	0.8637
0.15 to 1	45	0.838	0.434	0.7081

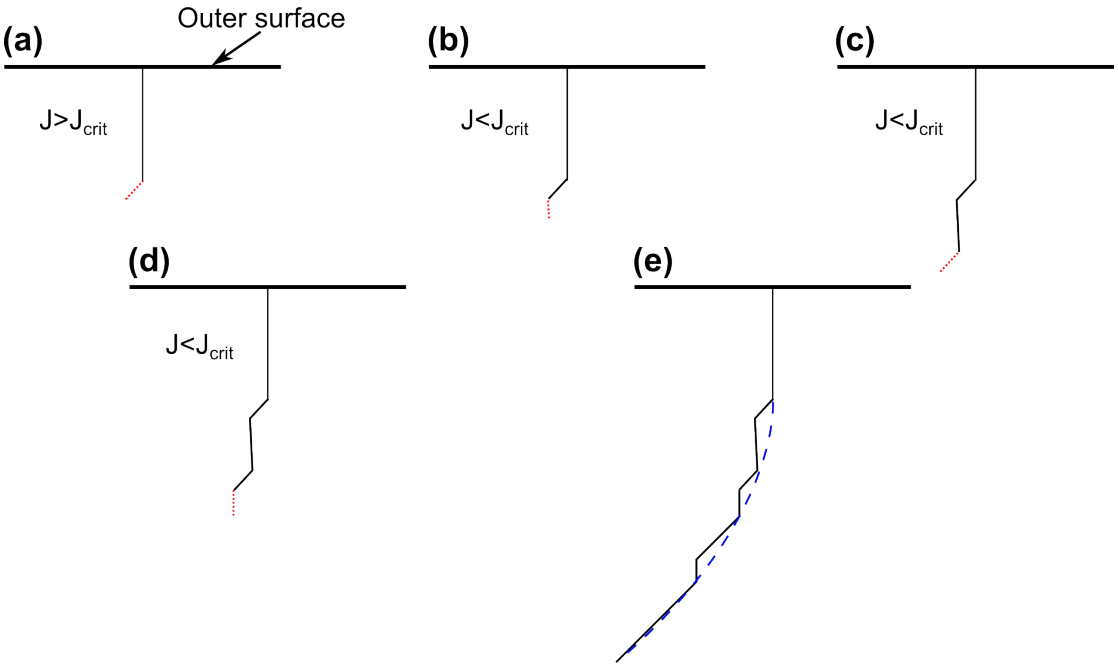

FIGURE 4.3: Evolution of an inclined crack through a strain enhanced growth mechanism, where red lines in (a)–(d) represent next growth step. (e) shows how the curve presents after 3 more growth segments.

Table 4.1 also allows us to estimate the depth over which the crack will gradually change propagation angle before the asymptotic limit is reached for verification purposes. The J integral is linearly proportional to the square of the stress intensity factors $K_I^2 + K_{II}^2$, and the stress intensity factors are linearly proportional to the square root of the crack length $c_1 + c_2$, as shown in Equations 4.2, 4.3 and 4.4. Thus the J integral is linearly proportional to the crack length for an isotropic linear elastic material. This linear proportionality implies that we can get an approximation for the depth at which an inclined crack will reach a stabilised growth angle, as in Figure 4.3e. The depth at which this stability occurs can be estimated as the depth of the initial straight section divided by the non-dimensional ratio J/J_0 (from Table 4.1) for a stable angled crack ($\frac{c_2}{c_1+c_2} = 0.15$ to 1). This gives the depth at which an angled crack would have the same J integral as the initial

straight crack. As an example using the values presented in Table 4.1, a crack of straight section of (c_1) will have a stabilisation depth of $c_1/0.7081$ when the stable final angle (θ) is 45 degrees. Similarly, if the final angle is 30 degrees, the stabilisation depth will be $c_1/0.8637$. Some error is expected in this, as there is no sharp kink and two easily defined straight sections for the field grown cracks, and also rolled steel is not an isotropic linear elastic body.

4.3 Crack path modelling method

A computational model was developed in this work which allows the generation of inclined SCC crack paths under the mechanism of strain enhanced electrochemistry. The model works through a combination of a MATLAB code, which generates a microstructure and propagates the crack through grain boundaries, and an ANSYS code which determines the stress state for the given crack geometry. The geometry determined in MATLAB acts as an input to the ANSYS code which outputs the stress state which returns as an input into the MATLAB code to generate a new geometry. This process continues until the specified end criterion, which was usually given as the lower of a depth or number of cycles. Input parameters for the model including grain geometry and critical J integral are determined using empirical data of isolated inclined SCC cracks. Produced crack paths are validated by comparing the produced crack paths with cracks grown in the field with the modelled conditions matching those in the field.

The algorithm defined in the previous section is combined with an intergranular growth code developed in-house across the modelling environments MATLAB and ANSYS, with the general program architecture shown in Figure 4.4. The microstructure is generated in MATLAB by Voronoi tessellation, as shown in Figure 4.5, with geometric parameters as determined from empirical studies of inclined SCC affected pipe [14]. Key parameters include grain width of 8 μm, and an average grain aspect ratio in the region of 0.5 ± 0.05 (consistent with pipe rolling), both found through EBSD measurements conducted in previous studies [29, 99]. These were accounted for in the MATLAB script by conducting a Voronoi tessellation over an area with the number of seeds such that the average diameter of the grains would be 8 μm. The grains were then compressed by scaling all the Y coordinates (the radial direction) by the desired aspect ratio to give grains with the correct average widths and aspect ratios. Textural characteristics are not included in the initial model, as there is an equally likely chance of a resistant boundary occurring on either side of the crack front, and over many cracks with many grain boundary fracture events, the average macroscopic crack path should remain fairly similar whether texture is taken into account or not. Texture is considered later however, once the hypothesis of crack tip strain dependent electrochemistry is tested.

The critical J integral criterion is taken to correspond to that of a straight crack with depth of 0.55 mm under field stress conditions, which was determined experimentally to be typical of isolated inclined Australian cracks [14]. While the initial conclusions of Zadow [14] presented a range of crack inclination depths, closer examination of the raw data showed the variations were occurring in the

cases where interaction would alter the stress field. Additionally, some cracks were represented with only one or two cross sectional slices and the maximum straight depth of the 3D crack (and hence inclination depth) could not be determined from so few data points. Of the cracks that showed limited interaction and were represented with multiple slices, the maximum straight depth was consistent at 0.55±0.05 mm. This indicates that the critical J value would occur at this depth under the stress state present in the field. This critical J would govern the crack growth direction, and the crack extension would be inclined or straight if the critical J value was exceeded or not respectively. Presence of crack interaction can change the stress magnitude and distribution, so only the simple case of a single isolated crack is considered in an attempt to reduce the varying nature of the cracking. Even still, slight variations in microstructure, anisotropy and electrochemistry will cause some differences between the ideal case modelled and the real life cracks, but the model provides basis for a proof of concept, and general agreement lends weight to potential for crack tip strain enhanced SCC growth.

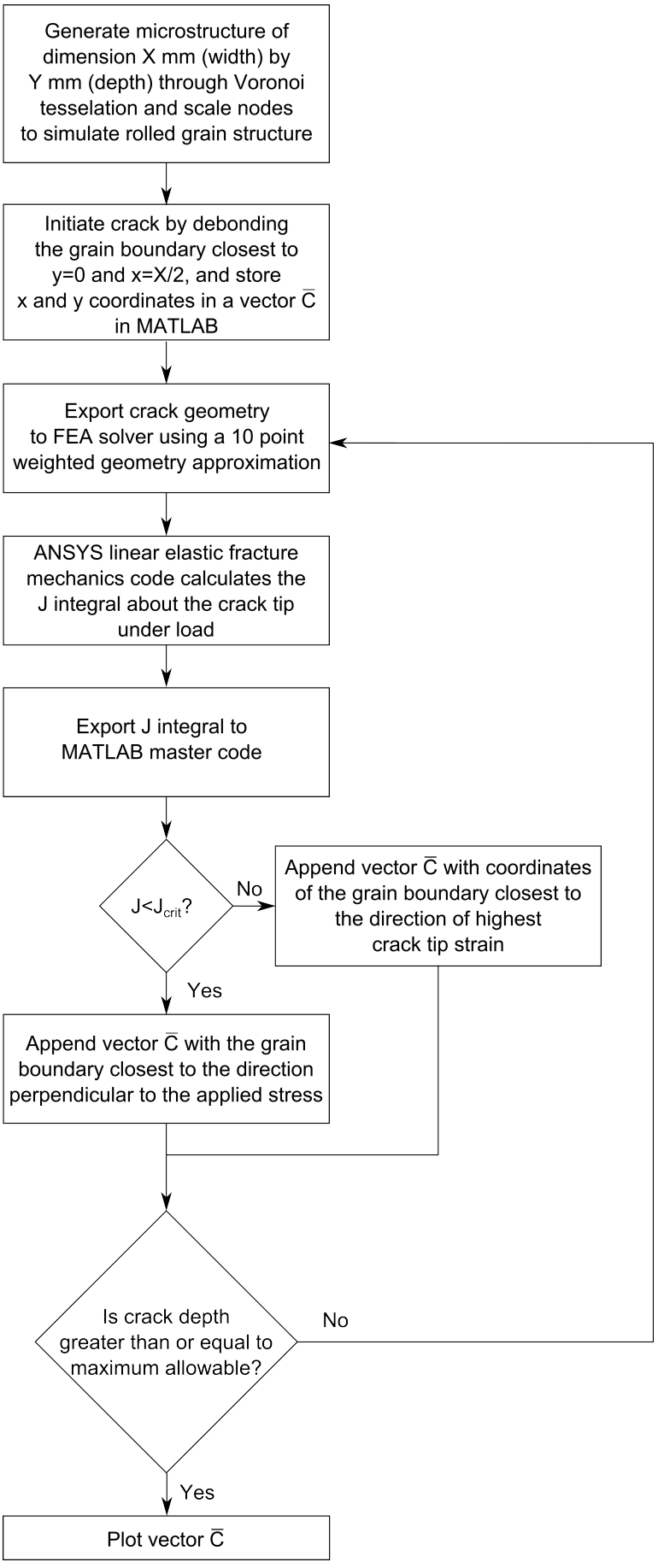

FIGURE 4.4: High level program architecture of the model.

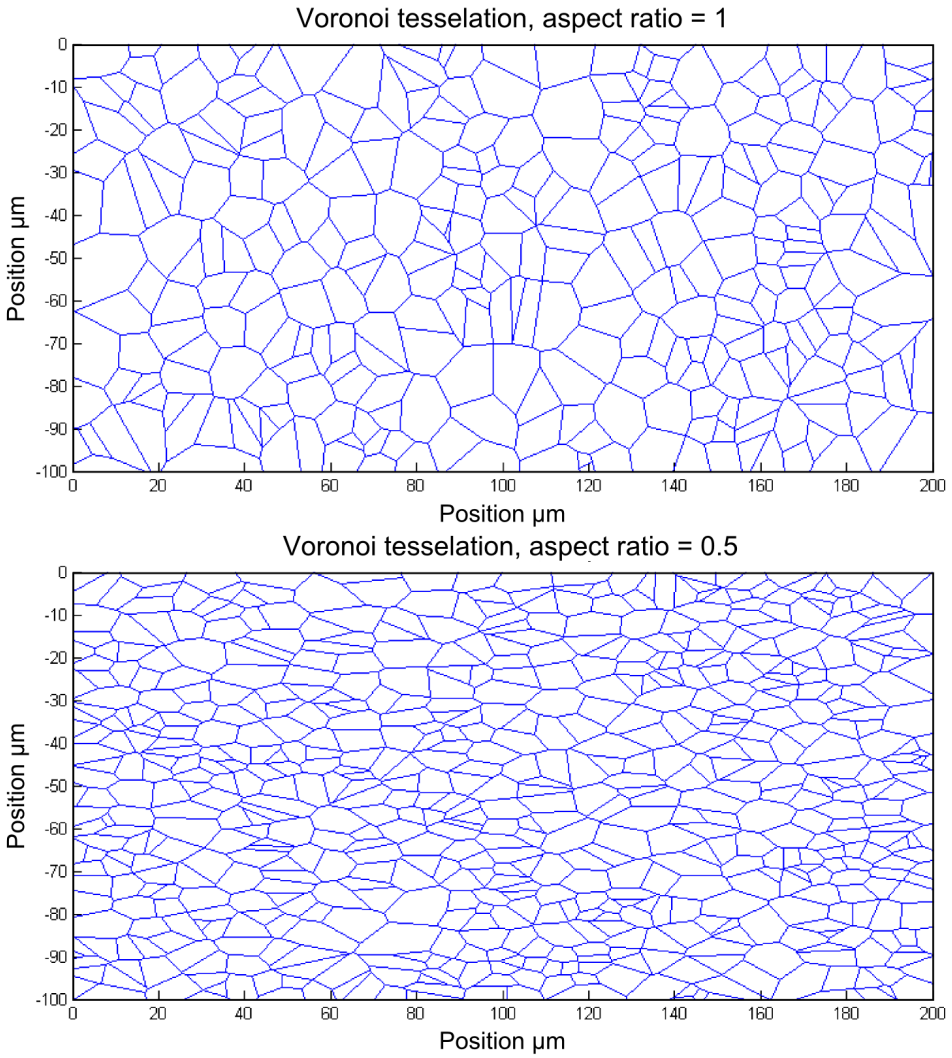

FIGURE 4.5: Example section of generated microstructure for average grain aspect ratios of 1 and 0.5, with a grain width of $8\mu m$.

The J integral is calculated within an ANSYS code represents the crack in a 2D semi-infinite body with depth of 8.3 mm and infinite width. Flat plate J integral results have been shown to not differ significantly from thin walled cylinders, and the assumption has been used for pipeline stress calculations previously [19]. The ANSYS model approximates the crack shape via a 10 point weighted representation. More key points are generated near the crack tip to represent the crack shape, as the geometry has less impact on the stress field the further it is from

the crack tip [43]. The body is meshed in 3 areas with PLANE183 elements, with smaller elements around the crack tip, and larger elements in the bulk to decrease computational time. 20 contours of J are taken, and mesh density is refined until convergence occurs within the first 5 contours, however the model produces similar results with mesh density coarsened such that convergence occurs after more contours which results in additional computational efficiency if required.

In order to validate this proposed mechanism, relatively isolated field grown cracks have to be selected for comparison to limit the effect of crack interaction (the most significant variable). Figure 4.6 shows five inclined SCC cracks from an Australian SCC colony [14], each crack with limited interaction so the mechanism can be examined with less variations caused by interaction. Interestingly all the isolated cracks tend to incline at a similar depth at their centreline, and a greater range of inclination depth is only seen in those cracks with altered stress fields from neighbouring cracks. These isolated cracks will not display all the features seen in a typical SCC crack with interaction, such as zig-zag, but will help identify if the root cause of the inclination being crack tip strain dependant electrochemistry is plausible.

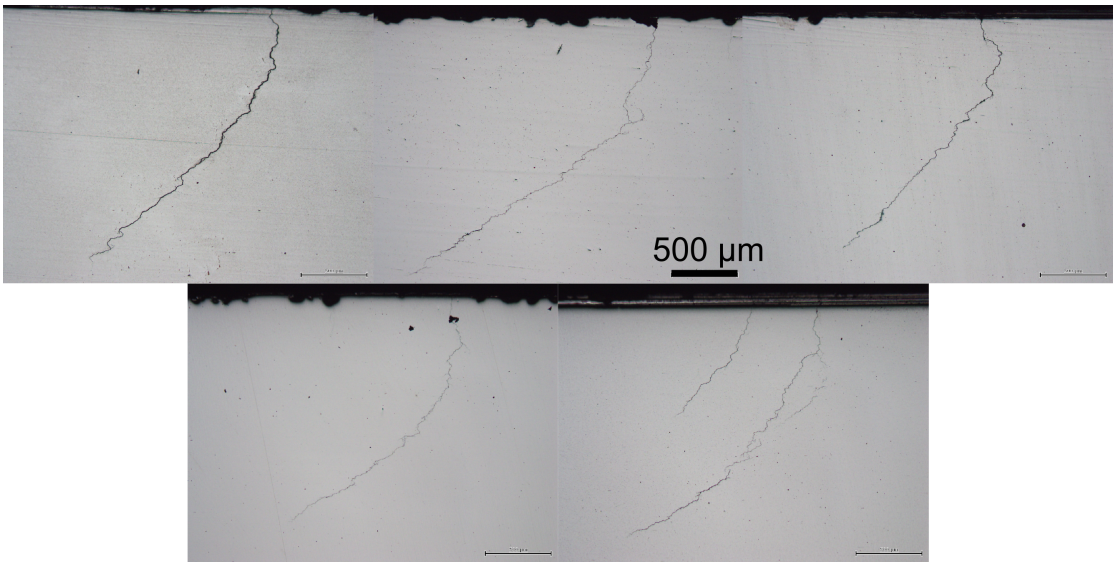

FIGURE 4.6: Five inclined SCC cracks with limited interaction from an Australian colony [14].

The combined MATLAB and ANSYS models generate intergranular crack paths in a given microstructure with grain size and aspect ratio and with a defined inclination criterion represented as a critical J integral. Crack geometry data is passed from MATLAB to ANSYS, and the corresponding J integral for that geometry is passed back from ANSYS to MATLAB. The geometry is then extended by one grain boundary and the cycle continues until the end criterion, which is 2 mm of growth. This area allows the crack path to stabilise based on the assumed mechanism, while also being more computationally efficient than representing the full thickness. The parameters used in the initial investigation are those from the field, such that the resulting crack paths can be validated against field grown crack paths. Once validation has been performed, the variables can be modified to see the impact of changing the stress state or microstructural properties on the crack path.

4.4 Results

Cracks were propagated in a simulated microstructure with properties gained from EBSD (grain width of $8\mu m$, average grain aspect ratio of 0.5) and a critical J integral criterion corresponding to a straight crack depth of 0.55 mm (Figure 4.7). Some cracks grown in these circumstances can then be compared to the isolated cracks from the field (Figure 4.8). The smaller crack arrowed in the lower right image of Figure 4.8 is not considered as its growth would have been influenced by interaction from the larger, pre-existing crack to its right.

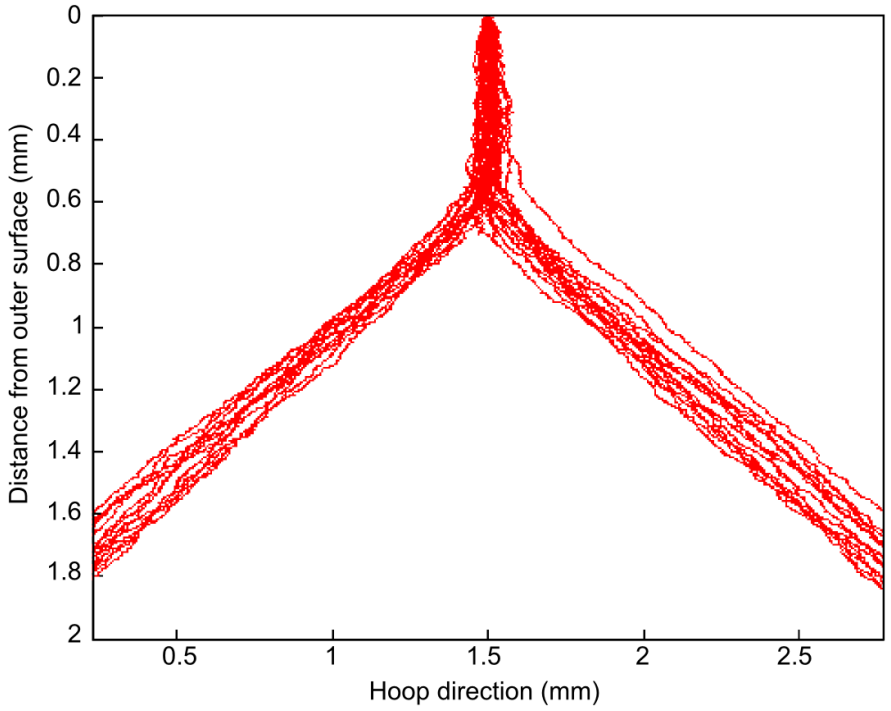

FIGURE 4.7: 30 modelled inclined SCC crack paths under a critical crack tip strain enhanced growth mechanism, with an average grain aspect ratio of 0.5.

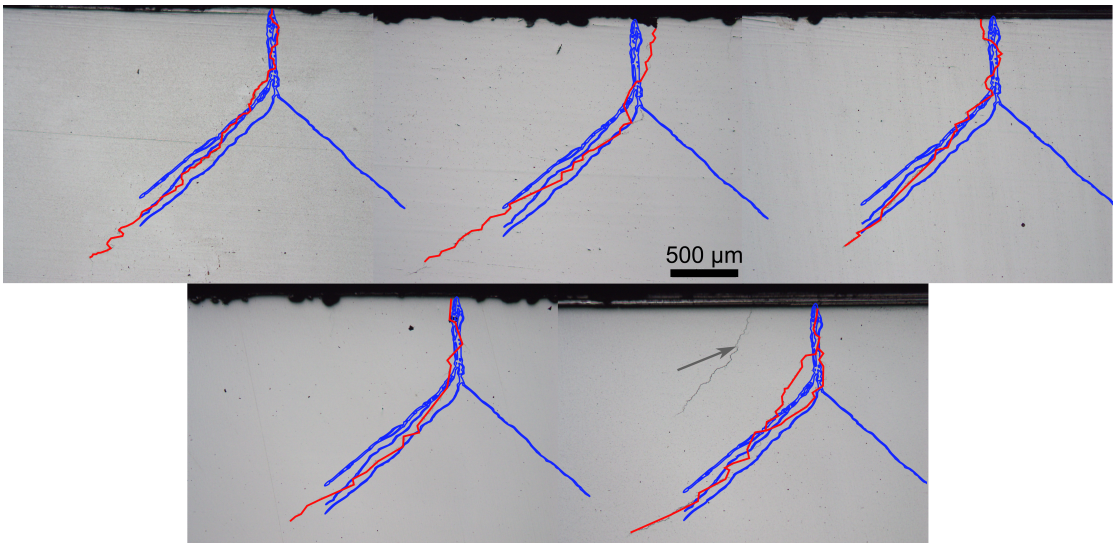

FIGURE 4.8: Five inclined SCC cracks with limited interaction from an Australian colony in red [14], with modelled 0.5 grain aspect ratio crack paths in blue. Arrowed crack is not considered due to presence of interaction from adjacent crack.

Figure 4.8 shows that the cracks grown by the model have a reasonable agreement with the cracks in the field, lending weight to the argument of crack tip strain dependant electrochemistry being a important driver behind inclined SCC. The curving nature of the cracks is represented rather well considering the simplicity of the model, which only considers geometric microstructural properties, a well as the critical strain growth criterion. More variation is seen in the real cracks due to the number of other influencing factors, such as interaction, possible residual stresses and strains, varying aspect ratio with depth and circumferential position, other microstructural variables (texture, vacancies, alloy concentrations) and varying electrochemistry. These factors can all account for the various deviations from the modelled cracks. An implication of this is that the crack tip strain criterion is of great significance to the inclined crack path, with variation influenced by the other variables. This can be further evidenced by the growth of a crack with a

criterion of film rupture of the weakest grain boundaries, which shows on average straight crack paths, even with the change in grain aspect ratio (Figure 4.9). Of the factors that are not included in the model, interaction is the one that could have the largest impact on crack path. Evidence for this lies in the fact that these cracks had relatively little interaction, and were fairly consistent, while cracks with more interaction can show vastly different crack paths. Regardless, the critical strain growth criterion seems to replicate the inclined cracking fairly well, with other factors contributing to the variations in the crack morphology.

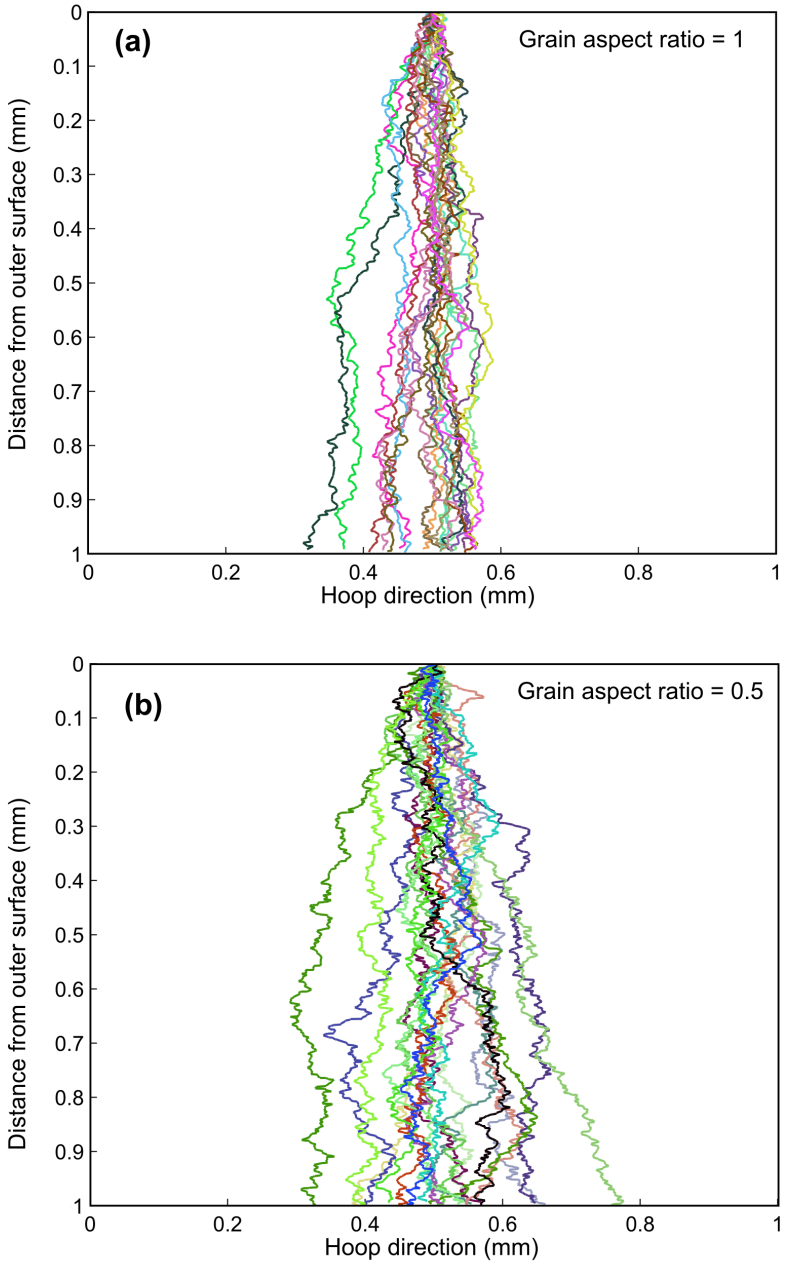

FIGURE 4.9: 20 modelled SCC crack paths under a maximum stress intensity factor film rupture based growth mechanism, with average grain aspect ratios of 1 and 0.5.

4.5 Extension: Further modelling

The effect of the grain aspect ratio was further investigated after the mechanism was seen to agree with real cracks. Two findings presented themselves during this investigation, (1) the grain aspect ratio can affect the final angle the crack path approaches, and (2) the rate with which it approaches that angle for the same critical strain. This difference is most easily visualised by modelling vastly different aspect ratios (Figure 4.10). Lower grain aspect ratios result in a greater inclination deviation, as well as taking longer before it stabilises on a steady state angle.

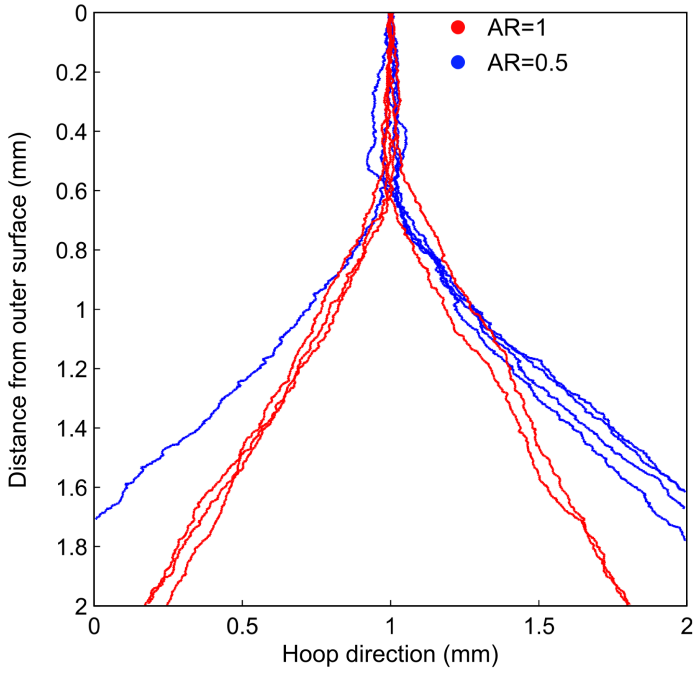

FIGURE 4.10: Five cracks with an average grain aspect ratios (AR) of 0.5 (blue) and 1 (red) showing the effect of grain aspect ratio on crack path.

Both of these results can be explained by looking at the calculated distribution of grain boundaries in the modelled space (Figure 4.11). The space with an average

grain aspect ratio of 1 has an even chance of propagating along any angle of boundary, however the modelled space with the lower aspect ratio has a far higher proportion of more horizontal boundaries, and as such the cracks will tend to travel more horizontally over time.

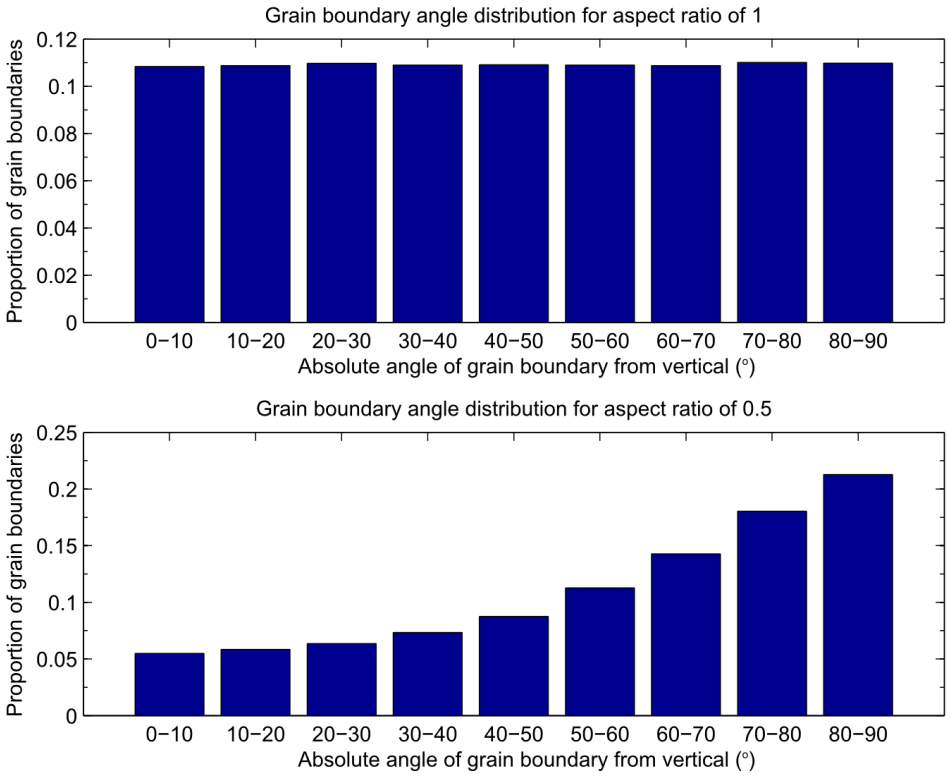

FIGURE 4.11: Distribution of the absolute grain boundary angles for average grain aspect ratios of 1 and 0.5.

Additionally, a crack with a higher inclination angle will have a lower stress intensity factor (as shown previously in Table 4.1, columns 3–5). This relationship between average grain aspect ratio and steady state growth angle can be calculated and quantified in 2D (Figure 4.12). The growth angle is relatively sensitive to aspect ratio, with a shift of approximately 5 degrees occurring from purely a change in aspect ratio from 0.45 to 0.55, which is the range found in the inclined SCC affected X65 pipes.

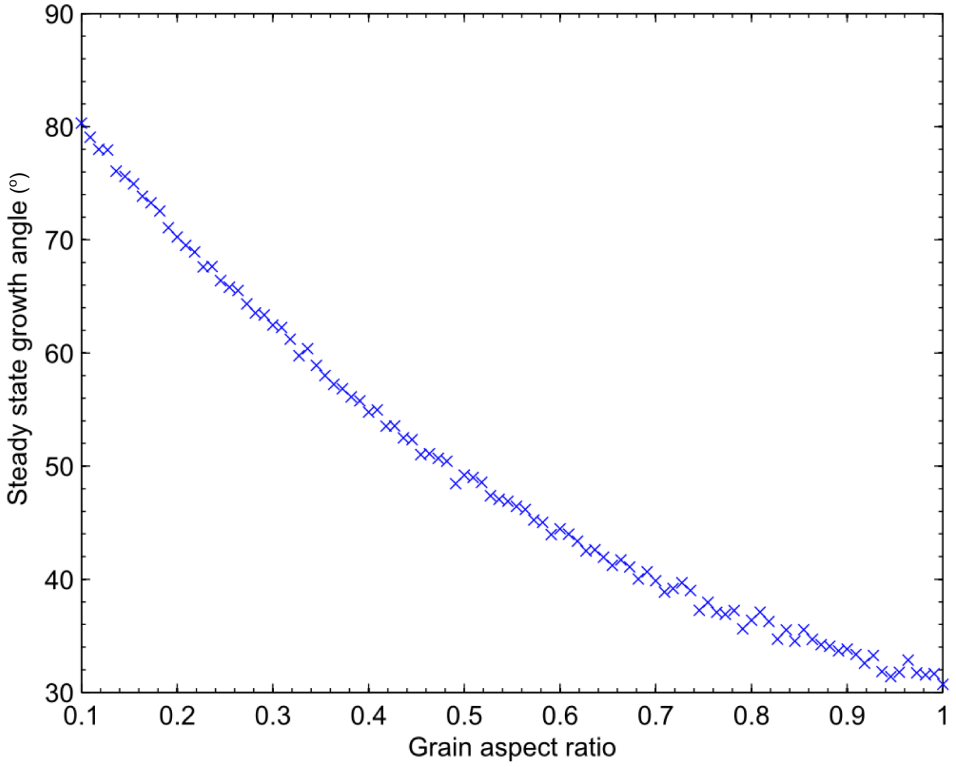

FIGURE 4.12: Distribution of the steady state growth angle over varying aspect ratios.

Crystallographic texture was also previously postulated to be a potentially influencing factor for inclined SCC growth [27, 99]. Texture has previously been shown to have an effect on the initiation and growth rates of SCC, particularly as low angle boundaries and other special boundaries are resistant to SCC while high angle boundaries are susceptible [48, 49]. Studies on the texture of the inclined SCC affected X65 against SCC resistant X65 showed a lower density initiation resistant texture in the SCC affected steel [29]. That study did not however look at whether the susceptible textures were evenly spread across all grain boundary angles, or whether they are more common in the direction of inclination. A MATLAB code

was generated for this study in order to assess the texture distribution on various grain boundary angles, which picked the angle of over 1000 grain boundaries from an EBSD scan of the centreline of SCC affected X65. The results of this are shown in Figure 4.13, which illustrates the distribution of susceptible and resistant boundaries in 5 degree grain boundary angle increments, and shows a similar total distribution to the simulated microstructure in Figure 4.11. The graph shows that there does seem to be some difference between the trends of resistant and susceptible boundaries. The relation can be quantified more simply by looking at the percentage of resistant boundaries for each 5 degree partition (Figure 4.14). We can see that grain boundary angles between 30 and 70 degrees have a higher proportion of resistant boundaries, while grain boundary angles under 20 degrees have a much lower proportion. This should act against the propensity for inclination.

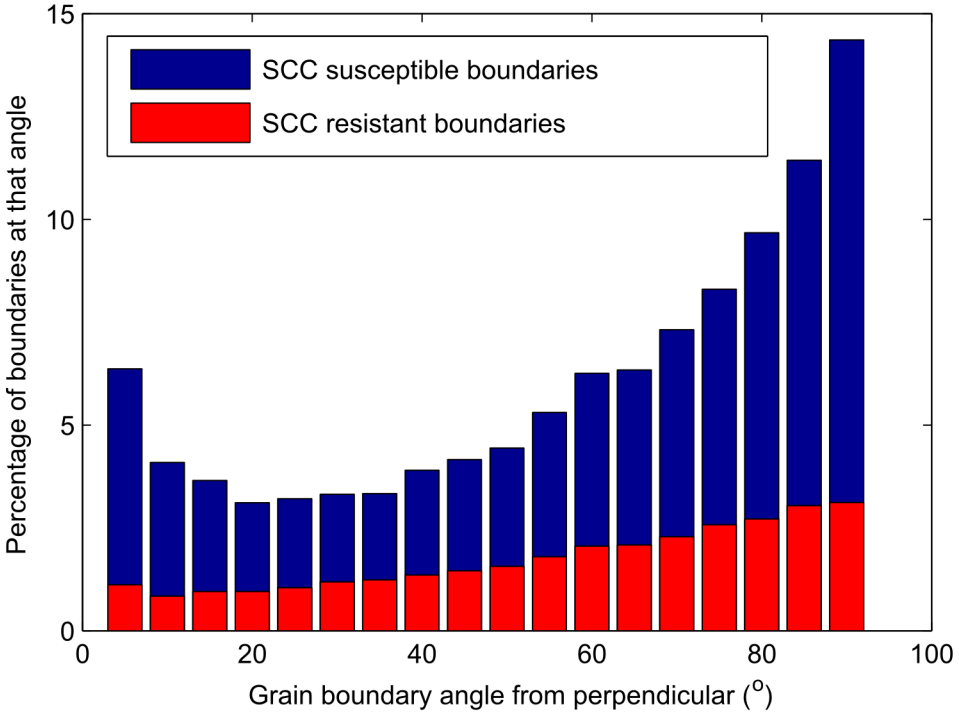

FIGURE 4.13: Texture distribution for various grain boundary angles for susceptible X65 pipe. Red represents the resistant boundaries while blue represents the susceptible boundaries.

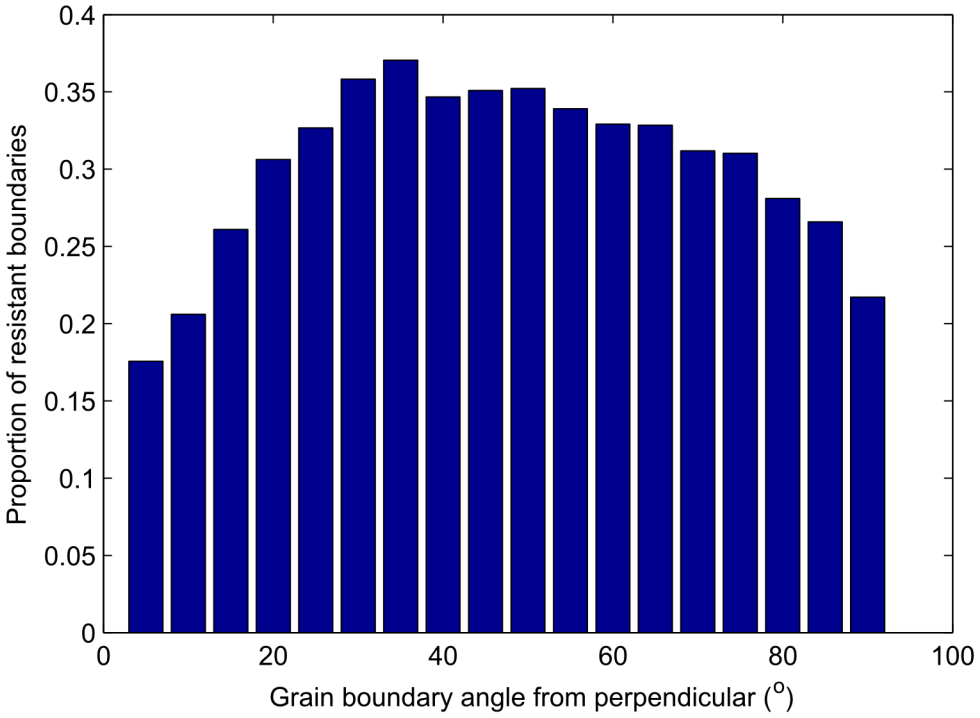

FIGURE 4.14: Proportion of resistant boundaries for different grain boundary angles.

The texture distribution was then used as an input for the growth code developed earlier in this chapter, with high angle boundaries gaining preference for failure over low angle boundaries. Modelled crack paths are shown overlayed on the cracks without texture in Figure 4.15. The influence of the texture appears to have a slight effect on the crack path, causing slightly less severe inclination. This may not be the case in reality however, as the model neglects the 3D nature of the cracks. In the full 3D scenario, the resistant boundary can be grown around entirely with the crack appearing to skip that boundary in the 2D plane. In any case, while texture has been linked to SCC susceptibility in general, it seems to have a minimal impact on the crack path in this instance.

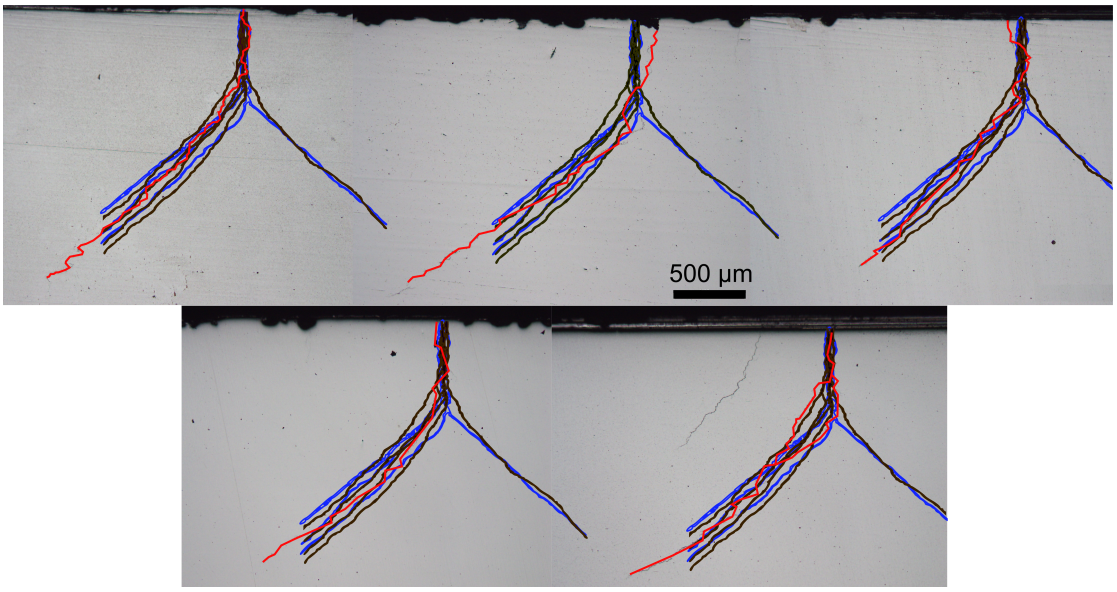

FIGURE 4.15: 5 cracks grown with included textural effects (black) overlayed on 5 non-texture inclusive simulated cracks (blue) and a field grown crack (red).

4.6 Discussion

The assumptions of the model lead to some minor deviations between the modelled cracks and the observed field cracks. For this model, it is assumed that there is no interaction from other neighbouring cracks. This assumption is rarely applicable to an SCC colony where interaction is one of the key driving forces behind the propagation. It is a point to note that the cracks observed were relatively isolated which would minimise the effects of interaction. Microstructural features such as vacancies and manganese sulphide inclusions were also neglected in the model, which in the field would have some effect on the crack path. There also is a source of small error in the model coming from the 2D representation of the crack, as the crack tip would be influenced by the movement of the rest of the crack front. Most of these assumptions have resulted in minimal errors as discussed in Section 4.4.

Assuming crack tip strain enhanced electrochemistry is the mechanism of inclined SCC, as is suggested by the results of this chapter, then certain implications can be projected onto adjacent topics of interest. These include the implications on growth rates, industry evaluation methods and manufacturing methods. Additionally, it provides clearer opportunities for further work in the understanding and prevention of inclined SCC.

The growth rate of an SCC crack is dependent on both rate of film rupture, and the current density (Equation 4.1). For the crack to grow at a preferential rate along the angle, its crack growth rate in that direction must be greater than the crack growth rate in the vertical direction. As during the turning portion of the growth, the crack alternates between inclined and straight propagation in small steps, the growth rates of these two sections will be similar, albeit in different directions. This means that for a final growth angle of 50 degrees (corresponding to a grain aspect ratio of 0.5), the radial growth of the crack will be 64% (cos(60)) of the equivalent straight crack from the inclination depth to the point of stabilisation. However, after the steady state region is reached, the crack growth rate will start to increase due to the increasing strain at the crack tip and corresponding current density, and it is predicted that the cracks should preferentially continue with a stable angle for the remainder of growth unless encountering a barrier in interaction or microstructural feature. This could potentially result in an increase in rate of radial crack growth and hence depth for very long inclined cracks relative to straight cracks, but further investigation is required to determine exactly what level of crack strain would be required, including quantitatively ascertaining the

crack tip strain dependant electrochemical response of the affected steel. This is discussed further in Chapter 5.

Industry evaluation methods for SCC (Canadian Energy Pipeline Association, CEPA) rely on both rate of crack growth, and potential for interaction [11]. This chapter has shown that inclined cracks could have different crack growth rates than those assumed by CEPA guidelines (even in a benign manner). Additionally, this work can help to quantity and assess the CEPA interaction guidelines. As the cracks grow in the direction of highest strain, stress shielding will still prevent adjacent parallel cracks from coalescing. Additionally, collinear cracks should still behave in the same manner as for straight cracks since inclination occurs in the hoop direction. The potential for unexpected interaction comes with closely spaced cracks with some hoop and axial offset, which incline towards each other subsurface (Figure 4.16). This configuration of cracks would allow an interaction region below the surface, but reduces the stress shielding effects that would retard the crack growth at the interacting surface tips. This crack configuration could create enhanced zones of strain at the leading and trailing edges of the subsurface cracks, and potentially cause subsurface coalescence with no obvious interaction on the surface. This potential subsurface coalescence would be outside of the stress shadow region as predicted by CEPA [11]. This interaction is a region of interest for future modelling endeavours, Chapter 6 determines whether closely spaced inclined cracks can still be assessed by CEPA guidelines.

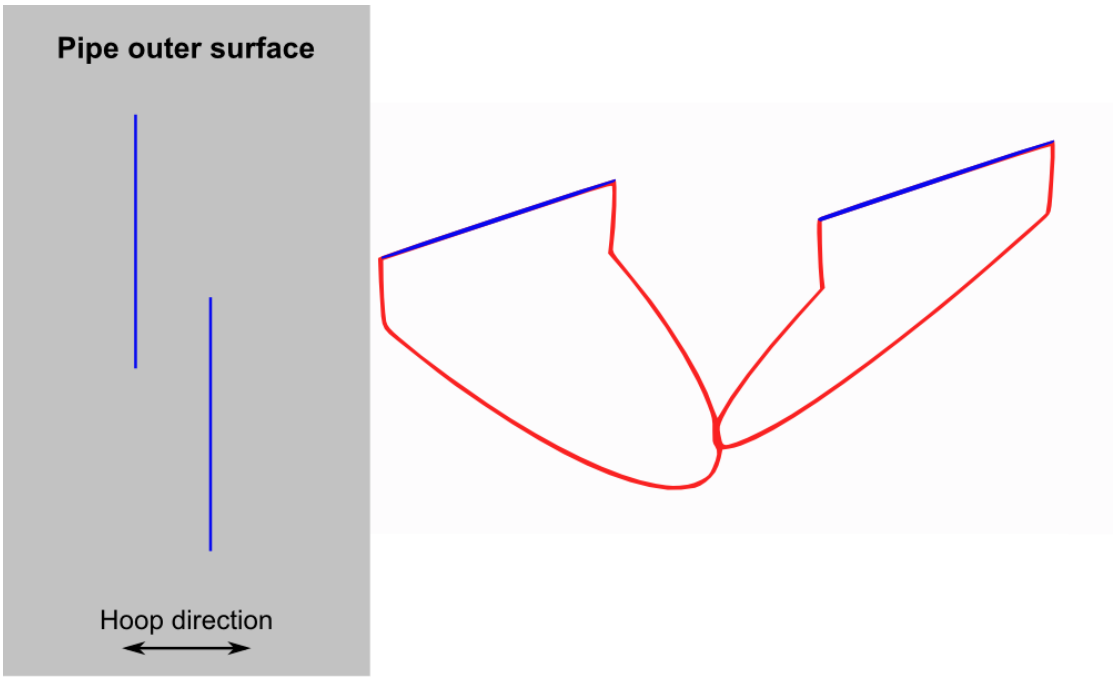

FIGURE 4.16: Schematic of potential unpredicted interaction between equal length parallel non-collinear inclined cracks. The blue lines represent the crack mouths on the outer surface of the pipe, while the red lines represent the crack front within the thickness.

Manufacturing methods are also of interest, as there could be potential to introduce inclined SCC resistance into pipe walls in the future. Many of the methods have changed since these X65 pipes were manufactured over 30 years ago, yet some areas are still of interest. Recrystallisation after rolling of the steel can move the grain aspect ratio back to an average of 1, and reduce the residual plastic strains that could aid the strain enhanced inclination. Additionally, the strain dependant electrochemistry of pipeline steels could be considered during steel design and manufacture, to provide greater understanding of whether SCC crack paths are likely to incline. More research is needed to determine why the X65 electrochemistry results in it being susceptible to inclined SCC in areas of high strain.

4.7 Conclusion

Crack tip strain dependant dissolution has been identified as being a possible cause for inclined SCC. A model has been developed using a bimechanistic growth algorithm of stress driven film cleavage and strain enhanced electrochemistry which can simulate inclined SCC cracks. These simulated cracks have shown to have similar crack paths to those seen in ex-service samples with equivalent microstructural geometric properties. This qualitative validation lends weight to the suggestion that this bimechanistic growth is a potential mechanism for inclined SCC in high pressure gas pipelines. Grain aspect ratio has also been investigated, and was found to have an influence on the appearance of the inclination, as well as the final steady state inclination angle. In particular, lower grain aspect ratios result in higher inclination angles with the angle being relatively sensitive to the grain aspect ratio. The distribution of SCC resistant textures was also assessed for its influence on crack paths, and was shown in this instance to have a relatively minor role. The model suggests that through thickness crack growth rates are fastest when the crack first initiates and grows perpendicular to the pipe free surface. After the crack starts to incline, the through thickness crack growth rate would slow down until the crack reaches a stable inclination angle, after which the through thickness crack growth rate will increase once again, and will be the focus for Chapter 5. Various possible implications for crack growth rates, interaction limits, and manufacturing methods have been discussed with some areas requiring further investigation identified. Now that the likely mechanism governing SCC inclination has been determined and examined with good agreement to field cracks,

the impact that this mechanistic shift has on SCC crack growth rates is assessed in the next chapter.

Chapter 5

Influence of strain on crack growth rate

5.1 Introduction

The previous chapter demonstrated that a strain enhanced electrochemistry mechanism is the likely cause of SCC inclination. This mechanism has various implications, particularly on the crack growth rate. SCC crack growth rates are dependent on current density, and current density has been shown to be dependent on strain in the literature review (Chapter 2). This implies that if the cracks follow the path of highest strain, the current density and hence crack growth rate would be altered. The radial crack growth rate would also be affected by the angle at which the crack is growing. The interplay between the change in current density and the crack path, and the impact on crack growth rates warrants investigation.

This chapter explores the effect of the mechanistic shift on crack growth rates. This achieves the second objective outlined in the Scope of "combining the found mechanism with proven and compatible SCC growth equations to predict the effect of the mechanism and inclination on crack growth rate." Not only does achieving this objective further the scientific understanding of inclined SCC, but it also can provide real world implications for inclined SCC management in pipelines.

In order to accomplish this objective both experiments and simulations were conducted. Experiments serve the purpose of providing insight into the degree that current density can be affected by bulk strain, while the simulations combine this with an industry validated equation [20, 21] and the geometric properties of inclined SCC to demonstrate the potential implications on the growth rate. This chapter first presents a brief background of crack growth rates in pipelines before outlining the methodology and results for the experiments and modelling respectively. Further work is then suggested to assist the understanding of the interplay between current density and micro-strain in the process zone of the crack tip, as well as contribute additional significance to the simulated results.

5.2 Background

Strain has been shown to have an effect on the electrochemical behaviour of steels, as discussed in Chapter 2, and has been identified as a possible driving factor in inclined SCC growth in X65 pipeline steels in Chapter 4. Since these cracks appear to be following the areas of higher crack tip strain, and strain is linked to current

density, it is logical to question the effect of this mechanistic shift on the growth rates of inclined cracks. Specifically, the equations that govern SCC growth can be analysed for how they would be affected by a change in strain and current density. The implications to industry of a growth rate that differs from that predicted for a straight crack are also of interest, as traditional prediction equations may under or overestimate the loss of wall thickness for an inclined crack.

The general mechanism of high pH SCC is understood as a combination of anodic dissolution advancing the crack front, and passive film formation which prevents the exchange of ions for dissolution. The stresses will eventually crack the film through fatigue or creep and expose the bare metal allowing further exchange of ions. The dissolution portion of this mechanism is described in work by Leis and Parkins [10] with Faraday's law, which is shown in Equation 5.1 (repeated for ease of reading).

$$\dot{a} = \frac{M_w}{zF\rho} i_a \tag{5.1}$$

This equation represents the upper limit of SCC growth which would occur if there was no film formation occuring. However the film formation does play a significant role in retarding the growth of SCC. In either case, this equation shows a proportional relationship between current density and the crack growth rate, as a higher current density implies a higher rate of transfer of metal ions.

Various authors have used an expanded form of Faraday's law which takes into account the strain rate of the crack tip, which incorporates the effect of the passive

film [7, 80]. This equation they is shown in Equation 5.2.

$$\dot{a} = \frac{M_w}{zF\rho} Q_F \frac{\dot{\epsilon}_{ct}}{\epsilon_F} \tag{5.2}$$

Here Q_F represents the charge passed in time between two passive film ruptures, $\dot{\epsilon}_{ct}$ is the crack tip strain rate, and ϵ_F is the strain required to rupture the film. This equation still shows a proportionality between the current density and the crack growth rate, as the charge passed between film ruptures, Q_F, is proportional to current density. Calculating the charge passed between ruptures is not so easy however, as the rate of exchange of ions varies between the maximum value specified by the current density and the minimum value once the film is at maximum thickness. This can be calculated by an integral of current density over one full film formation-rupture cycle. Lu [21] expanded on this and added some more easily obtainable material constants in Equation 5.3. This equation has to be modified for this work however due to the presence of plane strain and an error in the derivation of Equation 5.3 in the original paper. The plane strain correctly derived version used in this study is shown in Equation 5.4.

$$\dot{a} = (A_0 B i_a)^{\frac{1}{1-n}} \left[ln \left(\frac{K_M^2 - K_{ISCC}^2}{\pi r_0 \sigma_Y^2} \right) \right]^{\frac{n}{1-n}\frac{N+1}{N-1}} \tag{5.3}$$

$$\dot{a} = (A_0 B^n i_a)^{\frac{1}{1-n}} \left[ln \left(\frac{K_M^2 - K_{ISCC}^2}{3\pi r_0 \sigma_Y^2} \right) \right]^{\frac{n}{1-n}\frac{N+1}{N-1}} \tag{5.4}$$

In these equations, A_0, B, n, N, K_{ISCC} and σ_Y are material or electrochemical constants (explained in more detail in Section 5.5), K_M is the mean stress intensity

factor, and i_a is the peak current density. The power to which the current density is raised represents the integral over the full film rupture cycle. This shows a power relationship between the current density and the crack growth rate, although an inclined crack has a lower stress intensity factor than a straight crack. In all the equations used to predict high pH SCC crack growth rates, an increase in current density will give an associated increase in crack growth rate. This means that if the cracks are following the direction of highest strain and strain has an influence on current density, then the cracks are likely to grow faster, although not necessarily faster in the radial direction.

Inclined SCC tends to deviate between 30 and 60 degrees from the normal in the X65 steel samples that have been analysed. This value range is seen both in the field grown cracks and the simulated cracks. This means that the radial growth rate of the inclined cracks will be less than the growth in the inclined crack front plane. This relationship can be described in Equation 5.5, where $\dot{a}_r$ is the radial growth rate, and θ is the angle of inclination. For an angle of 50 degrees, $\cos(\theta)$ is 0.64. This means that the inclined crack growth rate could potentially be 1.5x higher than the straight crack but remove wall thickness at a slower rate. This relationship is interesting to quantify, particularly whether the reduction in radial growth rate due to the inclined growth direction could offset the increase in growth rate due to the increase in current density along the higher strained grain boundaries.

$$\dot{a}_r = cos(\theta) \cdot \dot{a} \tag{5.5}$$

Despite having equations that can describe the crack growth rate, various variables are still unknown and present challenges for simulation and crack growth rate prediction. Firstly, the current density at the crack tip is unknown for both the zero strain and shear plane strain cases. Polarisation curves at various strain levels have been generated to assist with this unknown, but two more unknowns that prevent quantitative modelling remained. The potential at the crack tip varies, and the exact value is unknown. This can be circumvented by selecting the potential that provides the worst case current density. Additionally, microstrain at the crack tip is highly sensitive to the local geometry and cannot be easily related to a fairly uniformly strained sample. This can again be taken into account by plotting the various cases to find the amount that the current density would have to increase in order for the radial growth rate of an inclined crack to exceed the rate of a straight crack.

Predicting growth rates of SCC colonies for pipelines is important for industry as it informs the inspection intervals, and the safe time remaining before a repair is necessary. Prediction is inherently challenging as crack growth rates can vary anywhere from zero to the faradaic limit even within one colony at a given time. This tends to lead to broad approximations, however it is important to establish a reasonable limit for the fastest that a colony would be expected to grow. Two obvious methods are available for predicting the growth rate, predictive models such as Leis and Parkins [10], Song et al. [20] and Lu [21], or extrapolation from historical data. Extrapolation is a good method for pipelines which have existed for long periods of time with fairly stable soil conditions, as the growth rates

should be fairly consistent. Predictive models on the other hand are useful when pipelines are being placed in new locations, or with new steels, and can also be a lot cheaper than collecting colony depth data. Considering the unknowns in the growth rate for inclined SCC, the only reliable method available to industry is extrapolation which is both costly and restrictive, as well as being potentially risky as there is no guarantee that the worst case crack growth rate would have yet been observed. Ideally the crack growth rates would be predictable with a model, which would allow steels that have been identified as candidates for inclined SCC to be properly maintained in new conditions. For existing pipes, a combination of both predictive modelling and data extrapolation is more robust and allows a method to ensure the inspection interval is reasonable.

Current density is one of the key parameters governing crack growth rates of SCC in X65 steel pipes, and is a fundamental variable used to predict crack growth rates in industry. Strain and current density have shown a link previously and thus in areas of high strain, the crack growth rate could vary significantly. Since the cracks appear to be following the direction of highest strain, it is integral to find the relation between current density and strain for X65 steels.

5.3 Experimental study

The nature of the relation between strain and current density for inclined SCC affected X65 steel is unknown. Whether residual plastic strain or applied elastic strain is of greater impact is also undetermined. Experiments were conducted to

quantify the interplay between current density and both residual plastic strains and applied elastic strains for inclined SCC affected X65 steel. These experiments were conducted with the intention of trying to understand why X65 specifically has shown inclined SCC and not other materials. These experiments provide a basis for sensitivity of current density to bulk strain, and can be used for comparison with other steels to determine if the current density for those steels are more or less sensitive to strain than for X65. This can then help predict whether other steel grades (such as X70 or X80) would be likely to present with inclined SCC. This section will outline the methods used to conduct these experiments.

5.3.1 Material

The material used was a ferritic API 5L grade X65 low carbon steel (0.085 wt.%C, 0.022 wt.%P, 1.58 wt.%Mn, 0.0045 wt.%S, 0.33 wt.%Si, 0.054 wt.%Nb, bal. Fe). Samples came from the pipe sections used in a previous study [29], extracted from the field after approximately 30 years of service. Nominal pipe diameter and wall thickness were respectively 864 mm and 8.3 mm. Pipes were manufactured through the UOE production process. The original coating was coal tar enamel.

5.3.2 Tensile test specimen preparation and mechanical testing

Flat dogbone tensile specimens were cut from the centreline of the pipe sections, in the longitudinal direction. Gauges were 5 cm length, 0.26 cm width and 0.28

cm thickness. The mechanical properties of the steel specimens (yield and ultimate tensile strengths) were determined by a typical tensile test using an Instron machine to strain the sample at 5mm/min. Vickers hardness was determined at a load of 0.5 kgf, three indents were made per sample and results were averaged.

5.3.3 Electrochemical measurements

5.3.3.1 Evaluation of the applied strain on the X65 electrochemical behaviour

Tensile specimens were exposed to the simulated high pH SCC medium defined in the literature: 1N carbonate + 1N bicarbonate solution at 70 ^{o}C [100]. The exposed surface of the specimens was limited to one face of each specimen gauge by covering the other faces with a layer of silicon rubber on the top of a layer of epoxy resin. Care was taken to avoid crevice effects. The exposed surface was thereby 0.91 cm^2 in area (3.5 cm length on 0.26 cm width). Surfaces were machine ground finished. A LIST machine [29] was used to apply different amount of loads (% of the measured yield strength) on the specimens. At each applied load, potentiodynamic curves with a scan rate of 0.1 mV/s were recorded from -1 $V_{Ag/AgCl}$ to 0.9 $V_{Ag/AgCl}$. Before each potentiodynamic measurements, a cathodic potential of -1 $V_{Ag/AgCl}$ was applied to the specimens for five minutes in order to remove the oxide layer formed on their surface, in air or during the previous experiments. At least three potentiodynamic curves per applied load were recorded to check the reproducibility of the results. The electrochemical tests were conducted with a Gamry interface

1000^{TM}, using the specimens as the working electrode, a platinum mesh as the counter electrode and a saturated silver/silver chloride electrode as the reference. The reference electrode was maintained at room temperature and connected to the electrochemical cell with a Luggin probe.

5.3.3.2 Evaluation of the residual strain on the X65 electrochemical behaviour

A series of 7 samples strained at different levels was produced (0, 2.2, 3.46, 5.4, 8.11, 11.6 and 14.8% strain). The strained dogbone gauges of these samples were then cut, embedded in epoxy resin and ground down to 1200 grit (Struers). The area of the exposed surface was approximately 0.6 cm^2. Samples were then immersed in the high pH SCC media at 70 ^oC and potentiodynamic tests as described in Section 5.3.3.1 were conducted.

5.4 Experimental results

The methods outlines in Section 5.3 produced mechanical and electrochemical results. These results can help give insight into the conditions that cause a current density increase in X65 steel, and thus on inclined SCC.

5.4.1 Mechanical tests

Figure 5.1 shows a typical stress-strain curve obtained for the X65 steel tested. The yield and ultimate tensile strengths were measured as 460 MPa and 590 MPa respectively. These values were consistent with X65 API 5L grade steel.

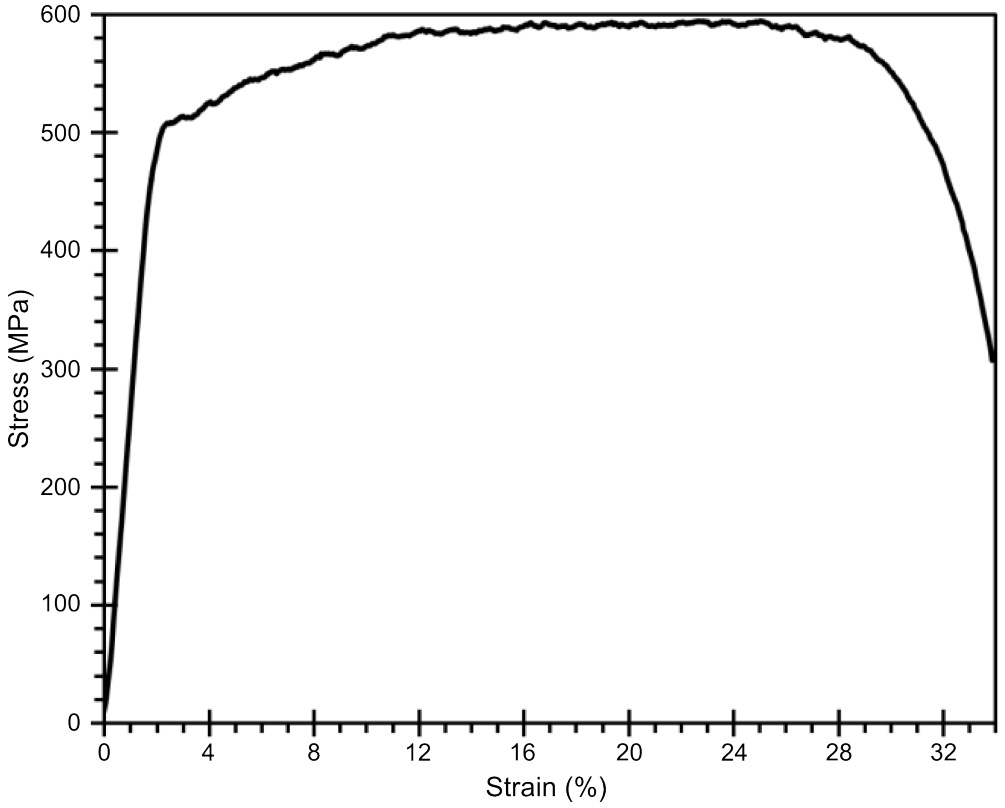

FIGURE 5.1: Stress strain curve for the X65 steel tested.

The hardness of the steel together with the hardness of the samples strained at 2.2, 3.46, 5.4, 8.11, 11.6 and 14.8% were measured and are presented in Figure 5.2. It can be seen that the microhardness of the X65 steel increases linearly with the amount of residual strain as is expected due to the strain hardening phenomenon.

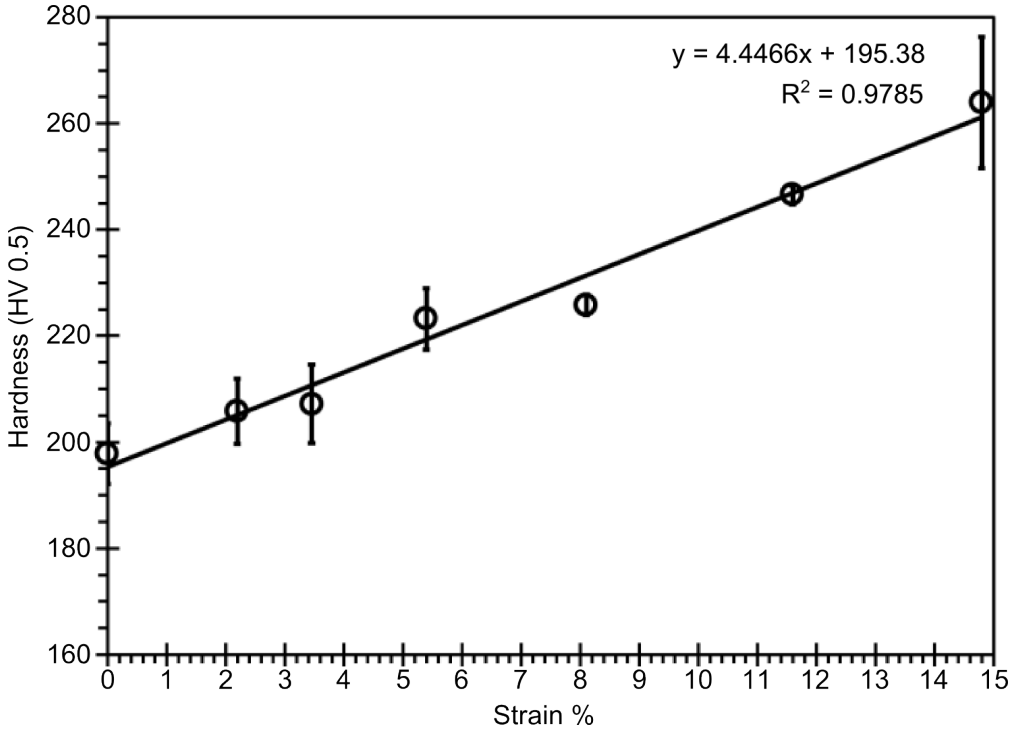

FIGURE 5.2: Hardness values for the X65 steel strained at different levels (average of the 3 measurements for each samples).

5.4.2 Electrochemical measurements

5.4.2.1 Effect of the applied strain on the X65 electrochemical behaviour

The polarisation curves recorded for different levels of residual plastic strain of the X65 steel are shown in Figure 5.3. It can be seen that the anodic current densities significantly increase with the increase of the elastic strain (for stress from 0 to 100% of YS) and the plastic strain (for a stress of 110% of YS). The corrosion potential tended to decrease with the increase of the applied strain.

According to the mechano-chemical theory developed by Gutman [61] the electrochemical corrosion potential of the steel is affected by the external load. An

external tensile load is expected to decrease the potential of the steel and enhance its corrosion activity [101]. Figure 5.3 shows a slight negative shift of 15 mV of the corrosion potential for the samples strained in the elastic range, and 30 mV for the sample strained in the plastic range. Additionally on the anodic edge of the SCC range, an increase in current density of up to 300% is observed at a potential of -500 $mV_{Ag/AgCl}$. This could have implications of up to a four times increase in the faradaic limit should the crack tip conditions be at a similar potential. According to the mechano-chemical theory also the anodic dissolution rate of the steel is expected to be accelerated by the external stress/strain [57] as observed in Figure 5.3.

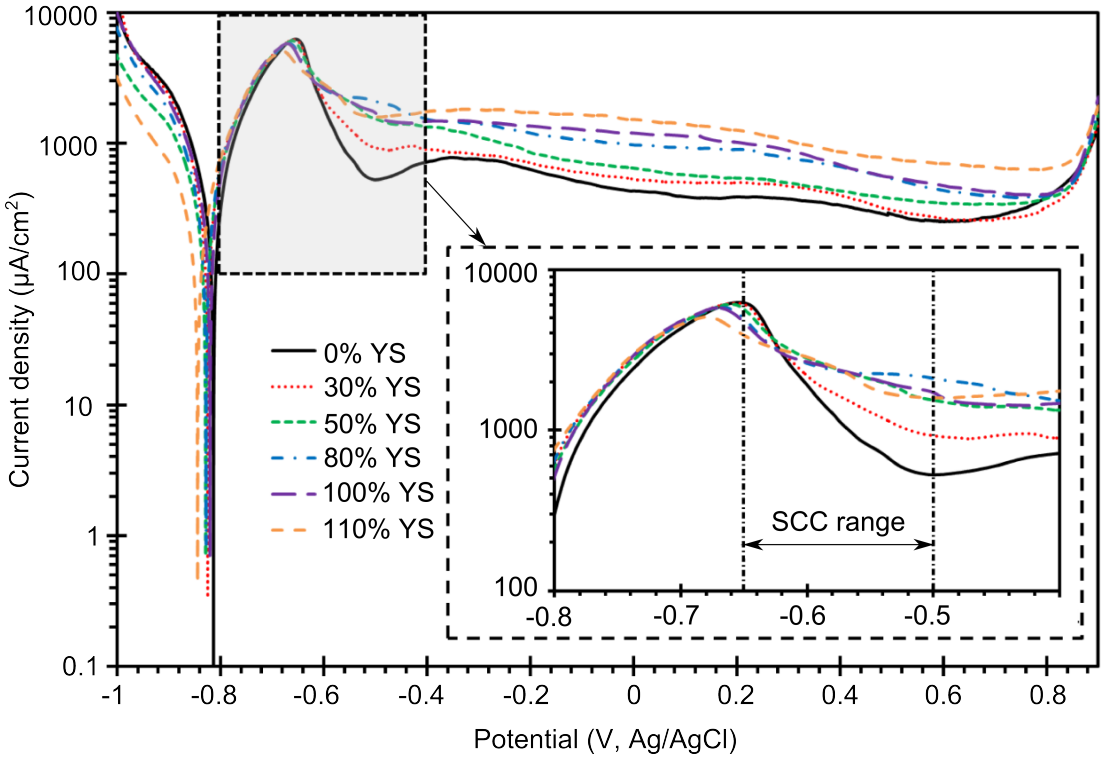

FIGURE 5.3: Polarisation curves for samples strained at different level in high-pH SCC medium with inset close-up of SCC range.

5.4.2.2 Effect of the residual strains on the X65 electrochemical behaviour

The polarisation curves recorded for samples strained at different level are presented in Figure 5.4. In this case no external load is therefore applied, and a very limited variation of the corrosion potential is observed. The residual strains do not significantly increase the current densities in the SCC region (within the active peak from -0.68 to -0.53 $V_{Ag/AgCl}$) suggesting that approximately the same amount of charge (supplied by the iron dissolution) is needed for the passive film to form. However, the residual strains significantly increase the current densities in the passive region suggesting that a higher amount of iron dissolution is needed to maintain the passive film formed. Since the lattice of the samples is distorted by the plastic strain, the dissolution of the steel may be stimulated [56]. The stability of the passive film is thus decreased with the presence of residual strains.

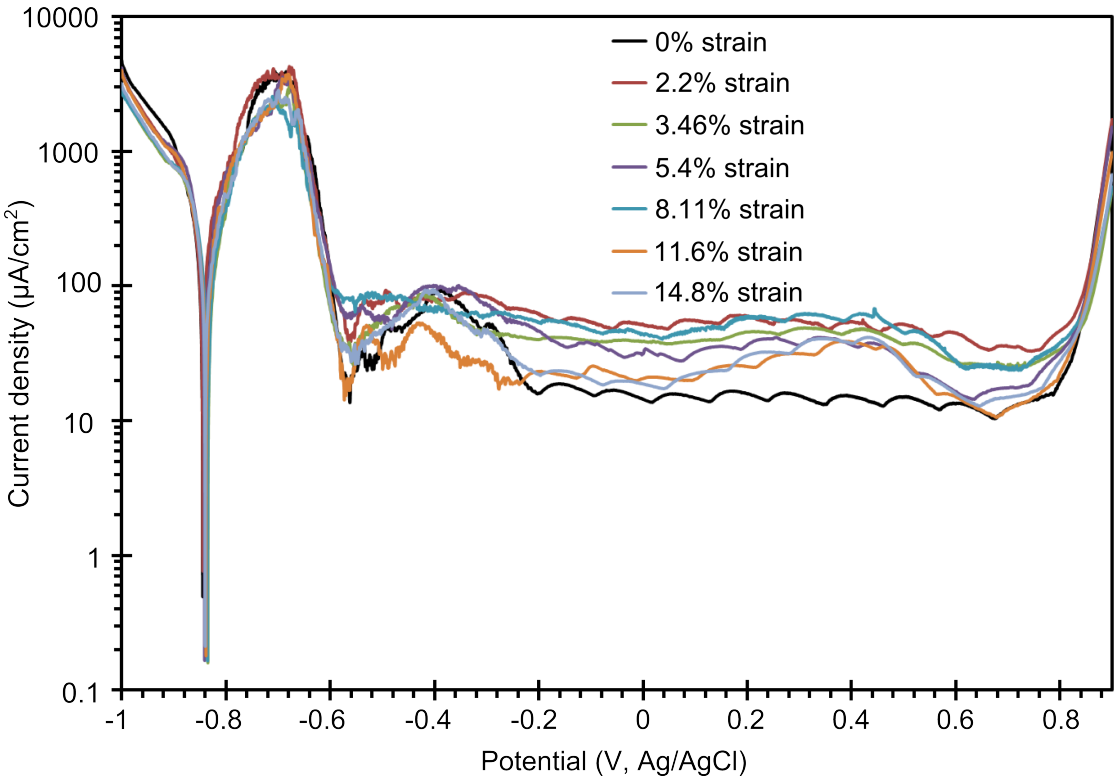

FIGURE 5.4: Polarisation curves for samples at different level of residual strain in high-pH SCC medium (no external load applied).

The results seem to indicate that applied strains have greater effect on the current density than residual strains in the SCC region. A large increase in current density was observed between 0% bulk strain and yield bulk strain, thus a similar relation could be expected at the different angles about the crack tip. The effect of such a change on crack growth rates will be explored with the use of simulations in the following sections.

5.5 Crack growth rate modelling

The experimental results of how current density varies with strain provide reason to believe that SCC growing along highly strained areas at the crack tip may have

a higher current density and potentially a higher growth rate than straight SCC. While it is difficult to relate macroscopic strain to local strain at the crack tip, clearly there should be some influence of the local strain on the current density. The theoretical stress singularity at the crack tip also makes it unreliable to quantitatively pair a current density increase from macroscopic strain to the current density increase seen along a locally strained grain boundary at the crack tip. Furthermore, the exact potential at the crack tip is not known which makes an equivalency between the polarisation curve and crack tip undependable. Nevertheless, the ranges for which the current density changes are known (up to 300% in the SCC region) and thus the growth rate for an inclined crack can be estimated for different ranges of current density. This could then serve as a basis for crack tip current density mapping in the future.

The growth rate of a high pH SCC crack is governed by the dual process of dissolution and passive film formation. The interdependency has been characterised in Equation 5.6 (repeated from Section 2.5.2 for ease of reading), which has been validated against industry growth rate data [20, 21]. A_0 and B are defined in Equations 5.7 and 5.8. The parameters used in these equations are summarised in Table 5.1.

$$\dot{a} = (A_0 B^n i_a)^{\frac{1}{1-n}} \left[ln \left(\frac{K_M^2 - K_{ISCC}^2}{3\pi r_0 \sigma_Y^2} \right) \right]^{\frac{n}{1-n}\frac{N+1}{N-1}} \tag{5.6}$$

$$A_0 = \frac{1}{1-n} \frac{M}{zF\rho} \left(\frac{t_0}{\epsilon_F} \right)^n \tag{5.7}$$

$$B = \frac{2N}{N-1}\frac{\beta\sigma_Y}{Er_0} \tag{5.8}$$

TABLE 5.1: Definition of parameters used for growth rate calculation, and the values used for those parameters.

Symbol	Description	Value used
$\dot{a}$	Crack growth rate	N/A
i_a	Crack tip peak current density	Varied
n	Repassivation kinetic exponent	0.667 [21]
N	Strain hardening exponent (Ramberd-Osgood Law)	6 [21]
K_M	Mean stress intensity factor in a cycle	Varied
$K_{ISCC}(MPa\sqrt{m})$	Critical stress intensity factor for SCC in X65	15 (average of [21] and [20]
$r_0(m)$	Specific length for crack tip strain rate calculation	1×10^{-6} [21]
$\sigma_Y(MPa)$	Yield strength of X65	460
$M(kg/mol)$	Molar mass of iron	55.845×10^{-3}
z	Valence of iron	2
F (C/mol)	Faraday constant	96485
$\rho(kg/m^3)$	Density of iron	7.847×10^3
$t_0(s)$	Incubation of repassivation	0.01 [21]
ϵ_F	Rupture ductility of passive film	0.001 [21]
E (GPa)	Elastic modulus of X65	200 [21]
β	Rice's coefficient	5.08

Equation 5.6 mostly consists of material constants that would not vary for an inclined crack as opposed to a straight crack. For the purposes of the model it is assumed that only the current density and stress intensity factor vary, and the other parameters remain constant. This equation was then used to determine

crack velocities for three key current densities found in the potentiodynamic tests. The results of this are shown in Figure 5.5.

Figure 5.5 illustrates the effect of current density and stress intensity factor on the crack growth rate. In the figure the stress intensity factor ranges from 20 to 50 MPa$\sqrt{m}$ as the stress intensity factor for a straight crack under loading conditions seen in inclined SCC affected pipes before inclination is approximately 20 MPa$\sqrt{m}$ (crack inclines at approximately 0.55mm depth [14]). The equation is valid for stress intensity factors as low as the critical stress intensity factor as well, though no difference would be seen between straight and inclined cracks as this stress intensity factor would be seen during the straight section of growth. The three current densities chosen represent the peak current density, 57.6 A/m^2, as well as the greatest percentage difference between strained and unstrained at one potential, 21A/m^2 and 5.3 A/m^2 respectively at a potential of -0.5 $V_{Ag/AgCl}$. Equation 5.6 shows that the crack growth rate is proportional to the current density cubed, and thus the differences between growth rate for the different potentials in the SCC range are significant. The maximum current density was chosen for the growth rate comparison between straight and inclined cracks as this would provide the most conservative estimates of time to failure.

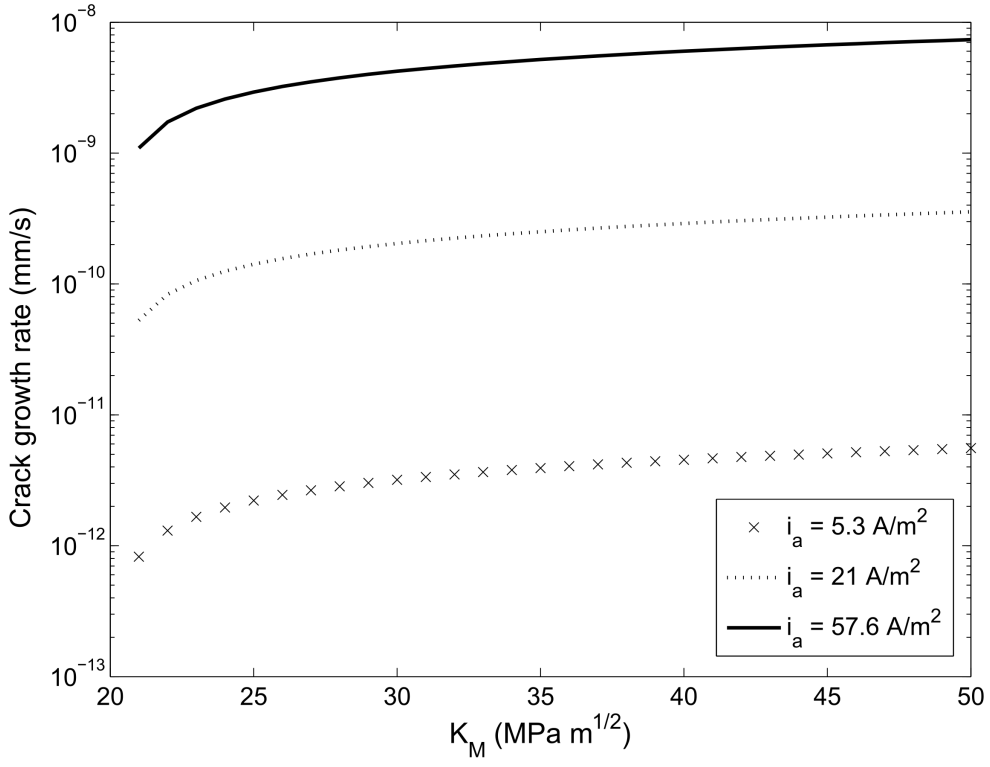

FIGURE 5.5: Crack growth rate against stress intensity factor for varied current densities using Equation 5.6.

The main point of interest of the simulation is to determine how large a difference in current density would be required to have an inclined crack exceed the crack growth rate of a straight crack. To accomplish this, straight and inclined SCC growth was simulated in MATLAB with Equation 5.6 as the governing equation. A time step of one hour was used in both cases, and radial growth/wall thickness loss was the output. This resulted in the growth rate for the inclined cracks being multiplied by $cos(\theta)$ where θ is the instantaneous growth angle measured from the radial direction (ie. for a straight crack $\theta = 0$), such that only the radial portion of the inclined growth was considered.

The inclined cracks are assumed to follow the path found in previous studies [14,

22, 102] and Chapter 4 where the inclination begins at 0.55 mm depth and slowly curves to a stable angle of approximately 50 degrees by 0.8 mm depth. During this curving section, the growth transitions between straight and inclined grain boundaries, which means that the growth rate is approximately equal to that of a straight crack with the same stress intensity factor between this 0.55 mm and 0.8 mm depth as discussed in Chapter 4. Once the inclined crack's path stabilises, the current density is assumed to increase by a ratio, F_n, of the straight crack current density, as shown in Equation 5.9. $i_{aStraight}$ was taken to be the maximum found in the potentiodynamic test for a conservative estimate of growth rate (57.6 A/m^2), and F_n was varied from 1 to 1.4 in the model.

$$i_{aInclined} = F_n i_{aStraight} \tag{5.9}$$

Validation of this method can be gained by comparing the straight crack growth values with those of Lu [21]. The parameters that are used in the Lu study are input to the MATLAB simulation and compared to the graph of Lu in Figure 5.6. Figure 5.6 shows a time to 7 mm depth for this present study (left) and the Lu study (right). Both graphs show a time to 7 mm of approximately 16 years at a current density of 80 A/m^2 when fatigue is neglected ($\dot{a}_e$ in the Lu study). The correlation of these results suggests that the methods used in this study provide realistic results.

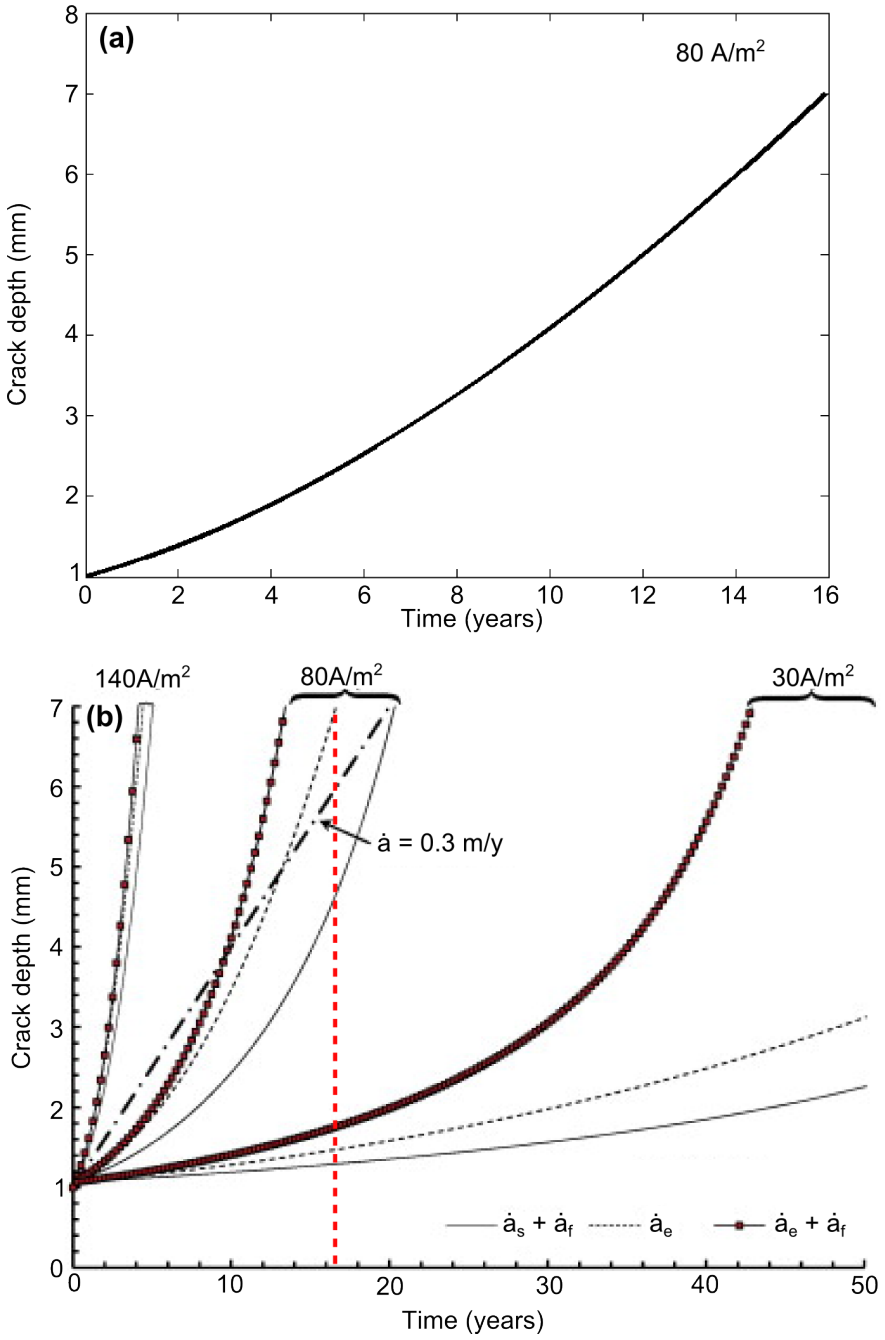

FIGURE 5.6: Validation of growth rate to 7mm with a current density of 80 A/m^2. (a) Simulation from this work shown, (b) Lu [21] shown on right. Time to 7mm of approximately 16 years found in both cases.

The current simulation is then extended to inclined cracks at a current density of 57.6 A/m^2 in Figure 5.7. It can be seen that the straight and inclined SCC growth over 50% wall thickness (4.15 mm) is very sensitive to F_n. The straight

crack reaches 1 mm depth, usually the minimum detectable depth, faster than an inclined crack for all presented values of F_n; however for a F_n of 1.2 or above, 50% wall thickness loss is achieved faster with an inclined crack. This means that only a 20% increase in current density is necessary in the highly strained areas around the crack tip for an inclined crack to grow faster than predicted for a straight crack over 50% wall thickness.

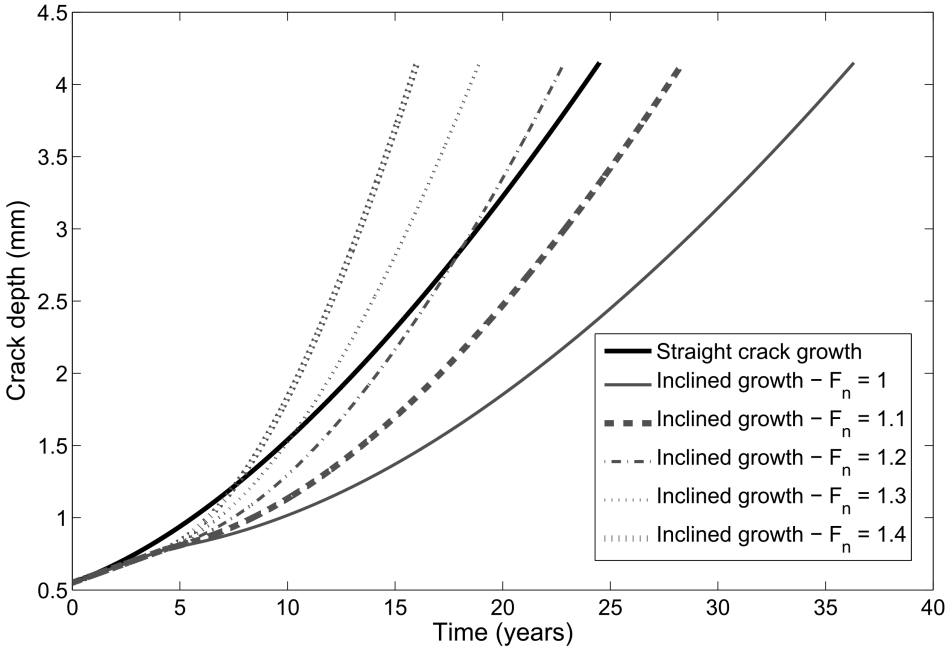

FIGURE 5.7: Radial growth for straight and inclined cracks for zero strain current density of 57.6 A/m^2. Inclined cracks grow with proportionally higher current density.

This finding reinforces the importance of strain mapping about the crack tip, where the current density increase can be quantitatively examined similar to work done by Tang and Cheng [33]. This would allow accurate predictions of inclined SCC growth rates in the future, and thus allow accurate decisions by industry on inspection intervals.

5.6 Discussion

The results of this chapter provide evidence of the strain dependent electrochemistry for the inclined SCC affected steel, and give some insight to the growth rate implications. Useful knowledge relating to the presentation and mechanisms of inclined SCC can be derived from this chapter. The implications for industry are also appreciable, but can be made more useful with the inclusion of future work. Some variables that are neglected and the impact that they can have on the results should also be addressed.

Several insights relating to the presentation of inclined SCC can be gleaned from this chapter. Firstly, applied strain appears to be of greater importance than residual strain in current density shifts, despite both showing some impact. This seems to indicate that the operating pressure may have more effect on the inclination than the material residual strains. A higher sensitivity of current density to strain was also observed at more anodic potentials than at the activity peak. This could help in the reproduction of inclined SCC in laboratory conditions, by utilising the potentials that result in the greatest sensitivity to of current density to strain. Simulations showed that while crack growth rates were slower for inclined SCC prior to when the stabilisation angle is reached, there is an exponential relation between depth and crack growth rate for inclined SCC. This is due to the time between film ruptures extending as the stress intensity factor increases, and the increased faradaic limit of inclined SCC playing a greater role in the growth.

Real world applications can be drawn from this chapter despite no one quantitative

growth rate difference between straight and inclined SCC being identified. Firstly, the model provides a platform that can easily provide crack growth rate predictions for inclined SCC should the variation in current density at the crack tip be estimated or determined experimentally. The results also suggest that predictive models that are not based on observations of inclined SCC affected pipes should be used with caution, with historical data from pigging or in-line inspection being the preferred tool. In addition, cracks of significant depth should be considered more dangerous than cracks of significant length, as the growth rates for inclined cracks seem to rise exponentially with depth. Colonies with the deepest cracks are already given priority for repair, and this result reinforces that practice. Lastly new pipeline materials could be tested for the sensitivity of their potentiodynamics to strain with the same experimental methods outlined in this chapter, which could help suggest if the pipe would be a candidate for inclined SCC or straight SCC. This can assist with management plans.

Various future works could help advance the knowledge already gained from this work. Experiments should be conducted to analyse the current density distribution about the crack tip of an SCC crack in X65 steel, to give quantitative inputs to the model developed in this chapter, and hence quantitative outputs. Additionally, the experiments conducted in this chapter could also be performed on straight SCC affected steels, such as X42. This would give insight as to whether potentiodynamic response to strain is an indicator of inclined SCC susceptibility. Long time scale inclined SCC growth experiments are also desirable, as it would give some data to validate a predictive growth rate model against, as well as provide a way to

test the sensitivity of the multitude of variables present in this model, such as the applied potential or steel characteristics.

Various parameters that are involved in SCC growth are somewhat neglected in the model, including the impact of fatigue, crack interaction, and textural impedances, however they are all somewhat accounted for in the industry validated equations upon which the model is based. These all can account for the wide variation in crack growth rates across a colony which inherently restricts crack growth rate predictions to setting an upper limit of growth. Of the various parameters omitted, the only one that would be likely to have an effect on the relative growth rates of inclined cracks as opposed to straight cracks is crack interaction, as inclined cracks are likely to encounter more cracks due to their hoop travel, which could both positively or negatively influence the crack growth rates. Additionally, the original model that the equation is sourced from uses some approximations for some of the parameters in the equations, including the repassivation kinetic exponent, and the incubation time of repassivation [21]. Both of these are candidates for change in the circumstance of inclined SCC, as a significant shift in the current density in the passive film region was observed, and further experiments to quantify these variables could add a slight improvement to the accuracy of the predictions. This potentially adds another source of error, and would underestimate the effect of inclined SCC. Furthermore, varied ranges for the critical stress intensity factor for SCC in X65 steel have been found, largely due to the fact that inclined SCC will grow below the critical stress intensity factor, just at a much slower rate. This can make the value of a critical stress intensity factor somewhat arbitrary, however

the results are not overly sensitive to the critical stress intensity factor. Lastly the cracks are assumed to travel in a 2D fashion with just the deepest cross section considered, where the 3D nature of the crack will also have some impact on the crack path and hence growth rate.

5.7 Conclusion

This chapter explored the effect of the strain enhanced electrochemistry mechanism on SCC crack growth rate estimates. This was accomplished by identifying the relationship between both residual and applied strain and current density experimentally, and subsequently the development of a model that accounts for inclination and increased current density at the growth angle. It was found that applied strain had greater impact than purely residual strains in the SCC region. A significant increase in current density of up to 300% in the SCC potential range was observed experimentally, yet simulations demonstrated that an increase in current density of only 30% at the inclined growth angle could result in faster growth rates to 50% wall thickness than straight SCC. This emphasised the importance of quantifying the relation between the microstrain at the crack tip and the current density at various angles, such that the actual increase in current density at the inclination angle at the crack tip could be known. This also seems to give some justification as to why X65 presents with inclined SCC, in X65 appearing fairly sensitive to strain. This helps achieve the aim of both furthering scientific understanding of the mechanisms of inclined SCC, as well as providing knowledge that can have implications for real world SCC management. Now that single inclined

cracks growth rates and crack paths have been thoroughly explored, the impact of inclination on interaction between adjacent cracks is of great interest, as crack interaction is one of the primary drivers in both stage 2 and 3 SCC growth.

Chapter 6

Result 3: 3D interaction

6.1 Introduction

The thesis thus far has focussed on finding the mechanism governing inclined SCC, along with the impact of this mechanism on crack growth rates. To reduce the number of unknown variables in this prior analysis, only single isolated cracks were considered and interaction was neglected. While this assumption can assist in the determination of the root cause of the inclination, SCC tends to grow in colonies with significant interaction between cracks. Interaction is considered so important in pipeline SCC that there are CEPA interaction guidelines for assessing the degree of interaction for pipeline operators [11]. The impact of inclination on interaction is thus integral to the understanding of inclined SCC in practical environments.

This chapter examines this relationship between inclination and subsurface crack interaction. This will be performed to achieve the third objective outlined in the

scope of "validating the CEPA guidelines by combining the constraints of crack growth set by the mechanism with the observed crack shape parameters from previous work [14] to create a 3D interaction model." Achieving this objective will provide the obvious benefit of confidence in assessing inclined SCC colonies for interaction, but also provide the theory with a new perspective on interaction of SCC. The existing guidelines and theory assume that interaction will occur first on the surface, however the presence of inclination can change the interaction point to be beneath the pipe surface with no indication of interaction on the surface plane.

This unknown is solved in this chapter through the use of computer simulation. Inputs from a prior study give realistic crack morphology data which provide a worst case scenario of inclination [14]. Simulations are then conducted through a combination of MATLAB and ANSYS which balance the worst case of geometrically possible interaction with the stress shielding that would prevent such interaction. This chapter first presents a brief background into interaction of SCC, before explaining the methods used and the results of interest. Discussions then indicate how the findings can best be applied, along with the limitations of the results.

6.2 Background

Interaction and coalescence dominate stage 3 and 4 growth in an SCC colony life cycle (Figure 2.18), and thus are vital to consider when attempting to prevent

SCC failures [4]. It has been shown that seven or more cracks are generally required to coalesce for a burst failure to occur rather than a leak [18]. The CEPA interaction guidelines for SCC cracks in gas pipelines were developed to determine whether two cracks would be potentially interacting [11]. These guidelines are based on a straight crack assumption though, and the potential for two cracks to incline towards each other would fall outside of the assumptions of the guidelines. The fracture mechanics of crack interaction must be looked into to determine the feasibility of two inclined cracks interacting outside of the guidelines.

The CEPA interaction guidelines deem two cracks to be potentially interacting if the hoop and axial spacing is less than 14% and 25% of their average lengths respectively (Figure 6.1) [11]. If two cracks are deemed to be interacting, then the two cracks are considered one crack and the process is repeated with the cracks adjacent to this now larger pseudo-crack. This process continues until the largest chain of potentially interacting cracks is found, which is then used as a parameter to assess the remaining life of the pipe section before repair or replacement is necessary. If two cracks are interacting but are considered not interacting by CEPA, it could cause not only an error between just two cracks, but potentially create large misreadings if further interaction would be predicted with the unison of those two cracks. Thus it is important to assess the validity of the CEPA criterion for the case of inclined cracks, which could potentially incline and interact below the surface.

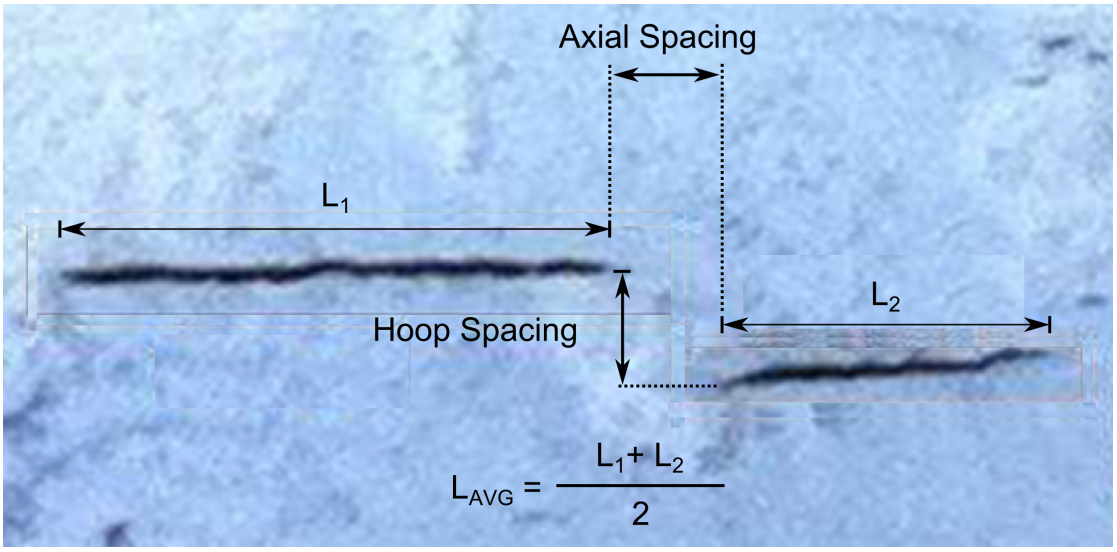

FIGURE 6.1: Axial and hoop spacing of two cracks is defined from the two closest crack tips, and length as the axial distance between the two tips of a single crack.

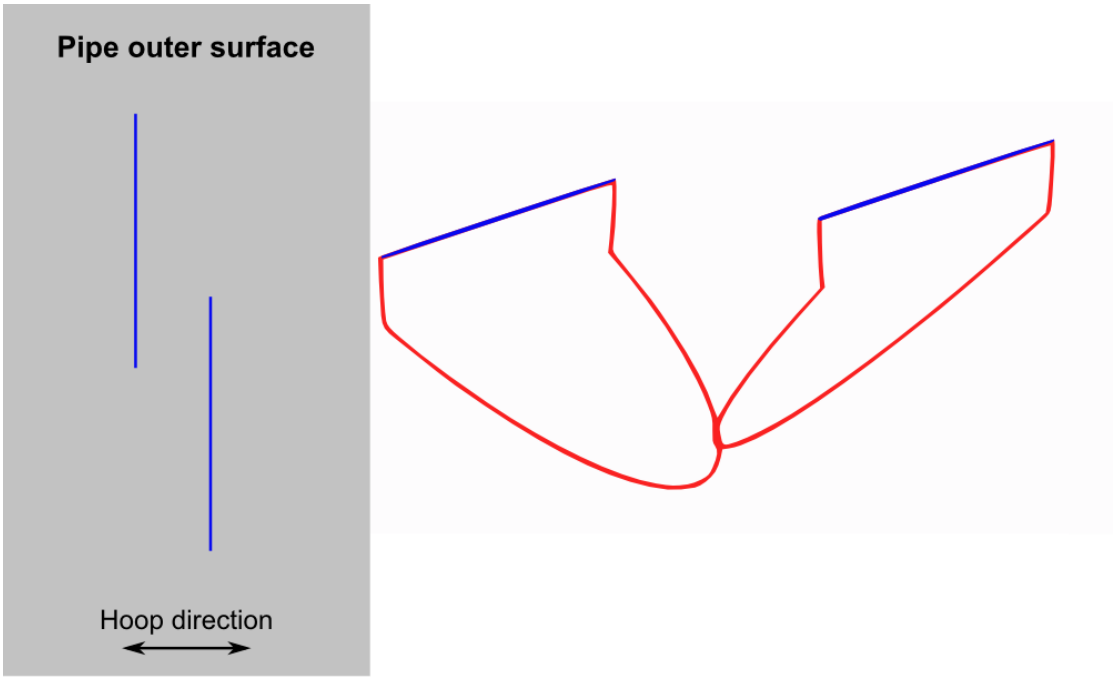

FIGURE 6.2: (Repeated for ease of reading) Possible interaction case where two equal length inclined cracks are partially overlapping on the surface view (left) and meeting at the tangent beneath the surface (right). Blue lines represent the crack mouth on the outer surface of the pipe while red lines represent the subsurface crack fronts.

Inclined cracks present a potential case for the violation of the CEPA interaction guidelines due to the significant hoop travel seen in prior studies. Zadow [14]

performed a study on inclined SCC in Australian gas pipelines and found that cracks approached an inclination angle of between 50^o and 60^o, a length to depth ratio between 1 and 14 and tended to incline with a centreline depth of 0.55 mm or greater. Both the angle and length to depth ratio increased with depth. This relates to the interaction of two cracks as a high angle means more hoop travel per unit length, while a high length to depth ratio means less hoop travel per unit length. As these two parameters counteract each other, a range of lengths must be considered with the worst case of the length dependent parameters seen in the Zadow study [14]. This means selecting the cracks which were both deepest and with the greatest angle for a given length.

While cracks could incline towards each other beneath the surface and potentially interact, stress shielding of the cracks relative to each other will generally influence the cracks to grow away from one another. Two parallel cracks with no axial offset for instance would be under the influence of a large degree of stress shielding and would have a tendency to incline away from each other both through a highest stress intensity factor or a highest plasticity mechanism. On the other hand, two collinear cracks with no hoop offset will tend to grow towards each other. Thus due to continuity, there must be some point in-between purely hoop offset and purely axial offset where the cracks will have an equal influence to grow towards and away from each other. This means that if two cracks were parallel to each other, offset in the hoop and axial directions and inclined towards each other, it would be geometrically possible for the crack fronts to meet where the surface cracks would appear to be outside of the CEPA guidelines, whilst also potentially

avoiding stress shielding. This configuration is outlined in Figure 6.2.

6.3 Modelling methodology

The modelling methodology can be divided into identifying the cases that need to be modelled and then implementation into MATLAB and ANSYS. A range of worst case scenarios is identified through a geometric case study with inputs from a prior study [14]. These cases are then analysed with finite element analysis for the effects of stress shielding, and whether it is possible for the cracks to reach the potentially infringing geometry.

6.3.1 Identifying a worst case scenario

Crack interaction of inclined cracks is a multi-variable problem. Relative crack lengths, length to depth ratios, inclination angle, and offset are all of importance. Identifying the worst case for crack interaction requires finding the worst cases for each of these variables.

Cracks of equal length can have a greater chance of violating CEPA guidelines [11] than cracks of unequal lengths. This is as the cracks can only interact at a depth as deep as the shallowest (and shortest) crack. Adding extra length to one of the cracks will make the average crack length longer with no addition to the combined subsurface hoop travel at the maximum depth of the shallowest crack. This would make CEPA interaction guidelines hold more easily. Thus, cracks of equal length

are considered in the analysis as the worst case. This idea can be easily visualised by considering the extreme case with one very long crack and one very short crack. The deepest point at which they could interact would be the deepest point of the shortest crack. Since hoop travel is proportional to depth, the maximum hoop travel would be twice the hoop travel possible at the depth of interaction. Instead if two cracks were of equal length but the same average length, the maximum possible depth of interaction would be deeper and hence allow greater hoop travel.

Length to depth ratio (L/D) and inclination angle both can affect the degree of subsurface hoop travel of an inclined SCC crack. A crack that is deeper for its length can have more subsurface hoop travel due to the inclination, and hence can interact with cracks that are further away. Similarly, cracks with a higher inclination angle will have more subsurface hoop travel per unit length, hence giving greater potential for interaction with cracks outside of CEPA limits. Ranges for L/D and inclination angle were chosen based on a prior study [14], with the modelled values having lower L/D ratios, and higher inclination angles (Figure 6.3). This creates a worst possible case for interaction.

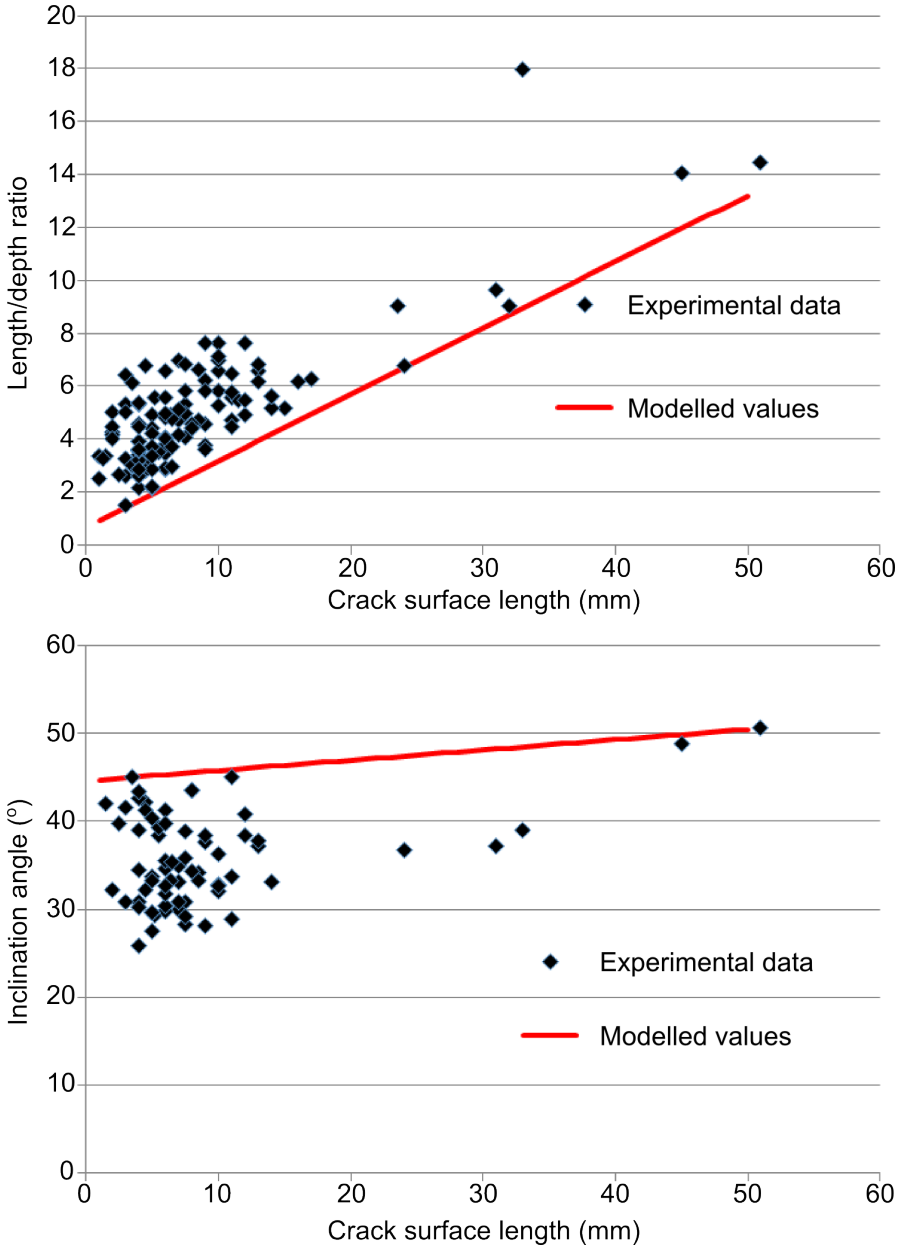

FIGURE 6.3: Data from Zadow [14] with modelled values representing the worst case for interaction predictions.

It is unclear as to exactly what hoop and axial offset of two adjacent cracks would create a worst case scenario. The cracks should overlap somewhat for interaction to occur without significant shielding, as in Figure 6.2. The exact configuration where shielding is minimal yet the cracks are far enough apart to be outside of

the CEPA guidelines is unknown. Thus both hoop and axial offset were varied to create a range of all geometrically possible interaction cases.

6.3.2 Modelling implementation and results

The analysis of whether cracks could interact outside of the CEPA guidelines occurred in three steps. Firstly, a range of geometrically possible worst case scenarios were created in MATLAB and assessed for interaction violations. Secondly these cases were tested in FEA by incorporating stress shielding effects. Lastly the results of the FEA analysis were input back into the MATLAB code and a revised field of interaction cases was generated.

The MATLAB code finds the points of interaction by using the ellipse projection of the cracks on the surface of the pipe. As the inclined cracks follow an approximately semi-elliptical shape, and the projection of a semi-ellipse is also a semi-ellipse, all possible angles of interaction for two cracks of a given length can be calculated by finding the interaction tangents of the two ellipse projections on the surface (Figure 6.4), then re-projecting them down to the appropriate depth. Only one tangential interaction point exists for each surface interaction angle α (as defined in Figure 6.5). The tangential point is used as this would result in two cracks that have only just started to interact, rather than two cracks that have been interacting for some time. Half crack length a (as defined in Figure 6.5) and interaction angle α are varied from 1-25 mm and 0 to 90^o respectively (angles from 90-180^o are symmetrical to 0-90^o). These cases are then tested for violation of the CEPA guidelines, and the output for each case ($\frac{d_2}{a}$–0.14) represents how

many percent above or below the CEPA hoop interaction limit they are. A positive output indicates CEPA being breached, while a negative output indicates CEPA holding. For instance, if the hoop spacing was 17% of the crack length for a given configuration, then the output for that configuration would be 17%-14% = 3%. The outputs for the full range of configurations are presented in Figure 6.6, with green representing all the crack configurations where CEPA holds, while the coloured region showing the degree to which CEPA could be breached.

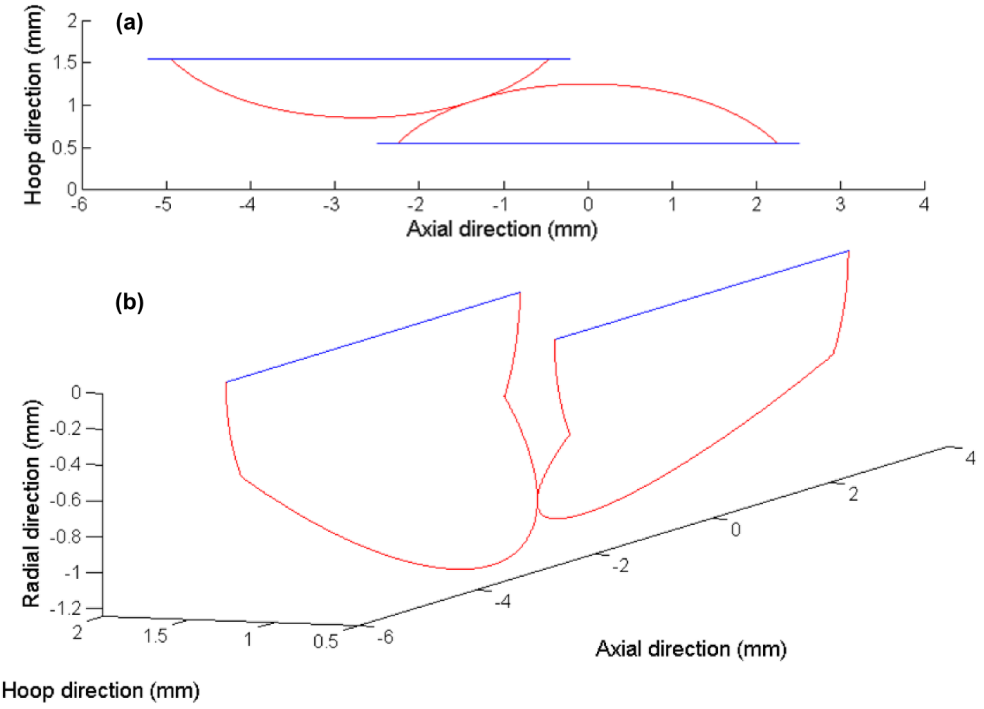

FIGURE 6.4: Tangent of interaction for the surface projected ellipse for two equal length cracks, (a) is a surface view and (b) is an isometric view. Blue line is the crack mouth on the surface while the red line is the crack front in the thickness.

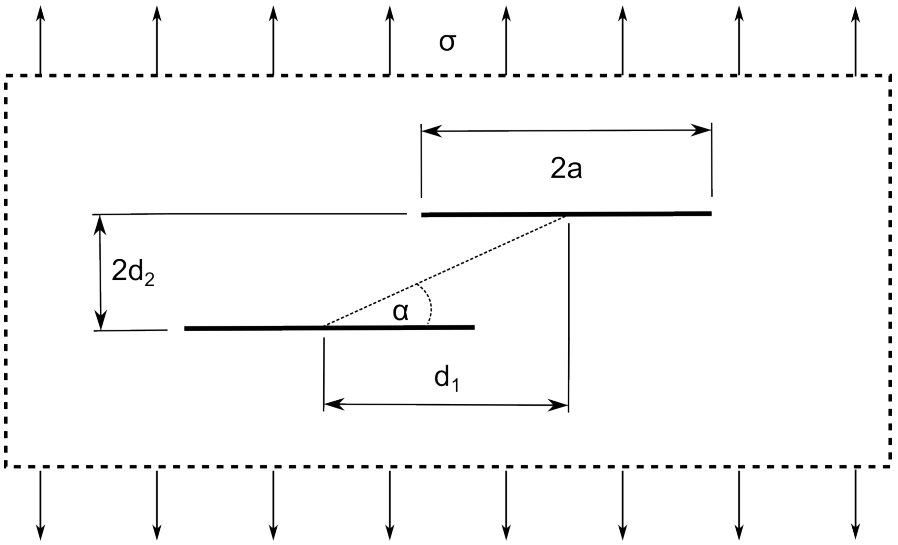

FIGURE 6.5: Surface view of two overlapping equal length cracks with parameter definition.

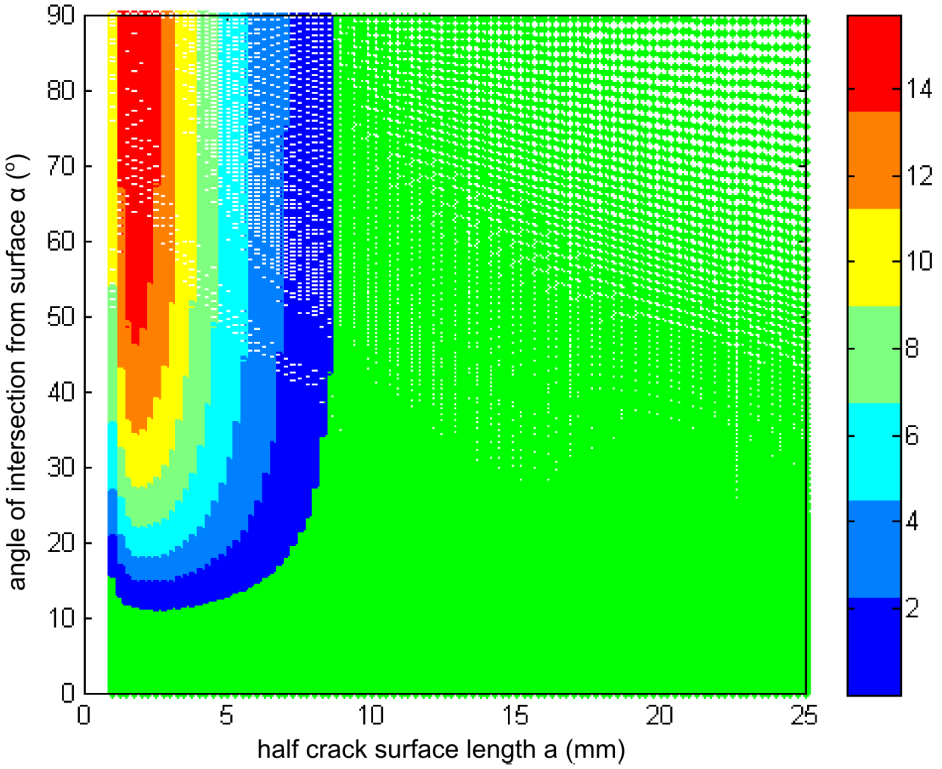

FIGURE 6.6: Worst case geometric interaction field. Green is within CEPA [11], coloured is outside of CEPA with the percentage the configuration falls outside of the predictions indicated by the colour bar.

The FEA code was then developed to test whether the cases identified would be possible, or whether they would be prevented due to shielding. The criteria set was that if the stress intensity factor at the inner crack tips on the surface were to fall below the minimum stress intensity factor required for growth, the crack would have arrested before that point and that crack geometry would be impossible. The critical stress intensity factor was taken as 25 MPa$\sqrt{m}$ or 790 MPa$\sqrt{mm}$, which was found as the limit for X60 (which has a similar chemical composition) in high pH solution [103]. A refined radial crack tip mesh of PLANE183 elements was used (Figure 6.7) with good convergence. Boundary conditions were a load of specified minimum yield strength (SMYS) for X65 (450 MPa) applied to the top surface, with the bottom surface being constrained (Figure 6.8).

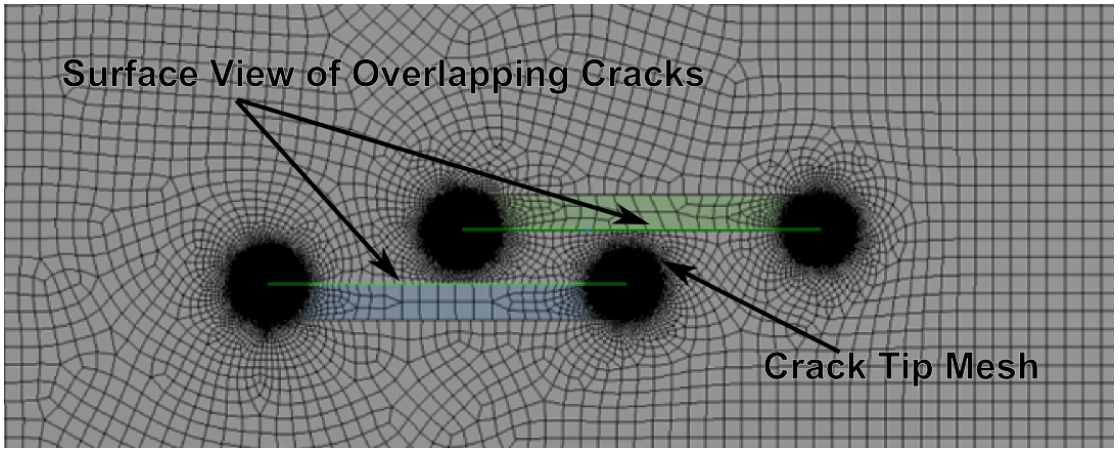

FIGURE 6.7: Visualisation of the mesh used for an example pair of overlapping cracks, showing refined, non-overlapping radial meshes at the crack tips.

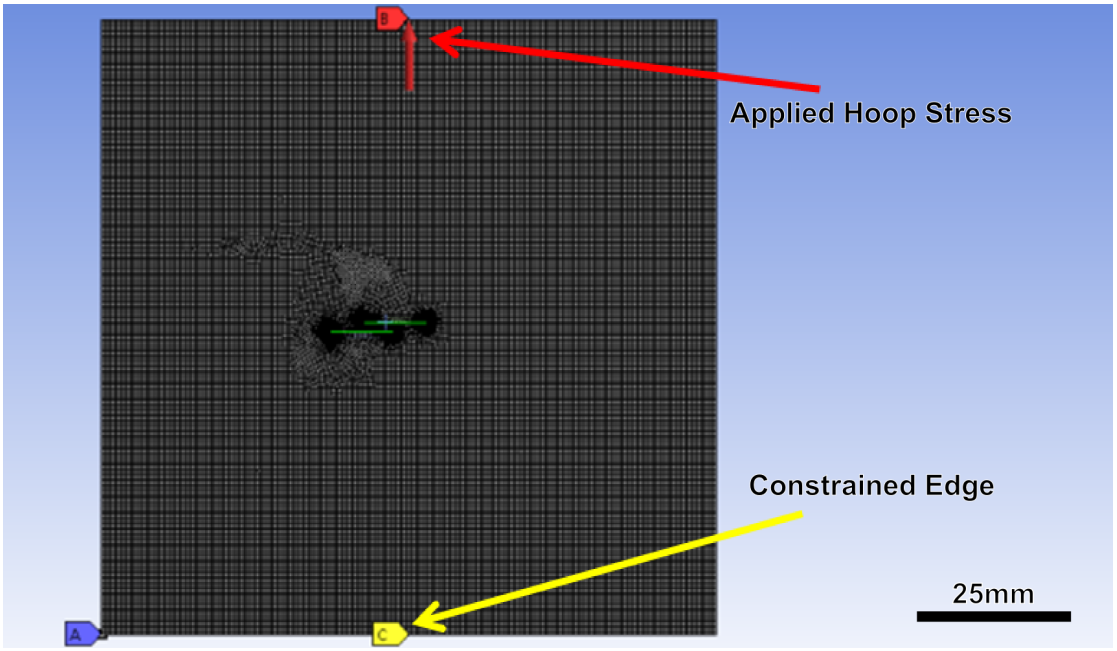

FIGURE 6.8: Visualisation of the boundary conditions used for the study relative to the crack geometry.

Rather than testing all the cases in Figure 6.6 explicitly (which could potentially be infinite depending on what step size is used), a dimensionless lookup table that was scalable with crack length was created. Inputs to the table were $2a/d_1$ and d_1/d_2, and the output was a ratio of the stress at the inner tip to the stress at the outer tip (or a crack of equal length with no interaction effects). If the stress intensity factor at the inner tip was lower than the outer tip, then the crack interaction was providing stress shielding. On the other hand, if the stress intensity factor at the inner tip was higher than the outer tip, the crack interaction was causing the cracks to preferentially grow together. FEA results were validated for two ratios of d_1/d_2 against published results [95] with good agreement (Figure 6.9).

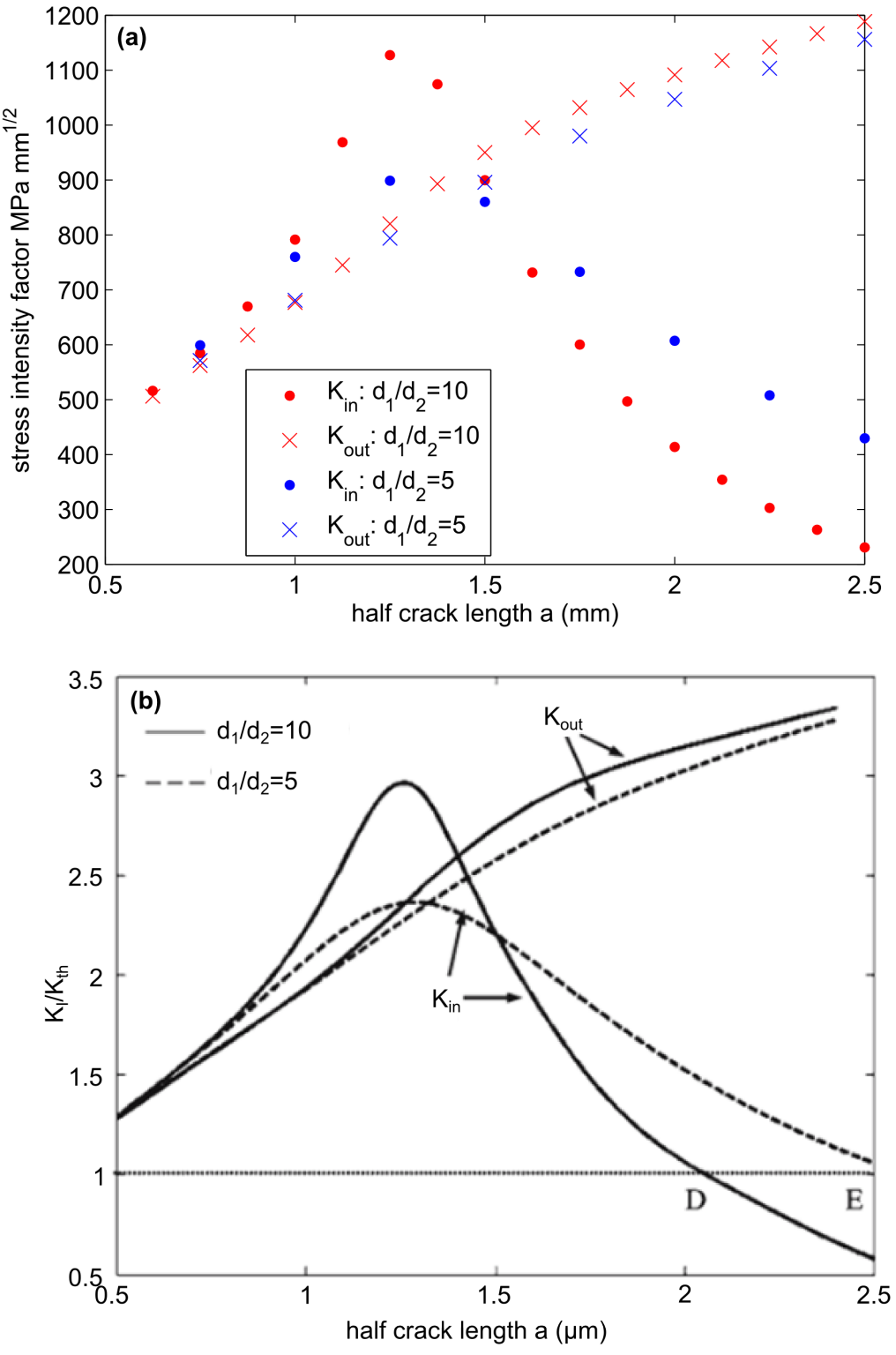

FIGURE 6.9: Validation of FEA results for two ratios of d_1/d_2 [95].

This process was repeated for additional values of d_1/d_2 and $2a/d_1$ across the

range of geometrically possible cases. The compilation of these curves combined with 3D cubic spline interpolation resulted in a lookup table that is visualised in Figure 6.10. The lookup table was then inserted back into the MATLAB code and values of stress intensity factor at the inner tip were compared to the critical stress intensity factor. If the stress intensity factor was below the critical value then the crack would have arrested and the configuration is impossible.

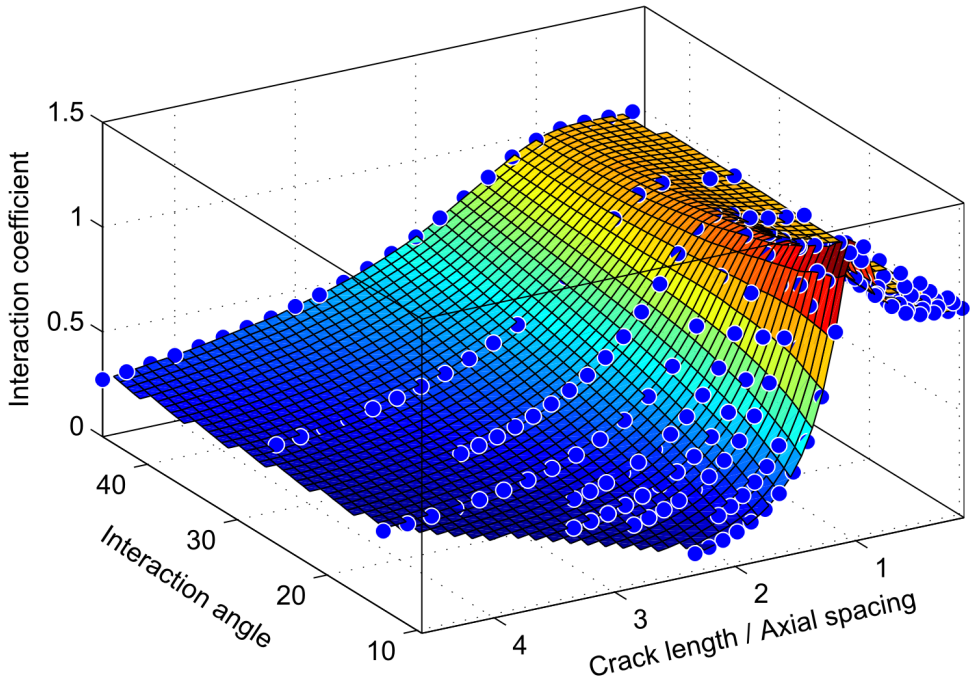

FIGURE 6.10: Graphical representation of the look up table determined through various FEA tests. The shielding coefficient represents K_{in}/K_{out}, and lower values represent a greater degree of shielding.

The results of the implementation of the look up table into the prior MATLAB code are shown in Figure 6.11. The area shaded green shows sections where shielding would allow the cracks to interact, albeit within the predictions of CEPA, while the area in pink shows the area where the inner crack tips would have arrested before the infringing geometry was reached, and thus shielding prevents

the interaction. Thus CEPA holds for all crack configurations. The worst case of interaction within CEPA that is possible including shielding effects occurs with a hoop spacing of 12.6% of the average crack lengths, with a half crack length of approximately 4.5 mm, and an interaction angle of approximately 12.5^o. CEPA holds especially well for longer cracks as the length to depth ratio tends to increase with length, with only shorter cracks with lower length to depth ratios proving to be close to the interaction limits.

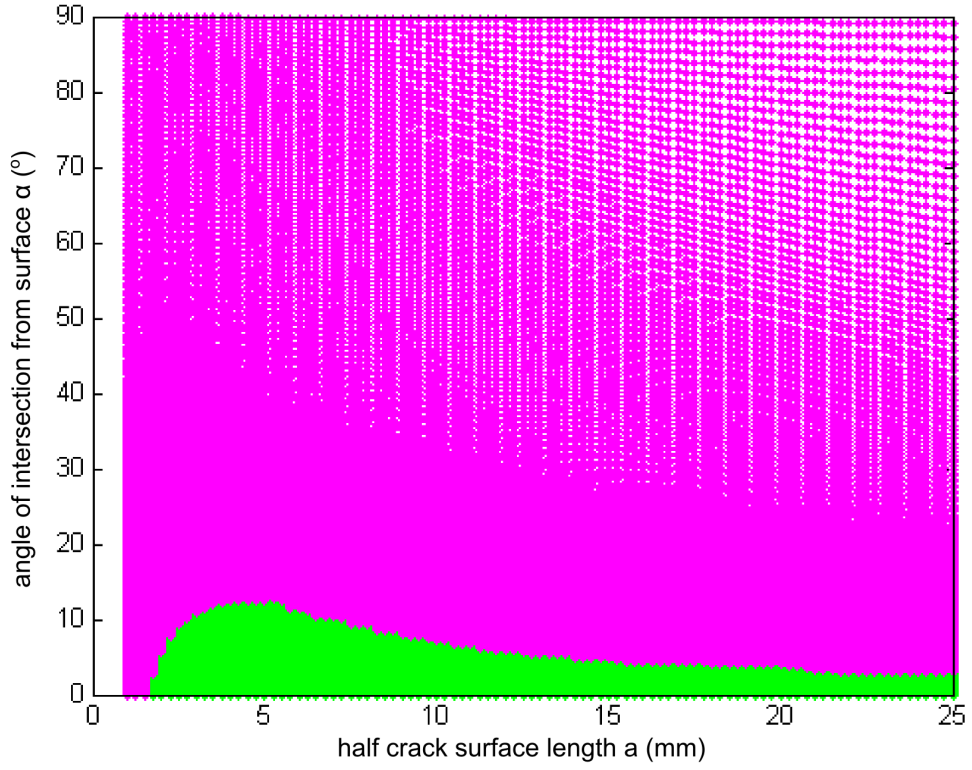

FIGURE 6.11: Geometric interaction possibilities with FEA shielding results. Pink = shielded so no interaction, Green = interaction within CEPA guidelines [11].

6.4 Extension to other cases

The results presented in this chapter thus far show extensively the possible subsurface interaction states of the colony analysed. While the methods used would be of assistance in assessing other SCC colonies with different input parameters for inclination, the results are not directly transferable. This section aims to address a wider range of inputs of straight section depth and stabilised inclination angle. This will provide value both in the determination of the relative sensitivity of the interaction of inclined SCC to these inputs, but also to help give a quick assessment of the conservativeness of the CEPA interaction guidelines for X65 pipes in slightly different scenarios.

The method for this extension follows an almost identical method to that described earlier in the chapter, but instead reduces the full range of interaction outputs to the sets global maximum. The other difference results in the change of the stabilised inclination angle from a length dependant variable to a constant, as the variation was fairly minimal and it still produces a worst case scenario. The critical stress intensity factor was taken to be that of X65 and the stress was 80% SMYS, and as such the results should not be transferred quantitatively to other steels, although the qualitative findings are still applicable. The depth of the straight section and stabilised inclination angle were varied over a range of feasible values and the global maximum stored for each data point. This allowed a visualisation of the effects of both the straight section depth and inclination angle on the interaction.

This relationship is illustrated in Figure 6.12. This figure shows the relationship between the maximum possible hoop spacing for interaction (Y axis) against the straight section depth (X axis) with the various curves representing different stabilised inclination angles. It is clear that as the depth of the straight section increases, less hoop travel would occur per unit length, and the maximum spacing is reduced. Through similar logic, a lower inclination angle also results in less hoop travel per unit length and that also results in a lower likelihood of the CEPA interaction limits being violated. This would imply that for inclined SCC colonies with high inclination angles and short straight section depths, CEPA is more likely to be violated and investigations should be conducted.

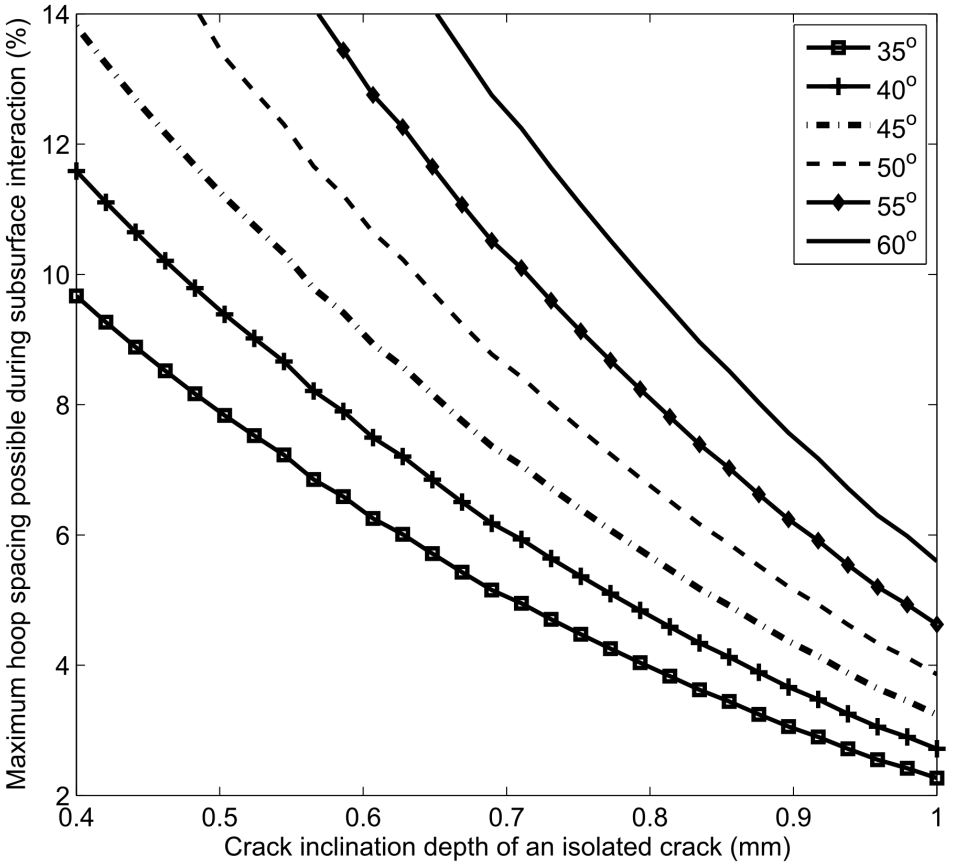

FIGURE 6.12: Maximum hoop spacing (abscissa) against the depth of the straight section for an isolated crack in the field conditions (coordinate) with multiple stabilised final inclination angles. Graph is given for an assumed applied load of 80% SMYS of X65 pipe steel, and should not be used for higher loadings or alternate materials.

The data was then manipulated to determine the critical limits of both straight section depth and inclination angle. This results in a fairly linear relationship as shown in Figure 6.13. The dashed line in this figure represents the conditions that cause the edge case where subsurface interaction could possibly occur at a spacing of 14% of the average crack lengths. The area to the left of this line is the region where interaction would be predicted with a spacing less than 14%, while the area

to the right of the line would warrant further investigation as these results suggest that interaction would be possible.

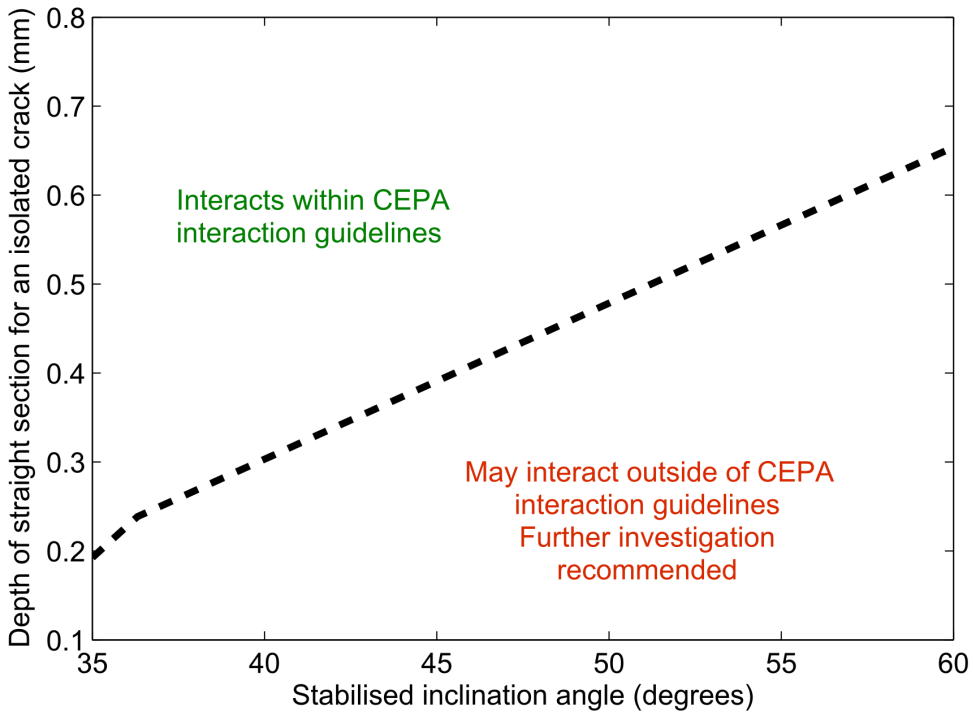

FIGURE 6.13: Safe boundary for subsurface interaction of inclined SCC in X65 pipe steel stressed at 80% SMYS. Region to the left of the line indicates subsurface interaction is not predicted to occur outside of the CEPA guidelines [11].

6.5 Discussion

This chapter has identified some key results which can both add to the knowledge base around inclined SCC as well as inform industry management tools. The findings also can be used to identify future research directions. The limitations of the results should also be discussed.

Numerous additions to the knowledge base of inclined SCC can be retrieved from the results of this chapter. Firstly, a maximum interaction spacing was found

for cracks with a length of 8-10mm, rather than long cracks which are usually considered most critical. The reasoning for this observation can be found in the inputs from the prior study (Figure 6.3). The L/D ratio was very sensitive to the length of the crack, causing longer cracks to be relatively shallower, meaning less hoop travel per unit length. This effect was expected to be offset by the increase of angle with length, however the data showed a relatively low sensitivity of the angle to crack depth, despite reports that the cracks from that study tended to curve with depth. The result was that the hoop travel for short cracks was relatively higher than for longer cracks. Additionally, the work also showed the sensitivity of the interaction to both the stabilised inclination angle and the straight section depth. Cracks that begin inclination at shallower depths or incline at a greater angle will see a higher chance for subsurface interaction with no indication on the surface plane. This is due to the fact that both of these conditions result in the potential for greater hoop travel per unit surface length. This finding can allow researchers to focus future analyses on colonies which present with the conditions most likely to result in an infringement of the existing standards. Lastly, the method for analysing subsurface interaction of inclined cracks can be utilised in the future on different steels that could present with inclined SCC, or even X65 steel in different conditions. Before this study there were methods for analysing surface interaction and subsurface interaction of straight cracks, yet no method for interaction of overlapping 3D inclined cracks which has now been developed.

The implications to industry from this chapter are very clear as part of the objective was to assess the CEPA interaction guidelines used in the pipeline industry.

Of most use to industry would be the result that the CEPA interaction guidelines are predicted to still be valid for inclined SCC under the field conditions and crack morphology determined in a prior study [14]. This means that the existing assessment techniques are still valid for that case, and additional investment in retraining and reassessment is not necessary in those conditions. The second main implication to industry would be the spacing limits should X65 steel be similarly stressed but contain cracks with different morphology (perhaps due to some electrochemical differences). The Figure 6.13 can be used to assess whether further investigation is required on the colony or whether the guidelines are most likely still valid. The extension work also produces one further implication to industry stemming from the finding that cracks which incline earlier and steeper are more likely to interact outside of the CEPA predictions. This can inform manufacture and operation to try and produce pipes that inhibit the inclination. Methods by which inclination could be inhibited in manufacture are a direct result of Chapter 4, and those results can be combined with the findings from this chapter to help produce safer pipes.

The findings of this chapter are of use to operators of X65 pipelines, stressed at 80% SMYS or below in conditions similar to that of the pipe discussed in the prior study [14]. However, there presents opportunities for future work in analysing X65 pipes in other conditions or even higher grade pipes that might be susceptible to inclined SCC. Additional surveys and subsequent modelling on different steels or circumstances would help provide a more precise band for what ranges of inclination morphologies are possible, and hence whether any cases could violate

the CEPA interaction guidelines. Additionally, this chapter assumed the use of semi-elliptical crack shapes, while in reality the shapes of cracks can vary from the ideal case due to material heterogeneity or even crack interaction. Lastly, while the results indicate when subsurface interaction can occur, there is no information on whether surface or subsurface interaction has the same impact on burst pressures. Additional experimental work with interacting inclined cracks and interacting straight cracks could assist in determining the degree to which the strength of the pipeline would be affected.

As with any simulation, the underlying assumptions lead to limitations. The most obvious limitation comes from the practical reality of only having inputs from one section of one pipeline. SCC conditions have been known to vary both between pipelines and also along the length of a single pipeline. It has been assumed that the crack morphology data is representative of the pipeline that it was extracted from, however the results cannot be feasibly applied to other pipelines without additional knowledge of the variation of crack morphology. Other limitations include the fact that the critical stress intensity factor is not a hard limit with zero growth rate prior to it and high growth rate afterwards [21], despite it often being treated as such. Instead it just represents a point at which the growth rate increases by several orders of magnitude. This means that the method is still sound, however there would be some growth once the stress intensity factor falls below the critical stress intensity factor. Additionally, the critical stress intensity factor used is that found for X60, which is chemically similar to X65, however the exact critical stress intensity factor for inclined SCC affected X65 steel would

improve the accuracy of the results. The cracks are also assumed to be perfect ellipses in the model, as is common practice for simulations on SCC. Various other crack shapes can occur in field conditions however, and the potential impact of these shapes has not been explored. The semi-elliptical assumption should still be accurate for most cases though, as it is the mathematically preferred shape of the crack. Lastly, the effects of microstructural defects such as vacancies or manganese inclusions could cause stress concentrators within the pipe wall thickness. This could give cause for hoop travel beyond what is expected. The magnitude of this effect warrants further investigation, however it is very unlikely that two symmetrical cracks would initiate in the correct spot relative to each other and the defect, as well as both inclining in the correct direction with the maximum magnitudes seen. Thus the results can still be seen as reasonable for field use.

6.6 Conclusion

This chapter aimed to explore how inclined SCC affects interaction between adjacent cracks in X65 steel pipelines, as there was concern that inclined cracks might interact beneath the surface where existing methods would predict no interaction. This relationship was examined through analysis of stress shielding conditions in a simulation developed across MATLAB and ANSYS which relied on prior field data as inputs to create worst case scenarios, before examining the geometric worst cases and the stress fields. The results show that the CEPA interaction guidelines hold across the entire range of possible geometries that were sourced from a number of worst case scenarios for the case examined. The findings also showed that

crack colonies with different geometric inclination variables such as length to depth ratio or inclination angle could pose a risk, and that further analysis of should be conducted on SCC colonies that present with lower length to depth ratios or higher inclination angles. This work has helped achieve the overall research aim of the thesis by both aiding the understanding of inclined SCC, and informing the existing guidelines used by industry. The specific knowledge gained and presented in Figures 6.12 and 6.13 would be of most use for informing industry guidelines as it identifies the conditions that would cause interaction of inclined SCC to still be entirely manageable within CEPA. These results will be presented to the advisory board who is looking into updating the CEPA guidelines. The results presented in Figures 6.12 and 6.13 should only be used with consideration to their limitations, which includes interaction of inclined SCC in X65 steel stressed at 80% SMYS or below. The addition to the knowledge base of inclined SCC from this chapter has been useful, especially when combined with that from the previous chapters. This new knowledge that has been identified throughout the thesis can be used to identify some key implications for industry, and how they can avoid, predict and manage inclined SCC.

Chapter 7

Conclusion

This research was undertaken in an attempt to help shed light on the mechanism of inclined SCC as well as provide the pipeline industry with an assessment of commonly used management techniques. As inclined SCC is a relatively new phenomenon, it was unknown as to whether the straight SCC management techniques would maintain the high level of safety and conservativeness demanded in the field of high pressure gas pipelines. Existing literature showed surveys of how inclined SCC presented in X65 pipe steels, but not the implication on safety. Three specific research goals were developed to address this gap:

- Determine a plausible mechanism for the inclination integrated into a model that can reproduce typical inclined crack paths.
- Determine how the mechanism affects crack growth rate predictions.
- Determine whether inclined SCC could interact outside of the Canadian Energy Pipeline Association (CEPA) interaction guidelines [11].

The first goal was achieved in Chapter 4 (and the second publication in Appendix B) with the identification of strain enhanced electrochemistry as a likely mechanism and the development of a model that produced crack paths similar to field grown cracks. The second goal was addressed in Chapter 5 (and the fourth publication in Appendix B) where simulation taking strain enhanced electrochemistry mechanism into account showed that growth rates were slower for shorter cracks but faster for longer cracks, and that only a 20% increase in current density is required along the inclination angle to cause faster growth to 50% wall thickness. The third goal was investigated in Chapter 6 (and the fifth publication in Appendix B) and showed that inclined SCC should not interact outside of the CEPA interaction guidelines given the conditions previously experimentally determined from field studies to date, but that it may potentially be possible if new steels, environments or stresses were to be present. Further work with the same methodology developed in Chapter 6 would be required if new conditions that are conducive to inclined SCC were to present in the field.

The results of this work do not tend to disagree with the wealth of SCC knowledge present in the literature. Rather it adds knowledge by combining the theories of high pH SCC and strain-dependant current density to give a reasonable explanation of inclined SCC. Knowledge of the mechanism can enable further experimental work to grow inclined SCC under laboratory conditions and look further into the sensitivity of the inclination to various parameters, such as potential or material properties. One point in particular where great addition to the literature is possible is in the area of hoop spacing for interaction guidelines for SCC. The existing

CEPA interaction guidelines [11] are based upon work by Wang et al. [19] which demonstrated that surface interaction would be possible at a hoop spacing of 14% or less. This work has demonstrated that subsurface interaction is not possible for inclined SCC under the conditions seen in the survey, but would be possible given slightly different crack morphology. These are two different types of interaction, so the results are not conflicting but should rather act in unison for accurate interaction prediction.

The study has provided a primarily theoretical analysis with a basis on limited real world crack data due to the practical realities of obtaining inclined SCC samples. As such there are various limitations to the work that should be considered. Firstly, the scope of the non-interaction analysis was restricted to 2D growth with a simplified microstructure and isolated cracks, while SCC typically presents with many cracks in a colony with complex 3D interactions and a microstructure with banding, vacancies and segregation. Methodological restrictions are also present in that the work was performed entirely through computer simulation which relies on just a few colonies from one pipeline for validation. The methodologies can be repeated for further scenarios of inclined SCC around the globe if additional samples become available, however applying the quantitative results directly to another X65 pipeline in a different location would have no assurance of accurate predictions due to the small sample size available for validation. Lastly, limitations are present due to the practical realities of the knowledge surrounding inclined SCC. Typical SCC management processes rely on non-destructive testing and repair rather than removal and replacement for both practical and financial

reasons. This results in many operators not knowing whether the SCC present in a pipeline would be straight or inclined, let alone the morphological characteristics required to inform a model. SCC also grows at too slow a rate for laboratory tests to give an alternate source of crack colonies in a reasonable time frame for this work. In an ideal world, a model would have a wealth of inputs from various sources to assist in isolating important variables and be able to predict every aspect of SCC growth, however due to the standard management practices, this is not realistically attainable. Despite this, the work conducted in this thesis were able to satisfactorily address the research aim and provide useful additions to the knowledge base around inclined SCC while addressing the goals and objectives.

This work has added significant knowledge to the literature as evident in the publications in the appendix, however there are also some important implications for industry. Particularly knowledge relating to management of growth rates and inspection intervals, interaction guidelines and the impact of stress and material properties on inclined SCC crack paths can all be utilised by pipeline manufactures and operators who wish to maintain safe and efficient practice when dealing with inclined SCC. These points have all been touched on in the thesis, but will also be summarised in the following section.

7.1 Industry implications

The primary aim of the thesis was to not only develop further understanding on the science of inclined SCC, but also to assess industry growth rate and interaction

management techniques with the gained knowledge. Implications for industry are not limited to just growth rate and interaction, with some general information gained also being of use. This section discusses how the various outcomes of this thesis may be of use to industry.

Chapter 4 looked at simulating crack paths for isolated SCC cracks, and validated against field growth cracks. It also investigated the effects of aspect ratio, resistant grain boundaries and stress on the crack path. The aspect ratio had the effect of changing the distance over which stabilisation of the crack was found, as well as impacting the stabilisation angle. Grains that were squashed to a higher degree by rolling showed crack paths at a higher angle then uniform grains. The texture survey showed a greater proportion of susceptible boundaries at the grain boundaries that were oriented towards the radial direction. This had the effect of reducing the inclination angle, however other distributions could have varying effects. Lastly, stress is shown to directly impact the inclination depth, as a higher stress will cause the critical strain to be achieved earlier. It also shortens the distance over which the stabilisation angle is reached.

The implications for industry for these results can be applied in both manufacture and management. If it is desirable to suppress inclination, then steel with a concentration of resistant boundaries at the inclination angles and uni-axial grains should be manufactured. Stress can also be modified in the field to impair or encourage the inclination of SCC cracks if so desired. Generally it would be advised to impair inclination in most cases, as this allows the use of existing management practices and standards that are created under the assumption of straight SCC.

Chapter 5 saw that bulk and crack tip strain has an impact on current density and hence crack growth rates. Simulations showed that growth rates to 50% wall thickness could be accelerated due to this strain enhanced electrochemistry governed inclination. While an exact quantifiable number for growth rate was unattainable without significant further experimental work, there are still implications for industry. Firstly, the model provides a framework to predict crack growth rates if the degree to which current density increases is discovered. Secondly, predictive models that have not been validated against X65 steels specifically should be avoided, but historical data trends for X65 pipelines should still be valid. Additionally, crack depth should be considered to be of great importance, as even a small increase in current density can cause an exponential rise in growth rate. The inclined cracks tend to be slower for the first mm of depth, but grow much faster afterwards. Thus SCC colonies with the deepest cracks should be given priority for repair.

Chapter 6 investigated the effect of inclination on subsurface interaction. The SCC analysed from a prior study [14] showed that the CEPA interaction criteria [11] would hold under those conditions. These conditions include X65 steel at 80% SMYS with an inclination depth of 0.55mm and an inclination angle upper limit of around 50 degrees. The study was extended to show the effect of varying inclination depths and inclination angles on the validity of CEPA providing the X65 steel is in a similar environment at 80% SMYS (Figures 6.13). This graph illustrates the primary result that could inform industry with regards to management of interaction of inclined SCC for X65 steels until further research would be

conducted for other specific cases. For different steels, different environments or higher stress states, repeating the method used in Chapter 6 for the new conditions is recommended to attain the conservativeness of the guidelines for the conditions.

Overall, the thesis has provided various implications that can be of use to industry both for management of inclined SCC and manufacture of inclined SCC resistant steels.

7.2 Future work

While this thesis has managed to answer some important questions, the development of new knowledge also results in the emergence of more gaps surrounding inclined SCC. These unknowns raise questions which in turn can guide future research to help further illuminate the area of inclined SCC. This section will explore some of these questions and the experiments that could provide some more enlightenment to inclined SCC.

7.2.1 Gaps in knowledge

This thesis has provided important understanding of inclined SCC that did not exist previously. Firstly, reviews of the literature found that only X65 steels had shown inclined SCC, and there were no reported cases of non-inclined SCC in X65 pipe steels. Secondly, a probable mechanism was proposed and modelled with good agreement with field grown crack paths. Other findings include the impact

of material and microstructural properties on crack paths, the fact that crack growth rates will be affected by the inclination and that inclined SCC with the morphological characteristics seen in prior surveys [14] will not interact outside of the CEPA interaction limits [11]. Each of these findings also identify some new research gaps that would be good candidates for further research in the field of inclined SCC.

Some interesting questions can be asked about inclined SCC's presence in exclusively X65 steels. Due to the limited number of samples examined in prior studies of field grown SCC in X65 pipe steel and the management techniques focussing on repairing rather than replacing, the data regarding X65 crack paths and sensitivity to various parameters is sparse. It is not known whether SCC in X65 steels will always grow inclined, or perhaps grow straight under certain conditions as crack path studies on X65 in the literature seem to be limited to inclined SCC. Additionally the crack path response of other higher strength pipe steels such as X70 and X80 is unknown, and could also potentially be inclined. It is also wondered if lab grown SCC in X65 steels would also appear inclined and thus make an easier testing platform to determine sensitivities of various parameters to inclined SCC as well as the crack path behaviour in other steels. Lastly it is wondered what differences there are between for example X42 (which is known to produce straight crack paths) and X65 that could explain the inclination present.

The mechanistic cause of inclined SCC appearing to be strain enhanced electrochemistry also raises some questions of note. Firstly it is pondered whether this likely mechanism can be proven experimentally, and if this were the case then if the

same methodology could be applied to other steels to see if they too are susceptible to inclined SCC. It is also unknown as to how much variance in current density exists about the crack tip in the areas of high local strain. It is also wondered as to what degree modifying the loading conditions, manufacturing techniques or steel would impact the presence of this effect.

Crack paths have also been simulated in this model and the sensitivity of various parameters on the crack path demonstrated through simulation. Of interest in the future would be conducting experiments to validate these findings of the impact of texture, grain aspect ratio and stress on the crack path. This would aid in determining if there would be a way to manufacture pipeline steel that would produce predictable SCC paths. Potential is another variable that could have an impact on the electrochemistry at the crack tip and hence the crack path, and it would too be interesting to analyse the influence of potential on the crack path. The simulations also focussed on isolated 2D cracks, while the cracks validated against in the survey would always be present with some interaction, so the idealised shape of a truly isolated inclined crack in 2D is also of interest. In particular this would possibly be helpful in revealing why SCC would incline clockwise or counter-clockwise, which would in turn allow better prediction of subsurface crack positions of in pipe colonies. In addition, it would be helpful to attempt to quantify the ideal crack path of a 3D SCC crack, in particular how the inclination depth varies with the location along the crack front. This would then allow more accurate prediction of crack paths when multiple cracks are involved.

Simulations in the thesis have shown that crack growth rates can be affected

by the mechanism associated with the inclination. Since the thesis could only provide qualitative results regarding the growth rate, there is a clear direction in quantifying the impact of inclination on the growth rate. This could be achieved through various means. Firstly, the impact of crack tip strain on the current density at the crack tip could be determined through methods similar to that of Tang and Cheng [33]. Secondly, a growth rate simulating experiment could be designed in the lab, which would allow comparison between straight SCC in X42 and inclined SCC in X65 in otherwise identical conditions. This would then also help clarify the influence of other variables such as stress, potential or material properties on the growth rate. It would then be interesting to compare how field growth rates compared to those found via these experiments, and if some sort of correlation would allow prediction of crack growth rates for new steels.

The work in Chapter 6 was able to show that inclined SCC grown in the field conditions observed in a prior study [14] did not interact outside of the current CEPA interaction limits [11]. However, due to the variance of conditions seen in X65 pipelines around the world, the results may not be directly applicable to all scenarios. As such it would be interesting to analyse a few scenarios which fall outside of the scope of this thesis. One such extension would be assessing cracks with a non-idealised elliptical shape, as the presence of other cracks or material heterogeneity can cause varying shaped cracks. Additionally different pipe operating conditions or material properties could cause different inclined SCC crack paths both within X65 or even potentially in other steels such as X70. This would then vary the results, and cracks which begin inclination at a shallower

depth or incline to a steeper angle could feasibly reveal cases which would interact at a spacing larger than those predicted in this thesis, and possibly CEPA. Lastly, it would also be useful to know whether the presence of inclined SCC would alter traditional burst pressure calculation when compared to a straight SCC colony with identical surface appearance.

7.2.2 Research directions

Some experiments present themselves as candidates to help answer some of the gaps identified in the prior section. In many of these cases, multiple questions can be answered with the same experimental set up. The recommended directions for research and the types of results that can be expected are discussed in this section.

The first experiment that would provide the greatest addition to new knowledge would be lab growth of 2D isolated SCC cracks from a fatigue pre-crack in a compact tension (CT) specimen. This would involve first growing a pre-crack in a CT specimen, the specimen would then be immersed in solution and placed under either a high or cyclic load such that the film will fracture quickly and the crack will grow at the faradaic limit. Preliminary calculations suggest that this would result in a growth rate of the order of 0.1mm per day. This would aid in the determination of various important pieces of information regardless of the steel used in the test:

- Crack paths of various pipeline steels (X42, X52, X60, X65, X70, X80) to determine whether inclination happens and when it would happen,

- Sensitivity of potential, load, environment and manufacturing techniques to both crack path and crack velocity,
- Determination of K_{ISCC} and the critical stress intensity factor/J integral for inclination,
- Determination of the ideal crack shape with no interference,
- Determination of effects that would cause clockwise or counter-clockwise inclination.

The second experiment which would aid in understanding inclined SCC is crack tip strain mapping similar to that performed by [33]. This method also begins with the growing of a fatigue pre-crack in a CT specimen and then performing a strain mapping experiment using a scanning probe. The current density distribution can then be equated to a given stress intensity factor. This would provide the link between the crack tip strain field and increase in current density. This would allow the quantification of the current density field around a strained crack tip, and the hence quantification of crack growth rate predictions for inclined SCC by informing the growth rate model described in Chapter 5.

Another study that would be of great interest is additional SCC surveys of SCC in other X65 pipes in different conditions, and other steels. The key result being looked for is crack morphology, and methods similar to Zadow [14] could be used. This could inform whether X65 only grows inclined SCC and how the variation in material properties, environment parameters, microstructural data and management techniques impact the crack path and growth rates. It would also be able to

help quantify whether the newer pipe steels such as X70 and X80 were susceptible to straight or inclined SCC, and inform what management tools they should be using. Any results can also be used as inputs into the models generated in this thesis to produce new results for the different conditions.

The last particularly useful research direction would be accelerated 3D growth of SCC in lab conditions. This is currently quite difficult due to the time taken to reach K_{ISCC}. However, this issue could be avoided in a similar manner to the first experiment described in this section where a pre-crack or notch is introduced to simulate the first stage of growth. The purposeful removal of material allows cracks to be placed with controlled interaction conditions and stressed above the critical stress intensity factor. The samples would involve either a buried pipe scenario in a box with sand or a plastic covering filled with solution and stressed either with internal pressure in a pipe scenario or through a similar loading scenario to the first experiment described in this section if the cracks were inserted into a plate. The cracks could then be grown for some time, and subsequently failed with a burst test or other destructive testing to determine the extent of the SCC growth, the direction of the crack path, the crack growth rate, the 3D crack shapes and the effects of interaction on all of the previous points.

The thesis has provided various valuable insights into both the mechanisms governing inclined SCC as well as the tools that can be used to manage it. Further gaps for research that build upon the work undertaken in this thesis have been outlined in this section, along with some experiments which would help to achieve

those gaps. It is important to continue research on pipe steels as operating conditions change and new steels are implemented. These research directions described not only help solve the problems of now, but also provide a platform for analysing the SCC issues of the future.

Straight SCC has had a rich history of research and management practices developed, but as high strength pipe steels have emerged, so too has inclined SCC. Various methods have been explored which can be used to analyse inclined SCC and inform both theorists and the pipeline industry, and possible future directions outlined. The aim of developing the understanding of the mechanism behind inclined SCC and informing industry management techniques has been thoroughly achieved, as evident through the production of the publications in the appendix and also various commercial in confidence reports to industry. It is hoped that this work can serve as a reference to help keep the next generation of pipelines safe from the next generation of SCC.

Bibliography

[1] The Washington Observer. 17 killed as gas line explodes, *March 5 1965*, 1965.

[2] R. N. Parkins and R. R. Fessler. Stress corrosion cracking of high-pressure gas transmission pipelines. *Materials in Engineering Applications*, 1:80–96, 1978.

[3] T. N. Baker, G. G. Rochfort, and R. N. Parkins. Pipeline rupture - conclusion - stress-corrosion cracking studies prompt changes in pipeline operating-conditions. *Oil & Gas Journal*, 85(5):37–38, 1987.

[4] R. N. Parkins. Factors influencing stress-corrosion crack-growth kinetics. *Corrosion*, 43(3):130–139, 1987.

[5] K. Sieradzki and R. C. Newman. Stress-corrosion cracking. *Journal of Physics and Chemistry of Solids*, 48(11):1101–1113, 1987.

[6] R. N. Parkins. Current understanding of stress-corrosion cracking. *Journal of the Minerals Metals & Materials Society*, 44(12):12–19, 1992.

[7] R. N. Parkins. Overview of intergranular SCC research activities: Pr-232-9401. Technical report, Pipeline Research Council International, Inc., 1994.

[8] R. N. Parkins. Mechanistic aspects of intergranular stress corrosion cracking of ferritic steels. *Corrosion*, 52(5):363–374, 1996.

[9] B. N. Leis and R. J. Eiber. Stress-corrosion cracking on gas-transmission pipelines: History, causes, and mitigation. *First International Business Conference on Onshore Pipelines, Berlin, Germany*, 1997.

[10] B. N. Leis and R. N. Parkins. Mechanics and material aspects in predicting serviceability limited by stress-corrosion cracking. *Fatigue & Fracture of Engineering Materials & Structures*, 21(5):583–601, 1998.

[11] Canadian Energy Pipeline Association. Stress corrosion cracking recommended practices, 2nd edition. Technical report, 2007.

[12] R. Sutherby and C. Weixing. Deflected stress corrosion cracks in the pipeline steel. *International Pipeline Conference, Calgary, Alberta, Canada, October 4–8*, pages 1–9, 2004.

[13] J. Xie, L. Yang, M. Sen, R. Worthingham, and F. King. Mechanistic investigation of deflected stress corrosion cracking in pipeline steels. *NACE International Corrosion 2009 Conference & Expo, Atlanta, Georgia, USA*, pages 1–19, 2009.

[14] L. Zadow. Characterisation of the morphology of inclined scc cracks in australian gas pipelines, 2014. M.A. Thesis, University of Adelaide, Adelaide.

[15] E. Gamboa, M. Giuliani, and O. Lavigne. X-ray microtomography observation of subsurface stress corrosion crack interactions in a pipeline low carbon steel. *Scripta Materialia*, 81:1–3, 2014.

[16] V. M. Linton, E. Gamboa, and M. Law. Fatigue crack extension and repair of pipes with scc cracks. *EPCRC Canberra Joint Technical Meeting*, 2007.

[17] F. Song. Overall mechanisms of high ph and near-neutral ph scc, models for forecasting scc susceptible locations, and simple algorithms for predicting high ph scc crack growth rates. *NACE Corrosion 2008: Conference and Expo, New Orleans, Louisiana*, 2008.

[18] R. N. Parkins and P. M. Singh. Stress corrosion crack coalescence. *Corrosion*, 46:485–499, 1990.

[19] Y. Z. Wang, J. D. Atkinson, R. Akid, and R. N. Parkins. Crack interaction, coalescence and mixed mode fracture mechanics. *Fatigue & Fracture of Engineering Materials & Structures*, 19(1):51–63, 1996.

[20] F. Song, B. T. Lu, M. Gao, and M. Elboujdaini. Development of a commercial model to predict stress corrosion cracking growth rates in operating pipelines. Technical report, Southwest Research Institute, 2011.

[21] B. T. Lu. Further study on crack growth model of buried pipelines exposed to concentrated carbonate-bicarbonate solution. *Engineering Fracture Mechanics*, 131:296–314, 2014.

[22] L. Zadow, E. Gamboa, and O. Lavigne. Inclined stress corrosion cracks in gas pipeline steels: morphology and implications. *Materials and Corrosion*, 66(10):1092–1100, 2014.

[23] Y. F. Cheng. *Stress Corrosion Cracking of Pipelines*. John Wiley & Sons, 2013.

[24] B. Y. Fang, A. Atrens, J. Q. Wang, E. H. Han, Z. Y. Zhu, and W. Ke. Review of stress corrosion cracking of pipeline steels in "low" and "high" ph solutions. *Journal of Materials Science*, 38(1):127–132, 2003.

[25] J. Wang and A. Atrens. Analysis of service stress corrosion cracking in a natural gas transmission pipeline, active or dormant? *Engineering Failure Analysis*, 11(1):3–18, 2004.

[26] A. P. Jivkov. Strain-induced passivity breakdown in corrosion crack initiation. *Theoretical and Applied Fracture Mechanics*, 42(1):43–52, 2004.

[27] O. Lavigne, E. Gamboa, V. Luzin, M. Law, M. Giuliani, and W. Costin. The effect of the crystallographic texture on intergranular stress corrosion crack paths. *Materials Science and Engineering: A*, 618:305, 2014.

[28] K. Spencer, U. Arumugam, and S. Kariyawasam. Improving interpretation of scc anomalies found by ultrasonic ili. *Pipeline & Gas Journal*, 235(6):8, 2008.

[29] O. Lavigne, E. Gamboa, W. Costin, M. Law, V. Luzin, and V. Linton. Microstructural and mechanical factors influencing high ph stress corrosion cracking susceptibility of low carbon line pipe steel. *Engineering Failure Analysis*, 45:283–291, 2014.

[30] S. Yaguchi and T. Yonezawa. Intergranular stress corrosion cracking growth perpendicular to fatigue pre-cracks in t-l oriented compact tension specimens in simulated pressurized water reactor primary water. *Corrosion Science*, 86: 326–336, 2014.

[31] Z. P. Lu, T. Shoji, F. J. Meng, Y. B. Qiu, T. C. Dan, and H. Xue. Effects of water chemistry and loading conditions on stress corrosion cracking of cold-rolled 316ng stainless steel in high temperature water. *Corrosion Science*, 53(1):247–262, 2011.

[32] T. Terachi, T. Yamada, T. Miyamoto, and K. Arioka. Scc growth behaviors of austenitic stainless steels in simulated pwr primary water. *Journal of Nuclear Materials*, 426(1-3):59–70, 2012.

[33] X. Tang and Y. F. Cheng. Micro-electrochemical characterization of the effect of applied stress on local anodic dissolution behavior of pipeline steel under near-neutral ph condition. *Electrochimica Acta*, 54(5):1499–1505, 2009.

[34] F. M. Song. Predicting the mechanisms and crack growth rates of pipelines undergoing stress corrosion cracking at high ph. *Corrosion Science*, 51(11): 2657–2674, 2009.

[35] G. R. Irwin. Relation of stresses near a crack to the crack extension force. Technical report, National research laboratory, 1956.

[36] I. N. Sneddon. The distribution of stress in the neighbourhood of a crack in an elastic solid. *Proceedings of the Royal Society of London Series A-Mathematical and Physical Sciences*, 187(1009):229–260, 1946.

[37] R. V. Goldstein and R. L. Salganik. Brittle-fracture of solids with arbitrary cracks. *International Journal of Fracture*, 10(4):507–523, 1974.

[38] B. Cotterell and J. R. Rice. Slightly curved or kinked cracks. *International Journal of Fracture*, 16(2):155–169, 1980.

[39] C. H. Wang. *Introduction to fracture mechanics*. DSTO Aeronautical and Maritime Research Laboratory, Melbourne, Victoria, 1996.

[40] M. Adda-Bedia. Path prediction of kinked and branched cracks in plane situations. *Physical Review Letters*, 93(18), 2004.

[41] S. Suresh. Crack deflection - implications for the growth of long and short fatigue cracks. *Metallurgical Transactions A-Physical Metallurgy and Materials Science*, 14(11):2375–2385, 1983.

[42] T. Fett, G. Rizzi, H. A. Bahr, U. Bahr, V. B. Pham, and H. Balke. A general weight function approach to compute mode-ii stress intensity factors and crack paths for slightly curved or kinked cracks in finite bodies. *Engineering Fracture Mechanics*, 75(8):2246–2259, 2008.

[43] S. Bechtle, T. Fett, G. Rizzi, S. Habelitz, and G. A. Schneider. Mixed-mode stress intensity factors for kink cracks with finite kink length loaded in tension and bending: Application to dentin and enamel. *Journal of the Mechanical Behavior of Biomedical Materials*, 3(4):303–312, 2010.

[44] A. A. Griffith. The phenomena of rupture and flow in solids. *Philosophical Transactions of the Royal Society of London. Series A, Containing Papers of a Mathematical or Physical Character*, 221:163–198, 1921.

[45] A. Chambolle, G. A. Francfort, and J. J. Marigo. When and how do cracks propagate? *Journal of the Mechanics and Physics of Solids*, 57(9):1614–1622, 2009.

[46] A. Salvadori. Crack kinking in brittle materials. *Journal of the Mechanics and Physics of Solids*, 58(11):1835–1846, 2010.

[47] M. A. Arafin and J. A. Szpunar. A new understanding of intergranular stress corrosion cracking resistance of pipeline steel through grain boundary character and crystallographic texture studies. *Corrosion Science*, 51(1): 119–128, 2009.

[48] M. A. Arafin and J. A. Szpunar. A novel microstructure - grain boundary character based integrated modeling approach of intergranular stress corrosion crack propagation in polycrystalline materials. *Computational Materials Science*, 47(4):890–900, 2010.

[49] M. A. Arafin and J. A. Szpunar. A microtexture-microstructure model to simulate intergranular stress corrosion crack propagation in pipeline steel. *Proceedings of the Asme International Pipeline Conference 2010, Vol 3*, pages 317–324, 2010.

[50] D. L. Li, R. Z. Zhu, and W. Q. Zhang. The acceleration mechanism of stress on anodic-dissolution of bare metal-surface. *Metallurgical Transactions a-Physical Metallurgy and Materials Science*, 21(12):3260–3264, 1990.

[51] P. J. Withers. Fracture mechanics by three-dimensional crack-tip synchrotron x-ray microscopy. *Philosophical Transactions of the Royal Society a-Mathematical Physical and Engineering Sciences*, 373(2036), 2015.

[52] M. Sahal, J. Creus, R. Sabot, and X. Feaugas. Consequences of plastic strain on the dissolution process of polycrystalline nickel in h2so4 solution. *Scripta Materialia*, 51(9):869–873, 2004.

[53] D. B. Wells, J. Stewart, R. Davidson, P. M. Scott, and D. E. Williams. The mechanism of intergranular stress-corrosion cracking of sensitized austenitic stainless-steel in dilute thiosulfate solution. *Corrosion Science*, 33(1):39–71, 1992.

[54] Y. X. Wang, W. M. Zhao, H. Ai, X. G. Zhou, and T. M. Zhang. Effects of strain on the corrosion behaviour of x80 steel. *Corrosion Science*, 53(9): 2761–2766, 2011.

[55] R. K. Ren, S. Zhang, X. L. Pang, and K. W. Gao. A novel observation of the interaction between the macroelastic stress and electrochemical corrosion of low carbon steel in 3.5 wt% nacl solution. *Electrochimica Acta*, 85:283–294, 2012.

[56] X. G. Feng, Y. Zuo, Y. M. Tang, X. H. Zhao, and J. M. Zhao. The influence of strain on the passive behavior of carbon steel in cement extract. *Corrosion Science*, 65:542–548, 2012.

[57] L. Y. Xu and Y. F. Cheng. Corrosion of x100 pipeline steel under plastic strain in a neutral ph bicarbonate solution. *Corrosion Science*, 64:145–152, 2012.

[58] L. Y. Xu and Y. F. Cheng. Development of a finite element model for simulation and prediction of mechanoelectrochemical effect of pipeline corrosion. *Corrosion Science*, 73:150–160, 2013.

[59] X. Wang, X. Tang, L. Wang, C. Wang, and W. Zhou. Synergistic effect of stray current and stress on corrosion of api x65 steel. *Journal of Natural Gas, Science and Engineering*, 21:474, 2014.

[60] A. R. Despic, R. G. Raicheff, and J. O'M. Bockris. Mechanism of the acceleration of the electrodic dissolution of metals during yielding under stress. *The Journal of Chemical Physics*, 49(2):926, 1968.

[61] E. M. Gutman, G. Solovioff, and D. Eliezer. The mechanochemical behavior of type 316l stainless steel. *Corrosion Science*, 38(7):1141, 1996.

[62] M. Sahal, J. Creus, R. Sabot, and X. Feaugas. The effects of dislocation patterns on the dissolution process of polycrystalline nickel. *Acta Materialia*, 54(8):2157–2167, 2006.

[63] A. Tafreshi. Simulation of crack propagation in anisotropic structures using the boundary element shape sensitivities and optimisation techniques. *Engineering Analysis with Boundary Elements*, 35(8):984–995, 2011.

[64] P. L. Chin. Stress analysis, crack propagation and stress intensity factor computation of a ti-6al-4v aerospace bracket using ansys and franc3d, 2011. Ph.D. Thesis, Rensselear Polytechnic Institute, Hartford, Connecticut.

[65] Y. Sun, K. Meciejewski, and H. Ghonem. A damage-based cohesive zone model of intergranular crack growth in nickel-based superalloy. *International Journal of Damage Mechanics*, 23(3):1–19, 2012.

[66] M. Kamaya and T. Kitamura. A simulation on growth of multiple small cracks under stress corrosion. *International Journal of Fracture*, 130(4): 787–801, 2004.

[67] M. Kamaya and M. Itakura. Simulation for intergranular stress corrosion cracking based on a three-dimensional polycrystalline model. *Engineering Fracture Mechanics*, 76(3):386–401, 2009.

[68] A. Stoll and A. J. Wilkinson. Use of a dislocation-based boundary element model to extract crack growth rates from depth distributions of intergranular stress corrosion cracks. *Acta Materialia*, 60(13-14):5101–5108, 2012.

[69] A. P. Jivkov, N. P. C. Stevens, and T. J. Marrow. A two-dimensional mesoscale model for intergranular stress corrosion crack propagation. *Acta Materialia*, 54(13):3493–3501, 2006.

[70] A. P. Jivkov, N. P. C. Stevens, and T. J. Marrow. Mesoscale mechanical model for intergranular stress corrosion cracking and implications for microstructure engineering. *Journal of Pressure Vessel Technology-Transactions of the ASME*, 130(3):21–27, 2008.

[71] A. P. Jivkov, N. P. C. Stevens, and Marrow T. J. A three-dimensional computational model for intergranular cracking. *Computational Materials Science*, 38:442–453, 2006.

[72] A. P. Jivkov and T. J. Marrow. Rates of intergranular environment assisted cracking in three-dimensional model microstructures. *Theoretical and Applied Fracture Mechanics*, 48:187–202, 2007.

[73] A. Musienko and G. Cailletaud. Simulation of inter- and transgranular crack propagation in polycrystalline aggregates due to stress corrosion cracking. *Acta Materialia*, 57:3840–3855, 2009.

[74] J. J. Rimoli. A computational model for intergranular stress corrosion cracking, 2009. Ph.D. Thesis, California Institute of Technology, Pasadena, California.

[75] M. Itakura, H. Kaburaki, and C. Arakawa. Branching mechanism of intergranular crack propagation in three dimensions. *Physical Review E*, 71(5): 055102, 2005.

[76] I. Simonovski, L. Cizelj, T. J. Marrow, J. Q. da Fonseca, and A. King. Towards modelling intergranular stress-sorrosion cracks using experimentally obtained grain topologies. *ASME Pressure Vessels and Piping Conference 2009, Vol 3: Design and Analysis*, pages 543–550, 2010.

[77] P. Zhang, M. Karimpour, D. Balint, J. G. Lin, and D. Farrugia. A controlled poisson voronoi tessellation for grain and cohesive boundary generation applied to crystal plasticity analysis. *Computational Materials Science*, 64: 84–89, 2012.

[78] D. M. Yan, W. P. Wang, B. Levy, and Y. Liu. Efficient computation of 3d clipped voronoi diagram. *Advances in Geometric Modeling and Processing, Proceedings*, 6130:269–282, 2010.

[79] H. Ledoux. Computing the 3d voronoi diagram robustly: An easy explanation. *ISVD 2007: The 4th International Symposium on Voronoi Diagrams in Science and Engineering 2007, Proceedings*, pages 117–129, 2007.

[80] B. T. Lu, F. Song, M. Gao, and M. Elboujdaini. Crack growth model for pipelines exposed to concentrated carbonate-bicarbonate solution with high ph. *Corrosion Science*, 52(12):4064–4072, 2010.

[81] T. Shoji, Z. P. Lu, and H. Murakami. Formulating stress corrosion cracking growth rates by combination of crack tip mechanics and crack tip oxidation kinetics. *Corrosion Science*, 52(3):769–779, 2010.

[82] S. Laham. Stress intensity factor and limit load handbook. *British Energy Generation Ltd*, (2), 1998.

[83] T. J. Marrow, L. Babout, A. P. Jivkov, P. Wood, D. Engelberg, N. Stevens, P. J. Withers, and R. C. Newman. Three dimensional observations and modelling of intergranular stress corrosion cracking in austenitic stainless steel. *Journal of Nuclear Materials*, 352(1-3):62–74, 2006.

[84] A. R. Khoei and K. Karimi. An enriched-fem model for simulation of localization phenomenon in cosserat continuum theory. *Computational Materials Science*, 44(2):733–749, 2008.

[85] W. Attaporn and H. Koguchi. Intensity of stress singularity at a vertex and along the free edges of the interface in 3d-dissimilar material joints using 3d-enriched fem. *Cmes-Computer Modeling in Engineering & Sciences*, 39 (3):237–262, 2009.

[86] A. R. Khoei, S. M. Taheri-Mousavi, S. O. R. Biabanaki, and M. Anahid. An enriched-fem technique for large frictional contact deformation. *Steel Research International*, 81(9):1478–1481, 2010.

[87] A. R. Khoei, M. Vahab, E. Haghighat, and S. Moallemi. A mesh-independent finite element formulation for modeling crack growth in saturated porous media based on an enriched-fem technique. *International Journal of Fracture*, 188(1):79–108, 2014.

[88] E. Ferrie, J. Y. Buffiere, W. Ludwig, A. Gravouil, and L. Edwards. Fatigue crack propagation: In situ visualization using x-ray microtomography and 3d simulation using the extended finite element method. *Acta Materialia*, 54(4):1111–1122, 2006.

[89] R. Pourmodheji and M. Mashayekhi. Improvement of the extended finite element method for ductile crack growth. *Materials Science and Engineering a-Structural Materials Properties Microstructure and Processing*, 551:255–271, 2012.

[90] Q. Z. Zhu. On enrichment functions in the extended finite element method. *International Journal for Numerical Methods in Engineering*, 91(2):186–217, 2012.

[91] S. S. Hosseini, H. Bayesteh, and S. Mohammadi. Thermo-mechanical xfem crack propagation analysis of functionally graded materials. *Materials Science and Engineering a-Structural Materials Properties Microstructure and Processing*, 561:285–302, 2013.

[92] K. Oguni, M. L. L. Wijerathne, T. Okinaka, and M. Hori. Crack propagation analysis using pds-fem and comparison with fracture experiment. *Mechanics of Materials*, 41(11):1242–1252, 2009.

[93] H. Chen, L. Wijeranthne, M. Hori, and T. Ichimura. Stability of dynamic growth of two anti-symmetric cracks using pds-fem. *Structural Engineering / Earthquake Engineering*, 29(1):1–8, 2012.

[94] R. B. Stonesifer, F. W. Brust, and B. N. Leis. Mixed-mode stress intensity factors for interacting semielliptic surface cracks in a plate. *Engineering Fracture Mechanics*, 45(3):357–380, 1993.

[95] R. Sankar and A. J. Lesser. Generic overlapping cracks in polymers: Modeling of interaction. *International Journal of Fracture*, 142(3-4):277–287, 2006.

[96] M. Kamaya. Growth evaluation of multiple interacting surface cracks. part ii: Growth evaluation of parallel cracks. *Engineering Fracture Mechanics*, 75(6):1350–1366, 2008.

[97] A. Kotousov and D. Chang. Theoretical and experimental study of fatigue growth of interacting cracks. *International Journal of Fatigue*, 70:130–136, 2015.

[98] D. Chang and A. Kotousov. A fatigue crack growth model for interacting cracks in a plate of arbitrary thickness. *Fatigue & Fracture of Engineering Materials & Structures*, 37(11):1254–1267, 2014.

[99] E. Gamboa, O. Lavigne, J. Griggs, M. Law, and V. Luzin. Comparison between Canadian and Australian inclined SCC samples. *20th Joint Technical Meeting, Paris, France, 3-8 May 2015*, 2015.

[100] J. M. Sutcliff, W. K. Boyd, R. R. Fessler, and R. N. Parkins. Stress-corrosion cracking of carbon-steel in carbonate solutions. *Corrosion*, 28(8):313–320, 1972.

[101] L. Y. Xu and Y. F. Cheng. An experimental investigation of corrosion of x100 pipeline steel under uniaxial elastic stress in a near-neutral ph solution. *Corrosion Science*, 59:103–109, 2012.

[102] O. Lavigne, E. Gamboa, J. Griggs, V. Luzin, M. Law, and A. Roccisano. High ph inclined stress corrosion cracking in australian and canadian gas pipeline x65 steels. *Materials Science and Technology*, 2016. DOI:10.1080/02670836.2015.1132030.

[103] A. K. Pilkey, S. B. Lambert, and A. Plumtree. Stress-corrosion cracking of x-60 line pipe steel in a carbonate-bicarbonate solution. *Corrosion*, 51(2): 91–96, 1995.

Appendix A

Code developed

A.1 Intergranular growth code

A.1.1 Intergranulargrowth.m

File type: Matlab code Purpose: Generates crack paths with the influence of texture (requires textural survey in the file resistantgrains.csv). Is a little slower than the code without texture. The code assumes a crack path governed by passive film fracture (highest SIF direction) for values below a critical strain, and a path governed by highest strain (strain enhanced dissolution) above that critical strain. Only the path is considered, and the growth rate is tackled in a separate electrochemical model. This model differs from the previous by assuming that some grain boundaries are resistant to crack propagation.

Key Inputs:

- benddepth (m): point at which code starts checking ansys for inclination initiation [to speed up run time]
- Jcrittable: Critical J integral of interest considering a 100MPa tensile stress (each value produces another cycle)
- xsize: Width of the area to generate
- ysize: Depth of the area to generate
- aspectRatio: Aspect ratio of interest (multiple aspect ratios can be seen in separate or the same figures by editing the figure outputs)
- resistantgrains.csv: input of bands of grain boundary angles and proportion of resistant boundaries at that angle. Described further in the following section.

Outputs: One figure for each aspect ratio requested, each filled with the length of Jcrittable of cracks. The top centre of the figure shows the initiation point, and the cracks grow in the negative Y direction. All values in mm.

Troubleshooting: If you stop a run of this code part way through, you will have to delete the lock file along with the error files in the working directory.

```
1 clc
2 clear all
3 close all
4
5 xsize=2;
```

```
6  ysize=2;
7  benddepth=-0.5;
8  print1=[1,2,3,4,5,6,7,8,9,10];
9
10
11
12 xsave=zeros(20,1000);
13 ysave=zeros(20,1000);
14
15 [StubbornAngles, ...
       StubbornFraction]=readresist(csvread("resistantgrains.csv"));
16
17
18 Jcrittable=[950 950 950 950 950];
19
20 aspectRatio=[0.51];
21
22 timetaken=zeros(length(aspectRatio),length(Jcrittable));
23
24 rr=[1 0 0 1 1 0];
25 bb=[0 1 0 1 0 1];
26 gg=[0 0 1 0 1 1];
27
28 for kkkk=1:length(aspectRatio)
29
30     ansysrunnumber=0;
31
32     Jint=0;
```

```
33      gcount=0;
34      xxx=0;
35      nocount=0;
36      noFEA=0;
37
38      tt=cputime;
39      for iiiii=1:length(Jcrittable)
40
41          tic
42
43          Jcrit=Jcrittable(iiiii);
44
45          vkinky=-1;
46          vkinkx=-1;
47          outarrayx=zeros(1,9);
48          outarrayy=zeros(1,9);
49          outarrayx2=zeros(1,8);
50          outarrayy2=zeros(1,8);
51          haskinked=0;
52          Plastic=45;
53          NegAngle=[0,0];
54          gcount=0;
55
56          vorrseeds=floor(xsize*ysize/aspectRatio(kkkk)*(1000/8)^2)+1;
57
58          randx=xsize*rand(1,vorrseeds);
59          randy=-ysize*rand(1,vorrseeds)/aspectRatio(kkkk);
60          [vx, vy]= voronoi(randx,randy);
```

```
61          clear randx
62          clear randy
63
64
65          vy=vy*aspectRatio(kkkk);
66
67          kk=1;
68
69          for ii=1:length(vy)
70              if vy(1,ii)>0
71                  if vy(2,ii)<0
72                      vstarty(kk)=vy(2,ii);
73                      vstartx(kk)=vx(2,ii);
74                      vstarty2(kk)=vy(1,ii);
75                      vstartx2(kk)=vx(1,ii);
76                      vstarti(kk)=ii;
77                      kk=kk+1;
78                  end
79              else if vy(2,ii)>0
80                      if vy(1,ii)<0
81                          vstarty(kk)=vy(1,ii);
82                          vstartx(kk)=vx(1,ii);
83                          vstarty2(kk)=vy(2,ii);
84                          vstartx2(kk)=vx(2,ii);
85                          vstarti(kk)=ii;
86                          kk=kk+1;
87                      end
88                  end
```

```
89              end
90
91          end
92          kk=1;
93          vnum=100;
94
95          for ii=1:length(vstartx)
96              vnumtemp=abs(vstartx(ii)-0.5*xsize);
97              if vnumtemp<vnum
98                  vnum=vnumtemp;
99                  vnumx=vstartx(ii);
100                 vnumy=vstarty(ii);
101                 vnumx2=vstartx2(ii);
102                 vnumy2=vstarty2(ii);
103                 vix=vstarti(ii);
104             end
105         end
106         vstarty=0;
107         vstartx=0;
108         vstarty2=0;
109         vstartx2=0;
110         vstarti=0;
111
112         x=[vnumx2; vnumx];
113         y=[vnumy2; vnumy];
114         disp([num2str(iiiii), "start chosen"])
115
116
```

```
117         for nn=1:1000000
118
119             [vnextx,vnexty,vnexti] = ...
    next2grains(vx,vy,vix,vnumx,vnumy); % gets the next 2 grains ...
    in vnextx and vnexty
120
121
122             if length(vnextx)>1 && kkkk==2
123                 [vnextx,vnexty,vnexti] = ...
    textureeffect(vnextx,vnexty,vnexti,vnumx,vnumy,StubbornAngles,StubbornFraction)
    % determines if grains are resistant
124             end
125
126
127             if haskinked==1;
128                 [xtemp,ytemp,vix,GrowAng] = ...
    whichgrainplastic(vnextx,vnexty,vnexti,vnumx,vnumy,Jcrit,Jint,Plastic); ...
    % picks which grain to break if plasticity criterion active
129             end
130
131             if haskinked==0;
132                 ...
    [xtemp,ytemp,vix,GrowAng,vkinkx,vkinky,haskinked,noFEA,Plastic] ...
    = ...
    whichgrainelastic(vnextx,vnexty,vnexti,vnumx,vnumy,Plastic,benddepth); ...
    % picks which grain to break before plasticity criterion active
133             end
134
```

```
135
136             if GrowAng==100 %in case of failure (no more possible ...
    boundaries)
137                 disp(["Crack number ", num2str(iiiii), " arrested ...
    after ", num2str(nn), " grain boundaries"])
138                 break
139             end
140
141
142
143             if nocount>xxx
144                 noFEA=0;
145             end
146
147
148             if ytemp<-ysize || xtemp<0 || xtemp > xsize
149                 break
150             end
151
152             vnumx2=vnumx;
153             vnumy2=vnumy;
154             vnumx=xtemp;
155             vnumy=ytemp;
156
157             x2=[vnumx2; vnumx];
158             y2=[vnumy2; vnumy];
159
160             x=[x x2];
```

```
161             y=[y y2];
162
163
164             if vkinky>outarrayy2(1)
165                 vfirstx=vkinkx;
166                 vfirsty=vkinky;
167             else
168                 vfirstx=outarrayx2(1);
169                 vfirsty=outarrayy2(1);
170             end
171
172             for oacount=2:9
173                 outarrayx(oacount-1)=outarrayx(oacount);
174                 outarrayy(oacount-1)=outarrayy(oacount);
175             end
176
177             outarrayx(9)=vnumx;
178             outarrayy(9)=vnumy;
179
180             if length(x)>10
181                 outarrayx2=[x(floor(0.25*length(x))) ...
    x(floor(0.5*length(x))) x(floor(0.7*length(x))) ...
    x(floor(0.8*length(x))) x(floor(0.85*length(x))) ...
    x(floor(7/8*length(x))) x(floor(15/16*length(x))) ...
    x(floor(31/32*length(x)))];
```

```
182                 outarrayy2=[y(floor(0.25*length(x))) ...
    y(floor(0.5*length(x))) y(floor(0.7*length(x))) ...
    y(floor(0.8*length(x))) y(floor(0.85*length(x))) ...
    y(floor(7/8*length(x))) y(floor(15/16*length(x))) ...
    y(floor(31/32*length(x)))];
183             end
184
185             tofilex=[(vfirstx-xsize/2)/1000 ...
    (outarrayx2(2:8)-xsize/2)/1000 (outarrayx(5)-xsize/2)/1000 ...
    (outarrayx(9)-xsize/2)/1000];
186             tofiley=[vfirsty/1000 outarrayy2(2:8)/1000 ...
    outarrayy(5)/1000 outarrayy(9)/1000];
187
188             timecyc=0;
189             if noFEA==0 && haskinked ==1
190
191
192                 crackoutx=fopen("cracklocx.txt","w");
193                 fprintf(crackoutx,"%7.5f ",[1 print1]);
194                 fprintf(crackoutx,"\r\n%7.5f ",1);
195                 fprintf(crackoutx,"%10.8f ",tofilex);
196                 fclose(crackoutx);
197
198                 crackouty=fopen("cracklocy.txt","w");
199                 fprintf(crackouty,"%7.5f ",[1 print1]);
200                 fprintf(crackouty,"\r\n%7.5f ",1);
201                 fprintf(crackouty,"%10.8f ",tofiley);
202                 fclose(crackouty);
```

```
203
204                 !"C:\Program Files\ANSYS ...
    Inc\v150\ANSYS\bin\winx64\ANSYS150.exe" -b -i ...
    ANSYSinClined10pts.txt -o ANSYSoutClined10pts.txt
205
206                 load Jintegral.txt
207                 Jint=abs(Jintegral);
208
209
210                 nocount=0;
211                 gcount=gcount+1;
212                 ansysrunnumber=ansysrunnumber+1;
213
214             end
215
216
217             if gcount≥10
218                 noFEA=1;
219                 xxx=100;
220                 nocount=0;
221                 gcount=gcount+1;
222                 vnumx
223                 vnumy
224             end
225
226             if mod(gcount,10)==0 || gcount==15
227                 noFEA=0;
228
```

```
229             end
230
231             if gcount>100
232                 noFEA=1;
233             end
234
235             if Jint<Jcrit && haskinked==1
236                 noFEA=1;
237                 xxx=(Jcrit-Jint)/Jcrit*6/aspectRatio(kkkk);
238                 gcount=0;
239                 nocount=nocount+1;
240             end
241
242
243             end
244
245         figure(kkkk)
246         axis([0 xsize -ysize 0]);
247         line(x,y,"Color",[bb(kkkk) 0 rr(kkkk)],"LineWidth",1)
248         xlabel("Hoop direction (mm)")
249         ylabel("Distance from outer surface (mm)")
250         axis equal
251
252
253         clear vx
254         clear vy
255         clear x
256         clear y
```

```
257
258         timetaken(kkkk,iiiii)=toc
259
260     end
261 end
262 disp("donesies")
```

A.1.1.1 Required functions for Intergranulargrowth.m

```
1  function [vnextx,vnexty,vnexti] = ...
       next2grains(vx,vy,vix,vnumx,vnumy) % gets the next 2 grains in ...
       vnextx and vnexty
2  kk=1;
3  vnextx=0;
4  vnexty=0;
5  vnexti=0;
6  for ii=1:length(vx);
7      if vx(1,ii)==vnumx && vy(1,ii)==vnumy && ii≠vix
8          vnextx(kk)=vx(2,ii);
9          vnexty(kk)=vy(2,ii);
10         vnexti(kk)=ii;
11         kk=kk+1;
12
13     else if vx(2,ii)==vnumx && vy(2,ii)==vnumy && ii≠vix
14             vnextx(kk)=vx(1,ii);
15             vnexty(kk)=vy(1,ii);
16             vnexti(kk)=ii;
```

```
17              kk=kk+1;
18
19          end
20      end
21      if length(vnexty)==2
22          break
23      end
24  end
```

```
1  function [f1,f2] = readresist(test2) % f1=angle limits, ...
       f2=percent chance of resistant boundary
2
3  f1=test2(1:length(test2)/2);
4  f2=test2(length(test2)/2+1:length(test2));
```

```
1  function [vnextx,vnexty,vnexti] = ...
       textureeffect(vnextx,vnexty,vnexti,vnumx,vnumy,StubbornAngles,StubbornFraction
       % tells which grain will bust
2
3  myAngle=zeros(1,length(vnextx));
4  myRands=rand(1,length(vnextx));
5  vres=zeros(1,length(vnextx));
6  for ii=1:length(vnextx)
7      myAngle(ii)=atand(abs((vnumx-vnextx(ii))/(vnumy-vnexty(ii))));
8      for jj=1:length(StubbornAngles);
```

```
9           if myAngle(ii)≤StubbornAngles(jj) && ...
    myAngle(ii)≥StubbornAngles(jj)
10              if myRands(ii)<StubbornFraction(jj)
11                  vres(ii)=1;
12              else
13                  kk=ii;
14              end
15          end
16      end
17  end
18
19  if sum(vres)==1
20      vnextx=vnextx(kk);
21      vnexty=vnexty(kk);
22      vnexti=vnexti(kk);
23  end
```

```
1   function ...
        [xtemp,ytemp,vix,GrowAng,vkinkx,vkinky,haskinked,noFEA,Plastic] ...
        = ...
        whichgrainelastic(vnextx,vnexty,vnexti,vnumx,vnumy,Plastic,benddepth) ...
        % tells which grain will bust
2
3   GrowAng=100;
4   GrowAngTemp=0;
5   AngleFromPlastic=[0,0];
6   vkinky=-1;
```

```
7  vkinkx=-1;
8  haskinked=0;
9  noFEA=0;
10 NegAngle=[0,0];
11
12
13 for ii=1:length(vnextx)
14     ...
       GrowAngTemp(ii)=atand(abs(vnumx-vnextx(ii))/abs(vnumy-vnexty(ii))); ...
       %calculates the angles if it grew that way
15     if (vnumx-vnextx(ii))>0
16         GrowAngTemp(ii)=-GrowAngTemp(ii);
17
18     end
19
20     AngleFromPlastic(ii)=abs(Plastic-GrowAngTemp(ii));
21
22
23     if vnexty(ii)<vnumy %&& IsGrow>StubbornFraction
24         if GrowAng==100
25             GrowAng=GrowAngTemp(ii);
26             xtemp=vnextx(ii);
27             ytemp=vnexty(ii);
28             vix=vnexti(ii);
29         else
30             if vnumy>benddepth
31                 if abs(GrowAngTemp(ii))<abs(GrowAngTemp(ii-1))
32
```

```
33                      GrowAng=GrowAngTemp(ii);
34                      xtemp=vnextx(ii);
35                      ytemp=vnexty(ii);
36                      vix=vnexti(ii);
37
38                  end
39              end
40
41              if vnumy<benddepth
42
43                  if AngleFromPlastic(ii-1)>45;
44                      ...
    AngleFromPlastic(ii-1)=abs(AngleFromPlastic(ii-1)-90);
45                      NegAngle(ii-1)=1;
46                  end
47                  if AngleFromPlastic(ii)>45;
48                      ...
    AngleFromPlastic(ii)=abs(AngleFromPlastic(ii)-90);
49                      NegAngle(ii)=1;
50                  end
51
52                  if AngleFromPlastic(ii)<AngleFromPlastic(ii-1)
53                      ja=ii;
54                  else
55                      ja=ii-1;
56                  end
57                  if NegAngle(ja)==1;
58                      Plastic=-45;
```

```
                end

                haskinked=1;
                noFEA=0;
                GrowAng=GrowAngTemp(ja);
                xtemp=vnextx(ja);
                ytemp=vnexty(ja);
                vix=vnexti(ja);
                vkinkx=xtemp;
                vkinky=ytemp;
            end
        end
    end
end
```

```
function [xtemp,ytemp,vix,GrowAng] = ...
    whichgrainplastic(vnextx,vnexty,vnexti,vnumx,vnumy,Jcrit,Jint,Plastic) ...
    % tells which grain will bust

GrowAng=100;
GrowAngTemp=0;
AngleFromPlastic=[0,0];

for ii=1:length(vnextx)
    ...
    GrowAngTemp(ii)=atand(abs(vnumx-vnextx(ii))/abs(vnumy-vnexty(ii))); ...
    %calculates the angles if it grew that way
```

```
9       if (vnumx-vnextx(ii))>0
10          GrowAngTemp(ii)=-GrowAngTemp(ii);
11
12      end
13
14      AngleFromPlastic(ii)=abs(Plastic-GrowAngTemp(ii));
15
16      if vnexty(ii)<vnumy %&& IsGrow>StubbornFraction
17          if GrowAng==100
18              GrowAng=GrowAngTemp(ii);
19              xtemp=vnextx(ii);
20              ytemp=vnexty(ii);
21              vix=vnexti(ii);
22          else
23              if Jcrit>Jint
24                  if abs(GrowAngTemp(ii))<abs(GrowAngTemp(ii-1))
25
26                      GrowAng=GrowAngTemp(ii);
27                      xtemp=vnextx(ii);
28                      ytemp=vnexty(ii);
29                      vix=vnexti(ii);
30
31                  end
32              end
33
34              if Jcrit<Jint
35
36                  if AngleFromPlastic(ii)<AngleFromPlastic(ii-1)
```

```
37                      ja=ii;
38                  else
39                      ja=ii-1;
40                  end
41
42                  GrowAng=GrowAngTemp(ja);
43                  xtemp=vnextx(ja);
44                  ytemp=vnexty(ja);
45                  vix=vnexti(ja);
46
47
48              end
49          end
50      end
51  end
```

A.1.2 ANSYSinclined10pts.txt

File type: text file (ANSYS input APDL code)

Purpose: Calculates J integral for the crack geometry

Use: Leave in the working directory

Inputs: Crack geometry (automatic generated in MATLAB code)

Outputs: J integral (automatically generated in ANSYS code and read in MATLAB code)

```
1
2  finish
3  /clear
4  /nerr,,99,999,999
5  /PREP7
6
7  BTOL,1e-5
8
9  !straight crack
10 !units: SI
11 *SET,height,8.3/1000 !m - height of the rectangle
12 *SET,width,100/1000 !m - width of the rectangle
13 *DIM,keyvecx,TABLE,1,10
14 *TREAD,keyvecx,cracklocx.txt
15
16 *SET,kinkx,keyvecx(1,10) !m - crack tip depth
17
18 *DIM,keyvecy,TABLE,1,10
19 *TREAD,keyvecy,cracklocy.txt
20
21 *SET,kinky,keyvecy(1,10) !m - crack tip depth
22
23 *SET,depth,-keyvecy(1,10)
24
25
26 !Keypoints to define area
27
28 k,1,0,0
```

```
29 k,2,0,0
30 k,3,width/2,0
31 k,4,width/2,-height
32 k,5,keyvecx(1,10),-height
33 k,6,-width/2,-height
34 k,7,-width/2,0
35
36 l,7,6              !        ----------  -----------
37 l,3,4              !      |           |           |
38 l,6,5              !   L1 |           \           |  L2
39 l,5,4              !      |-----------------------|
40                    !             L3          L4
41
42 k,10,keyvecx(1,1),keyvecy(1,1)                     !1 is root, 10 ...
       is tip
43 k,11,keyvecx(1,2),keyvecy(1,2)
44 k,12,keyvecx(1,3),keyvecy(1,3)
45 k,13,keyvecx(1,4),keyvecy(1,4)
46 k,14,keyvecx(1,5),keyvecy(1,5)
47 k,15,keyvecx(1,6),keyvecy(1,6)
48 k,16,keyvecx(1,7),keyvecy(1,7)
49 k,17,keyvecx(1,8),keyvecy(1,8)
50 k,18,keyvecx(1,9),keyvecy(1,9)
51 k,19,keyvecx(1,10),keyvecy(1,10)
52
53 k,20,keyvecx(1,1),keyvecy(1,1)                     !1 is root, 10 ...
       is tip
54 k,21,keyvecx(1,2),keyvecy(1,2)
```

```
k,22,keyvecx(1,3),keyvecy(1,3)
k,23,keyvecx(1,4),keyvecy(1,4)
k,24,keyvecx(1,5),keyvecy(1,5)
k,25,keyvecx(1,6),keyvecy(1,6)
k,26,keyvecx(1,7),keyvecy(1,7)
k,27,keyvecx(1,8),keyvecy(1,8)
k,28,keyvecx(1,9),keyvecy(1,9)

K,30,keyvecx(1,10),keyvecy(1,10)/2

!Create area from keypoints

A,1,10,11,12,13,14,15,16,17,18,19,5,6,7
A,2,20,21,22,23,24,25,26,27,28,19,5,4,3



circle,19,depth/1.9 !Creates sub area for face split
circle,19,depth/6

lsel,s,line,,28,31

CM,dacircle,LINE

lsel,s,line,,32,35

CM,innercircle,LINE
```

```
83
84 allsel,all
85
86 ASBL,ALL,dacircle
87
88 allsel,all
89
90 ASBL,ALL,innercircle
91
92
93
94
95
96 et,1,plane183,0,,2 !sets element plane183
97 !Sets material properties for element type 1
98 MP,EX,1,75 000 000 000 ! Youngs modulus GPa
99 MP,PRXY,1,0.3 ! Poissons ratio
100
101 esize,depth/200
102 amesh,1,2
103
104 esize,depth/100
105 amesh,7,8
106
107 esize,height/16
108 amesh,5,6
109
110
```

```
111
112 SFL,2,pres,-200 000 000 !applies a load out from the area (right ...
       edge)
113 DL,1,3,UX,0 !constrains the left edge
114 DL,3,3,UY,0 !constrains the bottom edge
115 DL,4,3,UY,0 !constrains the bottom edge
116
117 FINISH
118
119 /SOLU
120
121 !local coordinate system to align X direction with crack direction
122
123
124
125 CSKP,11,0,18,19,3
126 CSYS,0
127 ! select node located along the crack front and define it as ...
       crack front/tip node component
128
129 SELTOL,1e-10
130 NSEL,S,LOC,Y,kinky
131 NSEL,R,LOC,X,kinkx
132 CM,CRACK_TIP_NODE_CM,NODE
133
134 *GET,ctnodenum,NODE,0,NUM,MAX
135
136 ! Define a new J-Integral calculation (all from ANSYS help)
```

```
137 CINT,NEW,1
138 CINT,CTNC,CRACK_TIP_NODE_CM
139 CINT,NORM,11,2
140 CINT,NCON,20
141 CINT,SYMM,OFF
142
143 allsel,all
144
145 solve
146
147
148
149
150
151 finish
152
153 /POST1
154
155 PRCINT,1,CRACK_TIP_NODE_CM,JINT
156
157 *GET,Jintegriz,CINT,1,,ctnodenum,,18,,JINT
158  *cfopen,Jintegral.txt
159  *VWRITE,Jintegriz
160  (F10.4)
161  *cfclose
162
163 finish
```

A.2 Crack growth rate code

File type: Matlab code

Purpose: Show the difference in growth rates for a straight and inclined crack.

Comment: In it's current state, this model requires an input of the degree that the current density is higher along the inclined plane. Experimental data is not yet available for this, so only qualitative results can be obtained. Once experimental data is obtained that defines the increase of current density along the inclined plane, that can be incorporated into the variable "Fn". Fn is defined as the multiplier of the current density along the inclined plane, such that Ia(inclined plane)=Fn*Ia(radial plane).

Key Inputs:

- aend (m): final length of interest for crack.
- a0 (m): initial length of interest for crack.
- stress (Pa): mean stress
- ia0 (A/m^2): current density for a straight crack
- Fn: Degree that current density is higher at an angle than at the perpendicular (to be modified once experimental data is available)
- KIscc: Critical stress intensity factor. Keep in mind that the equations are only valid for SIFs above KIscc, so chose a0 and KIscc appropriately such that the crack SIF will exceed KIscc.

- thetastab: Stabalised angle seen in crack path analyses (degrees)
- astab: depth at which stabalised angle is seen (as calculated on page 6 of the milestone 3 report for RP2-09B)
- Fin: Mode 1 shape factor used in the stress intensity factor equation for an inclined crack with a steady angle of "thetastab"
- Various growth rate equation parameters (under the comment bar Equation parameters from Lu) used in "B. T. Lu, 'Further study on crack growth model of buried pipelines exposed to concentrated carbonate-bicarbonate solution', Engineering Fracture Mechanics, 2014, 131, 296-314". It is suggested to not change these unless familiar with the paper and equation.

Outputs: Graph of crack depth vs time for inclined and straight cracks. Legend identifies the straight crack (blue) and the inclined cracks Fn value (green to red).

```
%%
clc
clear all
close all


%%%%%%%%%%%%%%%%%%%%%%%%%%%%%%%%%%%%%%%%%%%%%
%                                           %
%                  Inputs                   %
%                                           %
%%%%%%%%%%%%%%%%%%%%%%%%%%%%%%%%%%%%%%%%%%%%%
```

```
12
13 %Important parameters
14 Fn=[1 1.1 1.2 1.3 1.4]; % current density at the angle verses ...
       straight
15 aend=7e-3; % Where the crack grows to (m)
16 ia0=80; % current density for the straight crack (A/m^2)
17 a0=1e-3; %initial length (m)
18 stress=400e6; %Avereage stress Pa
19 sigmay=480e6; %Yield (Pa)
20 Kiscc=20e6;
21 %%%%%%%%%%%%%%%%%%%%%%%%%%%%%%%%%%%%%%%%%%%%%%%%
22 %                                                 %
23 %       Inclined crack path constants             %
24 %                                                 %
25 %%%%%%%%%%%%%%%%%%%%%%%%%%%%%%%%%%%%%%%%%%%%%%%%
26 Fin=0.838; %shape factor for the stabalised angle (Found in a ...
       stress intensity factor handbook)
27 astab=a0/0.7; %Found from the text explaining Table 1 on page 6 ...
       of the Milestone 3 report for RP2-09B
28 thetastab=50; %Found from crack path analysis (degrees)
29
30 %%%%%%%%%%%%%%%%%%%%%%%%%%%%%%%%%%%%%%%%%%%%%%%%
31 %                                                 %
32 %       Equation parameters from Lu               %
33 %                                                 %
34 %%%%%%%%%%%%%%%%%%%%%%%%%%%%%%%%%%%%%%%%%%%%%%%%
35 n=0.667; %
36 ef=0.001;
```

```
t0=0.01;
r0=1e-6;
E=200e9;
N=6;
beta=5.08;
M=55.845e-3;
F=96485;
z=2;
rho=7.847e3;

%%%%%%%%%%%%%%%%%%%%%%%%%%%%%%%%%%%%%%%%%%%%%%
%                                            %
%               End of inputs                %
%                                            %
%%%%%%%%%%%%%%%%%%%%%%%%%%%%%%%%%%%%%%%%%%%%%%

%
%          ______________
%        /.--------------.\
%       //                \\
%      //                  \\
%     ||  .-..----.  .-.  .--.  ||
%     ||(  ( "-..-"|.-.||.-.|||
%     ||  \ \  ||  ||  ||||_||||
%     ||._) )  ||  \"-"/||-"  ||
%      \\"_"  ""   "_" ""   //
%       \\                //
%        \\______________//
```

```
%          "_________________"


%Straight crack

Δt=3600;
Fi=1.12; %shape factor for straight crack
ia=ia0;
t=0; %time
a=a0; %depth
adot=2e-9;

A0=1/(1-n)*M/(z*F*rho)*(t0/ef)^n;
B=2*N/(N-1)*beta*sigmay/(E*r0);

K=stress*Fi*sqrt(pi*a);
adot0= (A0*ia) ^ (1/(1-n)) * B^(n/(1-n)) * (log((K^2-Kiscc^2) / ...
    (pi*r0*sigmay^2))) ^ ( (n/(1-n))*(N+1)/(N-1) );
%%%%%%%%%%%%%%%%%%%%%%%%%%%%%%%%%%%%%%%%%%%%%%%%%%%%

%%%%%%for the loop%%%%%%%%%%%%%%%%%%%%%%%%%%%%%%%%
avec=a;
tvec=t;
jj=1;
%%%%%%%%%%%%%%%%%%%%%%%%%%%%%%%%%%%%%%%%%%%%%%%%%%%%

while a<aend
   K=stress*Fi*sqrt(pi*a);
```

```
92
93      adot= (A0*ia) ^ (1/(1-n)) * B^(n/(1-n)) * (log((K^2-Kiscc^2) / ...
        (pi*r0*sigmay^2))) ^ ( (n/(1-n))*(N+1)/(N-1) );
94
95      a=a+adot*dt;
96      t=t+dt;
97
98      jj=jj+1;
99      avec(jj)=a;
100     tvec(jj)=t;
101
102 end
103
104
105 tvec=tvec/3600/24/365;
106 figure(1)
107 plot(tvec,1000*avec,"b")
108 hold on
109
110 %%%%%%%%%%%%%%%%%%%%%%%%%%%%%%%%%%%
111 %                                   %
112 %       Inclined crack              %
113 %                                   %
114 %%%%%%%%%%%%%%%%%%%%%%%%%%%%%%%%%%%
115 Fi=Fin;
116 for kk=1:length(Fn)
117
118 t=t0; %time
```

```
119 a=a0; %depth
120
121 %%%%%%for the loop%%%%%%%%%%%%%%%%%%%%%%%%%%%%%%%%
122 avec2=a;
123 tvec2=t;
124 jj=1;
125 %%%%%%%%%%%%%%%%%%%%%%%%%%%%%%%%%%%%%%%%%%%%%%%%%%
126
127 while a<aend
128    K=stress*Fi*sqrt(pi*a);
129
130    ia=ia0*Fn(kk);%OR ia=ia0*(1+(a/aend)*(iarat-1));
131
132    if a<astab
133        adot=adot0;
134        theta=thetastab*(a-a0)/(astab-a0);
135        adotr=cosd(theta)*adot;
136    else
137        adot= (A0*ia) ^ (1/(1-n)) * B^(n/(1-n)) * ...
       (log((K^2-Kiscc^2) / (pi*r0*sigmay^2))) ^ ( ...
       (n/(1-n))*(N+1)/(N-1) );
138        adotr=cosd(thetastab)*adot;
139    end
140
141    a=a+adot*Δt;
142    t=t+Δt;
143
144    jj=jj+1;
```

```
145     avec2(jj)=a;
146     tvec2(jj)=t;
147
148 end
149
150 tvec2=tvec2/3600/24/365;
151 figure(1)
152 plot(tvec2,1000*avec2,"Color",[kk/length(Fn) 1-kk/length(Fn) 0])
153
154 end
155
156
157 str4leg=cell(length(Fn)+1,1,1);
158 str4leg{1}="Straight crack";
159 for ii=2:length(Fn)+1;
160     str4leg{ii}=["Inclined - F_n = ",num2str(Fn(ii-1))];
161 end
162
163 legend(str4leg,"Location","SouthEast")
164 xlabel("Time (years)")
165 ylabel("Depth (mm)")
166 ylim([a0*1000 aend*1000]);
```

A.3 Crack interaction code

File type: Matlab code

Purpose: Generates a plot which shows how various arrangements of cracks fall under the CEPA interaction guidelines. This model mainly calculates crack interaction based on fracture mechanics. Electrochemical considerations are included in the Kcrit value (usually known as KIscc).

Comment: This is for two equal length cracks, previously shown to be a worse case than two unequal length cracks.

Key Inputs:

- matrixfromansys - [d1/2d2 a/d1 Kin/Kout]: Generated from ANSYS code. First column values must be together with a/d1 in ascending order.
- kcrit: critical stress intensity factor Kiscc in MPa sqrt(mm)
- ai: half-surfacelengths to analyse (in mm) - Format [shortestlength:increment:longestlength]

Outputs: Figure 1 shows the crack configuration which is NOT possible to grow according to the model. Pink region means that crack configuration is prevented from growing due to shielding. Green means that shielding does NOT stop that configuration.

Comment: If Figure 1 shows any region which is neither green nor purple, it means that CEPA guidelines would be breached. However, work to date (analytical and using this model) has not shown a different result. Hence, CEPA guidelines hold for all crack configurations.

```
1 clc
```

```
clear all
close all

ai=1:0.25:25;
anglecounti=1:1:500;
ltdrati=3:0.5:14;
thetai=30:5:60;

cepafailcount=1;
cepasuccesscount=1;
cepabordercount=1;
cepaxcount=1;
contcount=1;

%%
super3dmatrix=[
1   0.2 1.009978946
1   0.4 1.009274703
1   0.6 1.009995221
1   0.8 1.003399841
1   1   0.972839264
1   1.2 0.917131736
1   1.4 0.845412675
1   1.6 0.771701783
1   1.8 0.699796562
1   2   0.634186855
1   2.2 0.57983544
1   2.4 0.532663702
```

```
1   2.6 0.490780577
1   2.8 0.455702813
1   3   0.42482167
1   3.2 0.394354535
1   3.4 0.37448942
1   3.6 0.352546553
1   3.8 0.330986008
1   4   0.314225576
1   4.2 0.299376853
1   4.4 0.285517705
1   4.6 0.272089574
1.5 0.2 1.003146514
1.5 0.4 1.013702466
1.5 0.6 1.029952446
1.5 0.8 1.04198371
1.5 1   1.012169436
1.5 1.2 0.920995597
1.5 1.4 0.804033141
1.5 1.6 0.690432381
1.5 1.8 0.594639982
1.5 2   0.514034669
1.5 2.2 0.45145442
1.5 2.4 0.399989585
1.5 2.6 0.354358858
1.5 2.8 0.317704826
1.5 3   0.286632514
1.5 3.2 0.259642285
1.5 3.4 0.236461116
```

```
1.5 3.6 0.218416601
1.5 3.8 0.200173235
1.5 4   0.18585398
2   0.15    0.997072168
2   0.3 1.006768169
2   0.45    1.020468387
2   0.6 1.039676683
2   0.75    1.073537549
2   0.9 1.093754606
2   1.05    1.047454567
2   1.2 0.941729631
2   1.35    0.815746748
2   1.5 0.701196486
2   1.65    0.601759664
2   1.8 0.521480064
2   1.95    0.454590873
2   2.1 0.400242921
2   2.25    0.354065951
2   2.4 0.31429601
2   2.55    0.282005374
2   2.7 0.253346338
2   2.85    0.229605632
2   3   0.209067075
2.5 0.2 0.996545525
2.5 0.4 1.013625118
2.5 0.6 1.04863316
2.5 0.8 1.116176868
2.5 1   1.13170675
```

```
2.5 1.2 0.96017517
2.5 1.4 0.747693801
2.5 1.6 0.580003244
2.5 1.8 0.46025757
2.5 2   0.371594436
2.5 2.2 0.305175273
2.5 2.4 0.254925626
2.5 2.6 0.215405462
2.5 2.8 0.184586977
2.5 3   0.160125226
2.5 3.2 0.140190351
2.5 3.4 0.123652756
2.5 3.6 0.109847508
2.5 3.8 0.09804261
2.5 4   0.088246446
3   0.133333333 0.993992441
3   0.266666667 1.003347204
3   0.4 1.011919558
3   0.533333333 1.027912661
3   0.666666667 1.071705141
3   0.8 1.138520988
3   0.933333333 1.189413813
3   1.066666667 1.137134674
3   1.2 0.968954306
3   1.333333333 0.793288389
3   1.466666667 0.644650759
3   1.6 0.531504062
3   1.733333333 0.444659266
```

```
114 3   1.866666667 0.377423795
115 3   2   0.32124873
116 3   2.133333333 0.276533285
117 3   2.266666667 0.240647236
118 3   2.4 0.210934549
119 3   2.533333333 0.186561358
120 3   2.666666667 0.166279245
121 3.5 0.142857143 1.000350089
122 3.5 0.285714286 1.001338969
123 3.5 0.428571429 1.011182735
124 3.5 0.571428571 1.039892469
125 3.5 0.714285714 1.097771878
126 3.5 0.857142857 1.195770202
127 3.5 1   1.237080404
128 3.5 1.142857143 1.068301505
129 3.5 1.285714286 0.835171539
130 3.5 1.428571429 0.648856833
131 3.5 1.571428571 0.512022729
132 3.5 1.714285714 0.412401558
133 3.5 1.857142857 0.336715641
134 3.5 2   0.279695276
135 3.5 2.142857143 0.235268277
136 3.5 2.285714286 0.200468654
137 3.5 2.428571429 0.172950246
138 3.5 2.571428571 0.150729016
139 3.5 2.714285714 0.13250651
140 3.5 2.857142857 0.117144164
141 3.5 0.142857143 1.000350089
```

```
142 3.5 0.285714286 1.001338969
143 3.5 0.428571429 1.011182735
144 3.5 0.571428571 1.039892469
145 3.5 0.714285714 1.097771878
146 3.5 0.857142857 1.195770202
147 3.5 1   1.237080404
148 3.5 1.142857143 1.068301505
149 3.5 1.285714286 0.835171539
150 3.5 1.428571429 0.648856833
151 3.5 1.571428571 0.512022729
152 3.5 1.714285714 0.412401558
153 3.5 1.857142857 0.336715641
154 3.5 2   0.279695276
155 3.5 2.142857143 0.235268277
156 3.5 2.285714286 0.200468654
157 3.5 2.428571429 0.172950246
158 3.5 2.571428571 0.150729016
159 3.5 2.714285714 0.13250651
160 3.5 2.857142857 0.117144164
161 4   0.125   1.000176709
162 4   0.25    1.000181537
163 4   0.375   1.007827469
164 4   0.5 1.023126892
165 4   0.625   1.051157616
166 4   0.75    1.120484934
167 4   0.875   1.233146798
168 4   1   1.288602434
169 4   1.125   1.114831621
```

```
4   1.25    0.877450948
4   1.375   0.67816662
4   1.5 0.536409027
4   1.625   0.431685256
4   1.75    0.35385404
4   1.875   0.292850832
4   2   0.245531251
4   2.125   0.209143009
4   2.25    0.180317898
4   2.375   0.156916284
4   2.5 0.137759248
4.5 0.155555556 1.004404036
4.5 0.311111111 1.003820503
4.5 0.466666667 1.016278478
4.5 0.622222222 1.049531958
4.5 0.777777778 1.144951598
4.5 0.933333333 1.315479739
4.5 1.088888889 1.21345374
4.5 1.244444444 0.866920434
4.5 0.8 1.164975597
4.5 0.888888889 1.273188769
4.5 0.977777778 1.335642533
4.5 1.066666667 1.253232295
4.5 1.155555556 1.059927513
4.5 1.244444444 0.866920434
4.5 1.333333333 0.709823201
4.5 1.422222222 0.58828923
4.5 1.511111111 0.486475794
```

```
198 4.5 1.6 0.413776417
199 4.5 1.688888889 0.352243344
200 4.5 1.777777778 0.303793741
201 4.5 1.866666666 0.25
202 4.5 1.955555555 0.2
203 5   0.1 1.000010555
204 5   0.2 1.000587077
205 5   0.3 1.003241982
206 5   0.4 1.008310918
207 5   0.5 1.01915431
208 5   0.6 1.040523111
209 5   0.7 1.084457086
210 5   0.8 1.169318856
211 5   0.9 1.299966467
212 5   1   1.374804951
213 5   1.1 1.203261849
214 5   1.2 0.94691756
215 5   1.3 0.734824565
216 5   1.4 0.581663296
217 5   1.5 0.466557612
218 5   1.6 0.379209122
219 5   1.7 0.316906251
220 5   1.8 0.265068764
221 5   1.9 0.225502409
222 5   2   0.194154367
223 5.5 0.127272727 1.006203654
224 5.5 0.254545455 0.9998778
225 5.5 0.381818182 1.006136886
```

```
226 5.5 0.509090909 1.018407762
227 5.5 0.636363636 1.047851668
228 5.5 0.763636364 1.125019683
229 5.5 0.890909091 1.301844056
230 5.5 1.018181818 1.402710965
231 5.5 1.145454545 1.083634007
232 5.5 1.272727273 0.765310306
233 5.5 1.4 0.550148285
234 5.5 1.527272727 0.409500875
235 5.5 1.654545455 0.315724487
236 5.5 1.781818182 0.248089653
237 5.5 1.909090909 0.200725933
238 6   0.116666667 1.000088098
239 6   0.233333333 0.998735212
240 6   0.35    1.006426397
241 6   0.466666667 1.013061058
242 6   0.583333333 1.033800473
243 6   0.7 1.080063623
244 6   0.816666667 1.185602862
245 6   0.933333333 1.394943764
246 6   1.05    1.379886218
247 6   1.166666667 1.016290805
248 6   1.283333333 0.721140237
249 6   1.4 0.521815526
250 6   1.516666667 0.390398172
251 6   1.633333333 0.302550735
252 6   1.75    0.24114238
253 6   1.866666667 0.195544158
```

```
254 6   1.983333333 0.162360795
255 6   2.1 0.136656826
256 6   2.216666667 0.116958818
257 6   2.333333333 0.101110493
258 7   0.1 1.00004909
259 7   0.2 0.995190693
260 7   0.3 1.002603083
261 7   0.4 1.005849429
262 7   0.5 1.017539595
263 7   0.6 1.038179856
264 7   0.7 1.074889124
265 7   0.8 1.16004525
266 7   0.9 1.345914235
267 7   1   1.525725212
268 8   0.1 0.998148148
269 8   0.2 1.000791789
270 8   0.3 1.003394428
271 8   0.4 1.010369335
272 8   0.5 1.017461118
273 8   0.6 1.035980219
274 8   0.7 1.073117805
275 8   0.8 1.153609572
276 8   0.9 1.352148947
277 8   1   1.597207594
278 9   0.1 0.998279576
279 9   0.2 1.000829955
280 9   0.3 1.003712662
281 9   0.4 1.008540458
```

```
9   0.5 1.017202896
9   0.6 1.035614172
9   0.7 1.071850828
9   0.8 1.150686198
9   0.9 1.352603743
9   1   1.659581935
10  0.1 0.999993462
10  0.2 1.000468011
10  0.3 1.002578049
10  0.4 1.00930604
10  0.5 1.016659927
10  0.6 1.035208802
10  0.7 1.070687357
10  0.8 1.145512126
10  0.9 1.354803489
10  1   1.7185604
10  1.1 1.236752081
10  1.2 0.766478873
10  1.3 0.49733304
10  1.4 0.344667364
10  1.5 0.253237016
10  1.6 0.193230964
10  1.7 0.152263465
10  1.8 0.123946357
10  1.9 0.102900506
7   1.1 1.24617724
7   1.2 0.879655366
7   1.3 0.632678563
```

```
310 7   1.4 0.46845764
311 7   1.5 0.358328688
312 7   1.6 0.280885293
313 7   1.7 0.225516979
314 7   1.8 0.185918072
315 7   1.9 0.155957668
316 7   2   0.132392386
317 8   1   1.597207594
318 8   1.1 1.248194019
319 8   1.2 0.842891671
320 8   1.3 0.58488649
321 8   1.4 0.419856781
322 8   1.5 0.315941493
323 8   1.6 0.245009264
324 8   1.7 0.196247157
325 8   1.8 0.159702226
326 8   1.9 0.133133577
327 8   2   0.113252549
328 9   1   1.659581935
329 9   1.1 1.242138286
330 9   1.2 0.802022827
331 9   1.3 0.540621366
332 9   1.4 0.379808927
333 9   1.5 0.280077597
334 9   1.6 0.21561178
335 9   1.7 0.172229147
336 9   1.8 0.139578124
337 9   1.9 0.116206182
```

```
14  0.1 1.000271194
14  0.2 1.001091995
14  0.3 1.003634642
14  0.4 1.008093818
14  0.5 1.017154003
14  0.6 1.034347579
14  0.7 1.068153415
14  0.8 1.138202488
14  0.9 1.341261532
14  1   1.931841648
14  1.1 1.173180948
14  1.2 0.624865985
14  1.3 0.37458683
14  1.4 0.247386688
14  1.5 0.176964698
14  1.6 0.134480078
14  1.7 0.105776939
0.833333333 1   0.965165127
0.833333333 1.2 0.922313142
0.833333333 1.4 0.868902538
0.833333333 1.6 0.810560949
0.833333333 1.8 0.753471598
0.833333333 2   0.699407559
0.833333333 2.2 0.651121832
0.833333333 2.4 0.608354796
0.833333333 2.6 0.570351352
0.833333333 2.8 0.536773159
0.833333333 3   0.507465359
```

```
366 0.714285714 1   0.967799924
367 0.714285714 1.2 0.93563258
368 0.714285714 1.4 0.892212705
369 0.714285714 1.6 0.845356691
370 0.714285714 1.8 0.796649118
371 0.714285714 2   0.750108953
372 0.714285714 2.2 0.706382511
373 0.714285714 2.4 0.66713906
374 0.714285714 2.6 0.631880872
375 0.714285714 2.8 0.600145955
376 0.714285714 3   0.571951195
377 0.5 1   0.98458429
378 0.5 1.2 0.966266923
379 0.5 1.4 0.944178586
380 0.5 1.6 0.917311902
381 0.5 1.8 0.88835107
382 0.5 2   0.858186136
383 0.5 2.2 0.827900939
384 0.5 2.4 0.799076213
385 0.5 2.6 0.771491936
386 0.5 2.8 0.745018858
387 0.5 3   0.72100016
388 0.5 3.2 0.698996832
389 0.5 3.4 0.678484108
390 0.5 3.6 0.659362521
391 0.5 3.8 0.642142008
392 0.5 4   0.626745874
393 0.5 4.2 0.611675665
```

```
0.5 4.4 0.598226178
0.5 4.6 0.585837855



];
%%

for aicount=1:length(ai)

        for angleicount=1:length(anglecounti)

            cepaspacing=0;
          ltdrat = 0.25*2*ai(aicount) + 0.76; %%% linear below ...
    all points

            anglecount=anglecounti(angleicount);

            theta=(44.5925+0.116421*2*ai(aicount))-90;



            a=ai(aicount); %a is half crack length
            b=a/(ltdrat*sind(-theta));



            x=linspace(-a,a,1000);
            y=linspace(-a,a,1000);

```

```
421
422
423             d=sqrt(b^2/(1+(tand(theta))^2));
424
425             yel=(d^2*(1-x.^2/a^2)).^0.5;
426             z=yel.*tand(theta);
427
428             xi=x(anglecount);
429             yi=yel(anglecount);
430
431
432             x2=x-2*xi;
433             y2=yel-2*yi;
434             z2=-z;
435
436             yp5=0;
437             for ii=1:length(z)
438                 if abs(real(z(ii)))>0.55
439                     yp5=yel(ii);
440                     break
441                 end
442             end
443
444
445              theangle=acosd(abs(xi)/sqrt(xi^2+(yi-yp5)^2));
446
447             if yp5>yi
448
```

```
449             elseif yp5==0
450
451             else
452                 cepaspacing=2*(yi-yp5)/(2*a);
453                 cca(contcount)=a;
454             ccltd(contcount)=ltdrat;
455             ccangle(contcount)=theangle;
456             ccspacing(contcount)=(cepaspacing-0.14);
457             contcount=contcount+1;
458             end
459 %%
460
461             ctest=0;
462             adrat=-2*a/(2*xi);
463             ddrat=-(2*xi/2*(yi-yp5));
464             ddratrnd=ceil(ddrat*2)/2;
465             upperlim=14;
466
467             if ddratrnd>6
468                 ddratrnd=ceil(ddratrnd);
469
470             end
471             if ddratrnd>upperlim
472                 ddratrnd=upperlim;
473             end
474             if ddratrnd>10 && ddratrnd<14
475                 ddratrnd=10;
476             end
```

```
477
478             if ddratrnd<2.5;
479                 ddratrnd=2.5;
480             end
481
482             xxx=super3dmatrix(:,1);
483             yyy=super3dmatrix(:,2);
484             zzz=super3dmatrix(:,3);
485             krat=1;
486             for i3count=1:length(xxx)
487                 if xxx(i3count)==ddratrnd
488
489                     if yyy(i3count)<adrat
490                         krat=zzz(i3count);
491                     end
492                     if yyy(i3count)<adrat && yyy(i3count+1)>adrat
493                         ...
    krat=zzz(i3count)+(adrat-yyy(i3count))*(zzz(i3count+1)-zzz(i3count))/(yyy(i3cou
494                         break
495                     end
496                     if yyy(i3count) == adrat
497                         krat=zzz(i3count);
498                         break
499                     end
500                 end
501             end
502
503
```

```
504              ktip=450*sqrt(2*a);
505              kratreq=(790.57/ktip);
506
507             if kratreq>krat || ktip<750.56
508             ctest=1;
509              end
510             if a==20 && theangle>20 && theangle<30
511                ...
    export=[a,theangle,ctest,krat,kratreq,ktip,ddrat,ddratrnd,adrat,2*xi,2*yi];
512             end
513
514
515              if cepaspacing>0.14 && ctest==0
516                  cfa(cepafailcount)=a;
517                  cfltd(cepafailcount)=ltdrat;
518                  cfangle(cepafailcount)=theangle;
519                  cfspacing(cepafailcount)=(cepaspacing-0.14);
520                  cepafailcount=cepafailcount+1;
521
522              elseif cepaspacing<0.142 && cepaspacing>0.14 && ctest==0
523                  cba(cepabordercount)=a;
524                  cbltd(cepabordercount)=ltdrat;
525                  cbangle(cepabordercount)=theangle;
526                  cepabordercount=cepabordercount+1;
527
528              elseif ctest==0
529                  csa(cepasuccesscount)=a;
530                 csltd(cepasuccesscount)=ltdrat;
```

```
531                 csangle(cepasuccesscount)=theangle;
532                 csspacing(cepasuccesscount)=(cepaspacing-0.14);
533                 cepasuccesscount=cepasuccesscount+1;
534             else
535                  cxa(cepaxcount)=a;
536                 cxltd(cepaxcount)=ltdrat;
537                 cxangle(cepaxcount)=theangle;
538                 cxspacing(cepaxcount)=(cepaspacing-0.14);
539                 cepaxcount=cepaxcount+1;
540
541             end
542
543         end
544 end
545 ax=figure;
546
547 plot(csa,csangle,"g.")
548 hold on
549 pointsize=10;
550 plot(cxa,cxangle,"m.")
551
552 xlabel(["half crack surface length a (mm)"])
553 ylabel(["angle of intersection from surface \theta"])
```

Appendix B

Publications

 DOI: 10.1002/maco.201508454

A review of modelling high pH stress corrosion cracking of high pressure gas pipelines

J. Griggs, E. Gamboa* and O. Lavigne

Modelling of intergranular stress corrosion cracking (SCC) in pipelines is an important field of study as predictive techniques are integral to pipeline integrity and management. An inclination of the SCC propagation direction has been observed for some pipelines, which is not predictable using existing models as they assume perpendicular crack growth. A review has been conducted to identify the applicable techniques from existing models, as well as the gaps in current knowledge. Existing work in crack growth rates, stress formulations and microstructural representations are reviewed. Mechanical dependency of the electrochemical response is identified as a gap and proposed for inclusion in a model alongside the other areas reviewed.

1 Introduction

Modelling of stress corrosion cracking (SCC) has been a vital part of predicting which SCC colonies are likely to cause a failure and how much time is available to repair a component before a failure occurs. In the case of high pH SCC of high pressure gas pipelines, various models have been developed which predict crack growth rates, as well as some that predict crack interaction limits [1–6]. These models assume that SCC cracks will follow a stress intensity factor dominated mechanism of film cleavage and propagate approximately perpendicular to the outer surface. Recent observations have shown, however, that this may not always be the case [7–13]. Sometimes SCC cracks do not grow perpendicular to the direction of the highest applied stress, indicating that the growth may switch from a stress driven film cleavage mechanism to a plasticity driven dissolution mechanism. As such, the models that are used to predict SCC failures with an assumption of a film cleavage mechanism may not be applicable in some cases. There is a need for a new model that can predict when a switch to a plasticity driven dissolution mechanism is likely to occur and whether that growth is more aggressive than straight SCC. A review of the existing SCC theory and models are presented to identify the important parameters to model this bimechanistic growth, as well as the various modelling methods that would be appropriate for such a model. The focus will primarily be the high pH SCC of high pressure gas pipelines, with some knowledge gained from allied fields of research when, pipeline specific research is lacking.

Classical SCC theory will be reviewed and shown to offer incomplete explanations of examples of inclined SCC found in Australia and Canada. The developments in modelling will then be addressed to identify what techniques are applicable and where gaps lie. A crack growth rate equation implicit in a current industry used model will be the benchmark for identifying which parameters are important and the methods by which they are identified will be assessed. The validity with which the electrochemical response is determined in SCC models will be identified as a possible gap in current knowledge. The electrochemistry will also provide a potential explanation for the inclined SCC phenomenon observed in recent years.

J. Griggs, E. Gamboa, O. Lavigne
School of Mechanical Engineering, The University of Adelaide, Adelaide, SA 5005 (Australia)
E-mail: Erwin.gamboa@adelaide.edu.au

2 Classical SCC

High pH SCC of gas pipelines can occur when an aggressive environment, a susceptible material and sufficient tensile stresses combine on the external surface of the pipe, usually under a defect in the coating [14]. Each of these elements is required for SCC propagation to occur, with the environment–metal pair resulting in dissolution along the crack front and the stresses resulting in the fracture of the passive brittle film that can form to prevent the dissolution. SCC usually presents as many axially directed cracks in a colony. The cracks are directed axially, perpendicular to the usually hoop stress dominated stress field; however, proximity to welds or notches can change the stress field and lead to cracks with different orientations [15]. The traditional view of a crack growth cycle is presented below and has been covered extensively by numerous other authors [14–21].

Initiation of high pH SCC in pipelines usually occurs under a holiday or defect in the coating, where the cathodic protection is shielded into the range of stress corrosion cracking. Pitting can then occur on the surface and the cracks can initiate at these stress concentrators [16].

Once the crack is initiated, growth continues intergranularly via a combination of anodic dissolution and film cleavage [14,16]. Anodic dissolution acts to dissolve the bonds between adjacent

grains into the solution. The speed of propagation has a ceiling determined experimentally of approximately 10^{-6} mm/s [18]. Growth in the field rarely reaches this limit though, as the propagation is rate limited by passive film fracture [18,21]. The conditions at the tip of the crack are usually transpassive and thus conducive to both dissolution and passive film formation. This passive film prevents further dissolution and advancement of the crack front. The film is brittle and much weaker than the base metal and can break through either creep or fatigue, depending on the loading pattern [21]. The crack can then advance a small amount through dissolution, as well as some penetration into the base metal from the fracture of the film. Overall, this results in fairly slow growth rates (between 2×10^{-8} and 10^{-6} mm/s) for individual cracks [18].

Cracks can start to grow with faster crack tip velocity once the colony develops and coalescence begins. The coalescence of neighbouring cracks can cause both temporary dormancy of some cracks due to stress shielding, and coalescence with crack acceleration, depending on the relative position of the cracks, as has been investigated by *Wang* and *Atrens* [22]. Cracks that are configured favourably relative to each other begin to link up, causing a much longer crack with a higher stress intensity factor. This larger crack will have a more significant stress field and thus the time between brittle fractures is reduced resulting in an increase in crack tip velocity [1]. Additionally, a single stress corrosion crack is insufficient to cause more than a leak in a pipeline, with at least seven coalescing cracks usually required for a critical failure to occur [1]. Failure occurs rapidly once the cracks reach a depth and length such that the fracture toughness of the material is exceeded by the mechanical stresses alone, with inspections of the final fracture surface usually showing no corrosive damage in the overload region [23].

The aforementioned growth cycle revolves around the rate limiting film fracture [6,18,24]. The cracks grow perpendicular to the outer surface of the pipe as this fracture will occur perpendicular to the principle stress, which is usually dominated by the applied hoop stress. A change in direction of the cracks is evidence of either a shift in the mechanism, or a change in the stress field due to interaction, welds or other stress concentrators. Within the last decade, examples of significant deviations from straight crack growth have been seen in both Canada and Australia [8–10,12,13], with the full global impact unknown due to the inconvenience of sample extraction while repairing SCC colonies in the field resulting in few reports of SCC growth direction.

3 Inclined cracks

Inclined SCC occurs when an SCC crack diverts from a crack path perpendicular to the surface and instead follows a new trajectory that is offset by a varying angle, often in the range of 30–60 °. It has been documented in both Australian [10] and Canadian [8,9] pipelines since 2004, with a failure report from 1984 also exhibiting the phenomenon [7]. Figure 1 shows the three cross sectional shapes of SCC found in *Xie's* colony. These studies documented cracks in high pressure gas pipelines that were inclined (Fig. 1c), as well as some that were straight (Fig. 1a). This occurrence has only been documented to date in X65 steels (0.085% C, 0.33% Si, 1.58% Mn, 0.0045% S, 0.054% Nb and 0.022% P [25]). Other occurrences of cracks growing in unusual directions have been observed in stainless steels in high temperature water [11,26,27], though these cases usually present simultaneously with branching, providing some mechanical explanation. The inclined SCC phenomenon could have some implications for both growth rates of individual cracks, as well as interaction zone limits for multiple cracks.

The first study into inclined SCC by *Sutherby* and *Weixing* [8] showed inclined SCC that grew perpendicular to the outer surface for 1.5 mm or less, before inclining at an angle of 30–60 °. They found that the entire crack was intergranular, both before and after inclination, and the shape was not semi-elliptical as is usually observed for SCC. They also determined that the crack inclination angle was generally proportional to the crack length and postulated that the crack does not incline at any one point, rather undergoing a slow turning process. Most of the cracks they showed supported this hypothesis (Fig. 2a: a slowly curving crack), although there were some exceptions (Fig. 2b: harsh kinks in a zig-zag pattern). *Sutherby* and *Weixing* [8] also proposed a 3D schematic sketch of an inclined crack, Fig. 3a, which rather than showing a semi-elliptical crack with a bend in the middle, shows the crack post-inclination behaving more like a centre crack, with the cross sectional chord peaking in the middle. Tomographical work performed later by *Lavigne* et al. [12] and *Gamboa* et al. [13] showed that the shapes are in fact far more complex due to the interaction intrinsic to SCC, and cannot simply be approximated as semi-elliptical. Figure 3b shows that the cracks can appear semi-elliptical, as in the light-blue crack, but also have steeper edges and a more rectangular shape, such as the dark blue crack. This presents the possibility that the inclined SCC could also be deeper and longer below the surface than would be expected

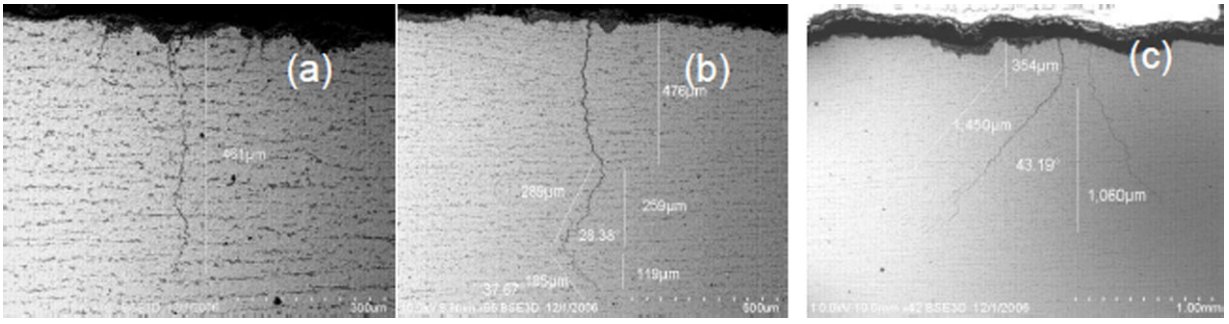

Figure 1. Three categories of SCC documented by *Xie* et al. [9]: (a) straight, (b) zig-zag and (c) inclined

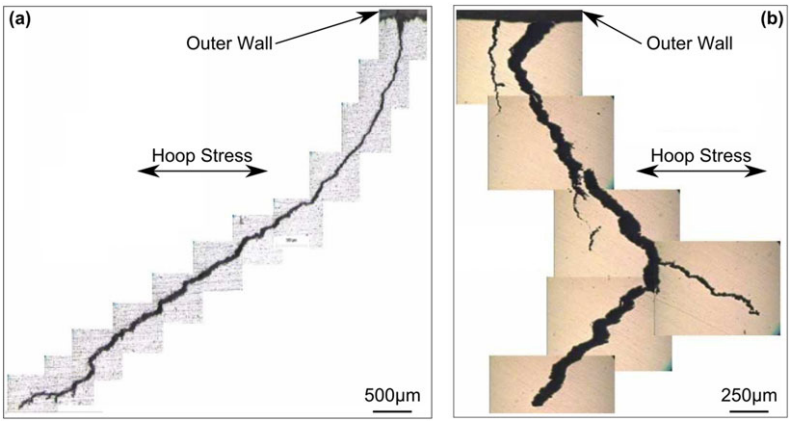

Figure 2. Some of the cracks surveyed by *Sutherby* and *Weixing* [8], (a): smooth curve, (b): harsher kinks

from surface inspection alone. *Sutherby* and *Weixing* [8] theorised that the crack inclination was caused by microstructural variance through the wall thickness that was itself caused during manufacture. This hypothesis was reinforced by their presentation of SEM images of the microstructure both at the surface and half way through the thickness, which showed banding as the depth increased. A hardened surface was also observed in the first 1.5 mm of pipe thickness, consistent with surface hardening techniques, which is similar to the length of the perpendicular section of growth in these specimens.

A follow up study was performed by *Xie* et al. [9]. *Xie* found that the cracks generally inclined in the range of 0.2–0.6 mm from the surface, with an inclination angle of 30–50 °, with more than 50% of all cracks with a straight length of 0.2 mm or more being inclined. The cracks *Xie* examined generally showed sharp kinking, as previously shown in Fig. 1b, but they also presented some cracks which curved more than kinked, similar to the findings of *Sutherby* and *Weixing* [8]. Banding of the microstructure was also found, however, no significant change in the banding was observed where the crack inclined. Contrary to *Sutherby's* findings, no significant change in hardness was present in the inclination zone and this result was also supported by *Zadow* [28] in the Australian case. *Xie's* [9] mechanistic analysis prompted the hypothesis, contrary to *Sutherby* and *Weixing's* proposals, that a combination of residual stresses and some abnormal corrosion were the causes of the inclination.

Zadow et al. [10] conducted a survey of a section of pipe from the Moomba–Sydney pipeline. They found that the straight section of significant cracks was between 0.2 and 0.9 mm, while the angle was between 30 and 60 °, with deeper cracks generally having a larger angle. Eighty-one percent of significant cracks showed some inclination. Thirty-two percent of all cracks analysed had some crack interaction occurring and 44% of those cracks had inclined and coalesced within the pipe thickness, but not necessarily on the surface [28]. Cracks showed both kinking and gradual curving towards the final inclination angle, as is seen in Fig. 4. The authors ascertained that the longitudinal subsurface travel may be significant, however, other work involving tomography is required to confirm this. While none of the interactions breached the guidelines for crack interaction provided by CEPA, *Zadow* et al. [10] suggest more work is required to quantify how conservative are the guidelines.

The studies to date on inclined SCC seem to imply that some of the influencing factors of inclined SCC could be residual stress/strains, microstructural variance, crack interaction, or other unspecified electrochemical mechanisms. Of these factors, residual stresses were found to be low in comparison with the applied hoop stress (although some were higher than non-affected samples) and not directional along the inclination angles [9,28]. Furthermore, the microstructure could have some effect, however, there were no smearing or other clearly visible microstructural features present that could easily explain

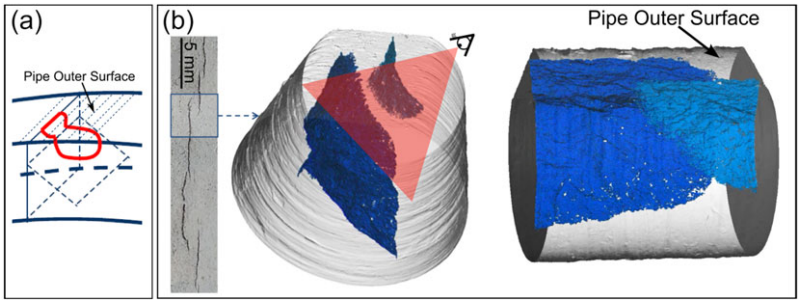

Figure 3. (a) Sketch of the 3D profile of an inclined crack [8]. (b) 3D tomography of an inclined crack in an Australian SCC colony, adapted from *Gamboa* et al. [13]

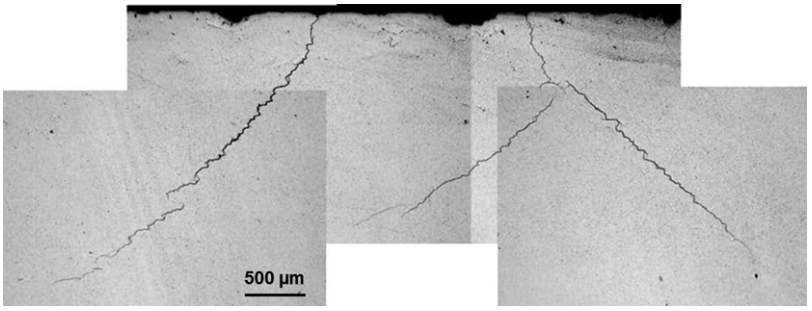

Figure 4. 2D cross section of inclined SCC in Australian X65 pipe, with curving seen on the left and kink-like branching on the right [28].

the inclination. Additionally, interaction could cause cracks to deviate from the perpendicular, however, interaction was not present for all the inclined cracks. Thus, the most likely cause for the inclination is related to the electrochemical mechanism. In the previous studies, the authors imply other electromechanical mechanisms as the cause of the issue but do not specify in detail which ones they could be. One such mechanism could be a preference towards dissolution or weak filming at areas of high plasticity, as seen by *Yaguchi* and *Yonezawa* [11] and *Lavigne* et al. [12] which could explain the angular deviation. So while this mechanistic change could be the cause for the inclination in general, the other factors such as residual stresses, microstructure and interaction should be included in the model to explain the differences found across different pipes and colonies. Existing models and theory will be examined, therefore, to determine what is applicable and where gaps exist.

4 Modelling crack growth rates

Pipelines experience a range of environmental conditions which affect SCC growth. The soil composition, the amount of cathodic protection and the temperature can vary along a pipeline due to its length [15]. Thus, it is logical that models have attempted to look at the relationships between the environmental properties and crack growth parameters.

To understand the effect of the environmental factors on SCC growth, it is necessary to understand the governing equations used. Traditionally, models have used Faraday's law to describe the dissolution process (Equation (1)) [29].

$$CGR = \frac{M_w}{zF\rho} i_0 \tag{1}$$

In this equation, CGR is the crack growth rate, M_w is the molar mass of iron, z is the valency of the ions in solution, F is Faraday's constant, ρ is the density and i_0 is the peak current density. Exclusive use of this equation will over-predict the growth rate in the field, as it neglects film passivation kinetics [24].

While Faraday's law describes the dissolution process very well, the inclusion of the film cleavage mechanism is important to ascertain the true rate of growth. It is common practice to consider the crack growth rate of pipeline steels in a high pH carbonate–bicarbonate solution by expanding Faraday's law to include strain rate effects (*Parkins* [30], *Lu* et al. [5]), such that the film cleavage drives Faraday's law (Equation (2)).

$$CGR = \frac{M_w}{zF\rho} Q_F \frac{\dot{\varepsilon}_{ct}}{\varepsilon_F} \tag{2}$$

Here Q_F represents the charge exchanged in the time between two passive film ruptures, $\dot{\varepsilon}_{ct}$ is the crack tip strain rate and ε_F is the strain required to rupture the film. *Lu* et al. [5] claim their results match well with crack velocities lower than 10^{-6} mm/s. Here, it is assumed that the mass transfer is negligible and that the crack will grow via a film cleavage dominated growth mechanism. This is a reasonable assumption as *Parkins* and *Fessler* [14] have said that dissolution mechanisms tend to grow at or above 10^{-6} mm/s.

In both of these equations, the current density is an important factor and various environmental and mechanical parameters can affect it. The adoption of the impact of environmental factors into a pipeline predictive model has been led by *Song* et al. [6,21] and *Lu* et al. [5], with full derivations of the relevant equations available in those papers. Some of the environmental parameters included are as follows:

- The cathodic protection which varies along the length of the pipe and which will shift the current density according to the potentiodynamic curves,
- The composition of the soil will affect the solution at the crack tip, which in turn has an effect on the current density, and
- The chemistry of the solution at the crack tip is dependent on crack depth, which affects reactivity and thus the current density.

These are the current state of the art pipeline SCC models and account for strain rate driven film rupture and environmentally dependant dissolution with validated and reliable results; however, there remains a gap in the lack of microstructural detail, interaction dynamics and plastic strain-dependant electrochemistry. Of these things, only strain-dependant electrochemistry has yet to be incorporated into an SCC model before. To facilitate the integration of this into a model, clearer empirical relationships need to be drawn between the potentiodynamic curves and the local plastic strain.

5 Stress field calculation

Regardless by which mechanism SCC grows, calculations of the stresses, strains or stress intensity factors are required for the governing crack growth rate equations [5,6,18,31–33]. Film rupture is often determined by either the stress intensity factor or strain rate, as was seen in Equation (2), while dissolution-based mechanisms are governed by current density, which could have a dependency on plastic strain [11]. Typically, models have addressed the micro- or macro-scale growth of cracks, but the methods are generally applicable for mesoscale growth with some concessions in either accuracy or processing time.

Various methods are available to calculate the stress fields around a crack tip. For simple geometries, approximations can be made from tables or simple equations [5,6,34–39]. These can provide relatively accurate stress intensity factor results with low computational effort, however, for more complicated crack geometries, interaction and detailed stress field analysis, more complex methods are required. To do this, finite element (FE) solvers, such as ANSYS, ABAQUS, Franc2D, Franc3D, Z-Cracks, or self-developed FE solvers have been used in several models [32,40–49] and offer robustness at a higher computational cost, particularly for three dimensions. Alternatively, boundary element methods are sometimes used [50,51] and although they can be more efficient in some cases, no clear case is present for the use of either the boundary element method or finite element method exclusively over the other and the solution remains a matter of preference. Assorted alternative methods exist for calculating fracture parameters around a crack tip, such as enriched FEM (E-FEM) [52–55], extended FEM (X-FEM) [56–59] and the particle discretisation scheme FEM (PDS-FEM) [60,61], which often involve enriched nodes and the

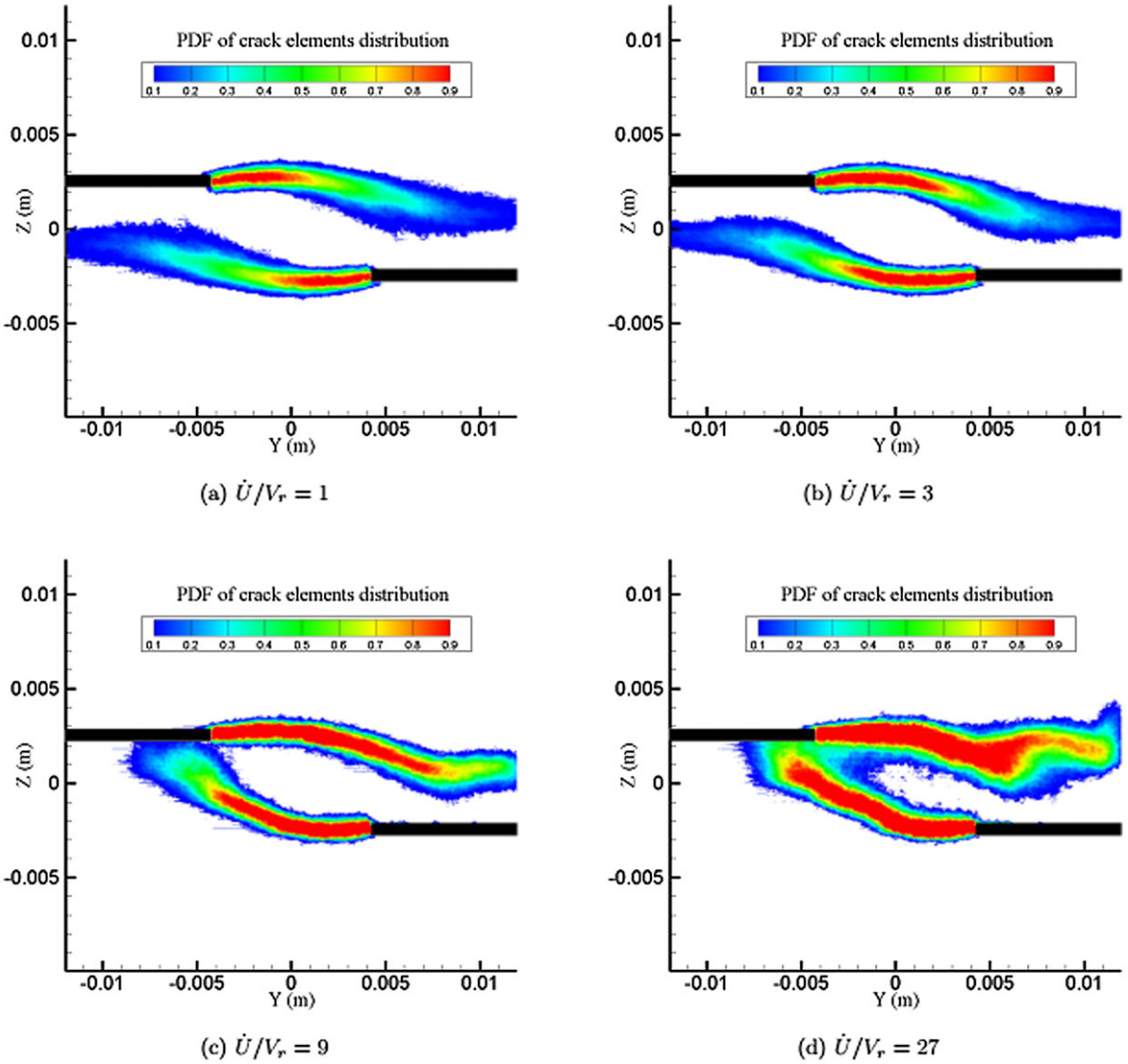

Figure 5. Plate surface view of a probability density function (PDF) of the crack path in PDS-FEM based on random material properties. Y and Z represent the coordinates of the surface, $\dot{U}$ is the loading rate (mm/s) and V_r is a constant equal to 0.1% of the P-wave velocity to non-dimensionalise the ratio [61]

advantage of mesh independence; however, they have scarcely been used in existing SCC models. PDS-FEM stands out from the others, as it provides a probabilistic crack path (Fig. 5), which is of great interest to intergranular SCC. Figure 5 shows two cracks in a flat plate from a surface view, with different loading rates depicted in the quadrants. The coloured contours are a probability density function representing the likelihood of the crack path growing through each point, with red being more likely than blue. The authors noted that the spread developed from their model could be a representation of the influence of material property variance from manufacture. The idea of a probabilistic crack response to material properties can equally be performed with existing methods though using a Monte Carlo approach, albeit at a lower computational efficiency.

PDS-FEM is based on random material properties. Y and Z represent the coordinates of the surface, $\dot{U}$ is the loading rate (mm/s) and V_r is a constant equal to 0.1% of the P-wave velocity to non-dimensionalise the ratio [61].

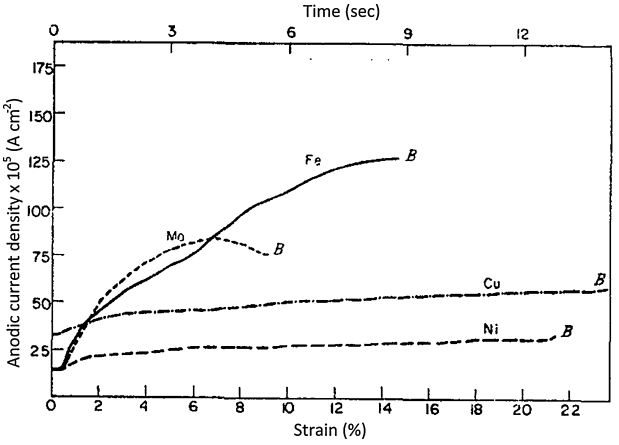

Figure 6. Current density variation with strain of iron, molybdenum, nickel and copper in various solutions. B represents breaking point. [67]

6 Electrochemistry

There is experimental evidence that supports the concept of the impact of electrochemical dependency on areas of high plasticity [31,62–66]. Not only does the strain result in an increase in current density, which is a driver of the dissolution rate in Faraday's law (Equation (1)), but also a shift in the relative propensity for dissolution and filming at the crack tip potential, which could mean a change in the charge passed between film ruptures, which is a driver of Equation (2) and hence the crack growth rate. A plasticity-dependant electrochemical response would result in different degrees of filming and dissolution at different angles (and grain boundaries) around the crack tip and thus angular-dependant SCC susceptibility, possibly explaining the inclined cracks discussed in Section 3. This has not been considered to a great extent in SCC before, as historically the film cleavage has been the rate limiting factor of the crack growth rate.

The electrochemical response of a metal in an environment can be described by its polarisation curve. The polarisation curve for a material in a given solution is often used for the design of preventative measures for corrosion in pipelines, but numerous studies have shown that these curves shift when the material is

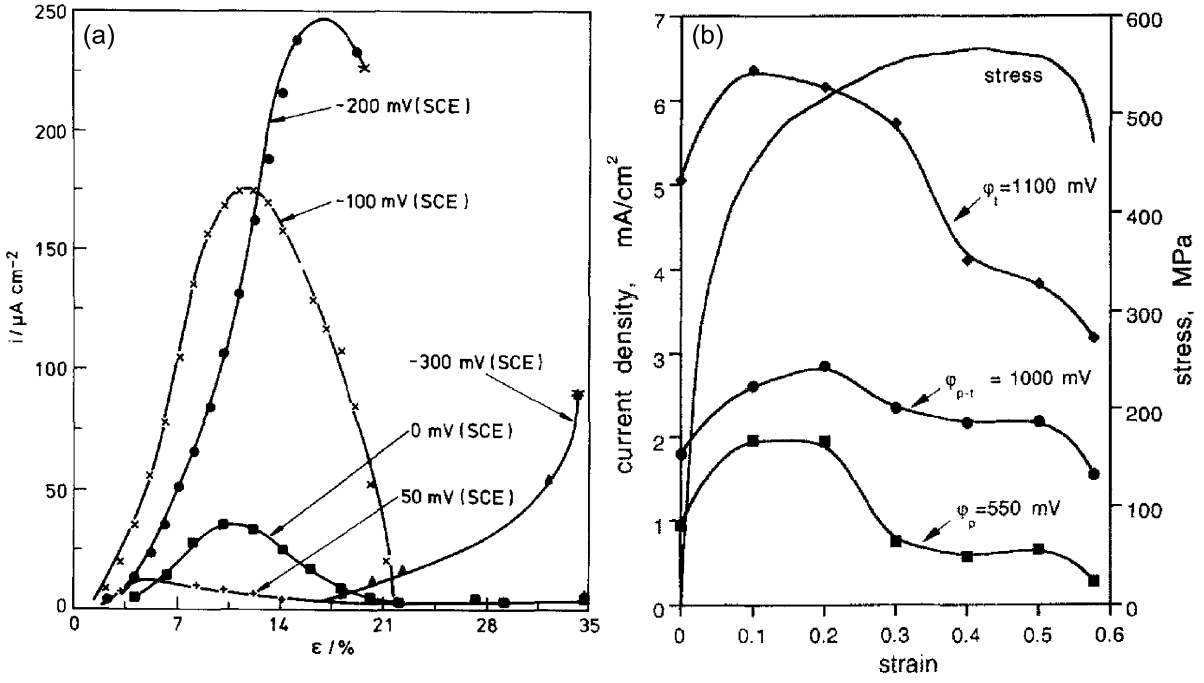

Figure 7. Current density variation with plastic strain of (a) type 304 austenitic stainless steel in 0.5 M $S_2O_3^{2-}$ for different levels of cathodic potential [62], and (b) type 316L stainless steel in 0.1% Na_2SO_4 + 5% H_2SO_4 for different levels of anodic potential (vs. SCE) [68]

strained [31,62–66]. The plastic strain causes an increase in the dislocation density in the material, which in turn provides higher diffusivity into the grain boundaries. This can cause a change in the effective current density (which is proportional to the dissolution rate) as well as the relative propensities for filming and dissolution.

The studies reviewed in this section have evaluated the effect of applying uniform plastic strain to a material and looking at the effect on the polarisation curves, with the exception of *Yaguchi* and *Yonezawa* [11]. This condition differs from that at the crack tip which is a non-uniform strain field, but the results should be transferable, especially with the evidence of *Yaguchi* and *Yonezawa* [11]. Some of the earliest work on this phenomenon was performed by *Despic* et al. [67], who demonstrated that the current density of iron in hydrochloric acid increased with strain fairly linearly until failure (Fig. 6). Later, *Wells* et al. [62] performed some slow strain rate tests on 304 stainless steel in dilute thiosulphate at different potentials in the cathodic range and documented the change in current density. Figure 7a shows some results from that study, including that the corrosion current varies strongly with the applied potential and goes through a maximum with the applied strain (aside from the most cathodic applied potential of −300 mV SCE). It can be seen also that the current density increases with the potential in the cathodic direction (aside again from the −300 mV SCE potential). Similar behaviour was observed for 316L stainless steel in 0.1% Na_2SO_4 + 5% H_2SO_4 solution (Fig. 7b) [68], that showed an increase of the current densities with the increase of the potential in the anodic direction and a maximum in the current with the applied strain.

Sahal et al. [31] went further and looked at the potentiodynamic curves of pre-strained nickel in sulphuric acid (Fig. 8). Figure 8a shows the different zones of the curve, where Section A is active dissolution, Section B is the transition zone comprising both filming and dissolution, Section C is the passive region and D is the film breakdown. Figure 8b shows that changing the strain shifts the active dissolution and transition zones negatively relative to the potential, as well as changing the peak current density. The results indicate that a small amount of strain increases the current density and further strain decreases it,

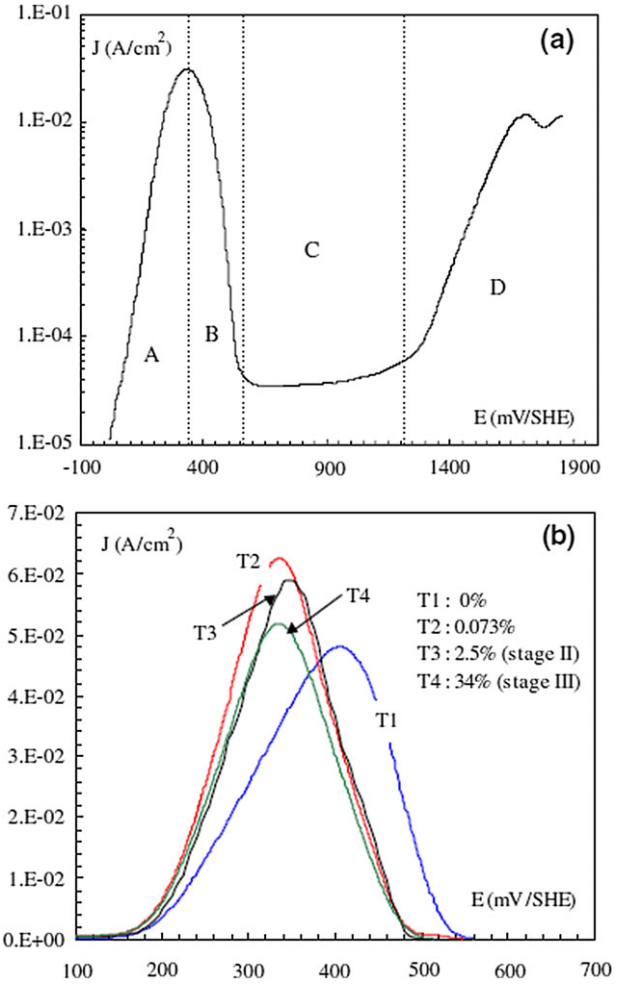

Figure 8. Effect of strain on potentiodynamic curves of nickel in H_2SO_4: (a) shows the various zones (A, B, C, D) of the curve, whilst (b) shows the current density against potential for different strains [31]

although the current densities are still higher than the non-strained values. Some properties of the hardening of nickel could be the cause of this movement, as suggested by *Sahal* et al. [31], with nickel known for its strain hardening and elongation at

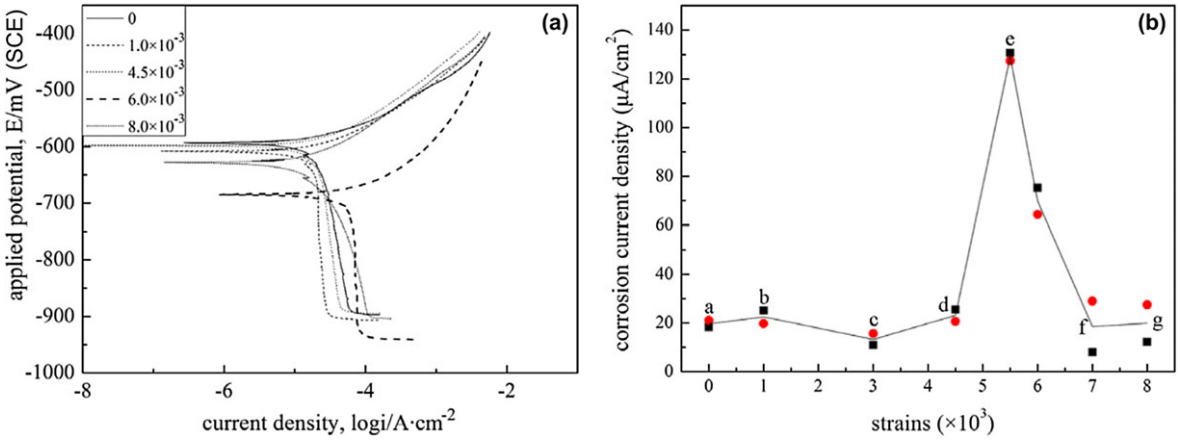

Figure 9. (a) Polarisation curve response of X80 in 0.62 M NaCl aqueous solution at different levels of strain. (b) Relationship between strain and current density at the corrosion potential. A sharp increase in the current density of X80 steel is illustrated at a strain of 6×10^{-3} [63]

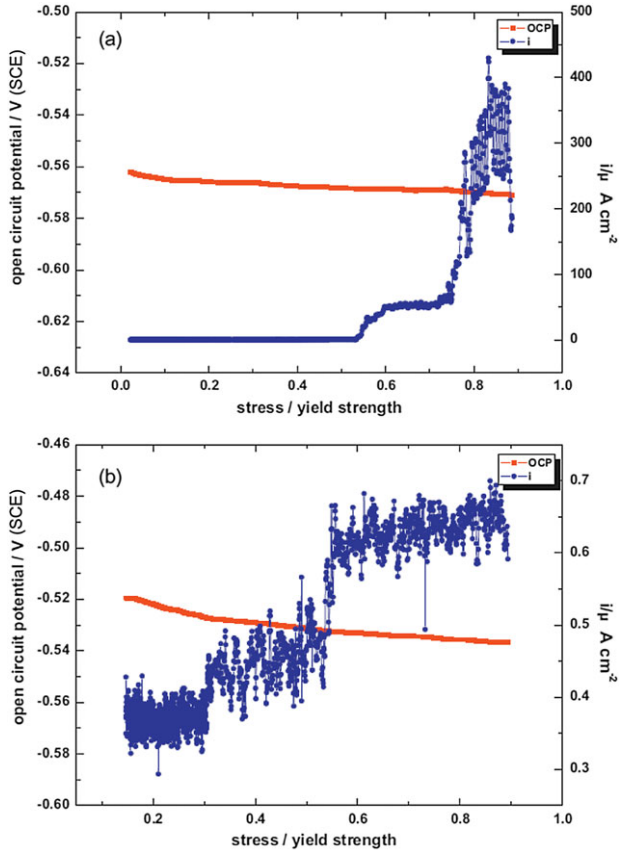

Figure 10. Change in current density and potential with increasing elastic strain for (a) low carbon bainitic steels and (b) low carbon ferritic steels, both in 3.5 wt% NaCl [64]

failure. As such, the presence of dependency is applicable to pipeline steels; however, the shape could be different due to the different stress–strain properties of the metals. Further work conducted by this group has shown that a good correlation exists between dislocation distribution and current density [69].

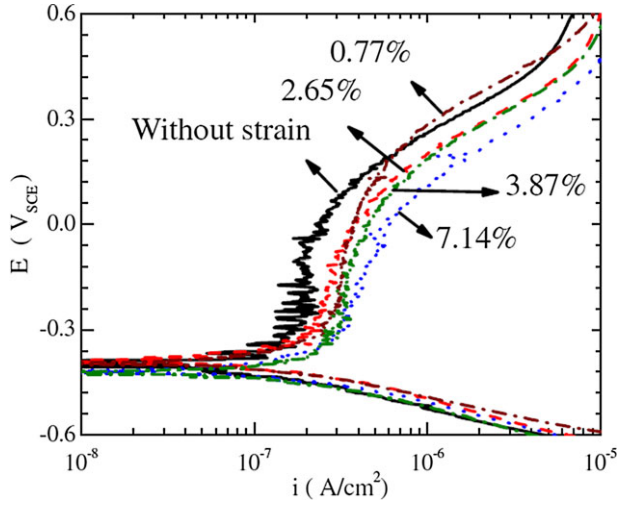

Figure 11. Effect of strain on polarisation response of carbon steel in cement extract [65]

The effect of strain on the current density for X80 pipeline steel (0.055% C, 0.2002% Si, 1.3917% Mn, 0.0019% S, 0.0318% Cr, 0.2636% Ni, 0.0017% P, 0.0173% Al, 0.3184% Mo) in NaCl aqueous solution has been investigated by *Wang* et al. [63] through potentiodynamic measurements (Fig. 9a). The corrosion potential appears to become more negative when the steel is strained, with a maximal shift in potential for a strain value of 6×10^{-3}. The current densities also tend to increase with strain, with a maximum effect observed also at the strain of 6×10^{-3}. Increasing strain further shifts the polarisation curve towards the zero strain condition. At this specific strain of 6×10^{-3}, the corrosion current density shows a sharp increase, while above and below this value the corrosion current densities are relatively stable and low (Fig. 9b). X80 is a higher grade of pipeline steel than the X65 on which this report focuses and has a slightly different composition. Thus, similar to the nickel results [31], the shape of the relationship between current density and strain may differ between X80 and X65, but studies done on this higher grade can still be of great interest for X65 pipes.

In a study of interest, *Ren* et al. [64] examined the electrostatic responses of marine structural steels to elastic strain in NaCl solution. The steels used in that study were low carbon bainitic (0.08% C, 0.35% Si, 1.12% Mn, 0.0083% S, 0.38% Cu, 0.52% Cr, 0.31% Ni, 0.0037% Nb, 0.008% P) and ferritic (0.0055% C, 0.16% Si, 0.79% Mn) steels. It was found that the relationship between strain and current density was non-linear with a more stepwise response seen (Fig. 10). It was proposed that this current density increases in the elastic region due to microplastic deformation events at local regions of instabilities inside the steel, despite the macroelastic stresses being below the yield strength. This plastic strain then increases the current density in the same manner as is seen in other studies. Pure elastic strain is shown to have little impact on the current density, indicating that plastic strain rather than total strain is the key factor to consider for electromechanical characterisation [67,70].

Feng et al. [65] considered structural carbon steel (0.37% C, 0.16% Si, 0.32% Mn, 0.053% S, 0.026% P) in cement extract solution and the effects of strain on the polarisation response. Figure 11 shows the relationship between strain and the

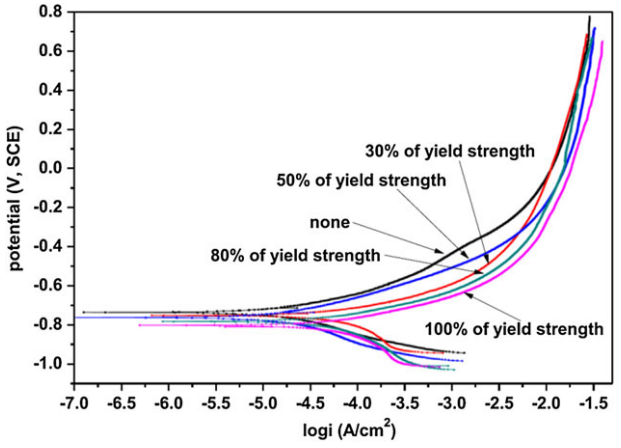

Figure 12. Effect of elastic stress on the polarisation response of pitted X65 steel in a soil representing alkaline solution [66]

polarisation response, and the results seem to be following the trend of proportionality between strain and current density seen in the aforementioned studies, however, this is without the previously seen reduction in current density as the strain is increased further. Strain seems to shift the curve more positively along the current density axis, with little movement along the potential axis. One possible reason for this difference relative to *Sahal* et al. [31] and *Wang* et al. [63] is that the strains all fall below the well-defined ultimate tensile strength of the carbon steel in *Feng's* case (similar to X65), while the nickel [31] and X80 steel [63] studies involve materials with flatter post yielding stress–strain responses. A similarly predictable response was also shown by *Wang* et al. [66] on X65 steel in the elastically stressed region (Fig. 12), however, the presence of pits and defects allowed regions of plastic strain. This could mean that for grade X65 and below steels, with strains below the ultimate tensile strength, strain may have a somewhat predictable effect on the polarisation response.

Yaguchi and *Yonezawa* [11] have shown intergranular SCC crack growth parallel to the applied stress. Their study subjected an existing fatigue crack to a corrosive environment and constant load conditions and showed SCC growth perpendicular to the crack, along its edge (Fig. 13). The cracks were deemed to be SCC rather than intergranular corrosion due to the formation of an oxide on the crack surface that was sufficient to halt extension after a small portion of growth. Higher zones of plasticity are present close to the crack walls due to its growth history as well as from the rolling process of manufacture. *Yaguchi* and *Yonezawa* [11] hypothesise that plasticity induced growth along susceptible grain boundaries. This result presents a possible case of polarisation curve shifting where the highly strained areas provide a weaker film and stronger dissolution and the less highly strained areas result in a stronger film, preventing dissolution. Crack tip plasticity enhanced dissolution has also been shown by *Tang* and *Cheng* [71] where the face of a pre-cracked X70 pipeline steel was exposed to corrosive media and significant attack was present in the crack tip plastic zone (Fig. 14). This increase in current density on the microscale was also reported by *Li* et al. [70], who showed that the current density of anodic dissolution increased significantly during plastic deformation of a single crystal (but not elastic deformation). They related this increase in current density to the higher dislocation density in the plastic region around a SCC crack tip. This reinforces the idea that the increase in current density seen with the bulk-strained samples should be relatable to plasticity on the microscale ahead of a crack tip.

Overall, this means that SCC crack growth does not follow a constant, strain-independent potentiodynamic curve. The higher and varied strains around the crack tip could result in different conditions for dissolution along differently strained grain boundaries. A model which represents intergranular SCC growth should be able to include not only the traditional stress response, microstructure, and filming and dissolution kinetics, but also demonstrate how those kinetics change radially around the crack tip. Additionally, as the cathodic protection differs down the length of the pipe, so too will the SCC equilibrium point. This could mean that the same pipeline could experience straight and inclined SCC along its length as the material properties, stresses, soil compositions and cathodic protection changes and thus these factors should also be considered when modelling SCC.

7 Modelling microstructure

As high pH SCC in gas pipelines propagates intergranularly, the properties of the microstructure will have an influence on the growth of the cracks. Various methods of creating a representative microstructure have been utilised in previous models with each

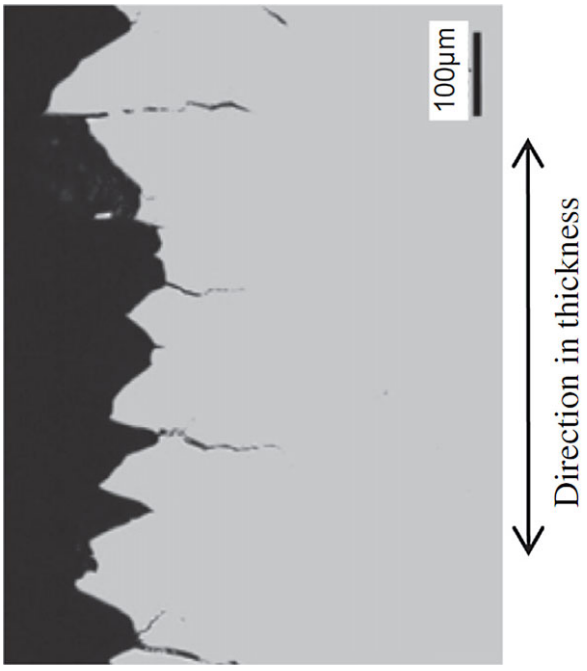

Figure 13. SCC cracks (horizontal) growing off parent fatigue crack (vertical on left of image) [11]

Figure 14. Preferential corrosion in the highly strained areas of pre-cracked X70 pipeline steel [71], with the theoretical linear elastic fracture mechanics strain contours overlayed

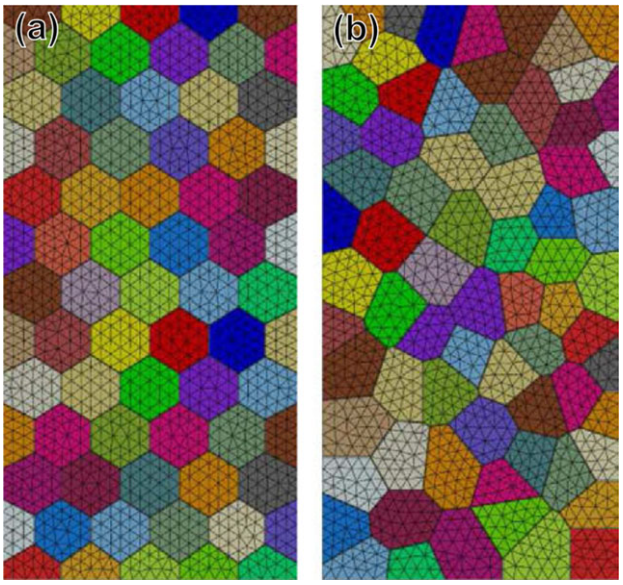

Figure 15. (a) Grains modelled using uniform tessellation; (b) grains modelled using Voronoi tessellation [46]

having their advantages and drawbacks [32,40,42–47,51,72–77]. Some of those studies have gone on to consider the effect of various microstructural properties, such as geometrical factors (shape/size) [75,76] and grain boundary properties (misorientation, special grain boundaries) [32,40,42–45,72,73,76].

The least complex method of generating a geometric microstructure is uniform tessellation of a shape, usually a hexagon or truncated octahedron, and this results in a uniform grain structure (Fig. 15a). This can be modified to add some shape skew to represent microstructural characteristics developed during fabrication and tends to be used for models where the specific path of a crack is not as important as the generic growth rate [32,42–44,47].

Following this, a grain growth method is sometimes employed [40]. This involves generating numerous grain nuclei, either randomly or via an algorithm, and then assigning each nuclei an incubation time and growth rate. The grain grows after an incubation period and forms a grain boundary when it collides with another grain. This requires significantly greater complexity than the uniform tessellation, but it does create geometrically realistic grain structures.

An alternate method to the grain growth method is Voronoi tessellation, which has been adopted in various models of polycrystalline solids as the primary method of microstructural representation [45,46,51,75,77]. Originally created in mathematics as a way of randomly dividing up a finite space into convex subspaces, Voronoi tessellation places a multitude of seed points within a 2D or 3D region [78]. Each point in the space then assigns itself to the closest seed point, creating Voronoi cells. While more complex than uniform tessellation, it is less complex than the grain growth method, while producing realistic grain structures (Fig. 15b). Furthermore, the multitude of research into Voronoi tessellation from the mathematics field has produced various algorithms for generating these diagrams more efficiently, such as with Delaunay triangulation [79]. Voronoi tessellation can even represent complex microstructural characteristics, such as banding or clusters [75] (Fig. 16). Both the grain growth algorithm and Voronoi tessellation's random nature require a Monte Carlo analysis to be performed, so that the most likely and worst case scenarios can be determined, which results in significantly more computational time than a repeating microstructure for a representative result.

Finally the grain structure of a specific sample can be found experimentally, for instance using a scanning electron microscope (specifically using an electron backscattered diffraction camera) [25,73], and then the microstructure can be imported directly into the model [74]. This method is good for validation of a model when compared with a failed component, but is generally impractical on a larger scale due to the time necessary to account for the random nature of the grains (performed in traditional models via Monte Carlo analysis).

Whichever representative method is used, the geometrical properties of the microstructure (e.g., aspect ratio, grain diameter, banding or clusters) should be determined experimentally and then replicated as closely as possible by one of the above methods.

The effect of special grain boundaries on stress corrosion cracking has also been a popular field of investigation. Certain textures (misorientation between grains) are more resistant to stress corrosion cracking [25,73] and various authors have examined their effect on crack growth rates [32,40,42–45,72,73,76]. Generally the authors considered the effect of increasing the fraction of special grain boundaries on the SCC growth rate, but with no directional consideration. The exception is *Itakura* et al. [72] who postulated that special grain boundaries can be a site for crack branching nucleation in three dimensions (Fig. 17).

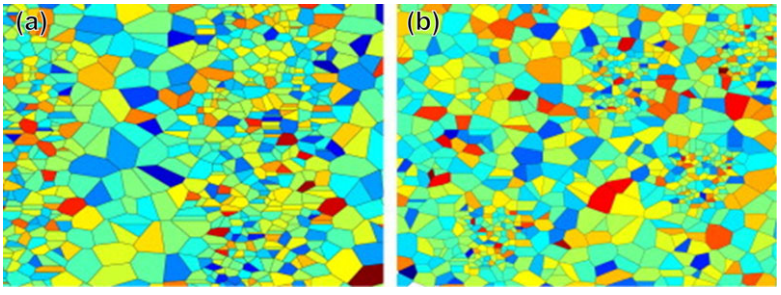

Figure 16. A Voronoi tessellation generated microstructure with (a) banding and (b) clusters [75]

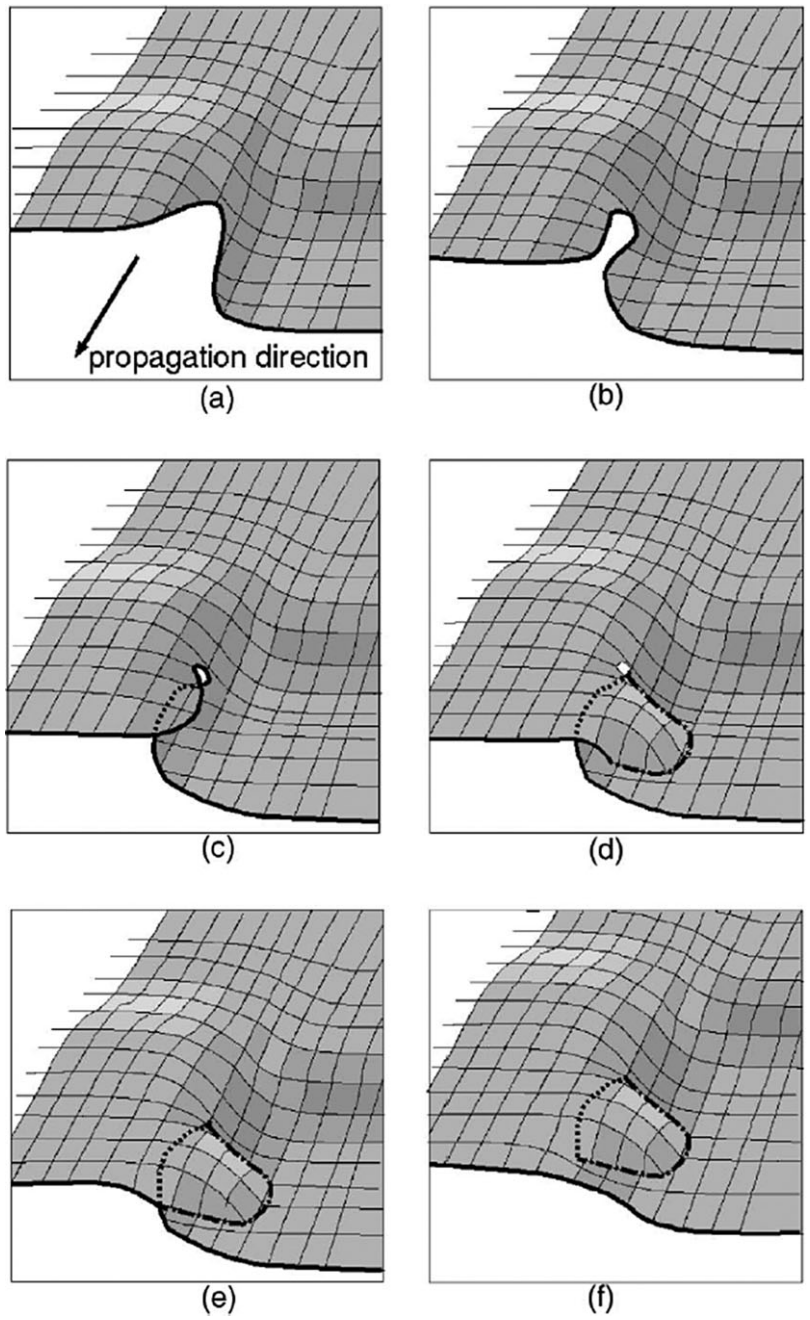

Figure 17. A step by step process of a resistant grain boundary causing crack branching in three dimensions [72]

Overall, these models show that special grain boundaries play a key role in SCC and their impact on the crack velocities should be considered in a model.

8 Conclusions

The overall rate of crack growth depends on the rates of film formation at the various crack fronts, the rate of film fracture and the rate of dissolution. These parameters, however, depend on environmental, mechanical and material properties. These must be combined and considered together to gain a holistic view of SCC growth on the mesoscale. In particular, multiple cracks in three dimensions must be modelled with consideration to the stress and strain responses, along with the effect of that stress and strain on the electrochemical behaviour and mechanisms for the different potential crack paths, which are in turn determined by the local microstructure. Existing models reveal great detail in some of these areas, but simplify one or more of the other aspects, and none of them have considered the effect of plasticity on the potentiodynamic response. A new model that can combine the existing modelling advances with this gap in

mechanically dependant electrochemistry would be required to model inclined SCC crack growth rates, as well as checking for interaction limits, as per the summary below:

1. Existing models provide reasonable predictions for straight SCC growth dynamics. In particular *Song* et al. [6] which is used by industry predicts good growth rates for film cleavage dominated growth on the macroscale, while others like *Arafin* and *Szpunar* [76] and *Kamaya* and *Itakura* [45] look at the microscale effects of microstructure and interaction.
2. A gap exists in the modelling of strain-dependant electrochemistry. A range of experimental evidence suggests that the electrochemical response will not be uniform at differently strained areas, for instance at crack tip.
3. To predict inclined SCC, a new model that takes this into account along with other factors from previous models is required. A new model would need to combine the macroscale predictive capabilities of *Song* et al. [6], the microscale interaction and microstructural properties of *Arafin* and *Szpunar* [76] and *Kamaya* and *Itakura* [45], the probabilistic tendencies of *Chen* et al. [61] and the mechanistic plasticity driven dissolution discussed in Section 6.

Such a model would allow both inclined and straight SCC to be modelled with increased certainty. It would provide a platform for additional research, guidelines or modelling tools to be developed.

Acknowledgements: This work was funded by the Energy Pipelines CRC, supported through the Australian Government's Cooperative Research Centres Program. The cash and in-kind support from the APIA RSC is gratefully acknowledged. The authors wish to further acknowledge Dr. *Andrei Kotousov* and Prof. *Valerie Linton*.

9 References

[1] R. N. Parkins, P. M. Singh, *Corrosion* **1990**, *46*, 485.
[2] Y. Z. Wang, J. D. Atkinson, R. Akid, R. N. Parkins, *Fatigue Fract. Eng. Mater. Struct.* **1996**, *19*, 51.
[3] Canadian Energy Pipeline Association, Stress corrosion cracking recommended practices, 2nd Edn., *Technical report*, **2007**.
[4] B. Choi, A. Chudnovsky, *Metall. Mater. Trans. A* **2011**, *42*, 383.
[5] B. T. Lu, F. Song, M. Gao, M. Elboujdaini, *Corros. Sci.* **2010**, *52*, 4064.
[6] F. Song, B. T. Lu, M. Gao, M. Elboujdaini, Development of a commercial model to predict stress corrosion cracking growth rates in operating pipelines, *Technical report*, Southwest Research Institute, **2011**.
[7] F. J. Barbaro, C. G. Chipperfield, *Technical Report*, Australian Iron & Steel Pty Ltd., Port Kembla **1984**.
[8] R. Sutherby, C. Weixing, Presented at *ASME International Pipeline Conference 2004*, Alberta, Canada, October 4–8, **2004**, iPC04-0600.
[9] J. Xie, L. Yang, M. Sen, R. Worthingham, F. King, Presented at *NACE International Corrosion 2009 Conference & Expo*, Atlanta, USA, March 22–26, **2009**, 09121.
[10] L. Zadow, E. Gamboa, O. Lavigne, *Mater. Corros.* **2015**, *66*, 1092.
[11] S. Yaguchi, T. Yonezawa, *Corros. Sci.* **2014**, *86*, 326.
[12] O. Lavigne, E. Gamboa, V. Luzin, M. Law, M. Giuliani, W. Costin, *Mater. Sci. Eng., A* **2014**, *618*, 305.
[13] E. Gamboa, M. Giuliani, O. Lavigne, *Scr. Mater.* **2014**, *81*, 1.
[14] R. N. Parkins, R. R. Fessler, *Int. J. Mater. Eng. Appl.* **1978**, *1*, 80.
[15] Y. F. Cheng, *Stress Corrosion Cracking of Pipelines*, John Wiley & Sons, Hoboken, New Jersey **2013**.
[16] K. Sieradzki, R. C. Newman, *J. Phys. Chem. Solids* **1987**, *48*, 1101.
[17] R. N. Parkins, *JOM* **1992**, *44*, 12.
[18] R. N. Parkins, *Corrosion* **1996**, *52*, 363.
[19] B. N. Leis, R. J. Eiber, Presented at *First International Business Conference on Onshore Pipelines*, Berlin, Germany, December, **1997**.
[20] B. Y. Fang, A. Atrens, J. Q. Wang, E. H. Han, Z. Y. Zhu, W. Ke, *J. Mater. Sci.* **2003**, *38*, 127.
[21] F. Song, Presented at NACE Corrosion 2008: Conference and Expo, New Orleans, Louisiana, March 16–18, **2008**.
[22] J. Wang, A. Atrens, *Eng. Failure Anal.* **2004**, *11*, 3.
[23] R. N. Parkins, *Corrosion* **1987**, *43*, 130.
[24] A. P. Jivkov, *Theor. Appl. Fract. Mech.* **2004**, *42*, 43.
[25] O. Lavigne, E. Gamboa, W. Costin, M. Law, V. Luzin, V. Linton, *Eng. Failure Anal.* **2014**, *45*, 283.
[26] Z. P. Lu, T. Shoji, F. J. Meng, Y. B. Qiu, T. C. Dan, H. Xue, *Corros. Sci.* **2011**, *53*, 247.
[27] T. Terachi, T. Yamada, T. Miyamoto, K. Arioka, *J. Nucl. Mater.* **2012**, *426*, 59.
[28] L. Zadow, *Master's Thesis*, The University of Adelaide, Australia, **2013**.
[29] B. N. Leis, R. N. Parkins, *Fatigue Fract. Eng. Mater. Struct.* **1998**, *21*, 583.
[30] R. N. Parkins, Overview of intergranular SCC research activities: Pr-232-9401, *Technical report*, Pipeline Research Council International, Inc., **1994**.
[31] M. Sahal, J. Creus, R. Sabot, X. Feaugas, *Scr. Mater.* **2004**, *51*, 869.
[32] A. P. Jivkov, N. P. C. Stevens, T. J. Marrow, *Comput. Mater. Sci.* **2006**, *38*, 442.
[33] T. Shoji, Z. P. Lu, H. Murakami, *Corros. Sci.* **2010**, *52*, 769.
[34] B. Cotterell, J. R. Rice, *Int. J. Fract.* **1980**, *16*, 155.
[35] S. Suresh, *Metall. Trans. A* **1983**, *14*, 2375.
[36] S. Laham, *Stress Intensity Factor and Limit Load Handbook*, British Energy Generation Ltd., UK, April **1998**.
[37] T. Fett, G. Rizzi, H. A. Bahr, U. Bahr, V. B. Pham, H. Balke, *Eng. Fract. Mech.* **2008**, *75*, 2246.
[38] A. Chambolle, G. A. Francfort, J. J. Marigo, *J. Mech. Phys. Solids* **2009**, *57*, 1614.
[39] S. Bechtle, T. Fett, G. Rizzi, S. Habelitz, G. A. Schneider, *J. Mech. Behav. Biomed. Mater.* **2010**, *3*, 303.
[40] M. Kamaya, T. Kitamura, *Int. J. Fract.* **2004**, *130*, 787.
[41] T. J. Marrow, L. Babout, A. P. Jivkov, P. Wood, D. Engelberg, N. Stevens, P. J. Withers, R. C. Newman, *J. Nucl. Mater.* **2006**, *352*, 62.
[42] A. P. Jivkov, N. P. C. Stevens, T. J. Marrow, *Acta Mater.* **2006**, *54*, 3493.
[43] A. P. Jivkov, T. J. Marrow, *Theor. Appl. Fract. Mech.* **2007**, *48*, 187.

[44] A. P. Jivkov, N. P. C. Stevens, T. J. Marrow, *J. Pressure Vessel Technol.* **2008**, *130*, 21.
[45] M. Kamaya, M. Itakura, *Eng. Fract. Mech.* **2009**, *76*, 386.
[46] A. Musienko, G. Cailletaud, *Acta Mater.* **2009**, *57*, 3840.
[47] J. J. Rimoli, *PhD. Thesis*, California Institute of Technology, USA, **2009**.
[48] P. L. Chin, *PhD. Thesis*, Rensselear Polytechnic Institute, USA, **2011**.
[49] Y. Sun, K. Meciejewski, H. Ghonem, *Int. J. Damage Mech.* **2012**, *23*, 1.
[50] A. Tafreshi, *Eng. Analysis Boundary Elements* **2011**, *35*, 984.
[51] A. Stoll, A. J. Wilkinson, *Acta Mater.* **2012**, *60*(13–14), 5101.
[52] A. R. Khoei, K. Karimi, *Comput. Mater. Sci.* **2008**, *44*, 733.
[53] W. Attaporn, H. Koguchi, *CMES* **2009**, *39*, 237.
[54] A. R. Khoei, S. M. Taheri-Mousavi, S. O. R. Biabanaki, M. Anahid, *Steel Res. Int.* **2010**, *81*, 1478.
[55] A. R. Khoei, M. Vahab, E. Haghighat, S. Moallemi, *Int. J. Fract.* **2014**, *188*, 79.
[56] E. Ferrie, J. Y. Buffiere, W. Ludwig, A. Gravouil, L. Edwards, *Acta Mater.* **2006**, *54*, 1111.
[57] R. Pourmodheji, M. Mashayekhi, *Mater. Sci. Eng. A* **2012**, *551*, 255.
[58] Q. Z. Zhu, *Int. J. Numer. Meth. Eng.* **2012**, *91*, 186.
[59] S. S. Hosseini, H. Bayesteh, S. Mohammadi, *Mater. Sci. Eng. A* **2013**, *561*, 285.
[60] K. Oguni, M. L. L. Wijerathne, T. Okinaka, M. Hori, *Mech. Mater.* **2009**, *41*, 1242.
[61] H. Chen, L. Wijeranthne, M. Hori, T. Ichimura, *Struct. Eng. Earthq. Eng.* **2012**, *29*, 10.
[62] D. B. Wells, J. Stewart, R. Davidson, P. M. Scott, D. E. Williams, *Corros. Sci.* **1992**, *33*, 39.
[63] Y. X. Wang, W. M. Zhao, H. Ai, X. G. Zhou, T. M. Zhang, *Corros. Sci.* **2011**, *53*, 2761.
[64] R. K. Ren, S. Zhang, X. L. Pang, K. W. Gao, *Electrochim. Acta* **2012**, *85*, 283.
[65] X. G. Feng, Y. Zuo, Y. M. Tang, X. H. Zhao, J. M. Zhao, *Corros. Sci.* **2012**, *65*, 542.
[66] X. Wang, X. Tang, L. Wang, C. Wang, W. Zhou, *J. Nat. Gas Sci. Eng.* **2014**, *21*, 474.
[67] A. R. Despic, R. G. Raicheff, J. O. Bockris, *J. Chem. Phys.* **1968**, *49*, 926.
[68] E. M. Gutman, G. Solovioff, D. Eliezer, *Corros. Sci.* **1996**, *38*, 1141.
[69] M. Sahal, J. Creus, R. Sabot, X. Feaugas, *Acta Mater.* **2006**, *54*, 2157.
[70] D. L. Li, R. Z. Zhu, W. Q. Zhang, *Metall. Trans. A* **1990**, *21*, 3260.
[71] X. Tang, Y. F. Cheng, *Electrochim. Acta* **2009**, *54*, 1499.
[72] M. Itakura, H. Kaburaki, C. Arakawa, *Phys. Rev. E.* **2005**, *71*, 055102.
[73] M. A. Arafin, J. A. Szpunar, *Corros. Sci.* **2009**, *51*, 119.
[74] I. Simonovski, L. Cizelj, T. J. Marrow, J. Q. da Fonseca, A. King, Presented at *ASME Pressure Vessels and Piping Conference 2009*, Prague, Czech Republic, July 26–30, **2009**, pp. 543–550.
[75] M. A. Arafin, J. A. Szpunar, *Comput. Mater. Sci.* **2010**, *47*, 890.
[76] M. A. Arafin, J. A. Szpunar, Presented at *ASME International Pipeline Conference 2010*, Calgary, Canada, September 27 to October 1, **2010**, pp. 317–324.
[77] P. Zhang, M. Karimpour, D. Balint, J. G. Lin, D. Farrugia, *Comput. Mater. Sci.* **2012**, *64*, 84.
[78] D. M. Yan, W. P. Wang, B. Levy, Y. Liu, *Adv. Geometric Modeling Processing* **2010**, *6130*, 269.
[79] H. Ledoux, Presented at *ISVD 2007: The 4th International Symposium on Voronoi Diagrams in Science and Engineering 2007*, Pontypridd, Wales, July 9–11, **2007**, pp. 117–129.

(Received: May 21, 2015) W8454
(Accepted: August 4, 2015)

FFEMS Fatigue & Fracture of Engineering Materials & Structures
ORIGINAL CONTRIBUTION
doi: 10.1111/ffe.12514

2D modelling of inclined intergranular stress corrosion crack paths

J GRIGGS, E GAMBOA and O LAVIGNE

School of Mechanical Engineering, University of Adelaide, Adelaide 5005SA Australia

Received Date: 8 April 2016; Accepted Date: 31 July 2016; Published Online:

ABSTRACT Inclined high pH stress corrosion cracking (SCC) is a type of intergranular environmental cracking in gas pipelines, which differs from typical SCC by propagating at an angle from the wall direction. Investigations of Australian and Canadian inclined SCC colonies have not provided a clear indicator of a cause for the abnormal crack growth direction. This paper addresses the possibility of crack tip strain enhanced electrochemistry causing the inclination. Potentiodynamic tests were conducted to quantify the influence of strain on the electrochemistry, and strain was found to increase current density up to 300% in the SCC region. A model was developed that incorporates crack tip strain driven SCC growth, which showed good agreement with field grown cracks, and the aspect ratio of the grains was shown to have an effect on the inclination angle. The results indicate that crack tip strain enhanced electrochemistry is a plausible cause for inclined SCC.

Keywords effects of strain; gas pipelines; modelling studies; polarisation response; stress corrosion cracking; X65 steel.

NOMENCLATURE

c_1 = depth of straight crack section
c_2 = depth of inclined crack section
CEPA = Canadian energy pipeline association
CGR = crack growth rate
$EBSD$ = electron backscatter diffraction
E = elastic modulus of steel
F = Faraday's constant
F_I = mode 1 geometric shape factor
F_{II} = mode 2 geometric shape factor
$IGSCC$ = intergranular stress corrosion cracking
$\mathcal{J}_0$ = $\mathcal{J}$ integral for a straight crack of equivalent depth
$\mathcal{J}_{crit}$ = $\mathcal{J}$ integral calculated at the critical strain criterion
K_I = mode 1 stress intensity factor
K_{II} = mode 2 stress intensity factor
LIST = linearly increasing stress test
M_{Fe} = molar mass of iron
OD = outer diameter
Q_F = charge exchanged in one rupture cycle
SCC = stress corrosion cracking
z = valence of iron
$\dot{\epsilon}_{ct}$ = crack tip strain rate
ϵ_F = failure strain of passive film
ν = Poisson's ratio
σ = applied stress

Correspondence: E. Gamboa. E-mail: erwin.gamboa@adelaide.edu.au

INTRODUCTION

Intergranular stress corrosion cracking (IGSCC) of gas pipelines has been a topic of research since the 1960s, and the theory and mechanisms are generally well agreed upon.[1–7] This mechanism involves both dissolution and film formation/cleavage process that advances the crack perpendicular to the applied stress. More recently, examples of IGSCC that does not grow perpendicular to the applied stress have been reported in some Canadian and Australian high pressure gas pipelines.[8–15] The cause of these observed unusual crack paths is unclear as purely mechanically driven cracks should not incline and continue to propagate inclined over considerable distances under fracture mechanics theory and the loading conditions. Previous studies have suggested that either microstructural properties, residual strains or mechanistic shift could be the cause.[9,10,12,13] This current study investigates the idea of a mechanistic shift, where the growth mechanism would switch from a stress-based film cleavage mechanism to a crack tip strain enhanced electrochemistry driven mechanism after a critical value. The possibility for this mechanism has been discussed at length previously.[16] Crack tip strain enhanced electrochemistry refers to both increased current density and hence dissolution, along with lower film stability in the areas of high strain near the crack tip. Evidence exists in the literature for a link between strain and current density.[17–22] Strain has also been shown to have an effect on film stability.[23] Experimental observations have shown SCC growth parallel to the applied stress at zones of high strain, although this was in part due to residual strains from plate rolling operations rather than purely crack tip strains.[24] Another study has shown that crack tip strain can enhance current density and dissolution.[25] Despite these links, there has been no investigation into the relationship between inclined SCC and strain enhanced dissolution, let alone a model that explores the idea. This paper aims to address this gap.

This present study quantifies the effect that strain plays on current density for the inclined SCC affected steel and also uses finite element and microstructural modelling to demonstrate that a crack tip strain enhanced criterion seems plausible for the case of isolated cracks in 2D, with a mechanistic reason for the change hypothesised. 3D cracks are outside the scope of this initial investigation, particularly as 3D IGSCC models are computationally expensive when modelling growth in the hundreds or thousands of grains.[26,27] Modelled crack paths are compared with cracks identified through a metallographical study on some Australian X65 inclined SCC affected pipe.[11,12]

BACKGROUND

Inclined cracks

Inclined SCC is a type of high pH intergranular SCC that grows at an angle from the perpendicular, rather than straight down into the steel (Fig. 1). To date, inclined SCC has only been investigated in X65 pipeline steels in Australia and Canada since 2004[9,10,12–15;] however, the extent of the global impact of inclined SCC is unknown because of industry assessment and repair techniques generally not involving metallographical or tomographical analysis of the cracks involved.[28] Cracks have also been reported to grow in atypical directions in stainless steels in high temperature water,[24,29,30] although these cases usually differ from inclined SCC by occurring simultaneously with branching, giving a mechanical explanation for the angular change that is not present for the case in pipelines. Various findings have been made by the investigations on inclined cracks that lead to suggestions on what is and is not likely to be the cause of the inclination.

Previous studies on both Australian and Canadian cracks have analysed the crack geometry, the mechanical properties of the X65 steel, the residual stresses and the microstructure.[9–15,31] The studies found that inclination

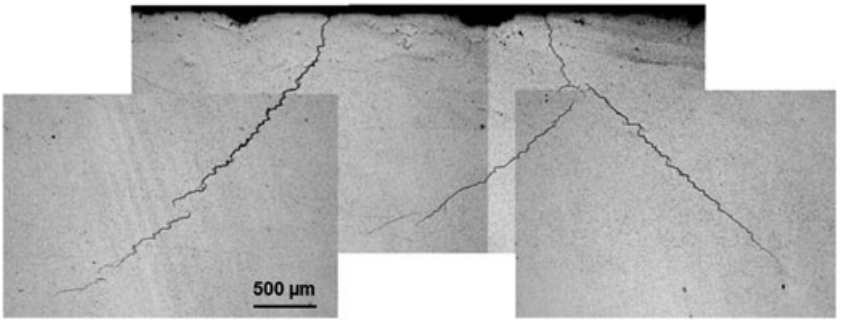

Fig. 1 2D cross section of inclined stress corrosion cracking in Australian X65 pipe transverse to pipe main axis, with curving seen on the left and branching on the right.[14]

usually occurred within 0.2 to 0.9 mm from the outer diameter, with an inclination angle between 30° and 60°,[12] however with slightly lower inclination angles for the Canadian samples.[10] The studies also showed the majority of cracks deeper than 0.2 mm from the outer diameter were inclined (81% in the Australian case).[12] The Canadian researchers reported seeing sharp kink-like inclination,[9,10] while the Australian researchers instead reported a slower curving inclination. Analysis of the cracks though shows similar crack paths in some cases (Fig. 2), and it is unclear whether the difference is due to nomenclature or actual differences in the crack path. In each case, the crack paths tend have more variance after inclination, as there are more types of crack interaction that can alter the stress fields depending on the relative inclination angles of the cracks.

Studies of the mechanical properties (yield strength, tensile strength, elastic modulus and hardness) showed little differences between the Australian and Canadian samples for the X65 steels, and authors from all studies are in agreement that mechanical properties are not indicative of propensity for inclination. Similarly, residual stresses were found to be relatively low and not in a direction such that the cracks would incline. Optical microstructural analysis showed no obvious features that could cause the inclination such as smearing.[10,12].Other microstructural findings included an average grain aspect ratio of approximately 0.5 across the Australian and Canadian specimens.[15]

One proposed reason for the inclination by the prior studies was an unspecified change in mechanism,[10] which other literature suggests may be from strain dependant electrochemistry.[17–22] In order to validate this proposed mechanism to limit the effect of crack interaction (the most significant variable), relatively isolated cracks have to be selected. Figure 3 shows five inclined SCC cracks from an Australian SCC colony,[11] each crack with limited interaction so the mechanism can be examined with

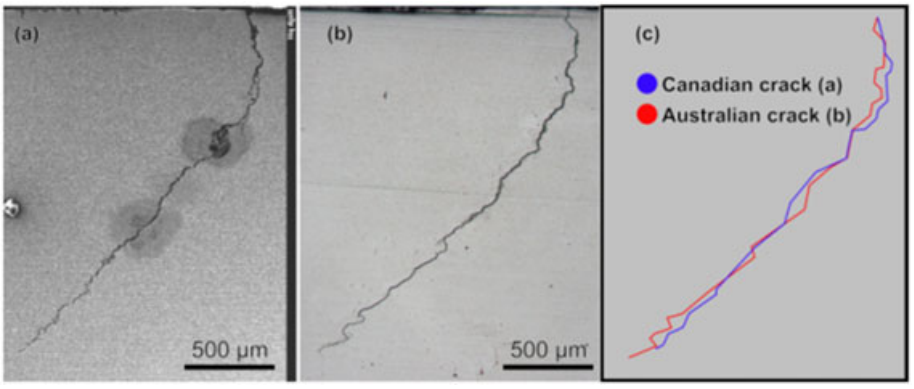

Fig. 2 (a) Canadian inclined stress corrosion cracking crack,[9] (b) Australian inclined stress corrosion cracking crack[11] and (c) tracings of the cracks overlayed on each other for comparison.

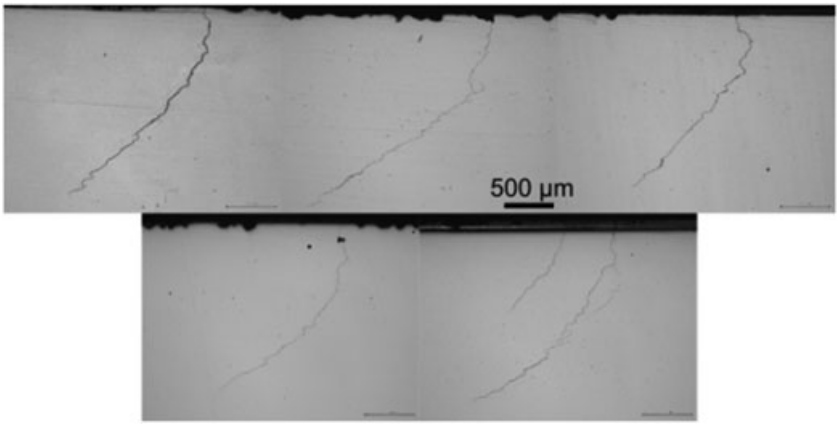

Fig. 3 Five inclined stress corrosion cracking cracks with limited interaction from an Australian colony.[11]

fewer variations caused by interaction. Interestingly, all the isolated cracks tend to incline at a similar depth, and a greater range of inclination depth is only seen in those cracks with altered stress fields from neighbouring cracks. These isolated cracks will not display all the features seen in a typical SCC crack with interaction, such as zig-zag, but will help identify if the root cause of the inclination being crack tip strain dependant electrochemistry is plausible. This cause can then be combined with the varied stress fields from interaction and presence of rolling residual strains which cause zig-zag patterns and inclination at more varied depths.

Fracture mechanics

Typical fracture mechanics based reasons for crack kinking such as mixed mode stresses would be a simple explanation for the cracks turning, with the mixed mode stresses possibly being caused by crack-crack interaction, crack-weld interaction and general residual stresses from pipe forming. All of these can be discounted however, as the cracks have occurred away from welds, sometimes inclined with no other nearby cracks, and inclined in both directions which discounts residual significant residual stress field effects (69% clockwise and 31% counter-clockwise of 95 inclined cracks surveyed).[12] Additionally, electron backscatter diffraction (EBSD) analysis has shown no obvious residual strain patterns or microstructural features that could explain the inclination on their own, although there is possibly some contribution from residual strain in the transverse direction of the pipe wall.[13] Other causes must be looked at for the cracking, and the electrochemical element of SCC propagation is the logical place to look for the shift in mechanism.

Shifting mechanism

The existing theory for predicting SCC growth involves the balance between dissolution and passive film cleavage. Film cleavage is usually the rate limiting factor and is represented as such in Eq. (1), which is a modified form of Faraday's law[32]

$$CGR = \frac{M_{Fe}}{zF\rho} Q_F \frac{\dot{\epsilon}_{ct}}{\epsilon_F}. \quad (1)$$

Here, CGR is the crack growth rate, M_{Fe} is the molar mass of iron, z is the valency of the ions in solution, F is Faraday's constant, ρ is the density, Q_F represents the charge exchanged in the time between two passive film ruptures, $\dot{\epsilon}_{ct}$ is the crack tip strain rate and ϵ_F is the strain required to rupture the film. Lu *et al.*[33] developed a model based on this equation, and they report good agreement with crack velocities lower than 10^{-6} mm s^{-1}. Their model assumed that the mass transfer is negligible and that the crack will grow via a film cleavage dominated growth mechanism.

Of note is that the dissolution is governed by charge exchanged, Q_F, which is also proportional to the current density at the crack tip.[32] Various authors[17–22] have shown that plastic deformation can change the current density at a given potential. There has also been an evidence of a shift in the corrosion potential under elastically strained X65 steel,[22] with pits causing microplastic events, which could suggest that the balance between dissolution and film formation could shift if the metal is locally strained. Because zones of high plasticity occur at shear angles ahead of the crack tip under mode I stresses, it follows that current density may be higher at these angles, increasing the propensity for dissolution. Strain mapping experiments conducted on a pre-cracked X70 steel specimen in concentrated carbonate/bicarbonate solution showed an increase in current around the crack tip, with the increases to current appearing to be primarily in the transverse direction,[25] giving justification to the idea of crack tip strain enhanced dissolution. The study also showed preferential dissolution in the crack tip plastic zone of pre-cracked X70 pipeline steel in longer time frame testing (Fig. 4).

For this crack tip strain enhanced mechanism to be worth investigating, it should be able to explain the macroscopic slow curving nature of the cracks seen in the majority of isolated cracks (the small deviations and perturbations can often be attributed to microstructural features or 3D effects). This can be most easily performed by following the assumption that above a critical strain value, the current density will be sufficient to cause inclined SCC extension in the direction of highest strain. Below that critical strain, the traditional film cleavage dominated mechanism will cause a straight crack extension. The J integral (as defined in Eq. (2)) is used as a relative measure of strain because of ease of calculation and

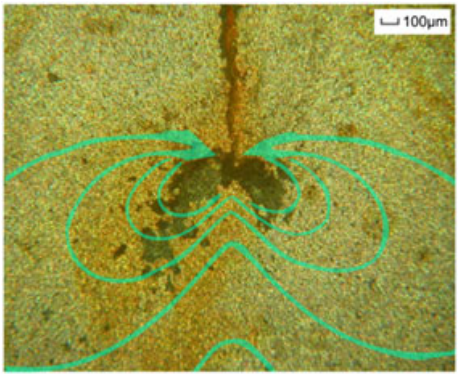

Fig. 4 Preferential corrosion in the highly strained areas of pre-cracked X70 pipeline steel,[25] with the theoretical linear elastic fracture mechanics strain contours overlayed.

comparison, and $\mathcal{J}_{crit}$ is defined as the $\mathcal{J}$ integral calculated at the critical strain criterion. In Eq. (2), K_I is the mode 1 stress intensity factor (defined in Eq. (3)), K_{II} is the mode 2 stress intensity factor (defined in Eq. (4)), ν is Poisson's ratio and E is the elastic modulus. In Eqs (3) and (4), σ is the applied stress, F_I a geometric shape factor and, c_1 and c_2 are as defined in Fig. 5. The crack would start by growing generally perpendicular to the applied stress with minor deviations due to microstructural features until the strain along the angles was sufficiently high such that the path of least resistance was along that angle, and the crack begins to incline. Using geometrical parameters defined in Fig. 5, Table 1 shows that a kinked crack under hoop stress will have a lower $\mathcal{J}$ integral than the straight crack of equal depth (row 1). Thus it can be seen that if $\mathcal{J}_{crit}$ is reached for a straight crack (i.e. $\mathcal{J}_0 = \mathcal{J}_{crit}$), the $\mathcal{J}$ integral will then fall below $\mathcal{J}_{crit}$ after a small extension at an angle in the direction of highest strain, and return to perpendicular film cleavage dominated growth. This alternating straight/inclined growth would continue until such a depth that the critical strain can be exceeded at a steady inclined angle, as illustrated in Figure 6.

$$\mathcal{J} = \left(K_I^2 + K_{II}^2\right) \cdot \left(\frac{1-\nu^2}{E}\right) \tag{2}$$

$$K_I = \sigma F_I \sqrt{\pi(c_1 + c_2)} \tag{3}$$

$$K_{II} = \sigma F_{II} \sqrt{\pi(c_1 + c_2)} \tag{4}$$

Table 1 also allows us to estimate the depth over which the crack will gradually change propagation angle before the asymptotic limit is reached. The $\mathcal{J}$ integral is linearly proportional to the square of the stress intensity factors $K_I^2 + K_{II}^2$, while the stress intensity factors are linearly proportional to the square root of the crack depth $c_1 + c_2$, as shown in Eqs (2), (3) and (4). Thus, the $\mathcal{J}$ integral is linearly proportional to the crack length for an isotropic linear elastic material. This linear proportionality implies that we can get an approximation for the depth

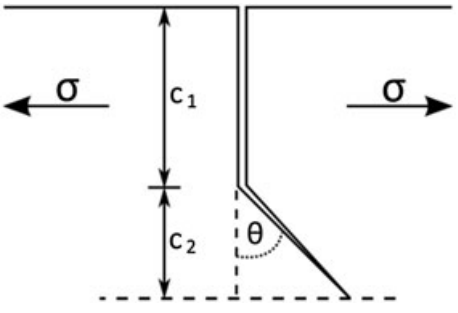

Fig. 5 Definition of crack geometric parameters.

Table 1 Stress intensity factors for various kink angles and length ratios,[36] along with the $\mathcal{J}$ integral relative to a straight crack of equal length, with parameters as defined in Fig. 5, and $\mathcal{J}_0$ is the $\mathcal{J}$ integral for a straight crack of equal depth.

$\frac{c_2}{c_1+c_2}$	$\theta(°)$	$\frac{K_I}{\sigma\sqrt{\pi(c_1+c_2)}}$	$\frac{K_{II}}{\sigma\sqrt{\pi(c_1+c_2)}}$	$\frac{\mathcal{J}}{\mathcal{J}_0}$
~0	0	1.1215	0	1
~0	15	1.093	1.1437	0.9662
~0	30	1.011	0.2695	0.8704
~0	45	0.877	0.3626	0.7160
0.03	15	1.05	0.159	0.8967
0.03	30	0.96	0.294	0.8015
0.03	45	0.82	0.3918	0.6566
0.05	15	1.061	0.1625	0.9160
0.05	30	0.967	0.304	0.8169
0.05	45	0.824	0.4044	0.6699
0.1	15	1.087	0.1696	0.9623
0.1	30	0.989	0.3172	0.8577
0.1	45	0.838	0.4255	0.7023
0.15 to 1	15	1.088	0.177	0.9661
0.15 to 1	30	0.989	0.329	0.8637
0.15 to 1	45	0.838	0.434	0.7081

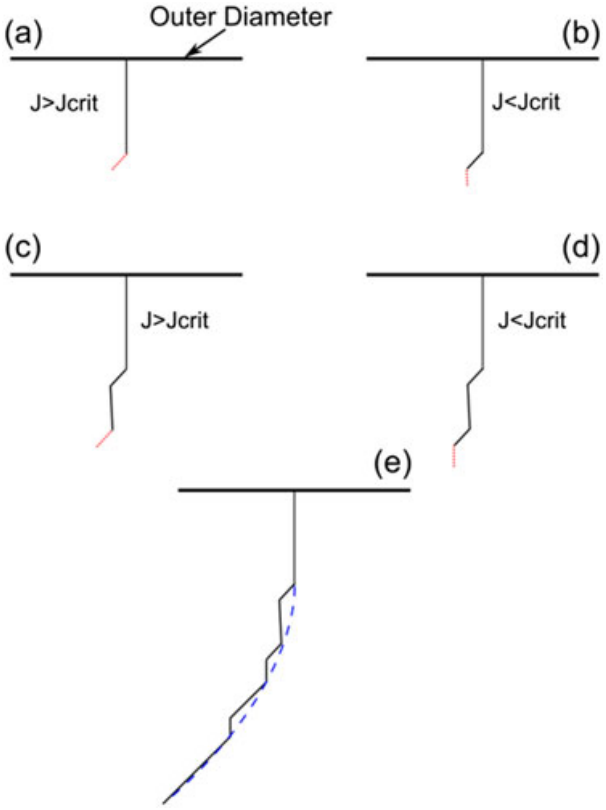

Fig. 6 Evolution of an inclined crack through a strain enhanced growth mechanism, where red lines in (a)–(d) represent next growth step. (e) shows how the curve presents after three more growth segments.

at which an inclined crack will stabilise its growth angle. The depth at which this stability occurs can be estimated as the depth of the initial straight section divided by the $\mathcal{J}$

integral for a stable angled crack $\left(\frac{c_2}{c_1+c_2} = 0.15 \text{ to } 1\right)$. As an example using the values presented in Table 1, a crack of straight section of depth c_1 will have a stabilisation depth of $c_1/0.7081$ when the stable final angle (θ) is 45°. Similarly, if the final angle is 30°, the stabilisation depth will be $c_1/0.8637$. Some errors are expected in this, as there is no sharp kink and two easily defined straight sections, and also, rolled steel is not an isotropic linear elastic body.

POTENTIODYNAMIC RESPONSE OF X65 TO STRAIN

Tests were conducted to quantify the relationship between strain and polarisation response for inclined SCC affected X65 steels in high pH environments. Flat tensile specimens were cut from the centreline of a pipe section in the longitudinal direction. This material came from one of the pipe sections that did not show any cracking used in a prior study.[28] Gauges were 50 mm in length, 2.6 mm in width and 2.8 mm in thickness. The mechanical properties of the steel specimens were first determined by a typical tensile test using an Instron machine. The yield and ultimate tensile strengths were measured as 460 and 590 MPa, respectively. Tensile specimens were then exposed to the simulated high pH SCC medium defined in the literature: 1 N carbonate + 1 N bicarbonate solution at 70 °C.[28] The exposed surface of the specimens was limited at one face of the specimen gauge by covering the undesired parts by a layer of silicon rubber on the top of a layer of epoxy resin. The exposed surface was thereby 0.91 cm^2 in area (35 mm in length and 2.6 mm in width). Surfaces were machine ground finished. A linearly increasing stress test machine[28] was used to apply different amounts of loads on the specimens. It should be noted that the range of loads available from the experimental setup were limited to the elastic range and that the process zone of the crack tip would be in the plastic region; however, the elastic relation between strain and current density is still of value. At each applied load, potentiodynamic curves with a scan rate of 0.1 $mV\,s^{-1}$ were recorded from −1 $V_{Ag/AgCl}$ to 0.9 $V_{Ag/AgCl}$. Before each potentiodynamic measurement, a cathodic potential of −1 $V_{Ag/AgCl}$ was applied to the specimens in order to remove the oxide layer formed on their surface in air or during the previous experiments. At least three potentiodynamic curves per applied load were recorded to check the reproducibility of the results. The electrochemical tests were conducted with a Gamry interface 1000^{TM}, using the specimens as the working electrode, a platinum mesh as the counter electrode and a saturated silver/silver chloride electrode as the reference. The reference electrode was maintained at room temperature and connected to the electrochemical cell with a Luggin probe. The results of these tests are presented in Fig. 7.

It can be clearly observed from Fig. 7 that strain results in an increase in current density for potentials on the anodic side of the activity peak (located at −665 m $V_{Ag/AgCl}$ approximately). This includes the SCC range as well as a clear difference for the passive region. This implies that the strain is causing a less stable film that is allowing more mass transfer and possibly increasing the amount of dissolution. At some areas in the passive region, an increase in the current density of up to 200% is seen between the zero strain and 100% YS strain condition, while in the SCC range up to a 300% increase is observed. These results seem reasonable and agree with the general trend seen in past studies.[17–22] This provides additional support that for the inclined SCC affected steel, even just elastic strain has a significant effect on the current density and film stability.

MODELLING METHOD

The algorithm defined in the previous section is combined with an intergranular growth code developed by the authors with MATLAB and ANSYS, with the general programme architecture shown in Fig. 8. The microstructure is generated in MATLAB by Voronoi tesselation, as shown in Fig. 9, with geometric parameters as determined from empirical studies of inclined SCC affected pipe.[11] Key parameters include grain width of 8 μm and an average grain aspect ratio in the region of 0.5 ± 0.05 (consistent with pipe rolling), both found through EBSD measurements conducted in previous studies.[15,31] Textural characteristics are not included in this model, as

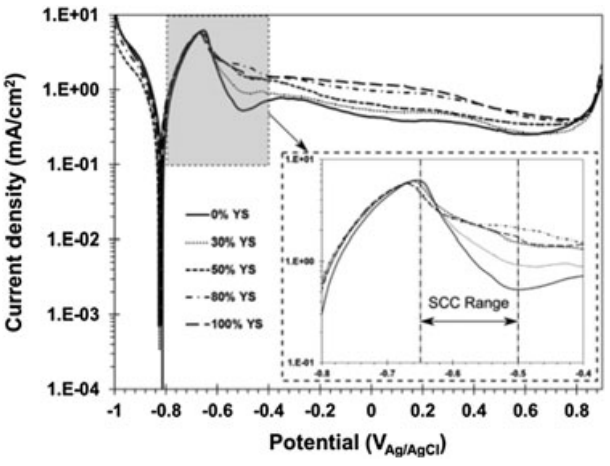

Fig. 7 Potentiodynamic curve of inclined stress corrosion cracking (SCC) affected X65 pipeline steel at different levels of *in situ* strain (YS = Yield strength).

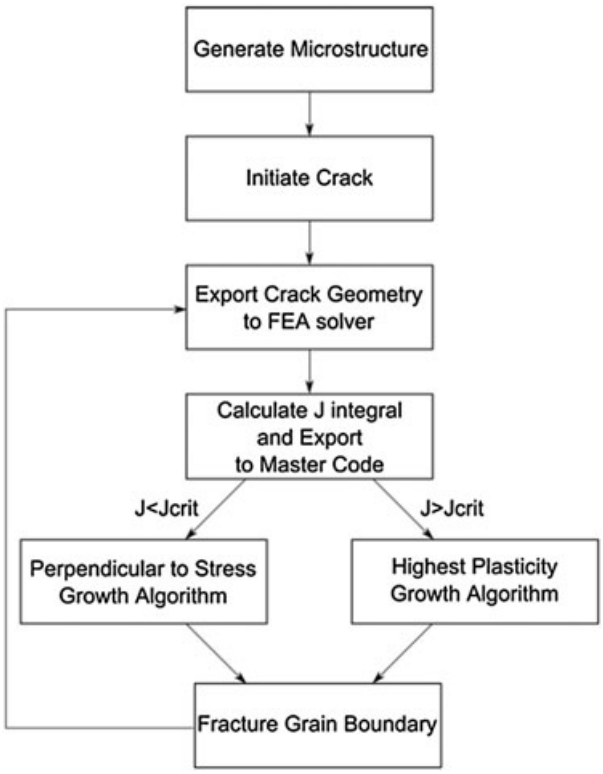

Fig. 8 High level programme architecture of the model.

there is an equally likely chance of a resistant boundary occurring on either side of the crack front, and over many cracks with many grain boundary fracture events, the average macroscopic crack path should remain fairly similar whether texture is taken into account or not. The critical J integral criterion is taken to correspond to that of a straight crack with depth of 0.55 mm, which was determined experimentally to be typical of isolated inclined Australian cracks.[11]

While the initial conclusions of Zadow[11] presented a range of crack inclination depths, closer examination of the raw data showed the variations were occurring in the cases where interaction would alter the stress field. Additionally, some cracks were represented with only one or two cross sectional slices and maximum straight depth of the 3D crack (and hence inclination depth) could not be interpolated accurately from so few data points. Of the cracks that showed limited interaction and were represented with multiple slices, the maximum straight depth was consistent at 0.55 ± 0.05 mm. This indicates that the critical J value would occur at this depth under the stress state present in the field. This critical J would govern the crack growth direction, and the crack extension would be inclined or straight if the critical J value was exceeded or not respectively.

Presence of crack interaction can change the stress magnitude and distribution, so for this study, we only consider the simple case of a single isolated crack in an attempt to reduce the varying nature of the cracking. Even still, slight variations in microstructure and electrochemistry will cause some differences between the ideal case modelled and the real life cracks, but the model provides basis for a proof of concept, and general agreement lends weight to potential for crack tip strain enhanced growth.

The J integral is calculated within an ANSYS code which approximates the crack shape via a 10-point weighted representation, with more key points towards the crack tip, as the crack geometry has less impact the further it is from the crack tip.[34] The model is meshed in 3 areas with PLANE183 elements, with smaller elements around the crack tip and larger elements in the bulk to decrease computational time. 20 contours of the J integral are taken, and mesh density is selected such that convergence is within the first five contours, however the model produces similar results with mesh density coarsened such that convergence occurs after more contours, which results in additional computational efficiency if required.

MODELLING RESULTS

Cracks were propagated in a simulated microstructure with properties gained from EBSD (grain width of 8 μm and average grain aspect ratio of 0.5) and a critical J integral criterion corresponding to a straight crack depth of 0.55 mm (Fig. 10). Some cracks grown in these circumstances can then be compared with the isolated cracks from the field (Fig. 11). The smaller crack arrowed in the lower right image of Fig. 11 is not considered as its growth would have been influenced by interaction from the larger, pre-existing crack to its right.

Figure 11 shows that the cracks grown by the model have a reasonable agreement with the cracks in the field, lending weight to the argument of crack tip strain dependant electrochemistry being an important driver behind inclined SCC. The curving nature of the cracks is represented rather well considering the simplicity of the model, which only considers geometric microstructural properties, as well as the critical strain growth criterion. More variation is seen in the real cracks because of the number of other influencing factors, such as interaction, possible residual stresses and strains, varying aspect ratio with depth and circumferential position, other microstructural variables (texture, vacancies and concentration of alloying elements) and varying electrochemistry. These factors can all account for the various deviations from the modelled cracks. An implication of this is that the crack tip strain criterion is of great significance to the inclined crack path, with variation influenced by the other variables. This can be further evidenced by the

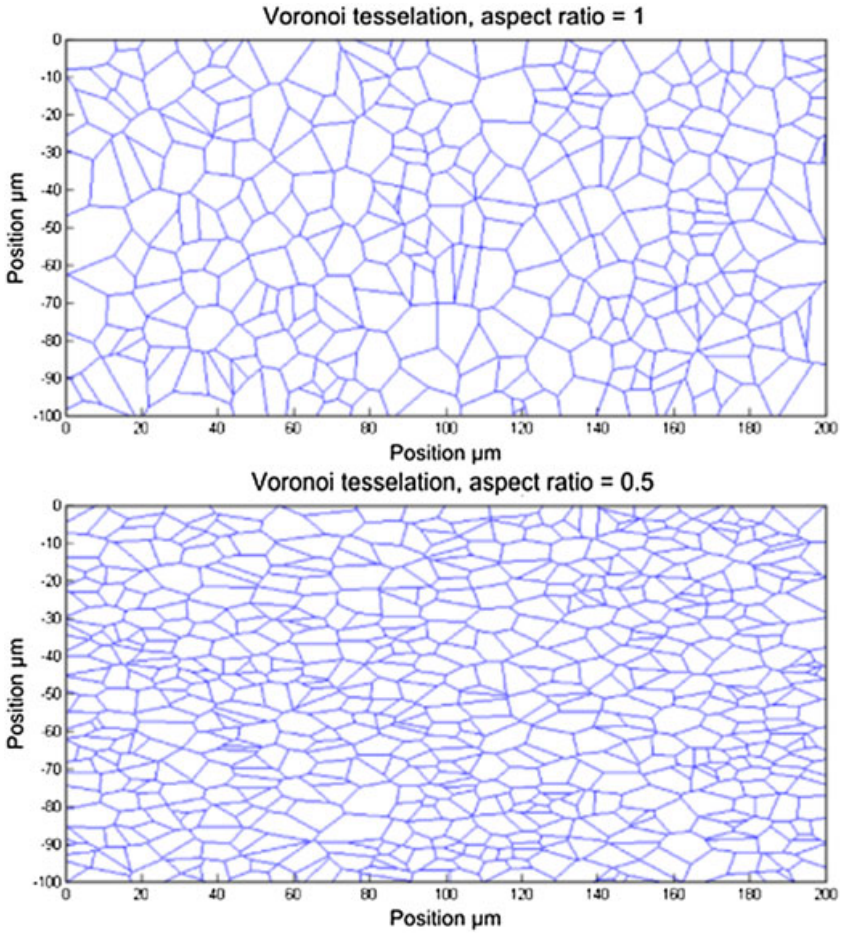

Fig. 9 Example section of generated microstructure for average grain aspect ratios of 1 and 0.5, with a grain width of 8 µm.

growth of a crack with a criterion of film rupture of the weakest grain boundaries, which shows on average straight crack paths, even with the change in grain aspect ratio (Fig. 12). Of the factors that are not included in the model, interaction is the one that could have the largest impact on crack path. Evidence for this lies in the fact that these cracks had relatively little interaction and were fairly consistent, while cracks with more interaction can show vastly different crack paths (Fig. 1). Regardless, the critical strain growth criterion seems to replicate the inclined cracking fairly well, with other factors contributing to the variations in the crack morphology.

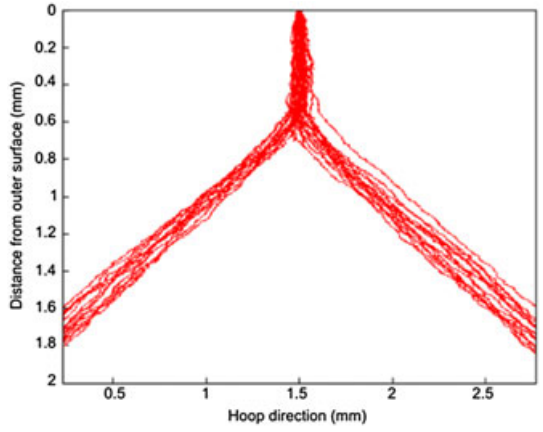

Fig. 10 Thirty modelled inclined stress corrosion cracking crack paths under a critical crack tip strain enhanced growth mechanism, with an average grain aspect ratio of 0.5.

The effect of the grain aspect ratio was further investigated after the mechanism was seen to agree with real cracks. Two findings presented themselves during this investigation, [1] the grain aspect ratio can affect the final angle the crack path approaches and [2] the rate with which it approaches that angle for the same critical strain. This difference is most easily visualised by modelling vastly different aspect ratios (Fig. 13). Lower grain aspect ratios result in a greater inclination deviation, as well as taking longer before it approaches a steady state angle. Both of these results can be explained by looking at the calculated distribution of grain boundaries in the modelled space (Fig. 14). The space with an average grain aspect ratio of 1

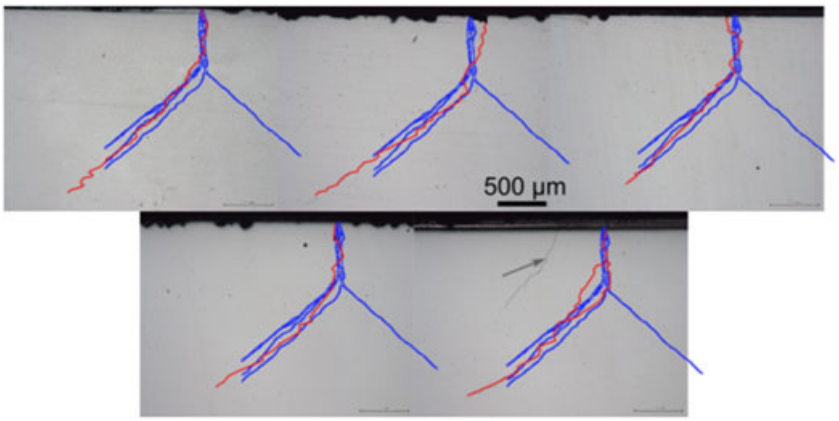

Fig. 11 Five inclined stress corrosion cracking cracks with limited interaction from an Australian colony in red[11], with modelled 0.5 grain aspect ratio crack paths in blue. Arrowed crack is not considered because of the presence of interaction from adjacent crack.

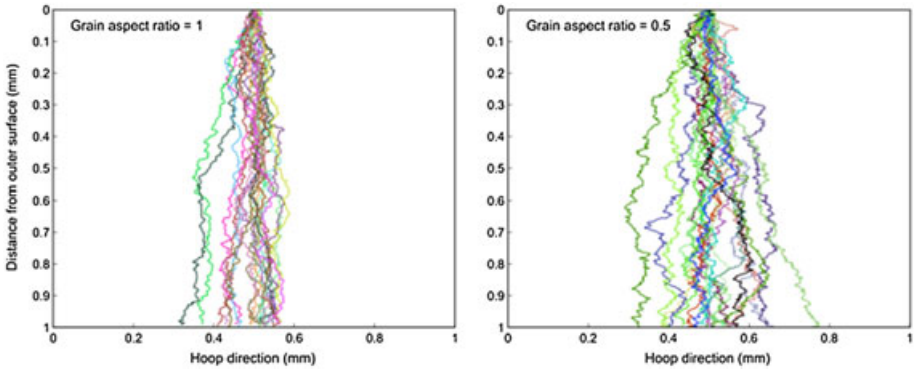

Fig. 12 Twenty modelled stress corrosion cracking crack paths under a maximum stress intensity factor film rupture based growth mechanism, with average grain aspect ratios of 1 and 0.5.

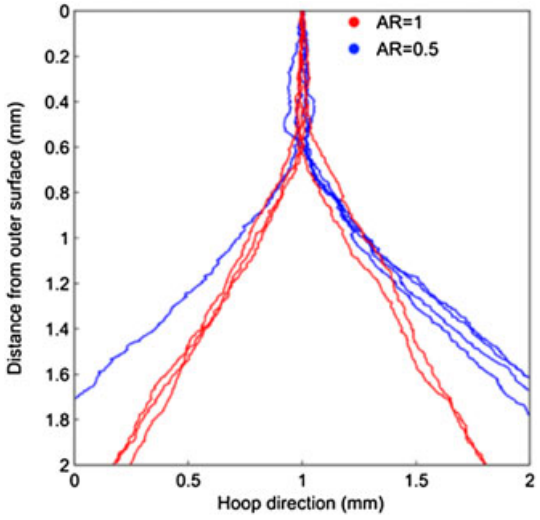

Fig. 13 Five cracks with an average grain aspect ratios of 0.5 (blue) and 1 (red) showing the effect of grain aspect ratio on crack path.

has an even chance of propagating along any angle of boundary, however the modelled space with the lower aspect ratio has a far higher proportion of more horizontal boundaries, and as such the cracks will tend to travel more horizontally over time. Additionally, a crack with a higher inclination angle will have a lower stress intensity factor (Table 1, columns 3–5). This relationship between average grain aspect ratio and steady state growth angle can be calculated and quantified in 2D (Fig. 15). The growth angle is relatively sensitive to aspect ratio, with a shift of approximately 5° occurring from purely a change in aspect ratio from 0.45 to 0.55.

DISCUSSION

The assumptions of the model lead to some minor deviations between the modelled cracks and the observed

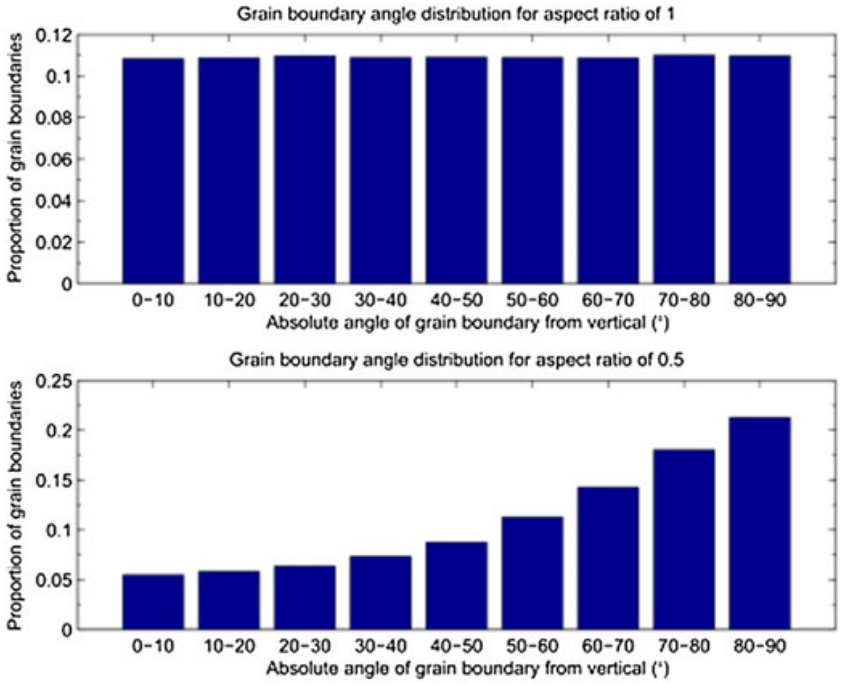

Fig. 14 Distribution of the absolute grain boundary angles for average grain aspect ratios of 1 and 0.5.

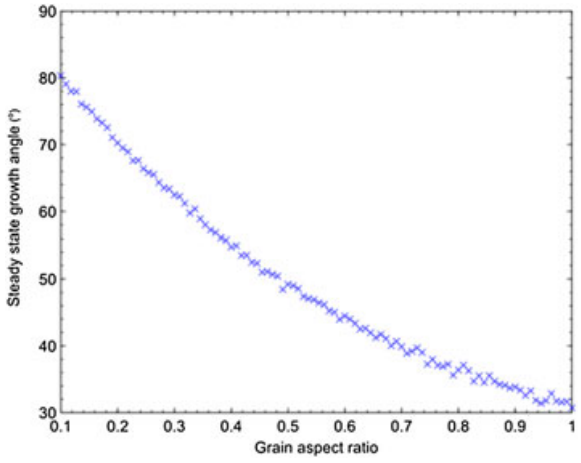

Fig. 15 Distribution of the steady state growth angle of inclined stress corrosion cracking over varying aspect ratios.

field cracks. For this model, it is assumed that there is no interaction from other neighbouring cracks. This assumption is rarely applicable to an SCC colony where interaction is one of the key driving forces behind the propagation. It is a point to note that the cracks observed were relatively isolated, which would minimise the effects of interaction. Texture and microstructural features such as vacancies and manganese sulphide inclusions were also neglected in the model, which in the field would have some effect on the crack path. There also is a source of small error in the model coming from the 2D representation of the crack, as the crack tip would be influenced by the movement of the rest of the crack front. Most of these assumptions have resulted in minimal errors as discussed in the previous Results section, but future works plan to incorporate these elements to quantify their effect on the crack path.

Assuming crack tip strain enhanced electrochemistry is a driver of inclined SCC, preliminary answers can be provided to other questions, such as the implications on growth rates, industry evaluation methods and manufacturing methods. Additionally it provides clearer opportunities for further work in the understanding and prevention of inclined SCC.

The growth rate of an SCC crack is dependent on both rate of film rupture, and the current density (Eq. (1)). For the crack to grow at a preferential rate along the angle, its crack growth rate in that direction must be greater than the crack growth rate in the vertical direction. As during the turning portion of the growth, the crack alternates between inclined and straight propagation in small steps, the growth rates of these two sections will be similar, albeit in different directions. This means that for a final growth angle of 50° (corresponding to a grain aspect ratio of 0.5), depth of the crack will be between 64% and 100% of the equivalent straight crack during prior to the stabilisation depth. However, after the steady state region is reached, the crack growth rate will start to increase because of the increasing strain at the crack tip and corresponding current density. This could

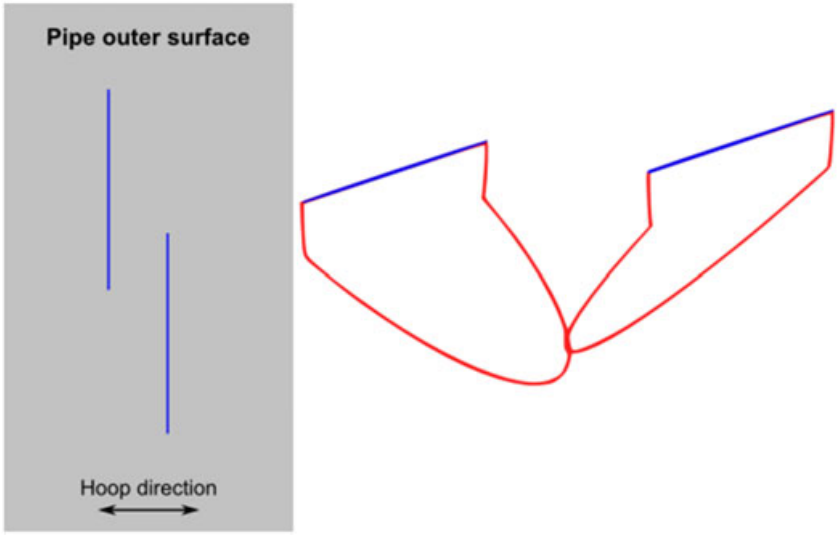

Fig. 16 Schematic of potential unpredicted interaction between parallel non-collinear inclined cracks. Blue lines represent the crack mouth on the surface, while red lines represent the crack front.

potentially result in an increase in rate of radial crack growth and hence depth for very long inclined cracks relative to straight cracks, but further investigation is required to determine exactly what level of crack strain would be required, including quantitatively ascertaining the crack tip strain dependant electrochemical response of the affected steel.

Industry evaluation methods for SCC (Canadian Energy Pipeline Association, CEPA) rely on both rates of crack growth and potential for interaction.[35] This paper has shown that inclined cracks could have different crack growth rates than those assumed by CEPA guidelines (even in a benign manner). Additionally, this work can help to quantity and assess the CEPA interaction guidelines. As the cracks grow in the direction of highest strain, stress shielding will still prevent adjacent parallel cracks from coalescing.[36] Additionally, collinear cracks should still behave in the same manner as straight cracks. The potential for unexpected interaction comes with closely spaced cracks with some hoop and axial offset, which incline towards each other sub-surface (Fig. 16). This configuration of cracks would allow an interaction region below the surface but reduces the stress shielding effects that would retard the crack growth at the interacting surface tips. This crack configuration could create enhanced zones of strain at the leading and trailing edges of the subsurface cracks and potentially cause subsurface coalescence with no obvious interaction on the surface. This potential subsurface coalescence could be outside the interaction region as predicted by CEPA.[35] This interaction is a region of interest for future modelling endeavours, and work is currently underway to determine whether closely spaced inclined cracks can still be assessed by CEPA guidelines.

Manufacturing methods are also of interest, as there could be potential to introduce inclined SCC resistance into pipe walls in the future. Many of the methods have changed since these X65 pipes were manufactured over 30 years ago, yet some areas are still of interest. Recrystallisation after rolling of the steel can move the grain aspect ratio back to an average of 1 and reduce the residual plastic strains that could aid the strain enhanced inclination. Additionally, the strain dependant electrochemistry of pipeline steels could be considered during steel design and manufacture, to provide greater understanding of whether SCC crack paths are likely to incline. More research is needed to determine why the X65 electrochemistry results in it being susceptible to inclined SCC in areas of high strain.

CONCLUSION

Crack tip strain dependant dissolution has been identified as being a possible cause for inclined SCC. A model has been developed using a bimechanistic growth code of stress driven film cleavage and strain enhanced electrochemistry, which can simulate inclined SCC cracks. These simulated cracks have shown to have similar crack paths to those seen in ex-service samples with equivalent microstructural geometric properties. This qualitative validation lends weight to the suggestion that this bimechanistic growth is a potential mechanism for inclined IGSCC in high pressure gas pipelines. Grain aspect ratio has also been investigated and was found to have an influence on the appearance of the inclination, as well as the final steady state inclination angle. In

particular, lower grain aspect ratios result in higher inclination angles with the angle being relatively sensitive to the grain aspect ratio. The model suggests that radial crack growth rates are fastest when the crack first initiates and grows perpendicular to the pipe free surface. After the crack starts to incline, the radial crack growth rate would slow down until the crack reaches a stable inclination angle, after which the radial crack growth rate will increase once again. Various possible implications for crack growth rates, interaction limits and manufacturing methods have been discussed with some areas requiring further investigation identified. The model developed in this study can be used to further examine the effect of inclined cracks on pipe integrity.

Acknowledgements

This work was funded by the Energy Pipelines CRC, supported through the Australian Government's Cooperative Research Centres Program. The cash and in-kind support from the APGA RSC is gratefully acknowledged. The authors wish to further acknowledge Dr Andrei Kotousov, Dr Michael Law and Prof. Valerie Linton.

REFERENCES

1 Parkins, R. and Fessler, R. (1978) Stress corrosion cracking of high-pressure gas transmission pipelines. *Mater. Eng. Appl.*, **1**, 80–96.
2 Sieradzki, K. and Newman, R. (1987) Stress-corrosion cracking. *J. Phys. Chem. Solids*, **48**, 1101–1113.
3 Parkins, R. (1992) Current understanding of stress-corrosion cracking. *JOM-J. Min. Met. Mat. S.*, **44**, 12–19.
4 Parkins, R. (1996) Mechanistic aspects of intergranular stress corrosion cracking of ferritic steels. *Corrosion*, **52**, 363–374.
5 Leis B., Eiber R. (1997). Stress-corrosion cracking on gas-transmission pipelines: history, causes, and mitigation. *First International Business Conference on Onshore Pipelines*, Berlin, Germany.
6 Fang, B., Atrens, A., Wang, J., Han, E., Zhu, Z. and Ke, W. (2003) Review of stress corrosion cracking of pipeline steels in "low" and "high" pH solutions. *J. Mater. Sci.*, **38**, 127–132.
7 Song F.(2008). Overall mechanisms of high pH and near-neutral pH SCC, models for forecasting SCC susceptible locations, and simple algorithms for predicting high pH SCC crack growth rates. *NACE Corrosion 2008*: *Conference and Expo*, *New Orleans*, *Louisiana*.
8 Barbaro F., Chipperfield C. (1984). Investigation of the failed Moomba-Sydney natural gas pipeline. Tech. Rep., *Australian Iron & Steel PTY LTD – Port Kembla*.
9 Sutherby R., Weixing C. (2004). Deflected stress corrosion cracks in the pipeline steel. *International Pipeline Conference*, Calgary, Alberta, Canada.
10 Xie J., Yang L., Sen M., Worthingham R., King F (2009). Mechanistic investigation of deflected stress corrosion cracking in pipeline steels. *NACE International Corrosion 2009 Conference & Expo*, Atlanta, Georgia, USA.
11 Zadow L. (2014). Characterisation of the morphology of inclined SCC cracks in Australian gas pipelines. *M.A. Thesis*, *University of Adelaide*, *Adelaide*.
12 Zadow, L., Gamboa, E. and Lavigne, O. (2014) Inclined stress corrosion cracks in gas pipeline steels: morphology and implications. *Mater. Corros.*, **66**, 1092–1100.
13 Lavigne, O., Gamboa, E., Luzin, V., Law, M., Giuliani, M. and Costin, W. (2014) The effect of the crystallographic texture on intergranular stress corrosion crack paths. *Mater. Sci. Eng. A*, **618**, 305–309.
14 Gamboa, E., Giuliani, M. and Lavigne, O. (2014) X-ray microtomography observation of subsurface stress corrosion crack interactions in a pipeline low carbon steel. *Scr. Mater.*, **81**, 1–3.
15 Lavigne, O., Gamboa, E., Griggs, J., Luzin, V., Law, M. and Roccisano, A. (2016) High-pH inclined stress corrosion cracking in Australian and Canadian gas pipeline X65 steels. *Mater. Sci. Tech. Ser.*, **32**, 684–690.
16 Griggs, J., Gamboa, E. and Lavigne, O. (2016) A review of modelling high pH stress corrosion cracking of high pressure gas pipelines. *Mater. Corros.*, **67**, 251–263.
17 Sahal, M., Creus, J., Sabot, R. and Feaugas, X. (2004) Consequences of plastic strain on the dissolution process of polycrystalline nickel in H2SO4 solution. *Scri. Mater.*, **51**, 869–873.
18 Wells, D., Stewart, J., Davidson, R., Scott, P. and Williams, D. (1992) The mechanism of intergranular stress-corrosion cracking of sensitized austenitic stainless-steel in dilute thiosulfate solution. *Corros. Sci.*, **33**, 39–71.
19 Wang, Y., Zhao, W., Ai, H., Zhou, X. and Zhang, T. (2011) Effects of strain on the corrosion behaviour of X80 steel. *Corros. Sci.*, **53**, 2761–2766.
20 Ren, R., Zhang, S., Pang, X. and Gao, K. (2012) A novel observation of the interaction between the macroelastic stress and electrochemical corrosion of low carbon steel in 3.5 wt% NaCl solution. *Electrochim. Acta.*, **85**, 283–294.
21 Feng, X., Zuo, Y., Tang, Y., Zhao, X. and Zhao, J. (2012) The influence of strain on the passive behavior of carbon steel in cement extract. *Corros. Sci.*, **65**, 542–548.
22 Wang, X., Tang, X., Wang, L., Wang, C. and Zhou, W. (2014) Synergistic effect of stray current and stress on corrosion of API X65 steel. *J. Nat. Gas Sci. Eng.*, **21**, 474–480.
23 Song, F. (2009) Predicting the mechanisms and crack growth rates of pipelines undergoing stress corrosion cracking at high pH. *Corros. Sci.*, **51**, 2657–2674.
24 Yaguchi, S. and Yonezawa, T. (2014) Intergranular stress corrosion cracking growth perpendicular to fatigue pre-cracks in T-L oriented compact tension specimens in simulated pressurized water reactor primary water. *Corros. Sci.*, **86**, 326–336.
25 Tang, X. and Cheng, Y. (2009) Micro-electrochemical characterization of the effect of applied stress on local anodic dissolution behavior of pipeline steel under near-neutral pH condition. *Electrochim. Acta*, **54**, 1499–1505.
26 Jivkov, A., Stevens, N. and Marrow, T. (2006) A three-dimensional computational model for intergranular cracking. *Comput. Mater. Sci.*, **38**, 442–453.
27 Kamaya, M. and Itakura, M. (2009) Simulation for intergranular stress corrosion cracking based on a three-dimensional polycrystalline model. *Eng. Fract. Mech.*, **76**, 386–401.
28 Gamboa, E. (2015) Inclined stress corrosion cracking in steel pipelines. *Corros. Eng. Sci. Tec.*, **50**, 191–195.
29 Lu, Z., Shoji, T., Meng, F., Qiu, Y., Dan, T. and Xue, H. (2011) Effects of water chemistry and loading conditions on stress corrosion cracking of cold-rolled 316NG stainless steel in high temperature water. *Corros. Sci.*, **53**, 247–262.

30 Terachi, T., Yamada, T., Miyamoto, T. and Arioka, K. (2012) SCC growth behaviors of austenitic stainless steels in simulated PWR primary water. *J. Nucl. Mater.*, **426**, 59–70.
31 Lavigne, O., Gamboa, E., Costin, W., Law, M., Luzin, V. and Linton, V. (2014) Microstructural and mechanical factors influencing high pH stress corrosion cracking susceptibility of low carbon line pipe steel. *Eng. Fail. Anal.*, **45**, 283–291.
32 Parkins R. (1994). Overview of intergranular SCC research activities: PR-232-9401. Tech. Rep., *Pipeline Research Council International, Inc*.
33 Lu, B., Song, F., Gao, M. and Elboujdaini, M. (2010) Crack growth model for pipelines exposed to concentrated carbonate-bicarbonate solution with high pH. *Corros. Sci.*, **52**, 4064–4072.
34 Bechtle, S., Fett, T., Rizzi, G., Habelitz, S. and Schneider, G. (2010) Mixed-mode stress intensity factors for kink cracks with finite kink length loaded in tension and bending: Application to dentin and enamel. *J. Mech. Behav. Biomed. Mater.*, **3**, 303–312.
35 Canadian Energy Pipeline Association (2007). Stress corrosion cracking recommended practices, 2nd Edition. Tech. Rep.
36 Wang, Y., Atkinson, J., Akid, R. and Parkins, R. (1996) Crack interaction, coalescence and mixed mode fracture mechanics. *Fatigue Fract. Eng. M.*, **19**, 427–439.

High-pH inclined stress corrosion cracking in Australian and Canadian gas pipeline X65 steels

O. Lavigne*[1], E. Gamboa[1], J. Griggs[1], V. Luzin[2], M. Law[2] and A. Roccisano[1]

High-pH stress corrosion cracking is a form of environmental degradation of gas pipeline steels. The crack path is intergranular by nature and typically perpendicular to the maximum applied (hoop) stress (i.e. perpendicular to the pipe outer surface). Some unusual instances of cracks have been observed in Canadian and Australian X65 pipes, where cracks grow away from the perpendicular for considerable distances. This paper presents a comparative study in terms of crack morphology, mechanical properties and crystallographic texture for these Australian and Canadian pipe steels. It is shown that the crack morphologies are quite similar, the main difference being the angle at which the cracks propagate into the material. This difference could be explained by the different through-wall texture and grain aspect ratio measured in the two materials. The interdependency of crack tip plasticity, crack tip electrochemistry and anisotropy in microstructural texture seems to heavily affect the resulting inclined crack path.

Keywords: Low-carbon steel, Stress corrosion cracking, Gas pipelines, Microstructure, Texture, EBSD

This paper is part of a Themed Issue on Advanced metallic alloys for the fossil fuel industries

Materials Science and Technology 2016.32:684-690.

Introduction

High-pH (pH > 9) stress corrosion cracking (SCC) is a form of environmental degradation observed in gas pipelines which requires three simultaneous conditions to occur: a tensile stress, a material that is susceptible to SCC and a cracking-inducing chemical environment.[1] High-pH SCC is characterised by an intergranular crack path and cracks theoretically propagate perpendicular to the maximum applied (hoop) stress.[1] However, several instances have been observed of high-pH SCC cracks growing at an angle away from the normal direction and propagating for considerable distances (several mm) in the pipe's hoop direction.[2–7]

A morphological survey carried out on 120 stress corrosion cracks located on various positions over a 59 m segment of an ex-service X65 Australian gas pipeline showed that 81% of the cracks had a tendency to grow away from the perpendicular.[7] A similar tendency for high-pH SCC cracks to grow at an inclined angle has also been reported for a Canadian pipe.[2,4]

The effect of the residual stress/strain and/or the effect of the texture have been examined to explain unusual intergranular stress corrosion crack paths observed in low-carbon steels and other materials such as stainless steels and nickel-based alloys.[2,7,8–15] This paper presents the characterisations of the Canadian pipeline samples used in previous studies[2,4] particularly in terms of texture and microstructure, subsequently comparing these results to those previously obtained for the Australian pipe samples.[3,5,7,14] These results are used to help evaluate whether anisotropy in these features (resulting mainly from pipe metallurgical and manufacturing processes) are responsible for the crack inclination path.

Materials and experimental methods

The Australian material used was a ferritic API 5L X65 low-carbon steel (0.085 wt-% C, 0.022 wt-% P, 1.58 wt-% Mn, 0.0045 wt-% S, 0.33 wt-% Si, 0.054 wt-% Nb, bal. Fe) extracted from the field after approximately 30 years of service and it contained SCC colonies. Nominal pipe diameter and wall thickness were, respectively, 864 and 8.3 mm. Pipe was manufactured through an UOE process. The original coating was coal tar enamel.

The Canadian pipe samples examined were also a grade X65 steel, extracted after 22 years of operation. Nominal pipe diameter and wall thickness were 1067 and 9.42 mm, respectively. The pipe was manufactured in accordance with the Canadian Standards Association standard Z245.2, with a double submerged arc welded longitudinal seam weld. Pipes were externally coated with a mastic primer, a hot-applied asphalt enamel coating and an asbestos and Kraft paper outer wrap.

The three-dimensional (3D) characterisation of the crack morphologies was made using X-ray micro-

[1]School of Mechanical Engineering, The University of Adelaide, Adelaide 5005, Australia
[2]Australian Nuclear Science and Technology Organisation, Lucas Heights, NSW 2234, Australia

*Corresponding author, email Olivier.lavigne@adelaide.edu.au, lavigneolivier@hotmail.com

Received 9 September 2015; accepted 8 December 2015
DOI 10.1080/02670836.2015.1132030

tomography. A detailed explanation of this method is given elsewhere.[5] For optical microstructure observation, the samples were photographed after standard sample preparation; coupons from pipe section were mounted in epoxy resin, ground down to 1200 grit paper and polished down to 1 μm diamond paste. The microstructure was revealed using 2% Nital etchant. The thickness-resolved texture was measured by neutron diffraction (ND) using the same experimental procedure as presented in Lavigne *et al.*[14] Electron-back scattering diffraction (EBSD) data were obtained using the parameters and the sample surface preparation as reported in Lavigne *et al.*[14]

Results and discussion

Cracks morphology

Figure 1 presents the 3D reconstructions of two different Canadian pipe volumes showing SCC scanned by X-ray micro-tomography. Figure 1*a* and *d* shows a top view of the outer surface of the pipes. Besides the cracks observed on the surface of the sample in Fig. 1*a*, some corrosion pits are also apparent. The volumetric segmentations of the cracks themselves are shown in blue (Fig. 1*b*, *c*, *e* and *f*). A different perspective of these cracks (as viewed from a different angle) are shown in Fig. 1*b*, *c* and *e*, *f*. Both cracks initially grew radially into the material (a straight crack section), subsequently showing crack branching and inclination (over several millimetres). While the two non-collinear cracks shown in Fig. 1*a* do not actually join on the surface of the pipe, some sub-surface interactions are visible (arrowed in Fig. 1*c*) as shown by a small tendril joining the two thumbnail-shaped cracks. The volumetric reconstructions for the cracks developed in the Australian samples are presented in Gamboa *et al.*[5] and Lavigne *et al.*[14] and display similar characteristics to the Canadian samples. The widths of the Australian inclined cracks are nevertheless smaller, showing less corrosion of the crack walls than in the Canadian samples. The larger width of the Canadian cracks could be due to that pipe being hydro-tested during service, whereas the Australian pipeline was not hydro-tested during service.

Figure 2 presents a comparison between the optical microstructure of both Canadian and Australian pipes. The observed microstructures are typical ferritic-pearlitic consistent with a rolling manufacturing process.[16] No decarburisation layer was observed in either sample. Both pipe outer diameter surfaces had similar roughness with a number of pits (it can be noted that Fig. 2*b*) do not show the rough surface due to other previous examination processes). Typical intergranular SCC cracks can be observed for both samples. Further qualitative optical observations did not show significant amount of voids, precipitates or inclusions in the microstructure.[4,17]

The main similarities or differences arising from these characterisations and from Xie *et al.*[2], Sutherby and Chen,[4] Zadow *et al.*[7] and Zadow[17] between the Canadian and Australian cracks morphology are:

- All cracks were in the longitudinal direction on the surface, with smaller cracks approaching each other and coalescing.
- All cracks were intergranular in nature, showing little to no branching.
- All cracks tended to grow initially perpendicularly into the pipe wall.
- The cracks started to incline and grow away from the normal after they reached a certain depth. For the Canadian case, this was within the first 200–800 μm from the surface, vs. 200–900 μm for the Australian case.

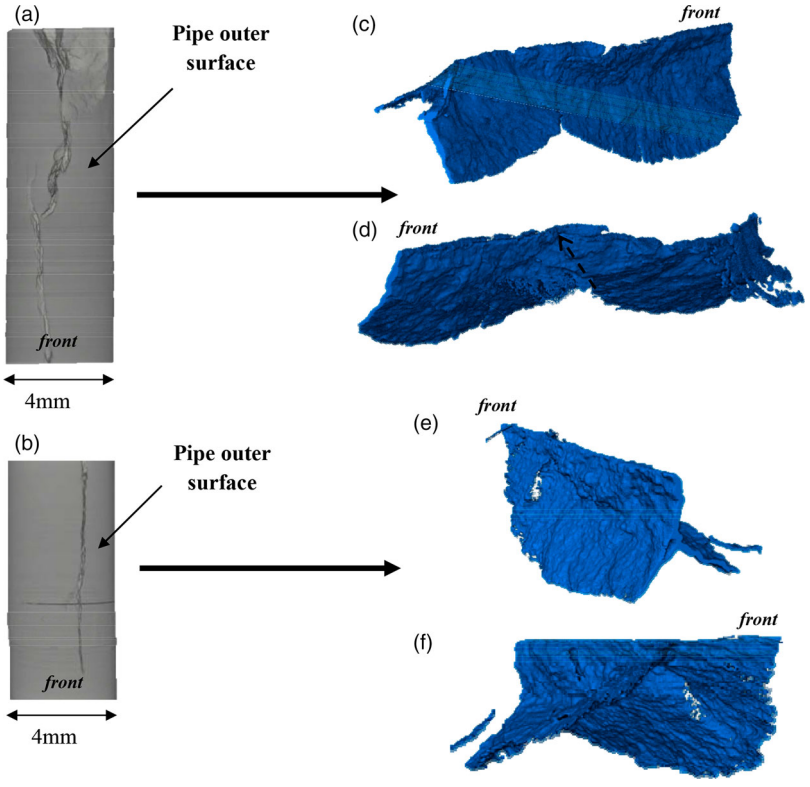

1 3D observations of typical stress corrosion cracks showing non-straight through-wall propagation for the Canadian samples

Materials Science and Technology 2016.32:684-690.

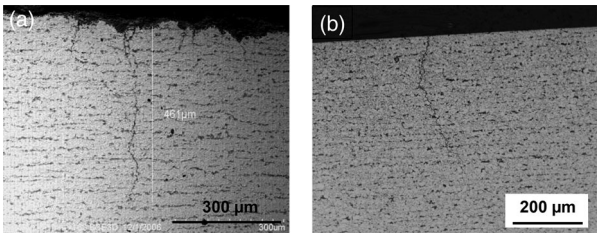

2 Transverse pipe section for *a* Canadian (from Xie *et al.*[2]) and *b* Australian, optical etched microstructures (2% Nital)

- There was no visible change in the optical microstructure in either sample associated with this change in propagation angle.
- Inclination angles in the Canadian case were between 30° and 50°, with a typical angle of 45°. Inclination angles in the Australian case were initially between 21° and 52°, but changed with increasing depth.
- Canadian cracks grew at a constant angle (see Fig. 3*a*), whereas Australian cracks increased in angle as they grew in depth. This means that as the crack grew deeper from the surface, the further the crack tip travelled in the hoop direction. This is illustrated in Fig. 3*b*, in particular for the two cracks highlighted by an arrow.
- Out of 18 (in one colony) and 56 (in another colony) Canadian cracks, the number of inclined SCC cracks were 67 and 52%, respectively. For the Australian cracks, 81% of 120 significant cracks (from 3 different colonies) were inclined. These high percentages show a high propensity of cracks to incline at different pipe segment locations.
- Thirty-two per cent of the Australian closely spaced cracks showed some form of sub-surface interaction. No number was quoted for the Canadian cases. No violation of the Canadian Energy Pipeline Association SCC cracks interaction guidelines[18] was observed at any instance.

This comparison shows that both sets of samples display some similarities in terms of tendency of SCC cracks to incline after a short straight section, but there are differences in crack path after the straight section (in particular changing angle with increasing depth for the Australian case).

Mechanical properties

The yield strength and the tensile strength of the Canadian SCC-affected steel were estimated by automated ball indentation to approximately 550 and 820 MPa, respectively,[2] although these values are likely high due to the conservative nature of the indentation test. The yield strength and the tensile strength of the Australian SCC-affected pipe were measured by the use of transverse gull-winged tensile specimens and by longitudinal tensile tests to approximately 542 and 618 MPa, respectively.[19] All values are consistent with API 5L X65 grade steel.

Figure 4 also shows small differences in the microhardness values (HV0.1) between the two samples. These values are typical of Vickers hardness values reported for X65 steel.[20] Several other mechanical property measurements (including further microhardness and strength measurements) were made on both Canadian[4] and Australian samples[7,17] that did not show clear differences between the two pipe steels. No significant correlation between the inclination of the cracks and the mechanical properties of the steels could be drawn.

Microstructural texture

The orientation distribution functions (ODFs) were plotted from the three pole figures obtained by ND measurements at different depths from the outer surface of the pipe (Fig. 5). ODFs quantitatively describe the texture of a crystalline phase. In body-centred cubic steels, ODFs at the $\phi_2 = 45°$ section display the major texture components.[21,22] The ideal locations of the main texture components on this ODF section are schematically shown in Fig. 5*a*. Fig. 5*b–e* are the ODFs obtained for the Australian sample. Fig. 5*f–i* and *j–m* are the ODFs obtained for two different Canadian samples coming from the same pipe section containing inclined cracks. Each column is a measurement taken at the same distance away from the pipe outer surface: at the free surface, at 0.8 mm depth, at 1.2 mm depth and at the centre line of the pipe wall, respectively.

Figure 5*b* shows that the outer surface of the Australian pipe sample does not show a strong texture, although a certain intensity of Goss orientation ({110}<100>) is measured. As the depth increases from 0.8 mm towards the centre line (Fig. 5*c–e*), a typical texture of a rolled sheet is found (i.e. along the <110>//RD (α-fibre) and

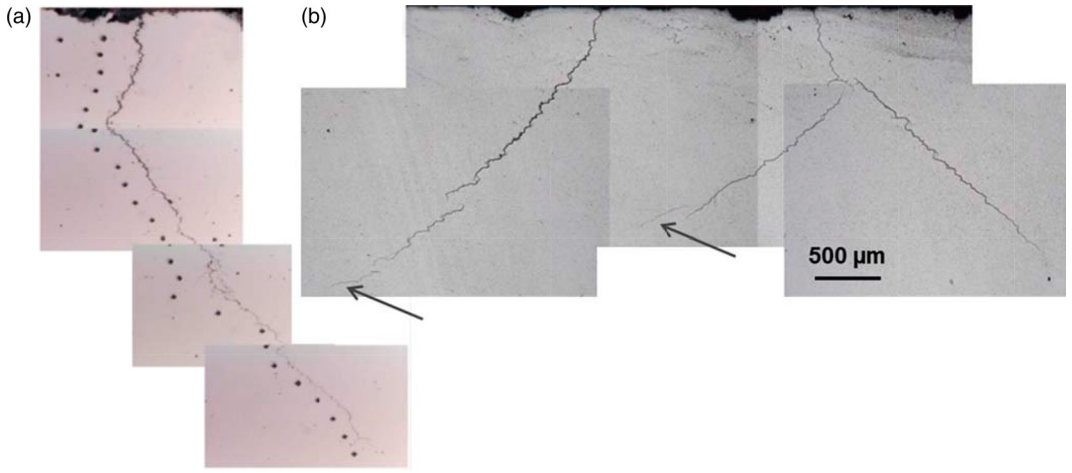

3 *a* Inclined Canadian SCC crack (no scale provided[2]) and *b* inclined Australian SCC cracks[5]

Materials Science and Technology 2016.32:684-690.

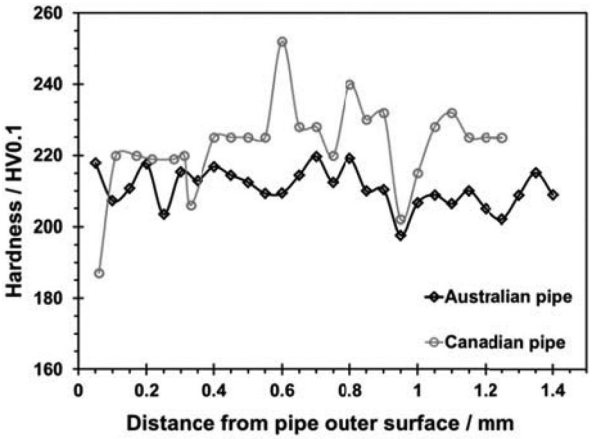

4 Vickers microhardness (HV0.1) traverse of Canadian (adapted from Xie *et al.*[2]) and Australian pipes (from Zadow[17])

<111>//ND (γ-fibre) orientations, with maxima measured here at the {100}<110>, {112}<110>, {111}<110> and {111}<112> orientations). A density of shear texture (along the <110>//TD (ε-fibre) with maxima at {110}<100> and {100}<110> orientations) is also measured at 0.8 mm from the outer surface. Some intensity of this orientation is still observed at 1.2 mm from the outer surface, but the main intensities of the shear texture are shifted towards the {111}<112> and to the {100}<110> orientations.

The two Canadian pipe samples, at the outer surface (Fig. 5*f* and *j*), show a similar texture than the Australian pipe sample (Fig. 5*b*), with different intensities. The typical texture of a rolled sheet is found at the centre line of these pipe samples (Fig. 5*i* and *m*) while the texture is weaker in comparison to the Australian pipe sample (Fig. 5*e*). It is interesting to note that even though the density of specific orientations is also lower at 0.8 and 1.2 mm from the outer surface of the Canadian pipe, these specimens also show some intensity of shear texture along the ε-fibre (<110>//TD) with maxima at {110}<100> and {112}<111> orientations.

Figure 6 shows an EBSD scan on a region located at 0.75 mm from the outer surface of the Australian X65 sample. The inverse pole figure showing the crystallographic orientation of the grains and the corresponding ODF of this region is shown in Fig. 6*a* and *b*, respectively. Figure 6*c* shows the Kernel average misorientation (KAM) map of this area. The KAM is an estimation of the residual strain distribution in the microstructure.[14] It can be seen that the crystallographic orientations along the ε-fibre (with maxima at {110}<100> and {112}<111> orientations (Fig. 6*b*) are related to a relatively high degree of plastic deformation, spread into the steel microstructure, along the transverse direction (Fig. 6*c*). SCC cracks preferentially propagating along the higher strained areas, the shear strain related to the shear texture would thus promote the cracks to propagate along the transverse direction.[14] This would help to explain the deflected crack path observed for the pipe samples.

As a side remark, it can also be noted that some variations of texture density are observed in the same pipe, especially at the outer surface (Fig. 5*f* and *j*). This difference in texture is expected to affect the localised SCC susceptibility of the pipe[19] although many other factors influence the crack initiation in buried pipelines.

The Australian pipe shows a different density of shear texture at different locations than the Canadian pipe which could help explaining the difference in crack paths morphology (steadily curving instead of fixed incline angle).

Crack paths modelling

Through a numerical model under development by the authors,[23] the grain aspect ratio (AR, defined as height of the grain divided by the width) was identified as another possible parameter influencing the crack paths. The model operates under the assumption that the strain in the crack tip plastic zone enhances the current density for dissolution and reduces film stability.[23–25] The critical plasticity at which the enhanced dissolution offsets, the higher stress intensity factor in the radial direction was determined from metallographic studies.[7] It also incorporates the geometry of the grain boundaries and how they influence the growth direction for the intergranular growth. Figure 7 shows the result of a simulation of five cracks running through two idealised microstructures: one having flattened grains of AR 0.5 (blue) and one having equiaxial grains with an AR of 1 (red). The growth of the cracks can be divided into three sections. The straight sections close to the outer surface of the pipes observed on the different samples and modelled in Fig. 7 occur via normal film fracture rate dependant SCC, with fracture occurring at the highest stresses.[26] After a certain depth, the crack tip strain increases such that the interplay between crack tip electrochemistry and plasticity[23–25] allows the crack preferential growth along an inclined angle. The growth mechanism switches back and forth between stress dominated and strain dominated growth until a depth where the growth angle stabilises and strain is the dominant factor. Assuming all other aspects such as stresses and electrochemical behaviour are equal, Fig. 7 shows that the change in AR can have an effect on the SCC crack path, especially the final angle at the crack tip. For cracks with lower ARs (i.e. flattened, typical of rolling processes), the crack tip will take longer to reach a more shallow angle (i.e. further away from the perpendicular). These cracks would hence have the appearance of a 'smooth' curve rather than a sharp turning point near the pipe surface.

ARs for the Canadian and Australian steel samples were thus measured through EBSD (Fig. 8). The grains in the Australian steel show a slightly lower AR than the grains in the Canadian steel with values of AR of, respectively, ~0.5–~0.52 and ~0.52–~0.55 depending of the depth. A peak at AR = 0.6 is observed for both steels due to the rolled nature of the pipe steel. The difference measured in AR between the two samples could thus play a role in the different crack paths observed; the cracks appear to incline more abruptly in the Canadian samples, whereas in the Australian steels the cracks tend to incline more gradually and reach a steeper angle (see Fig. 3*b*).

Preliminary validation of the model was conducted by simulating 10 cracks growing through a microstructure of AR = 0.51 (such as the Australian case), and by superimposing the modelled paths on a micrograph of a SCC crack from an ex-service pipe (Fig. 9). The general shapes

Materials Science and Technology 2016.32:684-690.

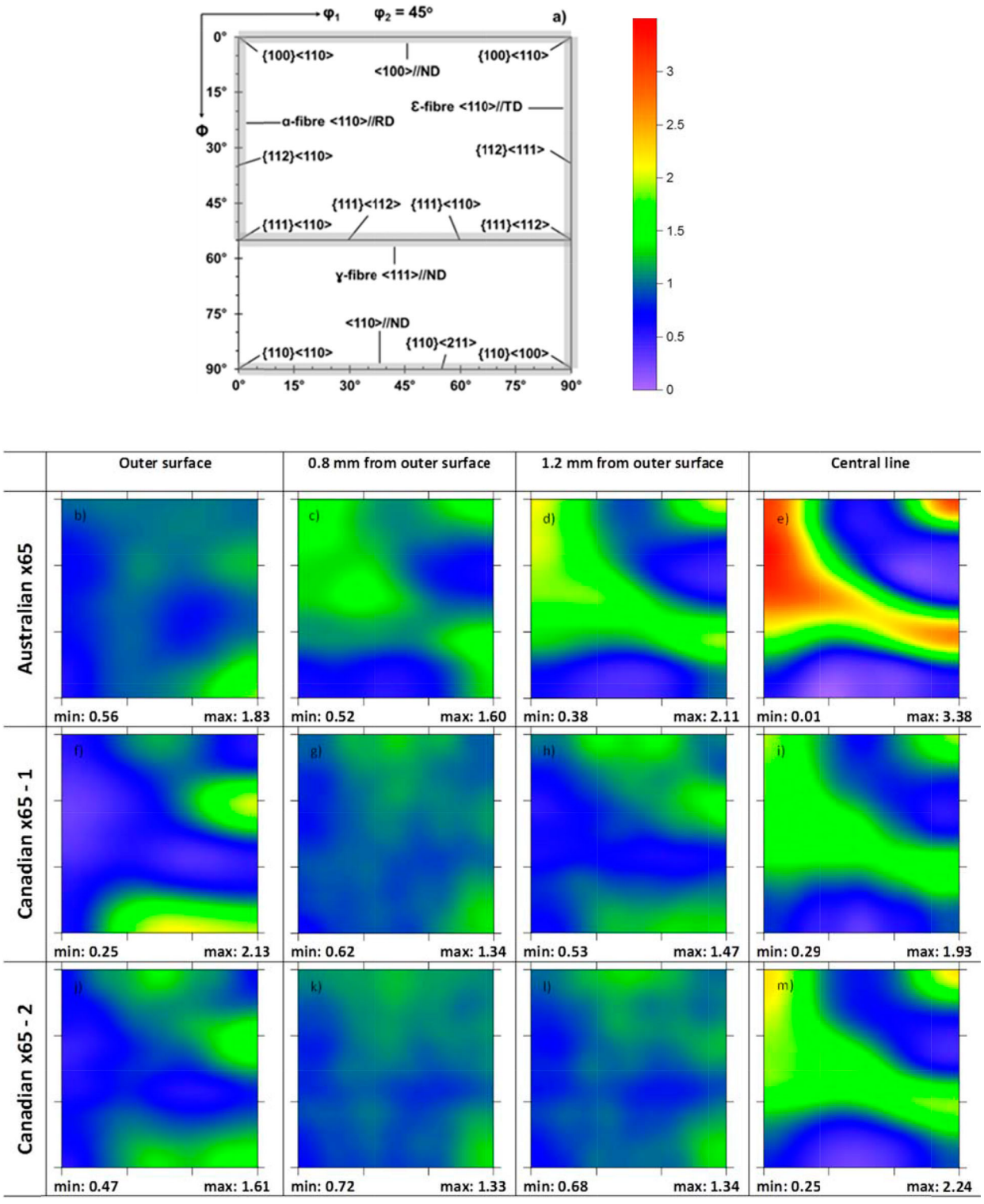

5 ODF results of Australian and Canadian samples at varying depths. The thickness of the analysed sample at each depth is 0.5 mm

of the modelled paths agree well with the observed ex-service crack for the full observed depth of the crack. This model suggests that the cracks' inclined growth is consistent with crack tip strain enhanced dissolution. The local variations between the modelled and observed crack paths in Fig. 9 could be thus explained by the residual localised plasticity/strain, random microstructural variance and microstructural features/defects resulting from manufacture.

Conclusions

The characterisations of two X65 steels experiencing the same form of unusual high-pH SCC paths in two different countries have been conducted. It is shown that the crack morphologies are quite similar with the main difference being the angle at which the cracks propagate after their similar straight sections. In the Canadian steel, the cracks tend to incline relatively sharply and maintain an

Materials Science and Technology 2016.32:684-690.

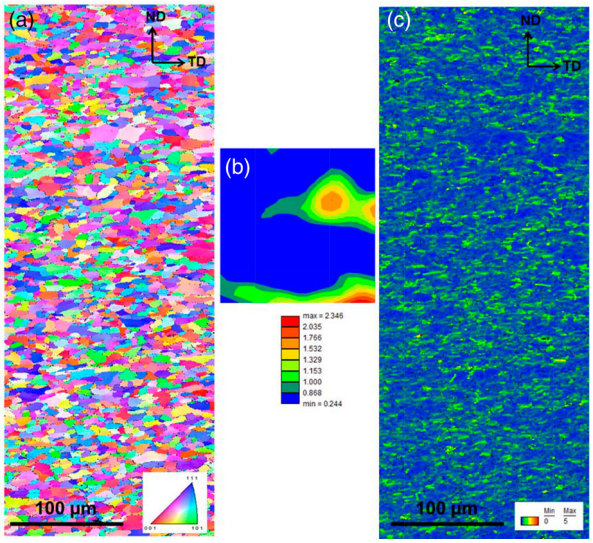

6 EBSD results (step size 0.5 μm). *a* Inverse pole figure, *b* ODF at $\phi_2 = 5^{\circ}$ and *c* KAM map

inclination angle, whereas in the Australian steels the cracks tend to curve gently, increasing the inclination angle as they get deeper. This feature could be explained by the different through-wall texture and different grain AR measured in the two materials. Overall, within the first 0.5 mm or so of the pipe thickness (for pipe walls of approximately 8–9 mm thickness), stress intensity factors are the main driving force causing the cracks to grow perpendicular to the free surface and into the material. Beyond this depth, the interdependency of crack tip plasticity, crack tip electrochemistry and anisotropy in microstructural texture seems to dictate the SCC crack path and related crack growth rates.

It has been shown that the mechanical properties (such as strength and microhardness) do not vary greatly between samples and should not be used to predict SCC susceptibility or SCC crack path.

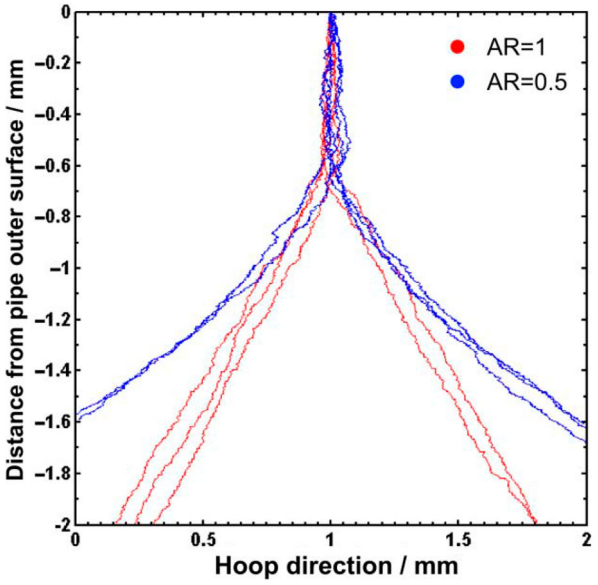

7 Simulation of SCC crack path through steels of two largely different AR ratios (blue = 0.5 and red = 1)

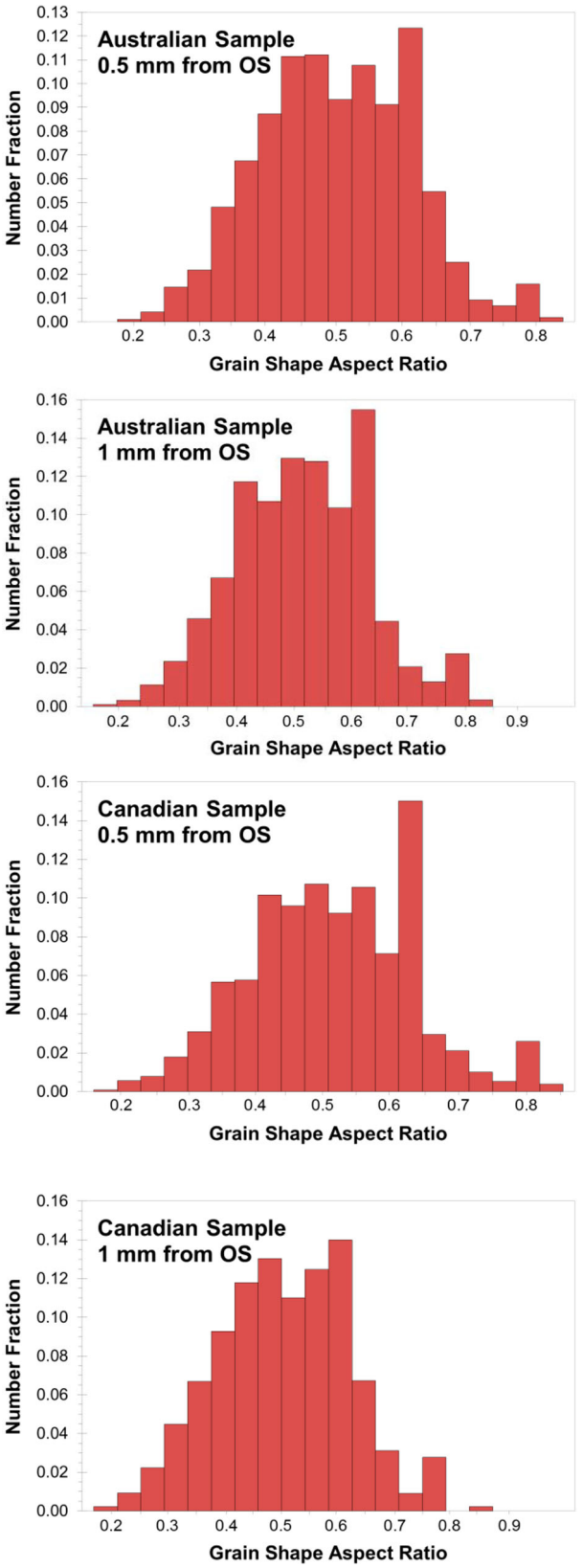

8 Fraction of grain shape AR for the Australian and Canadian steel pipes at different depths from the outer surface (OS)

Further work is being carried out in a model to incorporate the effects of strain (residual or induced) and crack tip electrochemical behaviour as well as crack interactions. This model will be used to help further understand crack paths, crack interaction regions and crack

Materials Science and Technology 2016.32:684-690.

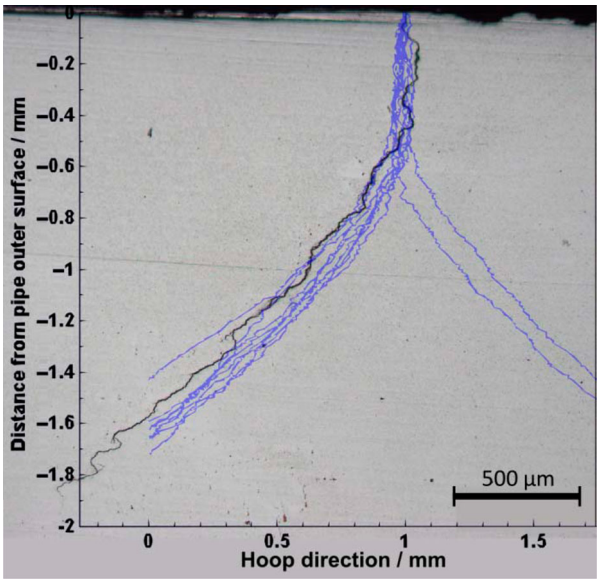

9 Simulated SCC cracks (blue) superimposed on a micrograph of an Australian ex-service crack

growth rates. The aim of this model is to provide pipe operators with more quantifiable, validated tools to manage and assess SCC and to provide pipe manufacturers with knowledge on SCC resistance of produced pipe steels. Initial validation work has shown this model to be representative of field observations.

Acknowledgements

This work was funded by the Energy Pipelines CRC, supported through the Australian Government's Cooperative Research Centres Program. The funding and in-kind support from the APGA RSC is gratefully acknowledged. The authors acknowledge the facilities, and the scientific and technical assistance, of the Australian Microscopy & Microanalysis Research Facility at the University of Adelaide. The authors also wish to thank Shahani Kariyawasam and Robert Sutherby at TransCanada for providing samples and advices.

References

1. V. S. Raja and T. Shoji: '*Stress corrosion cracking*', 2011, Cambridge, Woodhead Publishing Ltd.
2. J. Xie, L. Yang, M. Sen, R. Worthington and F. King: 'Mechanistic investigation of deflected stress corrosion cracking in pipeline steels', Annual NACE International Conference, Atlanta, GA, USA, March 2009, Paper 09121.
3. E. Gamboa and L. Zadow: 'Tomography of inclined SCC cracks in Australian gas pipelines', 9th International Pipeline Conference (IPC 2012), Calgary, Canada, September 2012.
4. R. Sutherby and W. Chen: 'Deflected stress corrosion cracks in the pipeline steel', 6th International Pipeline Conference (IPC 2004), Calgary, Canada, October 2004.
5. E. Gamboa, M. Giuliani and O. Lavigne: 'X-ray micro-tomography observation of subsurface stress corrosion crack interactions in a pipeline low carbon steel', *Scripta Mater.*, 2014, **81**, 1–3.
6. J. Wang and A. Atrens: 'Analysis of service stress corrosion cracking in a natural gas transmission pipeline, active or dormant?', *Eng. Fail. Anal.*, 2004, **11**, 3–18.
7. L. Zadow, E. Gamboa and O. Lavigne: 'Inclined stress corrosion cracks in gas pipeline steels: morphology and implications', *Mater. Corros.*, 2015, **66**, 1092–1100.
8. Z. Lu, T. Shoji, F. Meng, Y. Qiu, T. Dan and H. Xue: 'Effects of water chemistry and loading conditions on stress corrosion cracking of cold-rolled 316NG stainless steel in high temperature water', *Corros. Sci.*, 2011, **53**, 247–262.
9. Z. Lu, T. Shoji, F. Meng, H. Xue, Y. Qiu, Y. Takeda and K. Negishi: 'Characterization of microstructure and local deformation in 316NG weld heat-affected zone and stress corrosion cracking in high temperature water', *Corros. Sci.*, 2011, **53**, 1916–1932.
10. T. Terachi, T. Yamada, T. Miyamoto and K. Arioka: 'SCC growth behaviors of austenitic stainless steels in simulated PWR primary water', *J. Nucl. Mater.*, 2012, **426**, 59–70.
11. S. Yaguchi and T. Yonezawa: 'Intergranular stress corrosion cracking growth perpendicular to fatigue pre-cracks in T–L oriented compact tension specimens in simulated pressurized water reactor primary water', *Corros. Sci.*, 2014, **86**, 326–336.
12. M. A. Arafin and J. A. Szpunar: 'A new understanding of intergranular stress corrosion cracking resistance of pipeline steel through grain boundary character and crystallographic texture studies', *Corros. Sci.*, 2009, **51**, 119–128.
13. P. Scott, M. Foucault, B. Brugier, J. Hickling and A. McIlree: 'Examination of stress corrosion cracks in Alloy 182 weld metal after exposure to PWR primary water', 12th Int. Conf. on 'Environmental Degradation of Materials in Nuclear Power System', Warrendale, PA, USA, 2005.
14. O. Lavigne, E. Gamboa, V. Luzin, M. Law, M. Giuliani and W. Costin: 'The effect of the crystallographic texture on intergranular stress corrosion crack paths', *Mater. Sci. Eng. A*, 2014, **618**, 305–309.
15. J. Griggs, E. Gamboa and O. Lavigne: 'A review of modelling high pH stress corrosion cracking of high pressure gas pipelines', *Mater. Corros.*, 2015, http://dx.doi.org/10.1002/maco.201508454.
16. K. O. Findley, M. K. O'Brien and H. Nako: 'Critical assessment: mechanisms of hydrogen induced cracking in pipeline steels', *Mater. Sci. Technol.*, 2015. http://dx.doi.org/10.1179/1743284715Y.0000000131.
17. L. Zadow: 'Characterisation of the morphology of inclined SCC cracks in Australian gas pipelines', MA thesis, University of Adelaide, Adelaide, Australia, 2013.
18. Canadian Energy Pipeline Association (CEPA). '*Stress Corrosion Cracking: Recommended Practices*', 2nd edn, Canadian Energy Pipeline Association, Alberta, 2007.
19. O. Lavigne, E. Gamboa, W. Costin, M. Law, V. Luzin and V. Linton: 'Microstructural and mechanical factors influencing high pH stress corrosion cracking susceptibility of low carbon line pipe steel', *Eng. Fail. Anal.*, 2014, **45**, 283–291.
20. R. Chu, W. Chen, S. H. Wang, F. King, T. R. Jack and R. R. Fessler: 'Microstructure dependence of stress corrosion cracking initiation in X-65 pipeline steel exposed to a near-neutral pH soil environment', *Corrosion*, 2004, **60**, 275–283.
21. M. S. Joo, D.-W. Suh, J.-H. Bae and H. K. D. H. Bhadeshia: 'Toughness anisotropy in X70 and X80 linepipe steels', *Mater. Sci. Technol.*, 2014, **30**, 439–446.
22. E. El-Danaf, M. Baig, A. Almajid, W. Alshalfan, M. Al-Mojil and S. Al-Shahrani: 'Mechanical, microstructure and texture characterization of API X65 steel', *Mater. Des.*, 2013, **47**, 529–538.
23. J. Griggs, E. Gamboa and O. Lavigne: 'Modelling inclined high pH stress corrosion crack paths in 2D', *J. Nat. Gas Sci. Eng.*
24. X. Wang, X. Tang, L. Wang, C. Wang and W. Zhou: 'Synergistic effect of stray current and stress on corrosion of API X65 steel', *J. Nat. Gas Sci. Eng.*, 2014, **21**, 474–480.
25. T. Fett, G. Rizzi, H. A. Bahr, U. Bahr, V. B. Pham and H. Balke: 'A general weight function approach to compute mode-II stress intensity factors and crack paths for slightly curved or kinked cracks in finite bodies', *Eng. Fract. Mech.*, 2008, **75**, 2246–2259.
26. R. N. Parkins: Tech. Rep., Pipeline Research Council International, Inc., PR-232-9401, 1994.

Materials Science and Technology 2016.32:684-690.

Influence of strain on current densities and stress corrosion cracking growth rates in X65 pipeline steel

*James Griggs, Olivier Lavigne, and Erwin Gamboa.**

School of Mechanical Engineering, The University of Adelaide, Adelaide 5005, Australia

ARTICLE INFO

Article history:

Received 5 July 2016
Accepted 11 October 2016
Available Day Month Year

Keywords:

A. Stress Corrosion Cracking
B. Pipelines
C. Stress strain effects

*Corresponding author: +61 8 8313 5473; Email: erwin.gamboa@adelaide.edu.au

ABSTRACT

High pH stress corrosion cracking (SCC) in gas pipelines has been seen to grow along an incline angle rather than perpendicular to the outer surface. Crack tip strain enhanced electrochemistry has been previously postulated as a reason for the inclination, and recent computer simulations that take this effect into account produce realistic crack paths. This study attempts to determine the effect of strain on the electrochemical response of X65 steel, and the impact that the strain has on growth rates for inclined SCC. Potentiodynamic tests were conducted on X65 tensile specimens with residual plastic strain or in-situ elastic strain. An increase of the current density up to 300% was observed within the SCC potential range. Computer simulations were also conducted to show the qualitative effect of this increase in current density on the growth rate, and results indicated that inclined SCC could grow faster than straight SCC if the current density along the inclined angle is 20% higher than along the perpendicular. Further experimental work is suggested that can quantify this current densities difference in the strained area around the crack tip.

INTRODUCTION

High pH stress corrosion cracking (SCC) is a type of environmentally assisted cracking that is seen in high pressure gas pipelines. SCC requires a combination of a corrosive environment, a susceptible material, and sufficient stresses [1]. The mechanism generally involves crack tip anodic dissolution extending the crack tip, with passive film formation preventing further dissolution. The film rupture exposes bare metal to the solution again, and this previously has occurred in the direction of the highest stress intensity factor and is the rate limiting factor of growth [1, 2]. This highest stress intensity factor usually occurs in the radial direction of the pipe, as the hoop stresses are predominant; however since 2004, SCC that grows at an angle from the perpendicular has been observed in Australia and Canada in X65 steels [3, 4, 5, 6, 7]. This inclined SCC tends to grow straight for a depth of approximately 0.55 mm along its centreline before slowly turning to a stable angle of around 50 degrees from the radial direction. Various causes have been postulated for this change in direction, but it most likely seems to be related to the crack tip strain, which is highest along certain angles [8]. The inclined cracks have been observed to propagate along these angles [3, 4, 5, 6, 7].

Strain has been shown to have an effect on the electrochemical behaviour of steels [9, 10] and has been postulated as an influencing factor in inclined SCC growth in X65 pipeline steels [11, 12]. There exists the possibility that the current density could be higher at the high strain angles around the crack tip that inclined cracks appear to follow, and hence the growth rate could also be higher. Industry inspection intervals for pipelines containing inclined SCC could be altered if the growth rates for inclined SCC are significantly different than for straight SCC, as the estimates are mainly based on a straight crack assumption.

In order to determine the degree to which strain can influence current density, and hence SCC growth, the electrochemical response of X65 under different strain levels is needed. This is determined in this study through potentiodynamic tests of X65 tensile dogbone samples under the effects of both in-situ strain and residual plastic strain. The response in the SCC range is then used as a basis for a crack growth rate model developed in MATLAB to compare the crack growth rates of inclined and straight isolated SCC cracks.

Material and experimental details

Material

The material used was a ferritic X65 low carbon steel (0.085 wt.%C, 0.022 wt.%P, 1.58 wt.%Mn, 0.0045 wt.%S, 0.33 wt.%Si, 0.054 wt.%Nb, bal. Fe). Samples came from the pipe sections used in a prior work [7], extracted from the field after approximately 30 years of service. Pipe diameter and wall thickness were 864 mm and 8.3 mm respectively. Pipes were manufactured through the UOE production process. The original coating was coal tar enamel.

Tensile test specimen preparation and mechanical testing

Flat dogbone tensile specimens were cut from the centreline of the pipe sections, in the longitudinal direction. Gauges were 5 cm length, 0.26 cm width and 0.28 cm thickness. The mechanical properties of the steel specimens (yield and ultimate tensile strengths) were determined by a typical tensile test using an Instron machine at 5 mm/min. Vickers hardness was determined at a load of 0.5 kgf, three indents were made per sample and results were averaged.

Evaluation of the applied strain on the X65 electrochemical behaviour

Tensile specimens were exposed to the simulated high pH SCC medium defined in the literature: 1N carbonate + 1N bicarbonate solution at 70 °C [1]. The exposed surface of the specimens was limited to one face of each specimen gauge by covering the other faces with a layer of silicon rubber on the top of a layer of epoxy resin. The exposed surface was thereby 0.91 cm^2 in area (3.5 cm length on 0.26 cm width). Surfaces were machine ground finished. A LIST machine [7] was used to apply different amount of loads (% of the measured YS) on the specimens. At

each applied load, potentiodynamic curves with a scan rate of 0.1 mV/s were recorded from -1 $V_{Ag/AgCl}$ to 0.9 $V_{Ag/AgCl}$. Before each potentiodynamic test, a cathodic potential of -1 $V_{Ag/AgCl}$ was applied for 5 min to the specimens in order to remove the oxide layer formed on their surface either in air or during the previous experiments. At least three potentiodynamic curves per applied load were recorded to check the reproducibility of the results (an example is shown in Fig.1). The electrochemical tests were conducted with a Gamry interface 1000^{TM}, using the specimens as the working electrode, a platinum mesh as the counter electrode and a saturated silver/silver chloride electrode as the reference. The reference electrode was maintained at room temperature and connected to the electrochemical cell with a Luggin probe.

Evaluation of the residual strain on the X65 electrochemical behaviour

A series of 6 samples strained at different levels (0, 2.2, 3.46, 5.4, 8.11, and 11.6% strain) was produced from 6 different tensile specimens. The specimens were strained at a strain rate of 5 mm/min until a desired level, then released (Fig.2). The strain level for each sample was measured by measuring the gauge length variation of each specimen after the test. The strained dogbone gauges of the specimens were then cut, embedded in epoxy resin (Struers Epofix) and ground down to 220 grit. The area of the exposed surface was approximately 0.6 cm^2. Samples were then immersed in the high pH SCC media at 70 °C and potentiodynamic tests as described in the previous section were conducted.

Results

Mechanical tests

Figure 2 shows the typical stress-strain curve obtained for the X65 steel tested. The yield and ultimate tensile strengths were measured as 460 MPa and 590 MPa respectively. These values were consistent with X65 API 5L grade steel [13].

The hardness values of the X65 together with those of the X65 samples strained at 2.2, 3.46, 5.4, 8.11, 11.6 and 14.8% are presented in Figure 2. It can be seen that the microhardness of the X65 steel increases linearly with the amount of residual strain.

Effect of the applied strain on the X65 electrochemical behaviour

The polarisation curves recorded at different level of strain for the X65 steel are shown in Figure 4. It can be seen that the anodic current densities significantly increase with the increase of the elastic strain (for stress from 0 to 100% of YS) and the plastic strain (for a stress of 110% of YS). The corrosion potential, E_{corr}, tends to decrease with the increase of the applied strain.

According to the mechano-chemical theory developed by Gutman [14] the electrochemical corrosion potential of the steel is affected by the external load. An external tensile load is expected to decrease the potential of the steel and enhance its corrosion activity [15]. Figure 4 shows a slight negative shift of 15 mV of the corrosion potential for the samples strained in the elastic range, and 30 mV for the sample strained in the plastic range. In addition, according to the mechano-chemical theory, the anodic dissolution rate of the steel is expected to be accelerated by the external stress/strain [16] as observed in Figure 4.

Effect of the residual strains on X65 steel on the electrochemical behaviour

The polarisation curves recorded for samples strained at different level are presented in Figure 5. In this case no external load is therefore applied, and a very limited variation of the corrosion potential is observed (a negative shift within 11 mV compared to the 0% strained sample). The residual strains do not significantly increase the current densities in the SCC region (within the active peak from -0.65 to -0.50 $V_{Ag/AgCl}$) suggesting that approximately the same amount of charge (supplied by the iron dissolution) is needed for the passive film to form. The SCC region is approximately defined by the potential range between the top and the bottom of the anodic peak in the anodic direction [1, 17]. In the passive region however, an increase in the current densities for the strained samples is observed, suggesting that a higher amount of iron dissolution is needed to maintain the formation of the passive film. The lattice of the samples being distorted by the plastic strain, the dissolution of the steel may be stimulated [18]. The stability of the passive film is thus decreased with the presence of residual strains. Nevertheless, no trend can be drawn between the increase of the residual strains and the increase of the current densities, and any level of residual strain seems to increase the dissolution of the X65 in the passive range in the simulated high pH SCC media.

Crack growth rate modelling

The experimental results of how current density varies with strain provide reason to believe that SCC growing along highly strained areas at the crack tip may have a higher current density and potentially a higher growth rate than straight SCC. While it is difficult to relate macroscopic strain to local strain at the crack tip, clearly there should be some influence of the local strain on the current density [19]. The theoretical stress singularity at the crack tip also makes it unreliable to quantitatively pair a current density increase from macroscopic strain to the current density increase seen along a locally strained grain boundary at the crack tip. Furthermore the exact potential at the crack tip is not known which makes an equivalency between the polarisation curve and crack tip undependable. Nevertheless, the ranges for which the current density changes are known (up to 300% in the SCC region at the potential of 0.5 $V_{Ag/AgCl}$) and thus the growth rate for an inclined crack can be estimated for different ranges of current density. This could then serve as a basis for crack tip current density mapping in the future.

The growth rate of a high pH SCC crack is governed by the dual process of dissolution and passive film formation. The interdependency has been characterised in Equation 1, which has been validated against industry growth rate data [2, 20], and based on the work of Ford and Andresen [21, 22]. A_0 and B are defined in Equations 2 and 3. The parameters used in these equations are summarised in Table 1.

$$\dot{a} = (A_0 B^n i_a^*)^{\frac{1}{1-n}} \left[\ln\left(\frac{K_M^2 - K_{ISCC}^2}{3\pi r_0 \sigma_Y^2} \right) \right]^{\frac{n}{1-nN-1}\frac{N+1}{}} \quad (1)$$

$$A_0 = \frac{1}{1-n} \frac{M}{zF\rho} \left(\frac{t_0}{\epsilon_F} \right)^n \quad (2)$$

$$B = \frac{2N}{N-1} \frac{\beta \sigma_Y}{E r_0} \quad (3)$$

Equation 1 mostly consists of material constants that would not vary for an inclined crack as opposed to a straight crack. For the purposes of the model it is assumed that only the current density and stress intensity factor vary, and the other parameters remain constant. This equation was then used to determine crack velocities for three key current densities found in the potentiodynamic tests. The results of this are shown in Figure 6.

Figure 6 illustrates the effect of current density and stress intensity factor on the crack growth rate. 20 MPa.m$^{1/2}$ is the minimum value for the stress intensity factor shown as the stress intensity factor for a straight crack at the inclination point under loading conditions seen in inclined SCC affected pipes is approximately 20 MPa.m$^{1/2}$ (crack inclines at approximately 0.55 mm depth [12, 6]). The equation is valid for stress intensity factors as low as the critical stress intensity factor as well, though no difference would be seen between straight and inclined cracks. This is as a lower stress intensity factors would be seen before inclination where a straight and inclined crack path is identical. The three current densities chosen represent the peak current density, 57.6 A/m^2, as well as the greatest percentage difference between strained and unstrained at one potential, 21 A/m^2 and 5.3 A/m^2 respectively at a potential of -0.5 $V_{Ag/AgCl}$. Equation 1 shows that the crack growth rate is proportional to the current density cubed (for n=0.667), and thus the differences between growth rate for the different potentials in the SCC range are significant. The maximum current density was chosen for the growth rate comparison between straight and inclined cracks as this would provide the most conservative estimates of time to failure.

The main point of interest of the simulation is to determine how large a difference in current density would be required to have an inclined crack exceed the crack growth rate of a straight crack. To accomplish this, straight and inclined SCC growth was simulated in MATLAB with Equation 1 as the governing equation. A time step of one hour was used in both cases, and radial growth was the output. This resulted in the growth rate for the inclined cracks being multiplied by cos θ where θ is the instantaneous growth angle measured from the radial direction (i.e. for a straight crack, θ = 0), such that only the radial portion of the inclined growth was considered.

The inclined cracks are assumed to follow the path found in previous studies [12, 6, 23] where the inclination begins at 0.55 mm depth and slowly curves to a stable angle of approximately 50° by 0.8 mm depth. During this curving section, the growth transitions between straight and inclined grain boundaries, which means that the growth rate is approximately equal to that of a straight crack with the same stress intensity factor between this 0.55 mm and 0.8 mm depth. This idea has been elaborated on in a previous study [12]. The current density should be higher along the higher strained inclined plane than the radial direction. The exact degree to which it is higher is however unknown, therefore for this study the increase was treated with a ratio F_n (Equation 4). $i_{a\ straight}$ was taken to be the maximum current density found in the potentiodynamic test for a conservative estimate of growth rate (57.6 A/m^2 as found in Figure 4), and F_n was varied from 1 to 1.4 in the model.

$$i_{a\ inclined} = F_n i_{a\ straight} \quad (4)$$

Validation of this method could be gained by comparing the straight crack growth values with those obtained in [20]. The parameters used in [20] were input to the MATLAB simulation and compared to the graph obtained in Lu [20] (Fig.7). Figure 7 shows a time to 7 mm depth for this present study (left) and Lu's study (right). Both graphs show a time to 7 mm of approximately 16 years at a current density of 80 A/m^2 when fatigue is neglected ($\dot{a}_e$ in [20]). The correlation of these results suggests that the methods used in this study provide realistic results.

The present simulation is then extended to inclined cracks at a current density of 57.6 A/m^2 in Figure 8. It can be seen that the straight and inclined SCC growth over 50% wall thickness (4.15 mm) is very sensitive to F_n. The straight crack reaches 1 mm depth, usually the minimum detectable depth, faster than an inclined crack for all presented values of F_n; however for a F_n of 1.2 or above, 50% through wall growth is achieved faster with an inclined crack. This means that only a 20% increase in current density is necessary in the highly strained areas around the crack tip for an inclined crack to grow faster than predicted for a straight crack over 50% wall thickness.

Increase in current around a crack tip have been demonstrated for a stressed pre-cracked X70 steel specimen in a concentrated carbonate/bicarbonate solution [24]. The values of the current were also shown to increase with the increase of the applied potential (up to 250 mV from E_{corr}). Moreover the regions with higher current values seemed mainly in the transverse directions, in relation to stress field's presence at the crack tip. Another study from the same group also showed preferential corrosion at the inclined angles during longer time frame testing [25]. The values of the current densities at the crack tip estimated from [24] (by considering an area of 1.25 x 1.25 mm^2 on the scans) ranged from 45 to 320 A/m^2. These values were globally higher than the values used for the presented simulation due to the different electrochemical method, grade of steel and chemical environment employed. Current densities values and their distribution around the crack tip for the X65 grade could be of course different. However, the values used in the model for the X65 were realistic as they were chosen based on the polarisation curves (Fig.4) and were in the same order of magnitude than the current densities values measured at the crack tip for the X70 grade. A current densities mapping at the crack tip of a cracked X65 specimen would nevertheless, allow more accurate predictions of inclined SCC growth rates, and thus allow accurate decisions by industry on inspection intervals.

Various elements of SCC growth were neglected in the presented model, including the impact of fatigue, crack interaction, and textural impedances. Of these, the only one that would be likely to have an effect on the relative growth rates of straight and inclined cracks is crack interaction, as inclined cracks are likely to encounter more cracks due to their hoop travel, which could both positively or negatively influence the crack growth rates. Additionally, the original model that the equation is sourced from uses some approximations for some of the parameters in the equations, including the repassivation kinetic exponent, and the incubation time of repassivation [20]. Both of these are candidates for change in the circumstance of inclined SCC, as a significant shift in the current density in the passive film region was observed. This potentially adds another source of error, and would underestimate the effect of inclined SCC. Furthermore varied ranges for the critical stress intensity factor for SCC in X65 steel have been found, largely due to the fact that inclined SCC will grow below the critical stress intensity factor, just at a much slower rate. This can make the value of a critical stress intensity factor somewhat arbitrary, however varying it in this model doesn't cause a large shift in the result. Lastly the cracks are assumed to travel in a 2D fashion, where the 3D nature of the crack will also have some impact on the crack path.

Conclusion

- The effects of strain on current density, and hence crack growth rate, for inclined SCC has been shown to be an important relationship.
- Strain was shown to cause a significant increase in current density in the SCC affected region, and a small increase in current density was shown to result in a large increase in crack growth rate.
- A quantitative relationship between microstrain around the crack tip and current density is required, and could be paired with the model developed here to accurately predict the growth rates of inclined SCC, and hence optimise field inspection intervals.

Acknowledgements

This work was funded by the Energy Pipelines CRC, supported through the Australian Government's Cooperative Research Centre's Program. The cash and in-kind support from the APGA RSC is gratefully acknowledged. Thanks to the industry partners for providing ex-service samples used in this study.

References

1. R. N. Parkins, R. R. Fessler, "Stress corrosion cracking of high-pressure gas transmission pipelines", in Materials in Engineering Applications, 1978, 1, 80-96.
2. F. Song, B. T. Lu, M. Gao and M. Elboujdani, "Development of a commercial model to predict stress corrosion cracking growth rates in operating pipelines", Report by Southwest Research Institute, 2011, Project 20.14080.
3. R. Sutherby, W. Chen, "Deflected Stress Corrosion Cracks in the Pipeline Steel", 6th International Pipeline Conference (IPC 2004), Calgary, Canada, Oct. 4-8, 2004.
4. J. Xie, L. Yang, M. Sen, R. Worthington, F. King, "Mechanistic investigation of Deflected Stress Corrosion Cracking in Pipeline Steels", Annual NACE International Conference, Atlanta, GA, March 22-26, 2009, paper 09121
5. L. Zadow, E. Gamboa, O. Lavigne, "Inclined stress corrosion cracks in gas pipeline steels: morphology and implications", in Materials and Corrosion, 2015, 66, 1092-1100.
6. L. Zadow, "Characterisation of the morphology of inclined SCC cracks in Australian gas pipelines", M.A. Thesis, University of Adelaide, Adelaide, 2014.
7. O. Lavigne, E. Gamboa, W. Costin, M. Law, V. Luzin and V. Linton, "Microstructural and mechanical factors influencing high pH stress corrosion cracking susceptibility of low carbon line pipe steel", in Engineering Failure Analysis, 2014, 45, 283-291.
8. J. W. Hutchinson, "Plastic stress and strain fields at a crack tip", in J. Mech. Phys. Solids, 1968, 16, 337-347.
9. Y. X. Wang, W. M. Zhao, H. Ai, X. G. Zhou and T. M. Zhang, "Effects of strain on the corrosion behaviour of X80 steel", in Corrosion Science, 2011, 53, 2761-2766.
10. X. Wang, X. Tang, L. Wang, C. Wang and W. Zhou, "Synergistic effect of stray current and stress on corrosion of API X65 steel", in Journal of Natural Gas, Science and Engineering, 2014, 21, 474-480.
11. J. Griggs, E. Gamboa and O. Lavigne, "A review of modelling high pH stress corrosion cracking of high pressure gas pipelines", in Materials and Corrosion, 2016, 67, 251-263.
12. J. Griggs, E. Gamboa and O. Lavigne, "2D modelling of inclined intergranular stress corrosion crack paths", in Fatigue Fract. Eng. Mater. Struct. Accepted for publication, Aug. 2016.
13. American Petroleum Institute (API) Specifications 5L 44th Edition, Oct 1, 2007. ISO 3183:2007 (Modified), Petroleum and natural gas industries-steel pipe for pipeline transportation systems.
14. E.M. Gutman, "Mechanochemistry of Materials", in Cambridge Interscience Publishing, Cambridge, 1998.
15. L.Y. Xu and Y.F. Cheng, "An experimental investigation of corrosion of X100 pipeline steel under uniaxial elastic stress in a near-neutral pH solution", in Corrosion Science, 2012, 59, 103-109.
16. L.Y. Xu and Y.F. Cheng, "Corrosion of X100 pipeline steel under plastic strain in a neutral pH bicarbonate solution", in Corrosion Science, 2012, 64, 145-152.
17. F.M. Song, "Predicting the mechanisms and crack growth rates of pipelines undergoing stress corrosion cracking at high pH", in Corrosion Science, 2009, 51, 2657-2674
18. X. Feng, Y. Zuo, Y. Tang, X. Zhao and J. Zhao, "The influence of strain on the passive behavior of carbon steel in cement extract", in Corrosion Science, 2012, 65, 542-548.
19. D. Kolman and J. Scully, "Continuum mechanics characterization of plastic deformation-induced oxide film rupture", in Philosophical Magazine A, 1999, 79, 2313-2338.
20. B. T. Lu, "Further study on crack growth model of buried pipelines exposed to concentrated carbonate-bicarbonate solution", in Engineering Fracture Mechanics, 2014, 131, 296-314.
21. F.P. Ford and P.L. Andresen, "Development and use of a predictive model of crack propagation in 304/316L, A533B/A508 and Inconel 600/182 alloys in 288 °C water", The Third International Symposium on Environmental Degradation of Materials in Nuclear Power Systems – Water Reactors, Traverse City, Michigan, 1987, p. 789.
22. P.L. Andresen, F.P. Ford, "Life prediction by mechanistic modeling and system monitoring of environmental cracking of iron and nickel alloys in aqueous systems", in Materials Science and Engineering: A, 1988, 103, 167-184.
23. O. Lavigne, E. Gamboa, J. Griggs, V. Luzin, M. Law and A. Roccisano, "High-pH inclined stress corrosion cracking in Australian and Canadian gas pipeline X65 steels", in Materials Science and Technology, 2016, 32, 684-690.
24. G.A. Zhang and Y.F. Cheng, "Micro-electrochemical characterization of corrosion of pre-cracked X70 pipeline steel in a concentrated carbonate/bicarbonate solution", in Corrosion Science, 2010, 52, 960-968.
25. X. Tang and Y. F. Cheng, "Micro-electrochemical characterisation of the effect of applied stress on local anodic dissolution behaviour of pipeline steel under near-neutral pH condition", in Electrochemica Acta, 2009, 54, 1499-1505.

Table 1. Definition of parameters used for growth rate calculation

Symbol	Description	Value used
$\dot{a}$ (m/s)	Crack growth rate	N/A
i_a^* (A/m^2)	Crack tip peak current density	Varied
n	Repassivation kinetic exponent	0.667 [20]
N	Strain hardening exponent (Ramberd-Osgood Law)	6 [20]
K_M (MPa $\sqrt{\text{m}}$)	Maximum stress intensity factor in a cycle	Varied
K_{ISCC} (MPa $\sqrt{\text{m}}$)	Critical stress intensity factor for SCC in X65	15 (average of [2] and [20])
r_0 (m)	Specific length for crack tip strain rate calculation	1× 10^{-6} [20]
σ_Y (MPa)	Yield strength of X65	460
M (kg/mol)	Molar mass of iron	55.845× 10^{-3}
z	Valence of iron	2
F (C/mol)	Faradays constant	96485
ρ (kg/m^3)	Density of iron	7.847 × 10^3
t_0 (s)	Incubation of repassivation	0.01 [20]
ϵ_F	Rupture ductility of passive film	0.001 [20]
E (GPa)	Elastic modulus of X65	200 [20]
β	Rice's coefficient	5.08

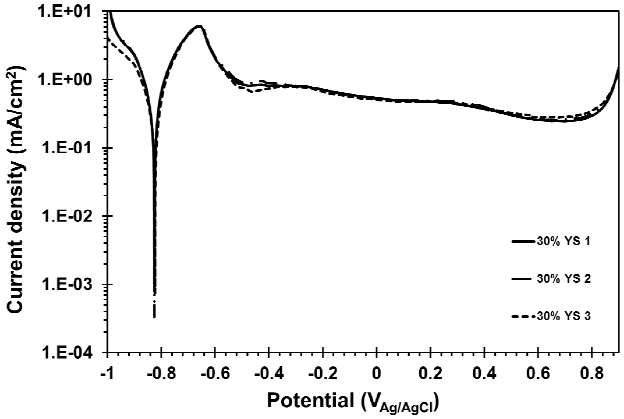

Figure 1. Example of 3 polarization curves recorded for a sample strained at one condition (30% YS). The measurements show a good reproducibility.

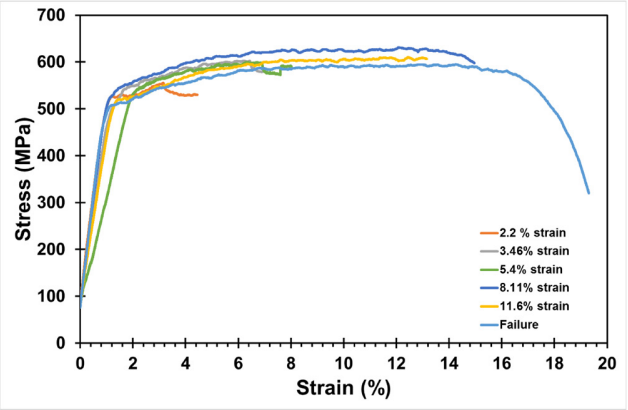

Figure 2. Stress strain curve for the X65 steel.

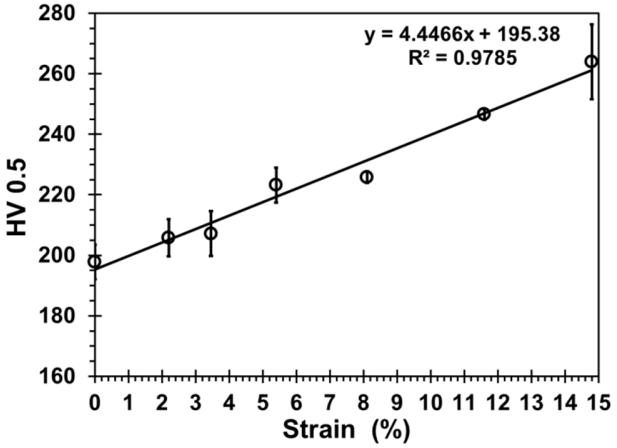

Figure 3. Vickers hardness values for the X65 steel strained at different level (average of the 3 measurements for each samples).

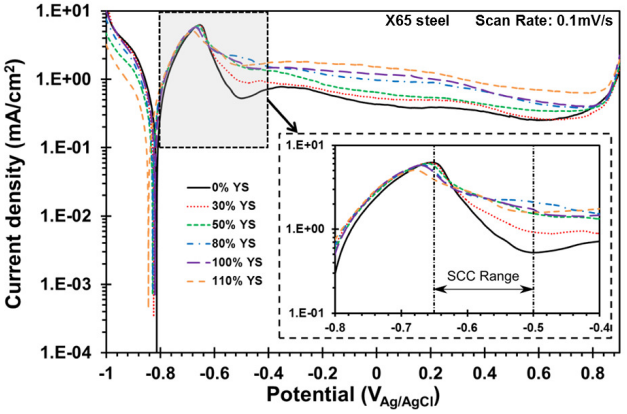

Figure 4. Polarisation curves for samples strained at different level in high-pH SCC medium with insert close-up of SCC range.

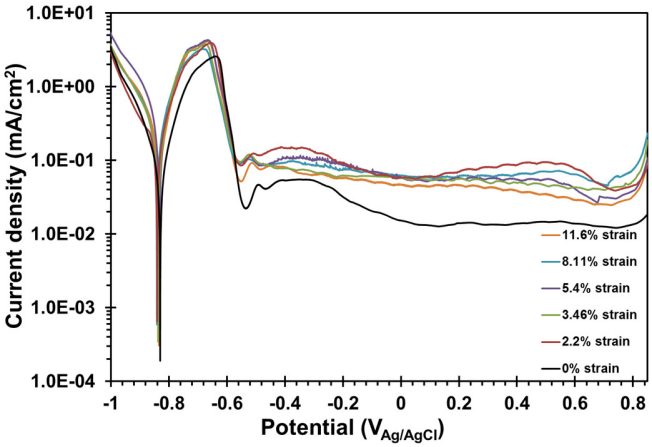

Figure 5. Polarisation curves for samples at different level of residual strain in high-pH SCC medium (no external load applied).

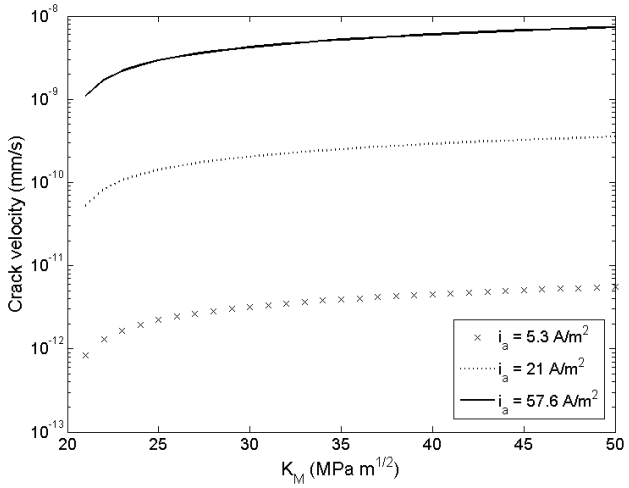

Figure 6. Crack growth rates for varied current densities using Equation 1.

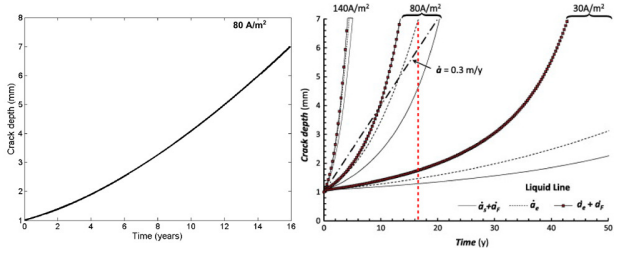

Figure 7. Validation of growth rate to 7 mm with a current density of 80 A/m^2. Present simulation shown on left, with Lu's simulations [20] shown on right. Time to 7 mm of approximately 16 years found for both.

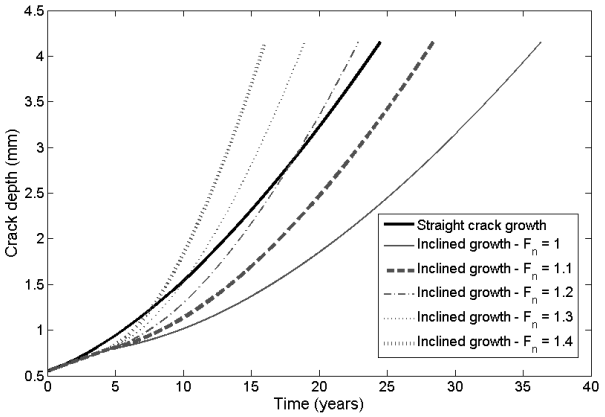

Figure 8. Radial growth for straight and inclined cracks for zero strain current density of 57.6 A/m^2. Inclined cracks grow with proportionally higher current density.

Modelling 3D interaction limits of inclined stress corrosion cracking

James GRIGGS[1], Olivier LAVIGNE[2], Erwin GAMBOA[3]

School of Mechanical Engineering, The University of Adelaide, Adelaide, 5005, Australia,
[1]james.griggs@adelaide.edu.au
[2]olivier.lavigne@adelaide.edu.au
[3]erwin.gamboa@adelaide.edu.au

Abstract: Assessment of high pH stress corrosion cracking in field inspections frequently involves using the Canadian Energy Pipeline Association (CEPA) interaction guidelines to determine whether two cracks could be interacting. These guidelines were created under the assumption of traditional SCC that propagates perpendicular to the applied stress (in the radial direction). Recently in both Canada and Australia, X65 pipelines have presented with stress corrosion cracking that instead grows at an angle from the perpendicular, termed inclined stress corrosion cracking. This raises the question that if two inclined cracks were angled towards each other, could they interact below the surface outside of the CEPA interaction guidelines?

This question is answered in this paper by developing an integrated MATLAB-FEA model that tests a series of worst case possibilities of inclined crack interaction based on previous field surveys of crack parameters. MATLAB is used to determine the worst case scenarios and finite element analysis (FEA) is used to test this range of cases for the effects of shielding, and whether these cases are feasible. It is found that the CEPA guidelines could be breached by a number of geometries, but all of those geometries are proven unattainable due to shielding effects. The significance of this result is that the CEPA interaction guidelines developed under a straight crack assumption are still valid for inclined SCC.

Keywords: Inclined stress corrosion cracking, modelling, crack interaction

Introduction and background

High pH stress corrosion cracking (SCC) usually grows in colonies, and as such quantifying the effects of crack-crack interaction is important for industry management. The guidelines used in the pipeline industry in Australia and Canada dictate that two cracks can be considered interacting if the closest crack tips are separated by less than 25% and 14% of their average lengths in the axial and hoop directions respectively [1]. These guidelines are based on prior studies that assume that the cross section of the SCC crack is perpendicular to the outer surface [2]. This assumption has been shown to not always hold true in recent years, as inclined SCC has been identified in both Australian and Canadian X65 steel pipelines [3-5].

Inclined SCC refers to high pH SCC with a subsurface crack path that deviates from the traditionally expected radial direction (Figure 1). Prior studies have shown cracks begin to incline at a depth of between 0.2mm and 0.9mm from the outer surface, and then incline to an angle of between 30 and 50 degrees from the radial direction [5]. Recent analysis has shown though that the depth of isolated cracks is more consistent at around 0.55mm from the outer surface for Australian inclined SCC [6].

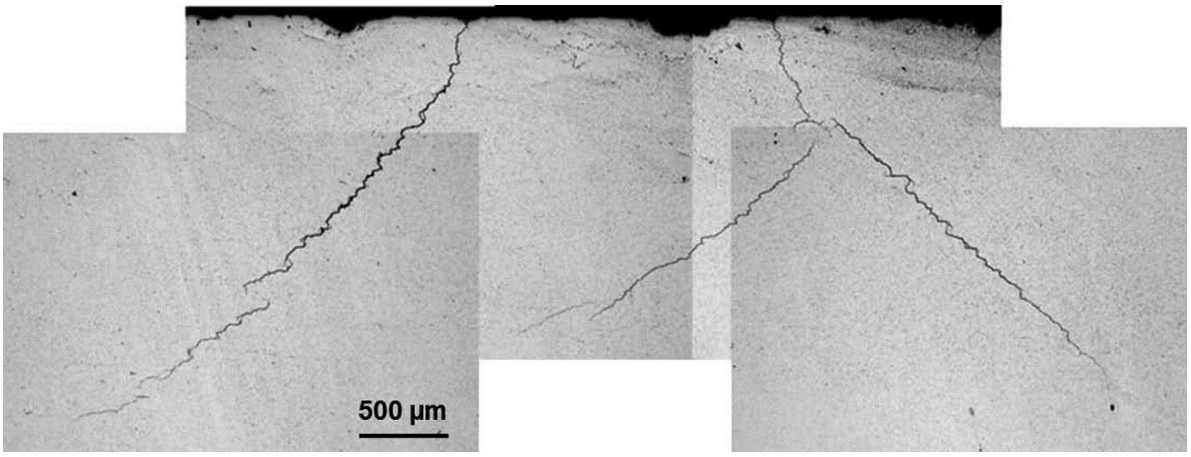

Figure 1: Inclined SCC cracks found in an Australian X65 steel pipeline [5].

While the surface interaction mechanics of adjacent cracks should not differ between straight and inclined SCC, there is potential for subsurface interaction where the existing guidelines would suggest that no interaction should occur. This study assesses inclined SCC for potential violations to existing guidelines [1]. This goal is achieved through first determining a range of worst case geometric scenarios using previously found statistical crack path parameters, and then tests those geometric cases using finite element analysis.

Method

The overall method to tackle this problem can be broken down into the methods required for the various tasks that needed to be achieved. These are determining a worst case range of crack path values, simulating two cracks touching beneath the surface and testing for spacing, and finally testing those geometric interaction cases for stress shielding, as was done by Wang et al. [2].

The worst case scenario for two interacting inclined cracks revolves on many variables. Relative crack lengths, length to depth ratios, inclination angle, and offset are all of importance.

Cracks of equal length have the ability to interact at a larger spacing than cracks of unequal lengths. This is as the cracks can only interact on a depth as deep as the shallowest (and shortest) crack. Adding extra length to just one of the cracks will make the average crack length longer whilst not changing the depth of interaction. Thus cracks of equal length were chosen for analysis.

Length to depth ratio (L/D) and inclination angle both have implications on the degree of subsurface hoop travel of the crack. A crack that is deeper for its length will have more subsurface hoop travel due to the inclination, and hence can interact with cracks that are further away. Similarly, cracks with a higher inclination angle have more subsurface hoop travel, and can therefore interact with greater surface spacing. Ranges for L/D and inclination angle were chosen based on RP2-05, with the modelled values having lower L/D ratios, and higher inclination angles (Figure 2). This creates a worst possible case for interaction.

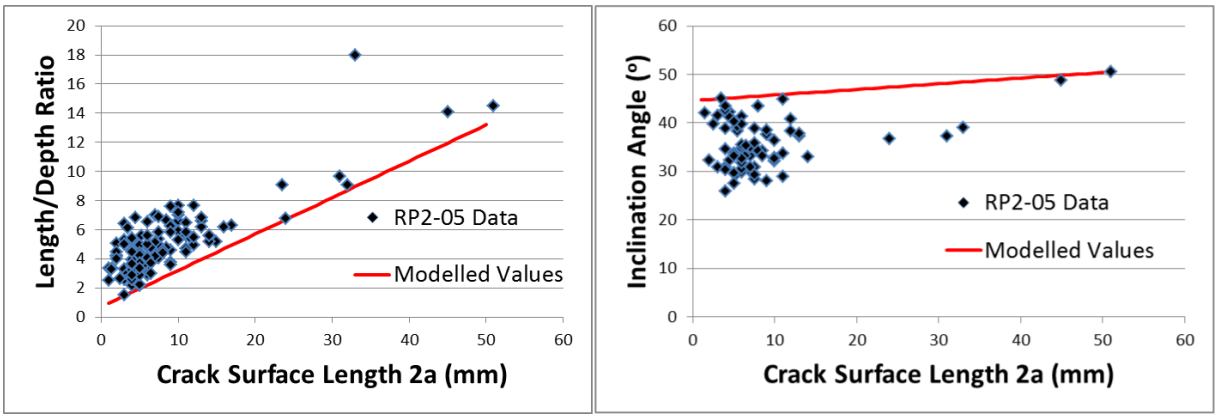

Figure 2: Crack path data sourced from Zadow [7] with modelled values taken for the greatest degree of inclination at a given depth.

Hoop and axial offset of the cracks is unclear as to what would create a worst case scenario. The cracks should overlap somewhat for interaction to occur without significant shielding, as in Figure 1, but the exact place where shielding is minimal yet the cracks are far enough apart to be outside of the CEPA guidelines is unknown. Thus these values were varied to create a range of all geometrically possible interaction cases.

The analysis of whether cracks could interact within CEPA occurred in three steps. Firstly a range of geometrically possible worst case scenarios were created in MATLAB and assessed for breaches. Secondly these cases were tested in finite element analysis (FEA) for shielding effects. Lastly the results of the FEA analysis were input back into the MATLAB code and a revised field of interaction cases is generated.

The MATLAB code finds the points of interaction by using the ellipse projection of the cracks on the surface of the pipe. As the inclined cracks follow an approximately semi-elliptical shape, and the projection of a semi-ellipse is also a semi-ellipse, all possible angles of interaction for two cracks of a given length can be calculated by finding the interaction tangents of the two ellipse projections on the surface (Figure 3), then re-projecting them down to the appropriate depth. Only one tangential interaction point exists for each surface interaction angle θ (as defined in Figure 4). The tangential point is used as this would result in two cracks that have

only just started to interact, rather than two cracks that have been interacting for some time. Half crack length a (as defined in Figure 4) and interaction angle θ are varied from 1-25mm and 0 to 90º respectively (angles from 90-180º are symmetrical to 0-90º). These cases are then tested for violation of the CEPA guidelines.

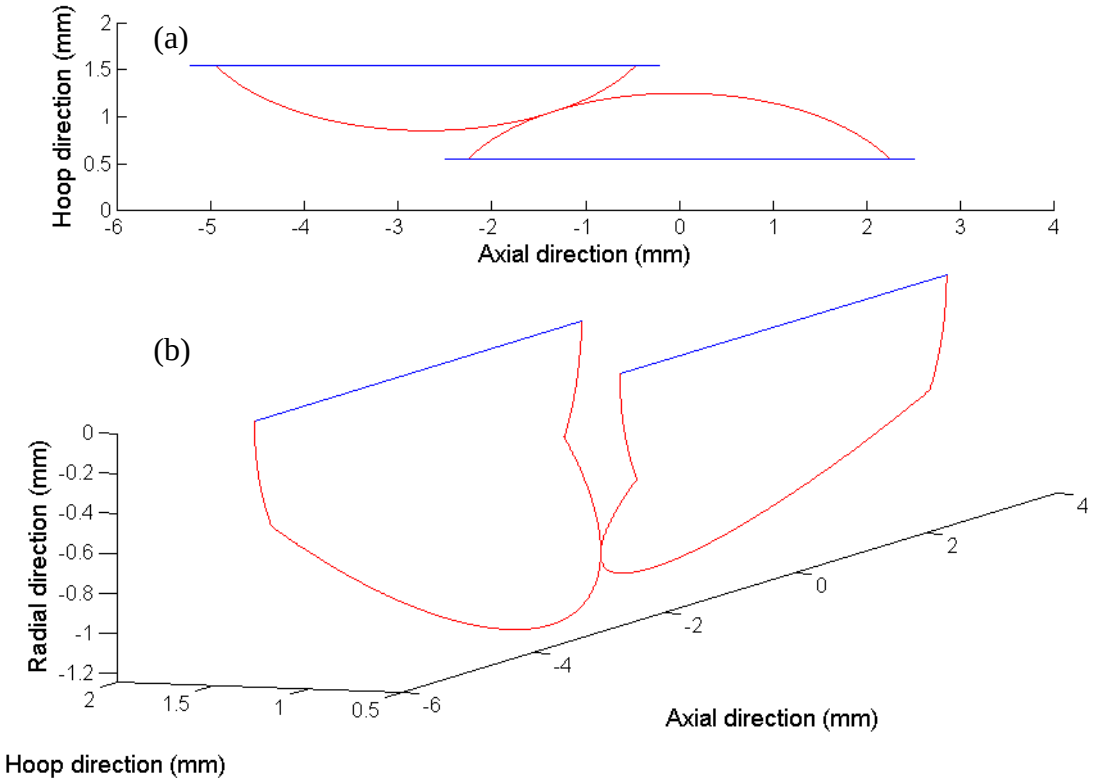

Figure 3: Tangent of interaction for the surface projected ellipse, (a) is a surface view and (b) is an isometric view. Blue line is the crack mouth on the surface while the red line is the crack front in the thickness.

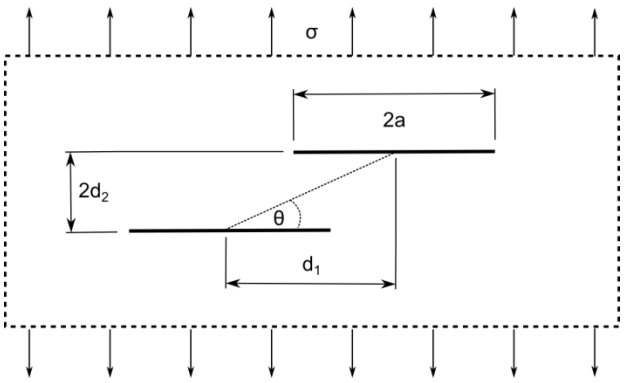

Figure 4: Surface view of two overlapping cracks with parameter definition.

The FEA code was then developed to test whether the cases identified would be possible, or whether they would be prevented due to shielding. The criteria set was that if the stress intensity factor at the inner crack tips on the surface were to fall below the minimum stress intensity factor required for growth, the crack would have arrested before that point and that crack

geometry would be impossible. The critical stress intensity factor was taken as 25 MPa√m or 790 MPa√mm, which is the limit for X60 in high pH solution [8]. Testing all geometric cases explicitly is not computationally efficient nor applicable to the creation of additional data points, thus a dimensionless lookup table that was scalable with crack length was created. Inputs to the table were the non-dimensional ratios $2a/d_1$ and d_1/d_2, and the output was a ratio of the stress at the inner tip to the stress at the outer tip (or a crack of equal length with no interaction effects). FEA results were validated for two ratios of d_1/d_2 against published results [9] with good agreement (Figure 5).

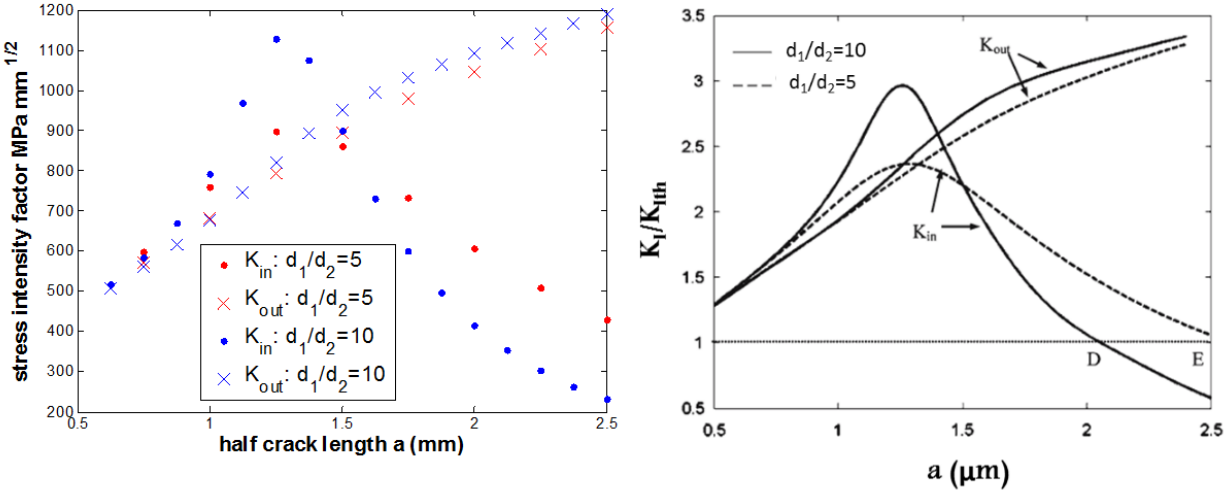

Figure 5: Validation of FEA results for two ratios of d_1/d_2 [9].

The lookup table was then inserted back into the MATLAB code and values of stress intensity factor at the inner tip were compared to the critical stress intensity factor. If the stress intensity factor was below the critical value then the crack would have arrested and the configuration is impossible. If all geometrically violating cases are shown to be prevented by shielding, the existing industry guidelines are also valid for inclined SCC.

Results

The surface spacing for the purely geometric subsurface interaction case is shown in Figure 6. Each crack configuration is represented by a point on the graph, and is assigned a key $(100\cdot(2d_2/2a) - 14)$ equal to how far above or below the CEPA hoop interaction limit they are. Positive numbers indicate interaction outside of the hoop spacing requirements set by the industry guidelines [1], while negative numbers indicate CEPA holding. For instance if the hoop spacing was 17% of the crack length, then the number that represents the spacing at that point would be 17%-14% = 3. Figure 6 shows the configurations that have a hoop spacing of less than 14% of their average lengths in green, while the configurations that lie outside of the guidelines are represented as per the colourbar.

It can be seen that all of the geometrically possible infringing cases occur with a relatively low surface crack length. This result is seen due to the tendency of SCC cracks have a higher length to depth ratio as their length increases, as previously shown in Figure 2. Additionally, the worst case inclination angle is relatively independent on the crack length when compared to the length to depth ratio. Thus the shorter cracks tend to be deeper relative to their surface length, and thus exhibit a greater subsurface hoop travel relative to their length. As specified in the methods,

these geometrically infringing cases would need to have the inner crack tips sufficiently stress shielded for the industry guidelines to hold for the inclined case.

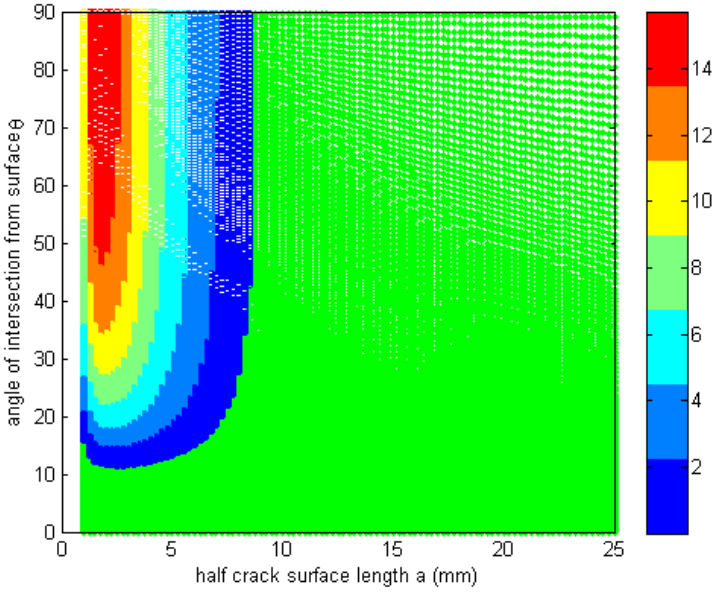

Figure 6: Worst case geometric interaction field. Green is within CEPA, coloured is outside of CEPA with degree indicated by the colour bar

The results of the addition of the FEA shielding is shown in Figure 7. The area shaded green shows sections where shielding would allow the cracks to interact, while the area in pink shows the area where the inner crack tips would have arrested before the infringing geometry was reached, and thus shielding prevents the interaction. Thus the existing CEPA interaction guidelines holds for all crack configurations. The worst case of interaction within the guidelines that is possible including shielding effects occurs with a hoop spacing of 12.6% of the average crack lengths, with a half crack length of approximately 4.5 mm, and an interaction angle (θ in Figure 4) of approximately 12.5º. CEPA holds especially well for longer cracks as the length to depth ratio increases, with only shorter deeper cracks proving to be close to the interaction limits.

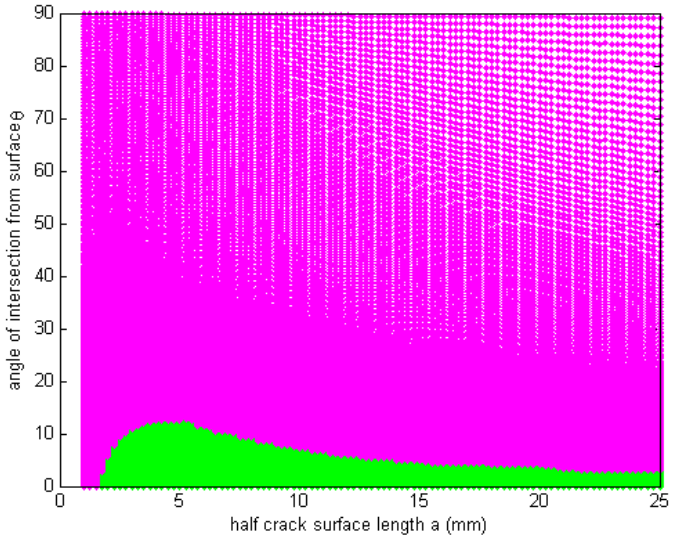

Figure 7: Geometric interaction possibilities with FEA shielding results. Pink = shielded so no interaction, Green = interaction within CEPA guidelines

Conclusion

Potential for inclined SCC interaction outside of CEPA guidelines was raised as a concern as the guidelines were developed with the assumption of a straight crack cross section. A range of worst case scenarios were generated using MATLAB and then tested for feasibility with finite element analysis. The results show that the CEPA guidelines hold across the entire range of possible geometries that were sourced from a number of worst case scenarios. CEPA was closest to being breached for shorter cracks which can have a lower L/D ratio than longer cracks, and thus would have more hoop travel per unit surface length. The researchers recommend no change to the currently used interaction guidelines for inclined cracks.

Acknowledgements

This work was funded by the Energy Pipelines CRC, supported through the Australian Government's Cooperative Research Centres Program. The cash and in-kind support from the APGA RSC is gratefully acknowledged. Thanks to the industry partners for providing ex-service samples used in this study.

References

1. Canadian Energy Pipeline Association, Stress Corrosion Cracking Recommended Practices, 2nd Edition. Canadian Energy Pipeline Association, (2007).

2. Y. Z. Wang, J. D. Atkinson, R. Akid and R. N. Parkins, Fatigue & Fracture of Engineering Materials & Structures, **19** (1996) 4

3. R. Sutherby, and C. Weixing, Proceedings of IPC 2004, Calgary, Canada, October 4-8, (2004).

4. J. Xie, L. Yang, M. Sen, R. Worthingham, and F. King, Proceedings of NACE International Corrosion 2009 Conference & Expo, Atlanta, Georgia, USA, March 22-26, (2009).

5. L. Zadow, E. Gamboa and O. Lavigne, Materials and Corrosion, **66** (2015) 10

6. O. Lavigne, E. Gamboa, J. Griggs, V. Luzin, M. Law and A. Roccisano, Materials Science and Technology, (2016) DOI: http://dx.doi.org/10.1080/02670836.2015.1132030

7. L. Zadow, Master's Thesis, The University of Adelaide (2014).

8. A. K. Pilkey, S. B. Lambert, and A. Plumtree, Corrosion, **51** (1995) 2

9. R. Sankar, and A. J. Lesser, International Journal of Fracture, **142** (2006) 3.